Universidad de Valladolid

FACULTAD DE CIENCIAS

Departamento de Química Física y Química Inorgánica

TESIS DOCTORAL:

Structural Studies of Biomolecular Building Blocks and Molecular Aggregates.

Presentada por **Montserrat Vallejo López** para optar al grado de **doctora en Química** por la Universidad de Valladolid

Dirigida por:
Alberto Lesarri Gómez

“What we know is a drop,

what we don´t know is an ocean”

Isaac Newton

Agradecimientos

No encuentro mejor manera de comenzar esta tesis que dando las gracias a todas aquellas personas que han contribuido de alguna manera en su desarrollo, así como al Ministerio de Ciencia e Innovación y al Ministerio de Economía y Competitividad la financiación recibida por el grupo a través de los proyectos de investigación: CTQ2009-14364-C02 y CTQ2012-39132-C02; y la concesión de la beca F.P.I. que he disfrutado.

En primer lugar, agradecerles a mis directores de tesis Alberto Lesarri y Emilio J. Cocinero la oportunidad que me han dado de trabajar con ellos durante estos años. En especial a Alberto por tener siempre tiempo para resolver mis innumerables dudas y a Emilio por haberme recibido siempre en su grupo como si formara parte de él.

Una persona imprescindible para que se haya realizado este trabajo es Patri. No tengo palabras para agradecerte todo lo que has hecho por mí, por enseñarme tantas cosas y tan diversas. Desde predecir un espectro (y no hablamos de espiritismo) hasta mostrarme lo difícil que es trabajar cuando fuerzas sobrehumanas como una prensa están en tu contra (lo mucho que esto puede llegar a unir). Y sobre todo, gracias por haberlo hecho SIEMPRE con una sonrisa. Creo que sabes lo importante que has sido en tantos momentos durante estos años para mí y tu gran contribución a esta tesis.

Agradecer también a todos los miembros de la sección de Química Física del departamento de Química Física y Química Inorgánica de la Universidad de Valladolid el haberme hecho sentir parte de él durante este tiempo. En especial quería dar las gracias a mi compañera Alicia, por todos los momentos que hemos pasado juntas, por los pequeños detalles iniciales que me hicieron saber que podía contar contigo y por conseguir hacerme reír por las mañanas con alguna aventura de tu peque. Tampoco puedo olvidarme de vosotros… los recién llegados: Adrián, Alberto, Álvaro, Germán, Pablo y por supuesto, la nueva microondera Elena. Ha sido una pena haber tenido que esperar tanto para conoceros, pero la espera ha merecido la pena porque, aunque nos conozcamos desde no hace mucho, ya tenemos juntos algunos momentos memorables como 'La cena de navidad de Quifis'. Gracias por los divertidos cafés y por tener buen gusto votando el 218 como el mejor despacho de becarios (o incluso de profesores) y hacerlo sede de las reuniones becariales.

A lo largo de este tiempo he tenido la oportunidad de visitar otros laboratorios. En primer lugar quería agradecer a los directores del grupo de espectroscopía de la Facultad de Ciencia y Tecnología de la UPV, los profesores Fernando Castaño y Francisco J. Basterretxea el haberme permitido formar parte de su laboratorio en diversos periodos durante estos años. Gracias también a Marian por tratarme siempre con tanto cariño y por preocuparse por mi bienestar en mis estancias en Bilbao. Y a todos aquellos con los que en algún momento he coincidido en el laboratorio, gracias por haberme hecho sentir una más entre vosotros. Sólo por eso puedo perdonaros que no tengáis clara la diferencia entre anchoa y bocarte/boquerón. Pero muy especialmente quiero dar las gracias a 'las chicas del lab'. A Lore por ser tan especial como eres, por ser tan 'dulce' (y no sólo por los chocolates de después de la comida), por tener siempre una frase bonita por las mañanas (aunque entre tú y Patri me sacarais los colores a diario). A Esti por comprender perfectamente la 'dura vida' del microondista y por recordarme que tengo una casa en Vitoria, ¡tomo nota!. Y por supuesto, gracias a las tres por preocuparos por mi agudeza visual y entrenarme en la búsqueda de objetos ocultos.

Un altro laboratorio che ho avuto l'opportunità di visitare per un lungo periodo di tempo è stato il laboritario del Prof. W. Caminati, la mia seconda casa. La sua gentilezza e ospitalità non si può descrivere a parole.

Grazie a tutto il gruppo per avermi fatto sentire gradita e benvenuta tra voi, per la vostra disponibilità e per avermi permesso di imparare tante cose di voi. Grazie a tutti: Sonia, Mina, Laura, Donatella, Annalisa, Luigi e, in modo speciale, un grazie a Camilla per essere la mia alleata con l´aria condizionata. Non vedo l´ora di ricontrarci in Spagna e andare in giro come abbiamo fatto a Firenze.

I would also like to thanks my work-team in Bologna for all the great moments we lived together in the lab and outside. You are more than workmates. Grazie a Luca e Lorenzo (i miei ragazzi del pranzo) per avermi fatto da guida turistica il mio primo giorno a Bologna e per non avermi lasciato indietro quando siamo dovuti scappare per il terremoto. Thanks Gang for your extremely kindness and for knowing what we need before asking anything. Devo avere un pensiero anche per imiei laureandi preferiti: 'Little Gloria' per essere così speciale, per avermi portato a conoscere il 'fisherman' e per i tanti momenti insieme; Andrea per essere stato il mio insegnante di

proverbi e di italiano (alla fine sei arrivato al top della mia piramide!). And last but for sure not least, Qian. Thank you for being my family in Italy, for understand me (we have proved it doesn´t depend on the culture) and for our funny 'karaoke' moments in the lab. I found more than a friend, a new sister.

Tengo que agradecer también a todos los que habéis estado conmigo desde mucho antes de que empezara este doctorado: las doctoras Ana, Clara y Lara (mira que es difícil decir vuestros nombres los tres seguidos). Desde nuestros comienzos como 'las chicas de la primera fila de Moreno' siempre habéis estado ahí. Gracias Ana por encontrar tiempo para un chocolate aún en tus momentos de estrés máximo y por ser la única de las tres que conoce mi casita de Valladolid. A ti Clara agradecerte tus chats, tus consejos con ojos sospechosos incluidos y por ser la mejor guía de todo Roma. Y a ti, Lara el ser tan detallista, aunque seas la que menos ruido hace, cuando no estás, te echamos de menos. Gracias a Jose, Carmen y Rocío por haberos unido al club de los UC´s y haber compartido tantos momentos especiales y grandiosos en la uni, en bodas o en paradas de metro (haced memoria y seguro que sonreís).

Por último agradecer a mi extensa familia todo el apoyo y cariño que cada uno me ha dado a su manera. Gracias a mis padres y a mis hermanos: Maica, Miguel, Magda y Luis por apoyarme siempre en las decisiones que he tomado y estar siempre disponibles para mí: bien con una llamada, acompañándome mi primer día en Valladolid o viendo series de las que sé que te avergüenzas. Sé que siempre puedo y podré contar con vosotros. Por supuesto a los peques (o ya no tanto) Pablo, Daniel, Lucía y Paula, vosotros aún en los momentos más duros, sabéis sacarme una sonrisa con vuestros goles, jugando a la 'caja registradora' o haciendo broches de papel. Finalmente, un especial agradecimiento a mi madre, porque ha conseguido dejarme, lo que en sus propias palabras, 'es la mejor herencia que se puede dejar a alguien: su formación'.

TABLE OF CONTENTS

III. Formaldehyde Complexes.

IV. Appendices: Other Studies.

Chapter 10.- **Trifluoroanisole**

Chapter 11.- **Trifluoroanisole···Water**

Chapter 12.- **Isoflurane···Water**

Chapter 13.- **Sevoflurane···Benzene**

Chapter 14.- **Pyridine···Fluoromethane**

Chapter 15.- **Pyridine···Difluromethane**

Chapter 16.- **Difluromethane···Dichloromethane**

Resumen.-

Esta memoria recoge el trabajo de doctorado realizado en el *Departamento de Química Física y Química Inorgánica* de la Universidad de Valladolid entre septiembre de 2010 y agosto de 2014. Asimismo, y con el fin de obtener la mención de *Tesis de Doctorado Internacional*, la memoria recoge los trabajos realizados en varias estancias científicas internacionales, en particular en la Università di Bologna.

La investigación llevada a cabo durante esta tesis doctoral ha comprendido el estudio teórico y experimental de diferentes unidades estructurales que juegan papeles importantes como bloques constructivos de diversos compuestos bioquímicos de relevancia, empleando técnicas de Química computacional y Espectroscopía de rotación.

Asimismo, se han llevado a cabo estudios de varios agregados débilmente enlazados generados en chorros supersónicos. De esta manera se han analizado tanto los factores intramoleculares responsables de las estructuras moleculares de cada monómero, como las interacciones de carácter intermoleculares que se ponen en juego en el caso de los agregados (en particular, enlaces de hidrógeno e interacciones dispersivas).

Se han estudiado tres familias de moléculas diferentes: tropanos, aminoésteres y decanos bicíclicos.

A la primera familia molecular pertenece la escopina y la pseudopeletierina, que tienen en común el azobiciclo de tropano que aparece en muchas moléculas de interés farmacológico. Al igual que en estudios previos llevados a cabo en nuestro grupo como la tropinona y la escopolina, para ambas moléculas se encontró que las estructuras estables eran las asociadas a configuraciones piperidínicas tipo silla, con el grupo metilamino en configuraciones axial o ecuatorial.

En el caso de la pseudopeletierina se midió el espectro de rotación de las especies isotópicas en abundancia natural, a partir de las cuales se obtuvo información acerca de la estructura del confórmero más estable de la molécula. Para la escopina no se pudo realizar el estudio isotópico dada la baja intensidad de las transiciones. Sin embargo, se detectó un efecto no encontrado en ninguno de los restantes tropanos: la rotación interna del grupo metilo.

La segunda familia estudiada es la de los aminoésteres, y en particular el isobutamben, de interés por su funcionalidad como anestésico local. Al igual que para otros compuestos de la familia como la benzocaína o el butamben se detectaron dos confórmeros, dependiendo de la orientación de la cadena lipofílica lateral.

La última de las familias es la de los decanos bicíclicos que comparten la estructura de la decalina, muy común en diferentes alcaloides y hormonas. En este trabajo se presentan los resultados correspondientes a la lupinina, donde además de confirmarse la configuración doble silla *trans* como la más estable, se observó un enlace de hidrógeno intramolecular que estabiliza la molécula.

La segunda parte de la tesis se centró en el estudio de las interacciones intermoleculares en complejos débilmente enlazados. En esta tesis se presentan los resultados de complejos en donde las moléculas involucradas en la formación de heterodímeros son el agua y el formaldehído.

El efecto de la solvatación tiene un claro interés bioquímico y en la actualidad se han estudiado diversos complejos por medio de espectroscopía de rotación. A pesar de que los sistemas microsolvatados no reproducen las condiciones de la materia condensada, proporcionan información acerca de los posibles lugares de interacción más favorables. En este trabajo se muestran los resultados obtenidos para los complejos monohidratados tropinona···agua y 2-fluoropiridina···agua.

En el primero de ellos existen dos posibles posiciones de enlace para la molécula de agua, bien a través de la del grupo carbonilo o amino. En este complejo se puso de manifiesto el papel del agua como donor de protones así como la importancia que tienen las interacciones secundarias del tipo $C-H\cdots O_w$ en el control de la estabilización del sistema hidratado.

En la 2-fluoropiridina se estudiaron los efectos de la fluoración en la piridina y cómo esto afecta al comportamiento del agua como donor o aceptor en el complejo. Finalmente se comprobó que el agua cuando se liga a la 2-fluoropiridina juega, al igual que en la tropinona···agua, el papel de donor interaccionando con el par electrónico del nitrógeno.

El segundo grupo de complejos intermoleculares es el de los dímeros formados con formaldehído. El objetivo inicial era el estudio de confórmeros que involucraban anestésicos volátiles como el isoflurano o el sevoflurano, pero finalmente se realizó un estudio previo de sistemas más sencillos (difluorometano y clorofluorometano) en los que se pusieran de manifiesto interacciones similares a las esperadas en los complejos con anestésicos volátiles.

Con la ayuda de estos sistemas de menor tamaño se pudo estudiar la competencia entre diferentes tipos de enlace, así como el análisis de los enlaces de hidrógeno cooperativos y cómo pequeños cambios en los monómeros afectan drásticamente a la geometría del complejo.

En ambos casos, se encontró un enlace bifurcado entre el grupo carbonilo del formaldehído con los hidrógenos del grupo metano, así como un enlace secundario entre alguno de los halógenos y los hidrógenos del formaldehído (C-Cl···H-C y C-F···H-C para el clorofluorometano y el difluorometano respectivamente). Adicionalmente, y para el complejo $CH_2FCl\cdots COOH$ se observaron dos estados diferentes correspondientes a la rotación interna del formaldehído.

Otra serie de aductos y monómeros han sido estudiados a lo largo de la realización de esta tesis doctoral, algunos de los cuales se muestran recogidos al final de esta memoria como apéndices (trifluoroanisol, trifluoroanisol···agua, isoflurano···agua, sevoflurano···benceno, piridina···trifluorometano, piridina···difluorometano y difluoro-metano···diclorometano).

Introduction

The investigation of biochemical molecules in the gas-phase using high-resolution spectroscopic methods has gained momentum in recent years and several reviews are available.[1-6] In the context of the research projects of our group (CTQ2009-14364 and CTQ2012-39132) in collaboration between the Universities of Valladolid (IP: A. Lesarri) and the Basque country (IP: José A. Fernández) our group was in charge of examining different families of compounds with rotational resolution, complementing the laser spectroscopy studies conducted in Bilbao. We present in this introduction the interest of the research objectives and structural problems that we have examined during the course of the doctoral work, which will be developed in the following chapters.

Biochemical compounds offer a large chemical variety and multiple degrees of complexity. Since high-resolution studies must progress constructively from simple units to more complex systems our main research lines were devoted to the spectroscopic investigation of several structural units that behave as molecular building-blocks of relevant biochemical compounds.

In parallel to this task we also participated in the instrumental objectives of the research projects, which in the Valladolid team included the construction of a new supersonic jet microwave spectrometer operating in the cm-wave region. This spectrometer follows the constructions of other microwave spectrometers in Bilbao in recent years and is now practically concluded.

We show in Figure 0.1 an outlook of the chemical families analyzed in the thesis. We chose three building-block families, first because of their biochemical and structural interest, and second to pursue previous studies done in our group. In this way the thesis contributes to the previous efforts on structural Chemistry done in Valladolid and provides a better understanding of the structural landscape of these molecular systems. This study was complemented with the investigation of several weakly-bound clusters generated in the gas-phase. While the study of isolated molecules focuses in the intramolecular factors controlling molecular structure, the analysis of molecular complexes allows examining intermolecular forces controlling aggregation. The relevance of molecular studies in the gas phase is the possibility to choose specific interactions in interacting groups, thus dissecting the different contributions of all intermolecular forces in play in these clusters (in particular hydrogen bonding or dispersive interactions).[7-9]

Some of the structural objectives on molecular clusters of the thesis have been carried out in the laboratory of Prof. Walther Caminati at the *Università di Bologna*, as part of the effort to obtain the qualification of "**International Doctoral Thesis**". During all the doctoral work the experimental collaboration with the Bilbao group has been also very fluid and is noted in several chapters. More occasional collaboration with other international groups, in particular those of Prof. Jens-Uwe Grabow (*Leibniz-Universität Hannover*) and Prof. Brooks H. Pate (*University of Virginia*) are noted when appropriate.

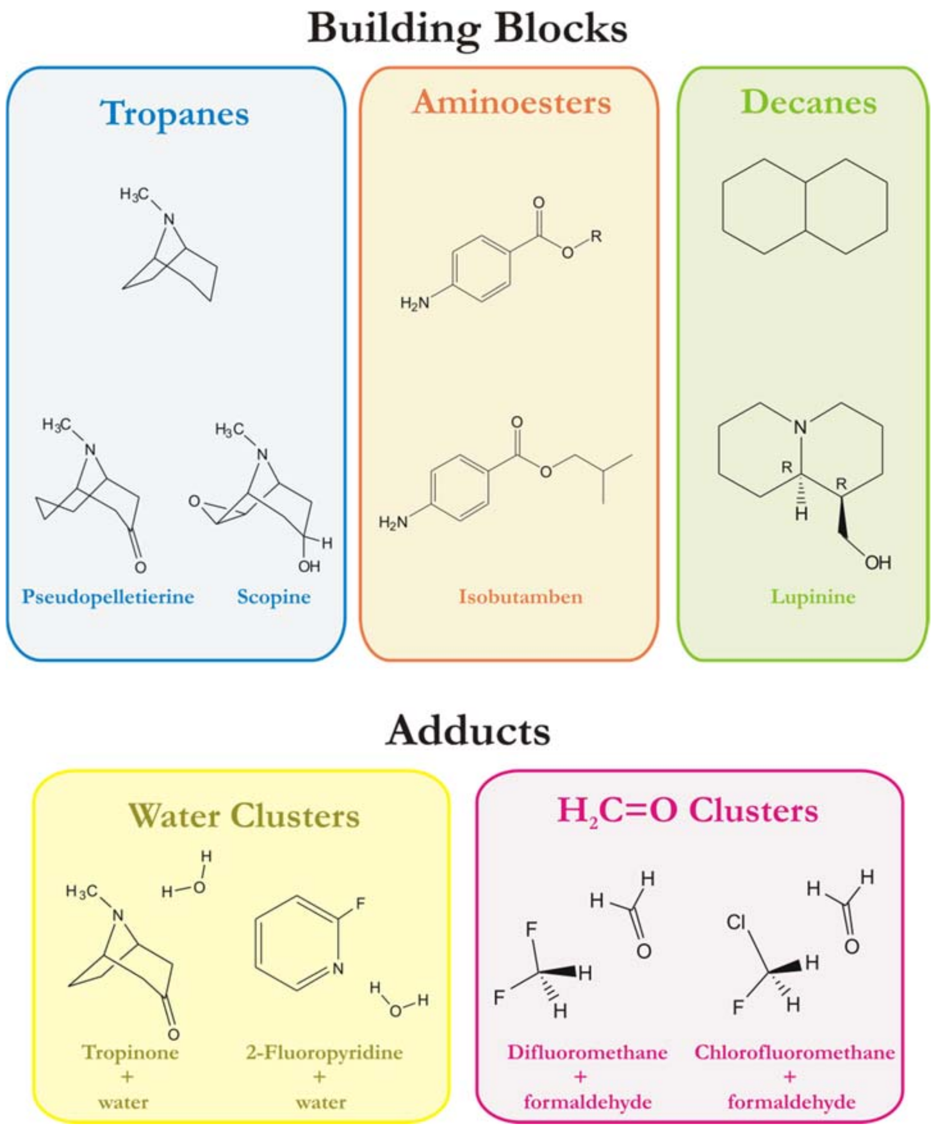

Figura: 0.1.- Structural targets examined during this thesis.

We examined three molecular families of biochemical building-blocks. The first family is that of tropane alkaloids. The common structural motif of these systems is the bicyclic unit of 8-azabicycle[3.2.1]octane, which appears in many molecules of pharmacological interest and drugs, some known from ancient times.[10] We studied in this thesis two tropane molecules, including pseudopelletierine (chapter 2) and scopine (chapter 3). These molecules are still relatively simple compared to larger pharmacological tropanes, but represent a logical extension of the previous work of our group on tropinone[11] and scopoline.[12] These studies examined basically problems of conformational equilibria, especially methyl inversion, and conducted multi-isotopic structural analysis which checked the conformational flexibility of the bicycle.

In pseudopelletierine and scopine the piperidinic skeleton adopts the most stable chair form. Six-membered twist or boat forms were not detected, offering a consistent description with the computational calculations predicting these conformations at much higher energies.

In pseudopelletierine the observation of isotopic species in natural abundance for the carbon and nitrogen atoms resulted in accurate structural information using the substitution and effective methods. This information has been useful to progress towards equilibrium structures in tropanes.[13]

In scopine we observed a phenomenon not observed in other tropanes, i.e., the internal rotation of the methyl group, splitting the rotational transitions by quantum chemical tunneling. This study allowed us to examine the treatment of internal rotation problems,[14] which results in the torsional barrier and rotor identification through its structural parameters.

The conformational equilibria in the studied tropanes is simple, as it is limited to the methyl inversion. We established the intrinsic conformational preferences in scopine and pseudopelletierine, which favor the equatorial form for scopine (as in tropinone) while the axial form is dominant in pseudopelletierine (as in scopoline). We measured conformational ratios in pseudopelletierine but this was not possible in scopine, where only the global minimum is observed. The conformational energies were modeled in all cases with ab initio calculations, giving arguments for the differences observed in scopine and other tropanes.

The second family of compounds analyzed in the thesis was that of the aromatic aminoesters. Compounds based on this chemical unit are also of pharmacological interest,[10] especially as local anesthetics, with different properties depending of the lipophilic and hydrophylics side chains. Our group examined previously two of these molecules with rotational resolution, including the ethyl and propyl sidechains in benzocaine[15] and butamben.[16] Some of these molecules had been studied also in the Bilbao group using laser spectroscopy,[17,18] offering the possibility to combine information from vibronic and rotational spectra.

In this thesis we examined isobutamben (chapter 4), where the *trans* and *gauche* conformers of benzocaine are further complicated by the two additional carbon atoms in the terminal isopropyl chain. Two conformers were detected for isobutamben, practically isoenergetic. Other conformations, despite being close in energy, were not observed, illustrating the importance of conformational relaxation in jets experiments.[19-22] This problem outlines the importance of a good description, not only of the stationary points on the PES, but also of the plausible interconversion paths in order to account for the conformational populations in jet spectra.

The third structural family we examined was that of bicyclic decanes, which are based in the structure of decalin. This chemical pattern is at the core of several biochemically relevant compounds, including steroids and alkaloids. The two rings in the fused system can adopt different conformations while still retaining the most stable double-chair, as our group observed in the investigation of 2-decalone, where three conformations were detected.[23] In this thesis we present the case of lupinine (chapter 5). Lupinine is a quinolizidine alkaloid, i.e, one of the carbon bridgeheads in decalin was substituted with a nitrogen atom, and also displays a hidroxymethyl group adjacent to the C bridge head.

Unlike decalone, the conformational landscape of lupinine is much simpler, as the formation of an intramolecular O-H$\cdots$N hydrogen bond (not possible in the diastereoisomer epilupinine) locks the molecule in a single most stable conformation. The molecule illustrates how intramolecular hydrogen bonding is the main stabilizing force in isolated molecules, as observed in many other systems.[1-9] We estimated computationally the contribution of the hydrogen bond to molecular stabilization by comparing the molecule with epilupinine and decalin.

The second part of the thesis is dedicated to the study of intermolecular interactions in weakly bound complexes. Molecular clusters can be formed easily in supersonic jets, offering the possibility to gauge specific interactions between neutral molecules. We present in the thesis complexes with two aggregation partners, including water and formaldehyde (other complexes are included as appendixes).

Solvation has an obvious biochemical interest and many compounds have been analyzed rotationally to date.[24] Microsolvated systems are far from the condensed media, but illustrate the preferences for binding sites and the interaction strengths. [25] Recent studies of the water clusters up to $(H_2O)_{15}$ have shown the possibilities of rotational investigations.[26] We present here results on the monohydrated complexes of tropinone···H_2O (chapter 6) and 2-fluoropyridine···H_2O (chapter 7).

Tropinone···H_2O was interesting because of the combination of a carbonyl and amino group in the molecule, offering two alternative binding sites to water. Somehow unexpectedly water binds to the amino group, acting as proton donor to the non-bonding orbital at the nitrogen atom. We observed also that the most stable equatorial conformation of tropinone was retained in the complex. This fact confirms the accepted view that monomer structures are not affected by complexation for weak or moderately intense hydrogen bonds. The structural information can be useful to suggest the presence of secondary interactions, for example weak C-H···O_w hydrogen bonds in hydrated tropinone. Secondary interactions were relevant also in the interpretation of the sevoflurane···benzene complex studied in collaboration with the University of Virginia, which is reported as an Appendix (chapter 13).[27]

In the case of 2-fluoropyridine we were interested in the effects caused by the fluorination of pyridine. In the predicted most stable configuration of the complex, water plays the role of proton donor to the electron lone pair at the nitrogen atom. This hypothesis was later confirmed by the experimental data. This behavior is the same as that found in pyridine···water. However, and due to the fluorine atom in position 2, an extra weak interaction is established between the two subunits. The stabilization of the adduct takes places also through the secondary weak interaction C-H···O, breaking the linearity of the hydrogen bond.

A second group of intermolecular complexes were those established with formaldehyde. Initially our objective was to explore the clusters with halogenated ethers used as volatile anesthetics (previously studied in our group),[28-29] but we finally preferred to first examine the simpler cases of difluoromethane···formaldehyde (chapter 8) and chlorofluoro-methane···formaldehyde (chapter 9), which might exhibit similar intermolecular interactions as those expected in the volatile anesthetics.

The advantage of the halogenated methanes, like the difluoro (HFC-32) and chlorofluoro (CFC-31) species is their small size and possibility of different competing interactions. In those molecules the C-H bonds are activated by the presence of the electronegative atoms and weak hydrogen bonds are relatively strong. [9] A final reason of interest is the possibility of cooperating effects between multiple hydrogen bonds, which has been observed in complexes bound by weak interactions. In these cases small changes in the monomers can affect dramatically the adduct geometry.

In the chlorofluoromethane-formaldehyde complex the cluster exhibits three simultaneous hydrogen bonds: a bifurcated contact between the methane hydrogens and the carbonyl group (C=O···H-C) and an extra interaction between the chlorine atom and one of the hydrogen atoms of formaldehyde. This geometry suggest that the C-Cl···H-C union is more favourable than the alternative C-F···H-C bond, which was not detected experimentally. Interestingly, we observed the inversion of the symmetric H atom of formaldehyde and information of the two first torsional states was obtained.

In the difluoromethane-formaldehyde complex the interactions are similar, sharing the bifurcated carbonyl to hydrogen bond, but now supplemented with a C-F···H-C union.

Other investigations conducted in this thesis are reported as Appendix (chapters 10 to 16), including six intermolecular complexes (trifluoroanisole···water, isoflurane···water, sevoflurane···benzene, pyridine···CHF_3, pyridine···CH_2F_2 and CH_2F_2···CH_2Cl_2) and one monomer (trifluoroanisole).

References.-

[1] J. P. Schermann, Spectroscopy and Modeling of Biomolecular Building Blocks, Elsevier, Amsterdam, **2008**.

[2] M. S. de Vries, P. Hobza, *Annu. Rev. Phys. Chem.*, 58, 585, **2007**.

[3] W. Chin, F. Piuzzi, I. Dimicoli, M. Mons, *Phys. Chem. Chem. Phys.*, 8, 1033, **2006**.

[4] J. P. Simons, *Mol. Phys.*, 107(23-24), 2435-2458, **2009**.

[5] T. R. Rizzo, J. A. Stearns, O. V. Boyarkin, *Int. Rev. Phys. Chem.*, 28, 481, **2009**.

[6] K. Kleinermanns, D. Nachtigallova, M. S. de Vries, *Int. Rev. Phys. Chem.*, 32, 308, **2013** and references therein.

[7] P. Hobza, K. Müller-Dethlefs, Non Convalent Interactions, Theory and Experiment, RSC Publishing, **2010**.

[8] G. A. Jeffrey, An Introduction to Hydrogen Bonding, Oxford UP, Oxford, **1997**.

[9] G. R. Desiraju, T. Steiner, The Weak Hydrogen Bond, Oxford UP, Oxford, **1999**.

[10] L. Brunton, B. Chabner, B. Knollman, Goodman and Gilman's The Pharmacological Basis of Therapeutics, 12th Ed., McGraw-Hill Professional, **2010**.

[11] E. J. Cocinero, A. Lesarri, P. Écija, J.-U. Grabow, J. A. Fernández, F. Castaño, *Phys. Chem. Chem. Phys.*, 12, 6076, **2010**.

[12] P. Écija, E. J. Cocinero, A. Lesarri, F. J. Basterretxea, J. A. Fernández, F. Castaño. *ChemPhysChem.*, 14, 1830, **2013**.

[13] J. Demaison, N. C. Craig, E. J. Cocinero, J.-U. Grabow, A. Lesarri, H. D. Rudolph, *J. Phys. Chem. A*, 116, 8684, **2012**.

[14] D. G. Lister, J. N. McDonald, N. L. Owen, Internal rotation and inversion, Academic Press Inc., New York, **1978**.

[15] A. Lesarri, S. T. Shipman, G. G. Brown, L. Alvarez-Valtierra, R. D. Suenram, B. H. Pate, L. Kan, Comm. RH07, 63rd. OSU Int. Symp. Mol. Spectrosc., Columbus (OH) **2008**.

[16] M. K. Jahn, D. Dewald, J.-U. Grabow, W. Caminati, E. J. Cocinero, A. Lesarri. In publication.

[17] E. Aguado, A. Longarte, E. Alejandro, J. A. Fernández, F. Castaño, *J. Phys. Chem. A*, 110, 6010, **2006**.

[18] E. Aguado, I. León, E. J. Cocinero, A. Lesarri, J. A. Fernández, F. Castaño, *Phys. Chem. Chem. Phys.*, 11, 11608, **2009** and references therein.

[19] D. H. Levy. *Science*, 214, num.4518, 263, **1981**.

[20] R. S. Ruoff, T. D. Klots, H. S. Gutowsky, *J. Chem. Phys.*, 93, 3142-3150, **1990**.

[21] G. M. Florio, R. A. Christie, K. D. Jordan, T. S. Zwier. *J. Am. Chem. Soc.*, 124, 10236-10247, **2002**.

[22] P. D. Godfrey, R. D. Brown, *J. Am. Chem. Soc.*, 12, 10724-10732, **1998**.

[23] D. Wachsmuth, M. K. Jahn, M. Vallejo-López, S. Blanco, A. Lesarri, J.-U. Grabow, in publication.

[24] S. Novick, Bibliography of rotational spectra of weakly bound complexes, http://wesfiles.wesleyan.edu/home/snovick/SN_webpage/vdw.pdf.

[25] L. Evangelisti, W. Caminati, *Phys. Chem. Chem. Phys.*, 12, 14433, **2010**.

[26] C. Pérez, M. T. Muckle, D. P. Zaleski, N. A. Seifert, B. Temelso, G. C. Shields, Z. Kisiel, B. H. Pate, *Science*, 336, 897, **2012**.

[27] N. A. Seifert, D. P. Zaleski, C. Perez, J. L. Neill, B. H. Pate, M. Vallejo-Lopez, A. Lesarri, E. J. Cocinero, F. Castaño, I. Kleiner, Angew. Chem. Int. Ed., **2014** (in press).

[28] A. Lesarri, A. Vega-Toribio, R. D. Suenram, D. J. Brugh, D. Nori-Shargh, J. E. Boggs, J.-U. Grabow, *Phys. Chem. Chem. Phys.*, 13, 6610, **2011**.

[29] A. Lesarri, A. Vega-Toribio, R. D. Suenram, D. J. Brugh, J.-U. Grabow, *Phys. Chem. Chem. Phys.*, 12, 9624, **2010**.

Chapter 1
Methodology

Following the presentation of research objectives in the Introduction, this chapter presents the methodology used in this work. The thesis deals with structural problems on biochemical building blocks and molecular aggregates. Understanding molecules requires a detailed description of their electronic distribution, vibrational properties and structure, usually demanding multiple pieces of information, both experimental and theoretical. Molecules interact and react, so we need to know not only the intramolecular factors defining the structure, but also which are the most important intermolecular forces controlling aggregation properties.

For this reasons each structural problem requires a combination of several theoretical and experimental methods to produce a comprehensive molecular description. Since many of these methods are well established we present a general overview with the most important features compatible with a condensed presentation. Detailed descriptions of the methods used can be found in the literature.

1.2. Computational Methods.-

Computational methods are used to investigate the electronic states, vibrational motions and structural properties of molecules and aggregates. All our investigations were limited to the electronic and vibrational ground states. Many of the systems studied possess multiple conformational degrees of freedom, so it was particularly important to obtain a good description of the conformational landscape of the studied molecules.

Once the most important features of the molecular potential energy surface (PES) were known, we examined the vibrational and structural properties of the global and most stable minima of the PES.

The theoretical methods are thus used before the experimental study in order to obtain predictions of relevant structural characteristics (moments of inertia) and electric properties (dipole moments and nuclear quadrupole coupling parameters). These results give the necessary information to simulate the rotational spectra of the molecular systems within the microwave region. The predicted transitions also help in the spectral assignment and later analysis.

In this work, several different kinds of theoretical calculations were performed, from the simplest molecular mechanics (MM) methods to relatively accurate molecular orbital ab initio calculations. Calculations intermediate in cost and accuracy terms, based in the Density Functional Theory (DFT) were also carried out.

The first task of the theoretical calculations is the analysis of the PES in the electronic ground state. The conformational screening can be done at different theoretical levels, but in all cases this is followed by more detailed structural and vibrational calculations. In consequence, this kind of calculations does not need to focus on accurate energetic or structural predictions but on the most systematic exploration of the PES. These arguments support the use of Molecular Mechanics for the survey of the PES due to the low computational cost and the powerful and new conformational search algorithms available. MM is implemented in many different programs, but we used especially Hyperchem[1] and Macromodel,[2] both having the possibility of doing automated conformational searches.

MM uses a combination of classical mechanics and empirical force fields to describe molecular motions and interactions.[3] Energy descriptions are usually partitioned into several contributions, both covalent (bond, angle and dihedral terms) and non-covalent (electrostatic, van der Waals, etc), and they are a fast and easy way to obtain initial information about the different structural configurations which can be adopted by a given molecular system. Molecular mechanics are highly dependent on the empirical force fields, which are adjusted to reproduce specific molecular properties or selections of compounds.

Some of the typical force fields include AMBER,[4,5] OPLS[6,7] or MMFF, [8-10] which are all appropriate for small organic compounds. In our case we used mostly the Merck Molecular Force Field (MMFF), which is a type-II extended potential that includes cross terms without truncation in order to better reproduce real systems. These kinds of potentials are suitable both in gas phase and condensed phases, and claim to have good transferability. In other words, it means that the empirical parameters of those potentials can be applied, to a certain extent, to molecules that have not been explicitly included in the empirical potential parameters.

An important advantage of MM methods is the availability of sophisticated conformational search algorithms, which can generate systematically a large number of starting structures. These procedures assure that the survey of the PES will be reasonably detailed. In particular, we used in this work two conformational search procedures based in a Montecarlo stochastic search and the so called large-scale low-modes exploration. These methods are implemented in Macromodel.[2] Other programs used different search procedures. All these searching procedures require a relatively low computational cost.[11]

In order to obtain reliable conformational energies and molecular properties, more sophisticated methods must be used on all the detected minima within reasonable energy windows (i.e., < 40 kJ mol^{-1}). Molecular orbital methods include ab initio (for example, MP2)

[12,13] and Density Functional Theory (DFT) [14] calculations with different functionals (i.e., B3LYP and M06-2X).[15,16]

The methods based in the density functional theory are widely used due to the good efficiency-cost ratio compared to the methods based in the wave function theory (WFT). However, the accuracy of the results provided by the DFT theory are directly related to the quality of the exchange-correlation potential energy (XC) used to describe the system under study.[16-18] Depending on the type of XC potential we can distinguish different methods which have been improved throughout the years. Hence, we can find functionals in which the exchange-correlation energy depends only on the electronic density (Local Spin Density Approximation LSDA), as well as other more sophisticated, among which M05[19] and M06[19] are noticeable.

In our case, we used both B3LYP[20-22] and M06-2X because of the reduced computational cost and because those methods use functionals that can reproduce, in principle with high accuracy, thermochemical variables that are overestimated or non- determined when other local functionals such as LSDA or GGA[23-25] (Generalized Gradient Approximation) are used. Normally both methods could produce satisfactory results for spectroscopic purposes in the kind of systems studied.

However, we should note that, despite the improvements with respect to the LSDA or GGA approximations, the B3LYP method has some inherent limitations and fails to fully describe some of the systems studied here. In particular, B3LYP does not account for middle-range dispersion interactions (~2-5 Å), which are very important in biological systems and in intermolecular clusters such as the dimers or hydrated molecules (chap. 6, 7, 8 and 9). Also B3LYP usually overestimates the height of torsion barriers[26] as a consequence of the auto-interaction error of the local DFT.

These issues of the B3LYP method motivated the development of other functionals, like the M05 and M06 approximations. [19] The M06-2X functional belongs to the so-called hybrid methods and was used extensively in our work. This method combines the characteristic local interchange of the DFT methods with the Hartree Fock (HF) theory. Another advantage with respect to B3LYP is the inclusion of a model for the interchange and correlation hole and some empirical fittings.

The M06 functional is very efficient for many chemical groups (not for transition metals), predicting with good accuracy the electronic states and different molecular properties. It is also very convenient for systems where the thermochemistry and the non-covalent interactions are relevant, especially intermolecular complexes.

In the case of the methods based in the WFT, the Møller-Plesset (MPn)[27,28] methods give a good balance between accuracy and computational cost for spectroscopic purposes. MPn calculations are post-Hartree-Fock methods which explicitly introduce electron correlation through perturbation theory, usually up to second (MP2), third (MP3) or fourth (MP4) order. We typically used MP2 in most cases, though occasionally MP4 or other more advance post-HF methods, like CCSD(T) have been used.

The ab initio and DFT calculations require an adequate selection of a finite set of orbital basis functions. A basis set is a description of the atomic orbitals centered at each nucleus of the molecule. Because of the computational difficulties of Slater functions, atomic orbitals are commonly described as linear combinations of gaussian orbitals, as suggested by Pople.[29] Depending on the number of gaussian functions involved in the definition of the orbitals, different basis sets are defined. In this work, we used basis sets which have in common the number of gaussian functions used to describe the core orbitals. For the valence orbitals different basis with different number of functions were used. In the double-ζ case, the valence orbitals are described by two basis sets, each one formed by a linear combination of different number of gaussian functions (X and Y respectively, or X-YZ-G, X being the number of Gaussian functions describing the core orbitals, six in our case: 6-YZ-G). For the triple-ζ case, three different basis sets form the valence orbitals (denoted X-YZW-G). A common modification of basis sets is the addition of polarization functions,[29,30] which supply the flexibility needed for deformation of the valence orbitals, either in heavy atoms (denoted *) or also in light atoms (H, He, denoted **). Other usual modification is the inclusion of diffuse functions (denoted + or ++ when it includes light atoms), helping to better reproduce the tails of the atomic orbitals far away from the atomic nucleus.[29] In the present work, the most common basis set employed were the 6-

31G(d,p) and 6-311++G(d,p) basis sets. The notation G(d,p) indicates that we add 'p' type functions to describe the hydrogen orbitals and 'd' functions for the elements of the first row of the periodic table.

The enlargement of the basis sets represent an improvement in the theoretical results used for the spectrum predictions, at the cost of a larger computational cost. The basis set used was selected because of the good relation between cost and efficiency in spectroscopic predictions.

1.2. Experimental Methods.-

The experimental methods used in this work were based in supersonic jet microwave spectroscopy, which provided the pure rotational spectrum in the cm-wave region. In fact, one of the main objectives of our research projects (CTQ2009-14364-C02, CTQ2012-39132-C02) in collaboration between the Universities of Valladolid (I.P.: A. Lesarri) and the Basque country (I.P.: J. A. Fernández) was to build a microwave spectrometer in our group. The design of this spectrometer, which is practically concluded, is shown below. In the meantime, the experimental measurements presented in this thesis were measured in different visits to the group of the University of the Basque country. Other experimental measurements were done in the group of Prof. W. Caminati at the University of Bologna, as part of the work to obtain the mention of "International Ph.D.". Collaborations with other groups are indicated in the publications.

The microwave spectrometer built in our group is based in the original Balle-Flygare design,[31] but includes many of the improvements developed in the last years, in particular in the group of Prof. J.-U. Grabow at the University of Hannover.[32,33]

The Balle-Flygare spectrometer is an instrument which combines techniques of supersonic jet expansions[34-36] with the spectroscopic characterization of the gaseous sample using Fourier-transform microwave (FT-MW) spectroscopy.[37] For this reason, we can distinguish two main parts related to the expansion chamber and the FT-MW spectrometer. A brief description of these components is presented below. More detailed explanations are available in the bibliography.

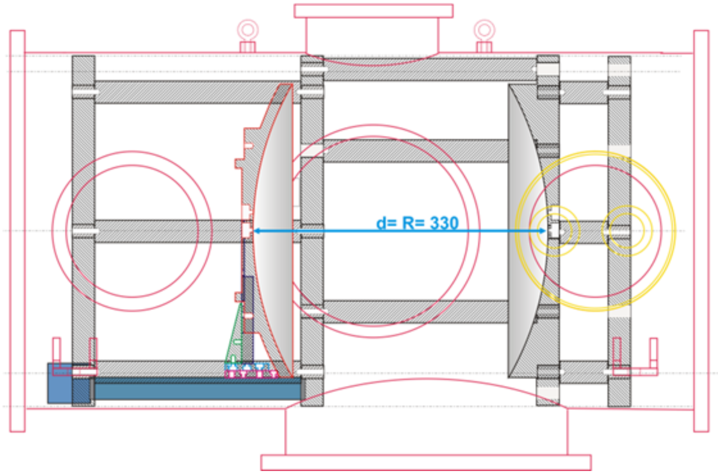

Figure: 1.1.- Fabry-Pérot resonator of the FTMW spectrometer at the UVa, showing the two spherical mirrors in confocal position.

a. Jet expansion.

The samples are prepared in the form of a molecular jet. The jet originates from a gas mixture at moderate pressures (1-5 bar), expanding through a small nozzle (ca. 1 mm) into an evacuated chamber (residual pressures of about 10^{-6} mbar). The nozzle is mounted in a solenoid pulsed valve, creating gas pulses of about 0.5 ms with repetition rates limited by the vacuum system (typ. < 10 Hz). The expansion pressures and the nozzle and chamber dimensions assures that most of the cell is within a "silence zone" (absence of intermolecular collisions), far from shock-waves.

The sample is typically diluted in a noble carrier gas (He, Ne) at very small concentrations (<1 %), favouring that the heavier sample molecules acquire the larger speeds of the light carrier. At the nozzle exit, the gas mixture reaches the speed of sound, allowing for spectroscopic probing in periods close to the time-scale of the expansion. During the expansion in the chamber, the random thermal movement of the sample is converted into a directional flux, so the energy of the internal modes is transformed into kinetic energy, due to the abundant collisions that take place in the nozzle proximities. The collisions decrease the rotational and vibrational temperatures (T_{rot} aprox. 2 K). Hence the adiabatic expansion causes a strong cooling that moves the population of the molecule to the lower rotational states within the ground vibrational state. At the end, only transitions between the lowest-lying rotational states can be detected in the jet.[38, 39]

Despite the difficult conditions required to work with supersonic jets, this technique has lots of advantages. Some of the benefits of working under supersonic expansions are explained below:

• The molecules in the jet can be considered in an effective way as isolated molecules, because they are in a collision-less environment.

• Under jet conditions, only the lowest-lying rotational states are populated within the ground vibrational state. It implies a great simplification of the rotational spectra allowing an easier assignment of complex spectra.

• Intermolecular complexes can be formed in the earlier stages of the jet, so they can be characterized spectroscopically. In this work we examined several complexes formed either by hydration or by aggregation with other partner molecules. The analysis of the process of microsolvatation is important in connection with the study of intermolecular forces like the hydrogen bond.

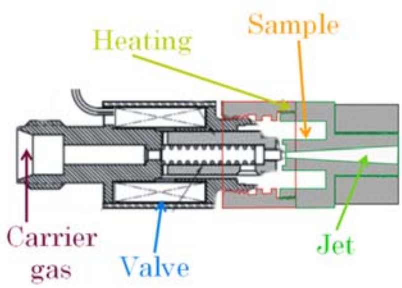

Figure: 1.2.- Solenoid-driven pulse injection valve with heating reservoir.

b. Fourier Transform Microwave Spectroscopy (FTMW).

The Fourier transform microwave spectrometer can detect the resonance frequencies of the rotational transitions following an initial excitation at microwave frequencies of the rotational energy levels. Initially, FTMW spectroscopy was conducted on a static gas confined in a waveguide.[40] Balle and Flygare introduced in 1981 the experiments in supersonic jets.[36] The use of a supersonic jet modifies the design of the spectrometer considerably, as radiation needs to interact with the large volume of the jet. To this purpose the jet is confined within a Fabry-Pérot microwave resonator. The advantages of this multipass cell are important, as power requirements are much reduced. Simultaneously, very weak emission signals can be amplified passively, enhancing the sensitivity of the experiment. The main problem associated to this resonator is the reduced bandwidth (about 1 MHz), which requires mechanical retuning of the resonator for each frequency. The resonator is formed by two spherical mirrors in a confocal arrangement, which simplifies the alignment. In our design the mirror diameter is 33 cm. One of the mirrors remains fixed to the chamber wall, while the second one is movable using a stepper motor. The excitation radiation and the molecular emission signals are transmitted to the Fabry-Pérot resonator using a L-shape ($\lambda/4$) antenna.

The electronic circuitry of the FT-MW spectrometer is shown in Figure 1.3. The radiation source is a microwave synthesizer that operates up to 20 GHz. The source produces both excitation and intermediate frequency signals. During the excitation period it generates a continuous wave (CW) which is upconverted 30 MHz with a single-sideband mixer. The CW is pulsed with a fast (25 ns) single-pole double-through (SPDT) pin-diode switch. The excitation pulses have typically a pulse length of 1 μs. The 30 MHz originates from a filtered multiplier operating on the 10 MHz frequency reference. Finally, the MW excitation pulses are amplified (ca. 150 mW) and transmitted to the Fabry-Pérot chamber. A programmable step attenuator regulates the excitation power.

The excitation induces a coherence state in which the absorbing molecules rotate synchronously, producing a macroscopic polarization.[41] The process can be described phenomenologically by the Bloch equations, similarly as in FT-NMR, but operating on the electric instead of the magnetic dipoles. When excitation is finished, the molecular ensemble loses coherence and emits spontaneously. This free-induced-decay (FID) can be recorded in the MW region following low-noise amplification. The FID length is about 400 μs for an expansion coaxial to the cavity axis. In order to obtain a digitizable signal the molecular emission at MW frequencies is mixed down with the original signal at frequency ν, producing an intermediate spectrum centered around the side-band frequency of 30 MHz. This signal can be downconverted again, but in our design it is digitized directly, simplifying the electronics.

The time-domain signal is recorded with a 200 MHz bandwidth digitizer. Sampling resolutions below 100 ns are sufficient for data acquisition. Finally, the frequency-domain spectrum is reconstructed using a fast Fourier transformation. The coaxial arrangement of the jet and the resonator axis incidentally produces an instrumental doubling in all transitions of about 50-80 kHz.

All the spectrometer frequencies are referenced to a single Rb frequency standard, in order to obtain reproducible phases and signal averaging. Depending on the transition intensities, hundreds or thousands of operating cycles may be necessary per step. The accuracy of the frequency measurements is below 5 kHz.

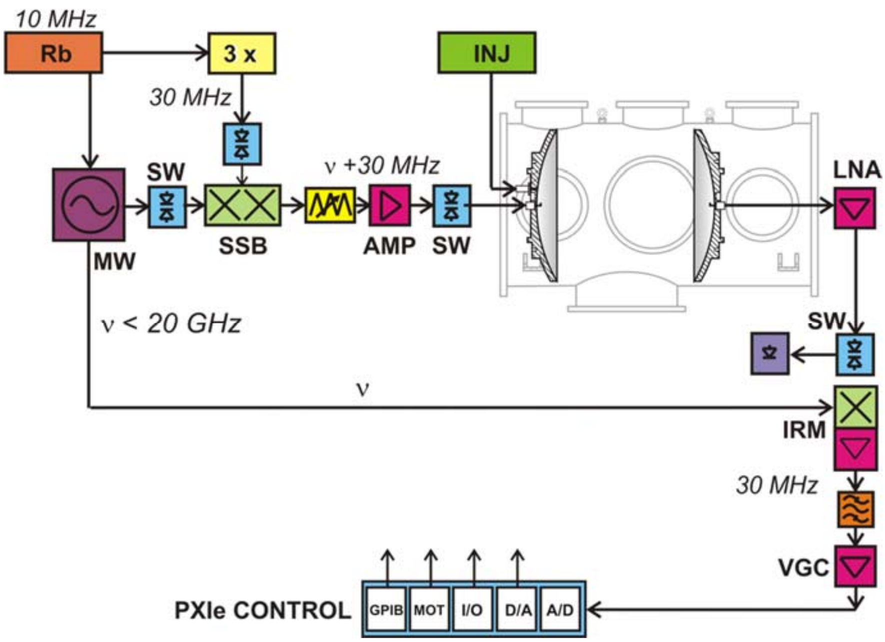

Figure: 1.3- Electronics of the FT-MW spectrometer. Rb: Frequency standard (Stanford FS725), MW Synthesizer (Hittite HMC-T2220, 10-20 GHz), SSB: Single-side-band mixer (Miteq SM0226LC1MDA), INJ: Valve Injector (Parker Iota One), AMP: Power amplifier (Miteq AFS5-06001800-50-20P-6, P=22 dBm), SW: SPDT switches (Sierra MW switching time 15 ns), LNA: low-noise amplifier (Miteq JS4-06001800-16-8P, G=30 dB, NF=1.5 dB), IRM: Image-rejection mixer (Miteq SM0226LC1A), VGC: Voltage gain controlled amplifier (VGC-7-30, G=10 dB), PXI: NI PXIe-1062Q.

c. Operating Sequence.

The operating sequence of the FT-MW spectrometer is shown in figure 1.4 and comprises four different steps. Each full cycle provides a measure of the spectrum around the excitation frequency. The repetition rate depends on the evacuation capacity and the time required for mechanically retuning the resonator. The typical speeds of the process are between 2 and 10 Hz. The operation of the spectrometer is automated. The control software (FTMW++) was developed at the group of Prof. J.-U. Grabow at the University of Hannover.

- **Step: 1.- Molecular pulse generation.**

The opening of the injection valve lasts about 0.1 to 1 milisecond. During this time, the near adiabatic expansion of the gas mixture (vaporized sample + carrier gas) originates a jet within the two mirrors of the microwave resonator inside the vacuum chamber.

- **Step: 2.- Polarization.**

The macroscopic polarization of the molecular jet takes place when the microwave pulse is transmitted through the Fabry-Pérot resonator. The resonator is tuned to the excitation frequency (as monitored by the cavity transmission modes). In order to achieve the optimum $\pi/2$ polarization conditions[44] the pulse length and power are adjusted for maximum signal. In case of unknown samples the prediction of electric dipole moments can be used to estimate the excitation powers.

- **Step: 3.- Cavity relaxation and molecular Emission.**

The excitation signal decays in the cavity, and the detection system can be opened to measure the molecular emissions or FID centered around the excitation frequency. A delay is necessary to dissipate the accumulated energy in the cavity.

• **Step: 4.- Detection.**

The emission molecular signal is registered in the time domain. This signal is later Fourier transformed, and the rotational spectrum in the frequency domain is obtained.

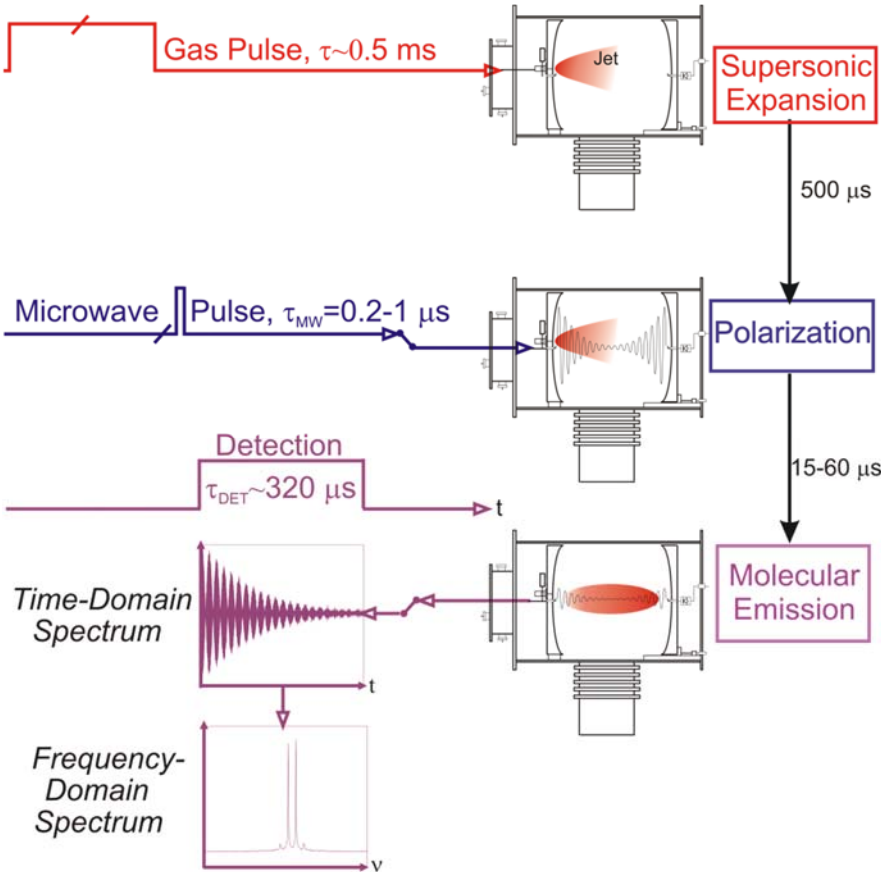

<u>Figure: 1.4.-</u> Pulse sequence of the FTMW spectrometer.

The sensitivity of the experiment is increased by using a coaxial rearrangement of the molecular jet and the axis of the Fabry-Pérot resonator, maximizing the interaction region.[41] However, this configuration also causes the splitting of the rotational transitions by the Doppler effect. In order to complete a frequency scan the spectrometer cavity is retuned sequentially by the control software. All operation is automatic.

1.3. Molecular Rotation Hamiltonian.-

The quantum mechanical description of molecular rotation is well known and has been treated extensively in the bibliography.[42-48] In consequence only a very brief summary of results is provided here.

Expressions for the rotational Hamiltonian depend on the values of the moments of inertia (conventionally $I_a \leq I_b \leq I_c$) or the reciprocal quantities known as rotational constants (*A*, *B*, *C*):

$$\boldsymbol{H}_{rot}^{(A)} = A^{(A)}\boldsymbol{J}_a^2 + B^{(A)}\boldsymbol{J}_b^2 + C^{(A)}\boldsymbol{J}_c^2$$

$$A = \frac{h^2}{8\pi^2 I_a}\ ; \qquad B = \frac{h^2}{8\pi^2 I_b}\ ; \qquad C = \frac{h^2}{8\pi^2 I_c}$$

For linear molecules ($I_a = 0 < I_b = I_c$) and symmetric rotors ($I_a < I_b = I_c$ or $I_a = I_b < I_c$) analytical expressions are easily derived for the molecular energy levels, with quantum numbers giving the total angular momentum (*J*) and the projections along the internal symmetry axes (*K*) or laboratory axes (*M*). For the most common asymmetric rotors ($I_a \neq I_b \neq I_c$) analytical expressions are not possible except for the lowest J values, so the Hamiltonian matrix is diagonalized by numerical methods. In asymmetric rotors no internal component of the angular momentum is constant of motion, so it does not commute with the Hamiltonian and K is no longer a good quantum number. The pseudo-quantum numbers K_a and K_c are used instead, corresponding to the limit cases of symmetric prolate and oblate molecules. Rotational energy levels are thus designated J_{K_a,K_c} (alternatively J_τ, with $\tau = K_a - K_c$). Energy levels can be classified according the symmetry of the rotational Hamiltonian (point group D_2 or *V*), given implicitly in the parity of the limiting indices. The notation is shown in Figure 1.5 below. We do not consider here additional orbital, spin or vibrational angular momentum contributions.

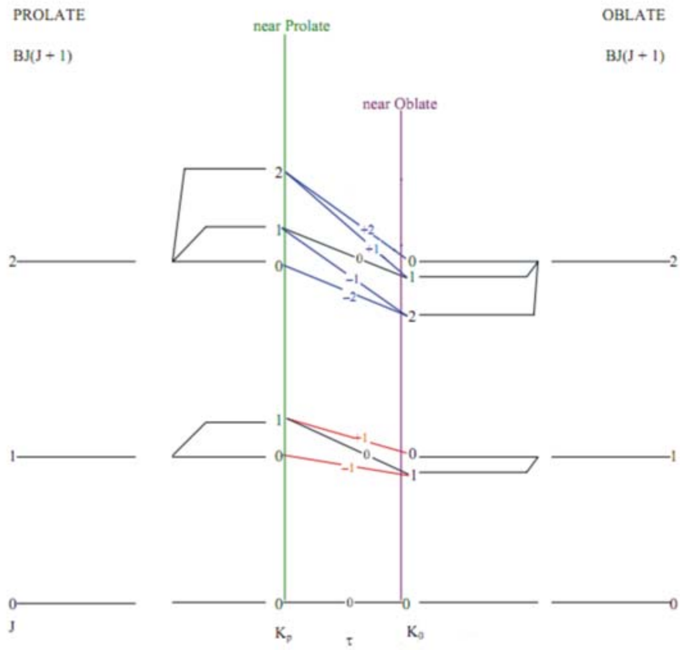

Figure: 1.5.- Correlation diagram between the rotational energy levels of the limiting prolate and oblate cases and the asymmetric rotor.

a. Selection rules.

The electric dipole selection rules indicate when the transition moments have a finite value, $\langle A(J_{K_a,K_c})|\mu|A(J'_{K_a',K_c'})\rangle \neq 0$. Asymmetric rotors follow the rules of symmetric tops, i.e., $\Delta J = 0, \pm1$, which are labeled as Q- ($\Delta J = 0$), P- ($\Delta J = -1$) and R-branch ($\Delta J = +1$) transitions.

The selection rules for the pseudo-quantum numbers can be derived from the symmetry properties of the ellipsoid of inertia in the D_2 point group, and can be expressed in terms of the variations of the limiting indices ΔK_a and ΔK_c as indicated in the table below. If the electric dipole moment is along one of the principal inertial axis then only that type of transitions is allowed. However, for molecules with non-zero components along the three inertial axes we can find simultaneously the three types of selection rules. Transitions are thus called *a*-, *b*- or *c*-type. The most intense lines for a molecule close to the prolate limit are those with $\Delta K_a = 0, \pm1$, while for an oblate case the most intense lines are $\Delta K_c = 0, \pm 1$. For a specific molecule the decision to examine a particular type of transition will depend primarily on the values of the components of the electric dipole moment $\mu_\alpha(\alpha = a, b, c)$. Molecules without electric dipole moment will give no spectrum.

Table: 1.1.- Selection rules for the pseudo-quantum numbers (K_a, K_c) of the asymmetric rotor. Larger variations in the indices (in parentheses) produce weak transitions.

Transition type	ΔK_a	ΔK_c
a	0 $(\pm 2, \pm 4)$	$\pm 1\ (\pm 3, \pm 5)$
b	$\pm 1\ (\pm 3, \ldots)$	$\pm 1\ (\pm 3, \ldots)$
c	$\pm 1\ (\pm 3, \ldots)$	0 $(\pm 2, \pm 4)$

b. Centrifugal distortion.

Molecules are not rigid, so we can conceive the atomic nuclei as held together by finite restoring forces. [42] As the rotational energy increases we can thus expect larger structural effects caused by centrifugal distortion forces. The calculation of centrifugal distortion parameters is important for the interpretation of the rotational spectra and to extrapolate the frequency predictions to higher angular momentum quantum numbers.

The theory of the centrifugal distortion was initiated by Wilson,[49] introducing a series of centrifugal distortion coefficients ($\tau_{\alpha\beta\gamma\delta}$) relating the molecular distortions and force constants. Kivelson and Wilson applied first-order perturbation theory, expressing the Hamiltonian for the semi-rigid rotor as

$$\boldsymbol{H} = \boldsymbol{H}_{rot} + \boldsymbol{H}_{cd} \tag{1}$$

$$\boldsymbol{H}_{rot} = A\ \ \boldsymbol{J}_a^2 + B\ \ \boldsymbol{J}_b^2 + C\ \ \boldsymbol{J}_c^2 \tag{2}$$

$$\boldsymbol{H}_{cd} = \frac{\hbar^4}{4} \sum_{\alpha\beta\gamma\delta} \tau_{\alpha\beta\gamma\delta}\ \boldsymbol{J}_\alpha \boldsymbol{J}_\beta \boldsymbol{J}_\gamma \boldsymbol{J}_\delta \tag{3}$$

In this expression many of the distortion constants are equivalent and there are only nine different τ coefficients, which can be later reduced to six using the commuting properties of the angular momentum operators. However, only five combinations can be finally determined experimentally. This is the reason to introduce reduced Hamiltonians, which are derived by a succession of contact transformations that preserve the original eigenvalues. Different reductions are possible. One of the most common is the Watson[42] asymmetric (A) reduction, which, including only quartic terms, is expressed as

$$\boldsymbol{H}^{(A)}_{Watson} = \boldsymbol{H}^{(A)}_{rot} + \boldsymbol{H}^{(A)}_{cd} \tag{4}$$

$$\boldsymbol{H}^{(A)}_{rot} = A^{(A)}\boldsymbol{J}_a^2 + B^{(A)}\boldsymbol{J}_b^2 + C^{(A)}\boldsymbol{J}_c^2 \tag{5}$$

$$\boldsymbol{H}^{(A)}_{cd} = -\Delta_J\boldsymbol{J}^4 - \Delta_{JK}\boldsymbol{J}^2\boldsymbol{J}_z^2 - \Delta_K\boldsymbol{J}_z^4 - 2\delta_J\boldsymbol{J}^2\left(\boldsymbol{J}_x^2 - \boldsymbol{J}_y^2\right) - \delta_K\left[\boldsymbol{J}_z^2\left(\boldsymbol{J}_x^2 - \boldsymbol{J}_y^2\right) + \left(\boldsymbol{J}_x^2 - \boldsymbol{J}_y^2\right)\boldsymbol{J}_z^2\right] \tag{6}$$

The A-reduction includes the following five centrifugal distortion constants: Δ_J, Δ_K, Δ_{JK}, δ_J and δ_K. This expression was originally intended for asymmetric rotors and is commonly reported for these molecules. However, the problem of this reduction is that for assymetric rotors close to the prolate or oblate limits rotational constants and centrifugal distortion constants are highly correlated. Watson also noticed that the centrifugal distortion constant δ_K blows up for near prolates because it contains the rotational constants (B–C) in the denominator.

For this reason it is sometimes convenient to use the alternative symmetric (S) reduction, which is expressed as

$$\boldsymbol{H}^{(S)}_{rot} = A^{(S)}\boldsymbol{J}_x^2 + B^{(S)}\boldsymbol{J}_y^2 + C^{(S)}\boldsymbol{J}_z^2 \tag{7}$$

$$\boldsymbol{H}^{(S)}_{cd} = -D_J\boldsymbol{J}^4 - D_{JK}\boldsymbol{J}^2\boldsymbol{J}_z^2 - D_K\boldsymbol{J}_z^4 + d_1\boldsymbol{J}^2(\boldsymbol{J}_+^2 + \boldsymbol{J}_-^2) + d_2(\boldsymbol{J}_+^4 + \boldsymbol{J}_-^4) \tag{8}$$

where $\boldsymbol{J}_\pm = \left(\boldsymbol{J}_x \pm i\,\boldsymbol{J}_y\right)$ and the centrifugal distortion constants are now D_J, D_K, D_{JK}, d_1, d_2.

c. Hyperfine effects: Nuclear quadrupole coupling.

The nuclear quadrupole coupling is a hyperfine effect arising from the electric interaction between a quadrupolar atomic nucleus and the molecular electric field gradient at the atomic position. [43,48] Nuclear quadrupole coupling effects are observed for atoms with nuclear spin *I* > ½. It is thus a common interaction in organic molecules containing typically ^{14}N (*I*=1), ^{35}Cl (*I*=3/2) or other nuclei. The electric quadrupole can be described as the result of a non-spherical nuclear charge distribution. The nuclear quadrupole moment is defined as

$$eQ = \int \rho\, r^2 (3\cos^2\alpha - 1) d\tau \quad (9)$$

where ρ is the nuclear charge density and r and α are the distance to the volume element and the angle between r and the spin axis. A quadrupolar nucleus inserted in a non-homogeneous electric field has a potential energy which depends on its orientation. Since orientations are quantized they may result in new energy levels within each rotational state.

For a single quadrupolar nucleus, this electric interaction couples the rotational (*J*) and spin (*I*) angular momentum. In the coupled representation the new state is represented by $|J, I; F, M_F\rangle$, which leaves the individual components of *I* and *J* unspecified. In other words, the angular momenta couple according to:

$$\boldsymbol{F} = \boldsymbol{I} + \boldsymbol{J} \quad (10)$$

where the new quantum number *F* takes values according to the Clebsch-Gordan series: $F= J+I, J+I-1, \ldots\ |J-I|$.

The effects of this electric interaction cause the splitting of the rotational energy levels and, as a consequence, a characteristic hyperfine pattern appears in the spectrum. The selection rules combine those of the rigid rotor, $\Delta J = 0;\ \pm 1$, with the condition that the nuclear spin do not change in the transition, $\Delta I = 0$. In consequence, we have

$$\Delta F = 0;\ \pm 1 \quad (11)$$

The calculation of the interaction energy has been treated in the bibliography.[50] The first-order contributions are given by

$$\boldsymbol{H_Q} = \frac{eQq_J}{2J(2J-1)I(2I-1)}\left[3(\boldsymbol{IJ})^2 + \frac{3}{2}\boldsymbol{IJ} - \boldsymbol{I}^2\boldsymbol{J}^2\right] \tag{12}$$

where we introduced the q_j coefficients which represent the average electric field gradient in the direction of maximum projection of the rotational angular momentum in the laboratory axes:

$$q_J = \left[\left(\frac{\partial^2 V}{\partial Z^2}\right)_0\right]_{M_J=J} \tag{13}$$

The equation can also be expressed in terms of the coordinates in the principal axis orientation as:

$$q_{i,j} = \frac{\partial^2 V}{\partial i \partial j} \qquad i,j = a,b,c \tag{14}$$

which can be related to the components of a nuclear quadrupole coupling tensor according to:

$$\boldsymbol{\chi}_{ij} = eQ\boldsymbol{q}_{ij} \tag{15}$$

With coupling constants $\chi_{\alpha\beta}$

$$\boldsymbol{\chi} = \begin{pmatrix} \chi_{aa} & \chi_{ab} & \chi_{ac} \\ \chi_{ba} & \chi_{bb} & \chi_{bc} \\ \chi_{ca} & \chi_{cb} & \chi_{cc} \end{pmatrix} \tag{16}$$

The diagonal elements of the traceless tensor ($\chi_{aa} + \chi_{bb} + \chi_{cc} = 0$) represent the electric field gradient in the principal axes of the molecule. The coupling constants are very sensitive to the electronic environment in the proximities of the quadrupolar and to the orientation of the inertial axes. For this reason the nuclear quadrupole coupling constants are a useful tool for the identification of different chemical species.

d. Internal Rotation.

The analysis of the internal rotation is one of the best known applications of rotational spectroscopy and is detectable in the spectrum for moderate barriers below ca. 10-15 kJ mol^{-1}. This phenomenon is a large-amplitude motion observed in molecules containing an internal group which rotates independently from the rest of the molecule.[50,51] In most cases the internal rotor is symmetric and we can observe a periodic variation of the potential energy with a period determined by the symmetry of the internal rotor. The best know case is the internal rotation of a methyl group, for which multiple determinations exists in the bibliography.

The effects of internal rotation on the rotational spectra result from a quantum mechanical tunneling effect. For an infinite torsional barrier a symmetric group like a methyl group will exhibit several equivalent minima. As the internal rotation barrier reduces, the degeneracy is partially lifted, so quantum mechanical tunneling appears. The symmetry group of the internal rotor must be a subgroup of the molecular symmetry group, so in the common case of a C_3 rotor the torsional levels are split into the irreducible representations of the point group (A and doubly-degenerate E in C_3). Since the Hamiltonian is invariant to operations within the internal rotor subgroup, the transition moment is finite ($\langle\psi_j|\mu|\psi_i\rangle \neq 0$) only for transitions of the same symmetry. This produce the selection rules $A \leftarrow A$ or $E \leftarrow E$. The magnitude of the torsional splitting increases as the levels approach the top of the barrier, so these measurements allow an accurate determination of the internal rotation barriers.[51] For large barriers this effect is not noticeable, but lower thresholds can be estimated.

The treatment of internal rotation has been given in many references. Kleiner reviewed recently the methods and codes used for analysis of C_3 rotor,[52] while Ilyushin presented a specific program for C_6 symmetry.

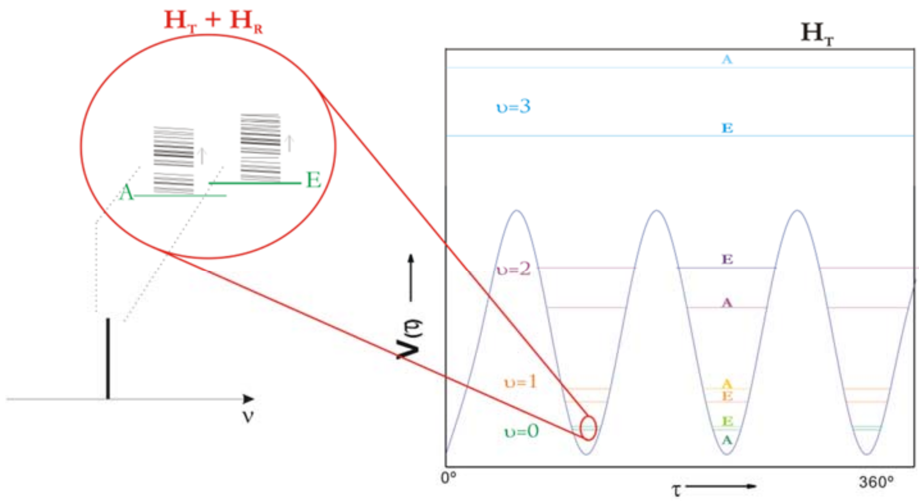

Figure: 1.6.- Schematic potential function for the internal rotation of a C_3 top.

To study the case of an asymmetric molecule or complex with an internal symmetric rotor, we consider the whole system like a set formed by a rigid asymmetric fragment linked to the symmetric internal rotor. We can use this approximation when the torsion is much less energetic (lower frequency) compared with the rest of vibrational motions. When this condition is satisfied we can assume the internal rotation as an independent motion from the rest of molecular vibrations.

In figure 1.6 we can observe the three identical minima in the internal rotation potential function, corresponding to the torsion angles of the E, C_3 and C_3^2 symmetry operations characteristic of the symmetry group, together with the potential barrier V_3. In cases of several internal tops or different symmetries the situation is more complicated.

The barrier height V_3 can be derived from the frequency splitting between the rotational transitions in different torsional states. For this purpose, the Hamiltonian of the molecule with an internal rotor must be solved. That Hamiltonian can be divided into three terms: the rotational ($\boldsymbol{H}_{\mathbf{R}}$) and torsional parts ($\boldsymbol{H}_{\mathbf{T}}$) and an extra term which describes the coupling between the angular momenta of the internal and overall rotations ($\boldsymbol{H}_{\mathbf{TR}}$).

$$\boldsymbol{H} = \boldsymbol{H}_{\boldsymbol{R}} + \boldsymbol{H}_{\boldsymbol{T}} + \boldsymbol{H}_{\boldsymbol{TR}} \tag{18}$$

where H_R, H_T and H_{TR} depend on the reduced angular momentum ($\mathcal{P}$), the adimensional moment of inertial of the internal rotor (F) and the barrier to internal rotation (V_n) as follows:

$$\boldsymbol{H_R} = \boldsymbol{H_r} + F\mathcal{P}^2 \tag{19}$$

$$\boldsymbol{H_T} = F\boldsymbol{p}^2 + \frac{1}{2}V_n(1 - \cos 3\alpha) \tag{20}$$

$$\boldsymbol{H_{TR}} = -2F\boldsymbol{\mathcal{P}}\boldsymbol{p} \tag{21}$$

The solution of the Hamiltonian depends on the selection of molecular axes. In particular, either the principal inertial axes (PAM method) or the internal rotor axis (IAM) can be selected. A particular selection will produce different coupling terms, and several procedures have been devised to solve the resulting equations.

In all cases the internal rotation analysis includes:

1.- Measuring of the frequency differences between the two rotational transitions (A and E in C_3, or other splitting in more complicated cases) associated to each torsional state. Large barriers will produce undetectable or very small splittings (kHz), while small barriers may result in huge splittings of GHz size.

2.- The frequency splittings are fitted to a selection of both structural parameters (orientation of the internal rotor in the principal axis system, moment of inertia of the internal rotor) and torsional barrier. The rotational parameters and centrifugal distortion are fitted simultaneously.

e. Molecular structure determination: Isotopic substitutions.

The analysis of the rotational spectra is the most accurate method to determine molecular geometries in the gas phase, and is generally applicable to polar molecules of small or moderate size (<450 amu).

The rotational spectra are extremely sensitive to the atomic masses and molecular geometries, so rotational methods are ultimately based in establishing a connection between the experimental moments of inertia and the molecular structure. As the molecular structure may depend of a large number of independent parameters, it is always convenient to have the largest possible experimental dataset. For this reason, a detailed structural determination requires examining the rotational spectra of several isotopic species (typically ^{13}C, ^{15}N or ^{18}O in organic molecules). The spectra of minor isotopologues may be examined in natural abundance (<1%) in cases of intense spectra. For other cases chemical synthesis should be required. In this thesis most of the experimental data originated from natural abundance isotopologues, though in some particular cases (i.e., water complexes with $H_2{}^{18}O$) we used special samples.

The main problem of the structural determination originates from the fact the experimental rotational constants do not represent the equilibrium moments of inertia, but the effective values in a particular vibrational state. As the moments of inertia always include vibrational contributions several methods have been devised to infer the near-equilibrium values from the effective ground-state (or vibrationally excited state) moments of inertia.

The most important rotational methods are the substitution (r_s) and the effective methods (r_0), which have been used repeatedly in this thesis. [48] Other methods, like the Watson's quasi-equilibrium treatments ($r_m^{(1)}$, $r_m^{(2)}$, etc.)[53] were explored occasionally. Several reviews are available on the different rotational methods,[54,55] but many of them require a large number of isotopic species, which is not always possible.

The substitution method was introduced by Kraitchman. Several other authors have contributed to this method and discussed its benefits and drawbacks.[56] The advantage of the substitution method is that it provides the Cartesian coordinates for each substituted atom in a sequential process which is not affected by other atoms. In this way the structure is constructed atom-by-atom. However, this method would require an isotopic substitution for each atomic position, so full substitution structures are uncommon or limited to small molecules. The Kraitchman equations assume that the vibrational contributions to the moments of inertia are constant for all isotopologues. In this assumption, it would be possible to cancel the vibrational contributions by subtracting the moments of inertia of each isotopologue from the values of the parent species. The method returns the absolute coordinates for each substituted atom, so additional information is required to fix the proper signs in the coordinates. The expressions for each coordinate are calculated as:

$$|x| = \left[\frac{\Delta P_x}{\mu}\left(1 + \frac{\Delta P_y}{I_x - I_y}\right) \cdot \left(1 + \frac{\Delta P_z}{I_x - I_z}\right)\right]^{1/2} \tag{22}$$

$$|y| = \left[\frac{\Delta P_y}{\mu}\left(1 + \frac{\Delta P_z}{I_y - I_z}\right) \cdot \left(1 + \frac{\Delta P_x}{I_y - I_x}\right)\right]^{1/2} \tag{23}$$

$$|z| = \left[\frac{\Delta P_z}{\mu}\left(1 + \frac{\Delta P_x}{I_z - I_x}\right) \cdot \left(1 + \frac{\Delta P_y}{I_z - I_y}\right)\right]^{1/2} \tag{24}$$

where,

$$\Delta P_x = \frac{1}{2} \cdot \left(-\Delta I_x + \Delta I_y + \Delta I_z\right) \tag{25}$$

$$\Delta I_x = I'_x - I_x \tag{26}$$

I'_x is the inertial moment of the monosubstituted species and I_x the corresponding value for the parent.

The structure obtained using the Kraitchman method is a good approximation to the physically inaccessible equilibrium structure, but there are many cases where it cannot be used. In particular the substitution method cannot be applied in the case of small molecular coordinates, as it can produce imaginary results. Isotopic substitutions with a large change of mass, typically H/D, are also not appropriate for this method.

Because of the problems associated to the substitution structures and/or the lack of sufficient isotopic information, other methods are available. The effective structure (*r*$_0$) method is defined operationally as the geometry that better reproduces the experimental rotational constants in a given vibrational state (usually the ground state, $\upsilon = 0$). The effective structure thus lacks a clear physical interpretation but provides an acceptable compromise for cases with the experimental data are limited. The quality of the effective structure is largely dependent on the number and quality of the experimental moments of inertial. Ideally the experimental dataset should be much larger than the number of independent structural parameters, making a least-squares fit valid. However, in cases where the number of data is limited the fit can be ill-conditioned or dependent of the assumed parameters.

1.4. References.-

[1] HyperChem Professional 7.51, Hypercube, Inc., 1115 NW 4th Street, Gainesville, Florida 32601, USA.

[2] MAESTRO, version 9.2, Schrödinger, LLc, New York, NY, **2012**.

[3] J. B. Foresman, Æ. Frisch, "Exploring chemistry with electronic structure methods", 2nd Edition, Gaussian Inc., Pittsburg, PA, USA, **1996**.

[4] S.J. Weiner, P.A. Kollman, D.A. Case, U.C. Singh, C. Ghio, G. Alagona, S. Profeta, P. Weiner, *J. Am. Chem. Soc.* 106, 765-784, **1984**.

[5] J. Wang, R.M. Wolf, J.W. Caldwell, P.A. Kollman, D.A. Case, *Journal of Computational Chemistry*, 25, 1157- 1174, **2004**.

[6] W.L. Jorgensen, D.S. Maxwell and J. Tirado-Rives, *J. Am. Chem. Soc.* 118, 11225-11236, **1996**.

[7] G.A. Kaminski and R.A. Friesner, *J. Phys. Chem. B*, 105, 6474-6487, **2001**.

[8] T.A. Halgren, *J. Comp. Chem.* 20, 720-729, **1999**.

[9] T.A. Halgren, *J. Comp. Chem.* 20, 730-748, **1999**.

[10] T.A. Halgren, R.B. Nachbar, *J. Comp. Chem.* 17, 587-615, **1996**.

[11] J.C. Grossman, L. Mitas, *Phys. Rev. Letters*, 94, 056403, **2005**.

[12] N. S. Ostlund, A. Szabo, "Modern Quantum Chemistry: Introduction to advanced electronic structure theory",Mc Milla,New York, **1982**.

[13] F. Jensen, "Introduction to computational chemistry", Gaussian Inc., Pittsburg, PA, USA, **1996**.

[14] W. Koch, M. C. Holthausen, A chemist´s guide to DFT, VCH, Weinhein, **1999**.

[15] Y. Zhao, D. G. Truhlar. *Acc. Chem. Res.*, 41, 157-167, **2008**.

[16] W. Kohn, A.D. Becke,R.G. Parr., *J. Phys. Chem.* 100, 12974-12980, **1996**.

[17] Y. Zhao, N. E. Schultz, D. G. Truhlar, *J. Chem. Theory Comput.,* 2, 364-382, **2006**.

[18] Y. Zhao, D. G. Truhlar, *Theor. Chem. Acc.,* 120, 215-241, **2008**.

[19] Y. Zhao, D. G. Truhlar, *Acc. Chem. Res.,* 41, 157-167, **2008**.

[20] C. Lee, W. Yang, R. G. Parr, *Phys. Rev. B,* 37, 785-789, **1988**.

[21] A. D. Becke, *Phys. Rev. A,* 38, 3098-3100, **1988**.

[22] P. J. Stephens, F. J. Devlin, C. F. Chabalowski, M. J. Frisch, *J. Phys. Chem.,* 98, 11623-11627, **1994**.

[23] R. van Leeuwen, E. J. Baerends, *Phys. Rev. A,* 49, 2421-2431, **1994**.

[24] A. D. Becke, *J. Chem. Phys.,* 109, 2092-2098, **1998**.

[25] J. P. Perdew, A. Ruzsinsky, J. Tao, V. N. Staroverov, G. E. Scuseria, G. I. Csonka, *J. Chem. Phys.,* 98, 5648-5652, **1993**.

[26] Y. Zhao, N. González-García, D. G. Truhlar. *Org. Lett.*, 9, 1967-1970, **2007**.

[27] C. Møllet, M. S. Plesset, *Phys. Rev.*, 46, 618, **1934**.

[28] D. Cremer, *Willey Interdiscip. Rev. Comput. Mol. Sci.*,1, 509, **2011**.

[29] W. J. Hehre, L. Radom, J. A. Pople, P. v. R. Schleyer, "Ab initio Molecular Orbital Theory", J. Willey & Sons, New York, **1986**.

[30] R. Krishnan, J. S. Binkley, R. Seeger, J. A. Pople, *J. Chem. Phys.*, 71, 650, **1980**.

[31] T. J. Balle, W. H. Flygare, *Rev. Sci. Instrum.*, 52, 33, **1981**.

[32] J.-U. Grabow, W. Stahl, H. Dreizler, *Rev. Sci. Instrum.*, 67, 4072, **1996**.

[33] J.-U. Grabow, W. Stahl, *Z. Naturforsch. Teil A*, 45, 1043, **1990**.

[34] D. H. Levy, *Science*, 214, 263, **1981**.

[35] D. H. Levy, *Annu. Rev. Phys. Chem.*, 31, 197, **1980**.

[36]B. Maté, I. A. Graur, T. Elizarova, I. Chiroikov, G. Tejeda, J. M. Fernández, S. Montero, *J. Fluid. Mech.*, 426, 177, **2001**.

[37] J.-U. Grabow, W. Caminati, *Microwave spectroscopy: Experimental techniques* in "Frontiers of molecular spectroscopy", Elsevier, **2008**.

[38] D. Phillips, "Jet spectroscopy and molecular dynamics", Glasgow, **1995**.

[39] G. Scoles, "Atomic and molecular beam methods", Vol.1, Oxford University Press, New York & Oxford, **1988**.

[40] T. G. Schmalz, W. H. Flygare, *Coherent transient microwave spectroscopy and Fourier transform methods* in "Laser and coherence spectroscopy", Ed. Jeffrey I. Steinfeld (MIT), Plenun Press, **1978**.

[41] R. Matheus, "Molecular spectroscopy: Modern Research", Academic Press, New York & London, **1972**.

[42] J. K. G. Watson, "Vibrational spectra and structure", Vol. 6, Elsevier, Amsterdam, Oxford & New York, **1977**.

[43] H. W. Kroto, "Molecular Rotation Spectra", Dover Publications, Inc., New York, **1992**.

[44] J. A. Wollrab, "Rotational spectra and molecular structure", Academic Press, New York & London, **1967**.

[45] J. M. Hollas, "High Resolution Spectroscopy", John Wiley & Sons Ltd, UK, **1998**.

[46] J. I. Steinfeld, "Molecules and radiation: An introduction to modern molecular spectroscopy", Dover Publications, Inc., New York, **2005**.

[47] J.-U. Grabow, *Fourier transform spectroscopy: measurements and instrumentation* in "Handbook of high resolution spectroscopy", Jonh Wiley & Sons, Inc., **1999**.

[48] W. Gordy, L.R. Cook, 'Microwave Molecular Spectra', John Wiley & Sons Inc., New York, **1984**.

[49] E. B. Wilson, J. B. Howard, *J. Chem. Phys.*, 4, 260, **1936**.

[50] J. M. Brown, A. Carrignton, "Rotational spectroscopy of diatomic molecules", Cambridge University Press, UK, **2003**.

[51] D. Lister, J. McDonald, N. Owen, "Internal rotation and inversion", Academic Press, New York & San Francisco, **1978**.

[52] I. Kleiner, *J. Mol. Spectrosc.*, 260, 1, **2010**.

[53] J. K. G. Watson, A. Roytburg, W. Ulrich, *J. Mol. Spectrosc.*, 196, 102, **1999**.

[54] H. D. Rudolph, Chapter 3 in "Advances in molecular structure research", JAI Press: Greenwich, CT, **1995**.

[55] J. Demaison, J. E. Boggs, A. G. Csaszar, Chapter 5 in "Equilibrium molecular structures: From spectroscopy to quantum chemistry", CRC Press, USA, **2011**.

[56] J. Kraitchman, *Am. J. Phys.*, 21,17, **1953**.

Molecular Building Blocks

Chapter 2
Pseudopelletierine

2.1. Introduction.-

Alkaloids are natural products containing a basic nitrogen atom (the name derives from the Arabic "alkali"). They are produced by a large variety of organisms, like plants, fungi, bacteria and animals, many of them as secondary metabolites. For these reasons alkaloids have very distinct chemical structures and biological functions. The pharmacological effects of alkaloids are also very diverse, and include stimulants, analgesics, antibacterial, etc. Many of these compounds are known since the ancient times and used therapeutically in various cultures.[1]

One of the best known alkaloid families is that of tropanes, which share an eight-membered bicycle with a nitrogen bridge, or 8-azabicycle[3.2.1]octane, often methylated in the nitrogen atom.

Tropane alkaloids include many compounds based on this chemical motif, like tropine, atropine, scopolamine, cocaine and ecgonine, among others. Some examples of these chemical derivatives are shown in the following figure.[2]

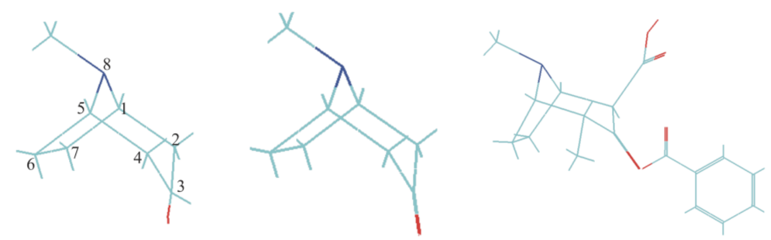

Figure: 2.1.- Tropine (hydroxytropane) and alkaloid derivatives: tropinone and γ-cocaine.

Previous works in our group using rotational spectroscopy have addressed the structure, conformational flexibility and N-methyl inversion in tropinone,[3] scopoline[4], and scopine (see chapter 3). These studies are a preliminary step for the investigation of larger systems and, at the same time, they provide a description of the molecular properties which is necessary to better understand its biochemical behavior in living organisms. As an example of the structure-function relationships, some studies on cocaine[5] have suggested that the methyl inversion could be related to its biological functions. This behavior has also been observed in other alkaloid systems like morphines.[6]

Previous studies using X-Ray diffraction[7] or NMR,[8,9] have demonstrated the prevalence of intermolecular interactions in condensed phases, sometimes forming networks of intermolecular interactions which mask the structure of the molecule.[10] For this reason, the characterization of the free molecule is necessary to determine the intramolecular factors controlling the molecular structure.

Following our previous studies we considered interesting the study in gas phase of pseudopelletierine, a tropinone derivative with an additional methylene group in the molecular skeleton (9-methyl-9-azabicyclo[3.3.1]nonan-3-one). Pseudopelletierine is a natural compound found in plants (pomegranate), but the chemical interest is directed to know how the larger ring can influence the conformational equilibria and ring inversion of the molecule.

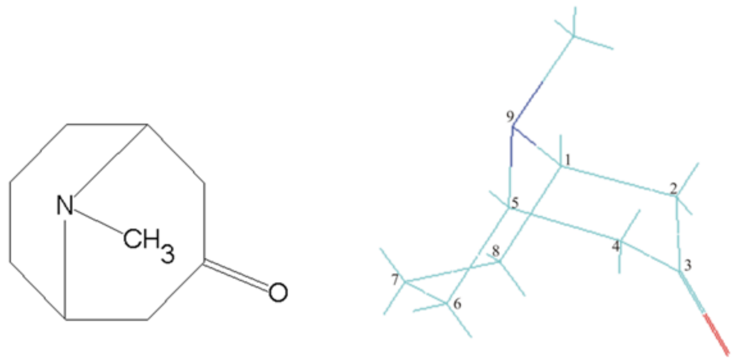

Figure: 2.2.- Molecular formula (left) and a plausible conformation of axial pseudopelletierine (right), with the IUPAC notation used for the heavy atoms.

The nine-atoms bicycle can be described as two fused six-membered rings, joined at the nitrogen bridge. In consequence we can use three independent dihedrals to define the molecular structure. Two of these dihedrals define the conformation of the six-membered rings: $\tau_1(N_9 - C_1 - C_2 - C_3)$ and $\tau_3(N_9 - C_5 - C_6 - C_7)$, which in principle results in four different conformational structures. These four conformers correspond to the chair and boat configurations of the ring. For each conformation, the axial/equatorial conformation of the N-methyl group can be specified by a third dihedral $\tau_2(C_{10} - N_9 - C_1 - C_2)$, generating a larger variety of structures. However, and despite the increase in the number of plausible structures, some of the inversion isomers may be impeded for certain ring configurations, making this study more complex than in the case of tropinone. It is also plausible that the inversion barriers and conformational preferences might change, offering a contrast to the previous findings in tropinone.

In the following figure eight different conformers are shown, classified according to the torsions τ_1, τ_2 and τ_3. For each configuration associated to the torsions $\tau_1$and τ_3, two different axial and equatorial orientations of the methyl group can be found depending on the value of the angle τ_2.

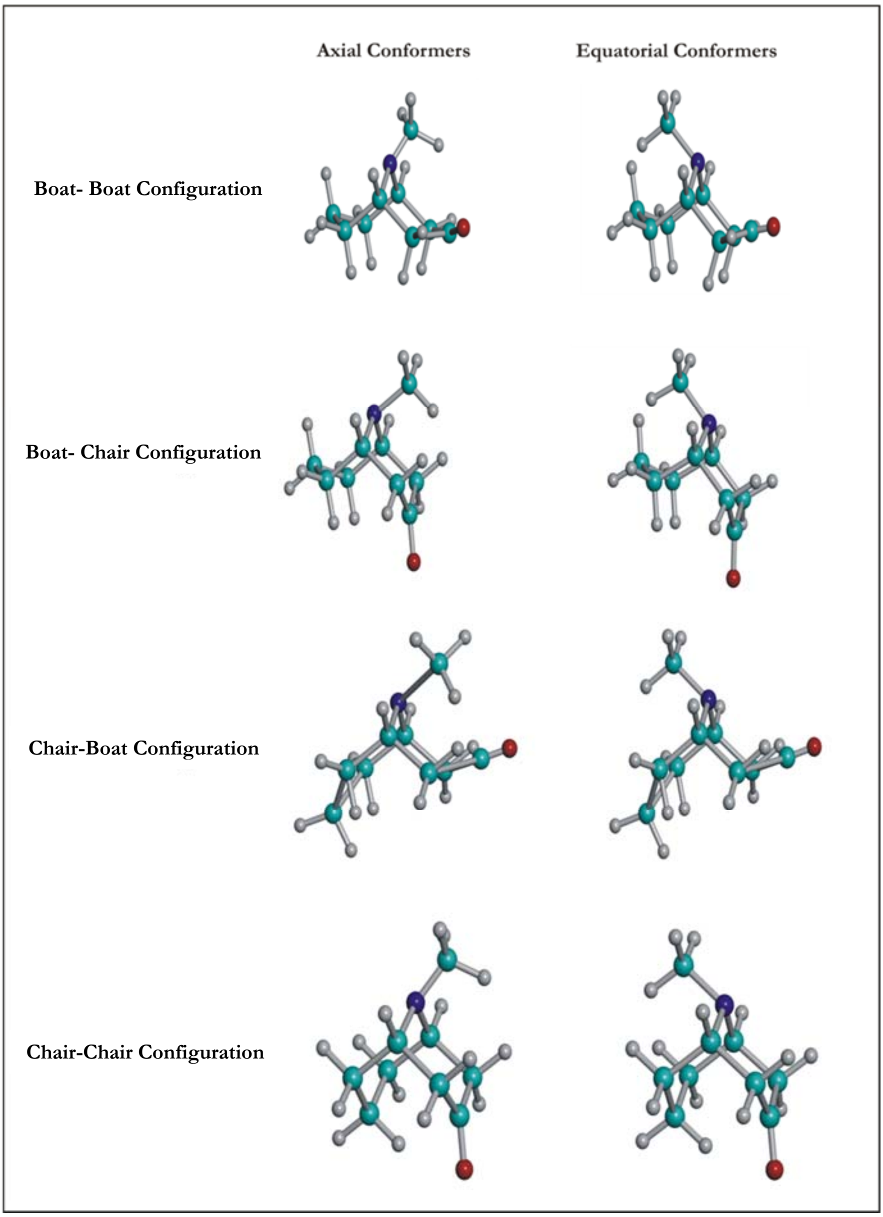

Figure: 2.3.- Some conformational species of pseudopelletierine, represented by the τ_1, τ_2 and τ_3 torsions.

In order to clarify which of the geometries are the most stable, it is necessary to do a previous theoretical study to characterize the PES. Hence, all the conformers can be sorted by energy.

2.2. Computational Methods.-

As we do for other molecules in the present work, a series of chemical and quantum mechanical calculations (described in chap. 1) were made in order to get information about the electric and structural properties of the molecule before the experimental data acquisition.

First, a conformational search was carried out using molecular mechanics (implemented in MACROMODEL),[11] and a list with the more stable structures was found. Those structures are shown in figure 2.3.

More sophisticated theoretical methods were later performed. In particular, geometry optimizations of the different structures have been made using second order perturbation methods (MP2) and hybrid methods based on the Density Functional Theory such as M06-2X. In both cases, the basis-set used was the Popple's triple zeta with polarization and diffusion functions, or 6-311++G(d,p). All the theoretical calculations were implemented in Gaussian 09[12].

Following the first geometry optimizations it was easily found that the most stables conformers are those with chair-chair configurations, both axial or equatorial. Other conformers are destabilized by more of 20 kJ mol^{-1}. The results are shown in table 2.1. Besides, it was possible to observe how the starting boat configurations converge to a chair-chair structure during the optimization process.

Table: 2.1.- Rotational constants (*A*, *B* and *C*), electric dipole moments (μ_α, α = a, b, c) and diagonal elements of the nuclear quadrupole tensor of ^{14}N ($\chi_{\alpha\beta}$, (α,β = a, b, c)) for the conformers optimized with ab initio and DFT methods. The centrifugal distortion constants are also shown (Δ_J, Δ_{JK}, Δ_K, δ_K and δ_K). The relative energies have been corrected with the zero-point energy (ZPE). ΔG was calculated at 298K and 1 atm.

	Theory MP2 / M06-2X					
	chair-chair		**boat-chair**		**boat-boat**	
	Ax	**Eq**	**Ax**	**Eq**	**Ax**	**Eq**
$\boldsymbol{A}$ **/ MHz**	1397.3/1393.9	1678.1/1679.5	1402.2/1406.6	1647.0/1650.7	1713.6/1706.6	1771.1/1650.9
$\boldsymbol{B}$ **/ MHz**	1197.0/1198.7	1018.8/1020.0	1198.9/1190.4	1034.4/1028.3	975.5/ 978.6	939.4/1027.8
$\boldsymbol{C}$ **/ MHz**	1037.8/1038.1	1012.6/1014.1	1033.0/1029.6	1013.2/1008.6	954.7/958.2	920.2/1008.3
χ_{aa} **/ MHz**	-3.2 / -3.9	2.0/2.1	-3.9 / -4.6	1.7/1.7	-4.3 -4.6	-2.7 / 1.6
χ_{bb} **/ MHz**	0.60 / 1.1	-4.7 / -4.9	1.3 / 1.8	-4.5 / -4.6	1.7/1.8	1.6 / -4.6
χ_{cc} **/ MHz**	2.6 / 2.8	2.6 / 2.8	2.6 / 2.8	2.7 / 2.9	2.6/2.8	1.1 / 2.9
$\lvert\mu_a\rvert$ **/ D**	2.5 / 2.8	3.4 / 3.6	2.3 / 2.5	3.2 / 3.4	2.4 / 2.7	3.9 / 3.4
$\lvert\mu_b\rvert$ **/ D**	0.68 / 0.73	0.02 / 0.07	1.7 / 1.8	0.78 / 0.89	0.35 / 0.44	0.04 / 0.88
$\lvert\mu_c\rvert$ **/ D**	0.0 / 0.0	0.0 / 0.0	0.0 / 0.0	0.0 / 0.0	0.44 / 0.42	0.92 / 0.00
$\lvert\mu_{TOT}\rvert$ **/ D**	2.6 / 2.9	3.4 / 3.6	2.9 / 3.1	3.3 / 3.5	2.5 / 2.8	4.0 / 3.5
Δ_J **/ Hz**	47.5 /	41.0/	134.38/	111.37/	32.71/	28.42/
Δ_{JK} **/ kHz**	0.20/	159.1/	-0.04/	0.05/	0.14/	0.49/
Δ_K **/ Hz**	-124.0/	-89.6/	-35.69/	-57.07/	244.79/	-386.24/
δ_J **/ Hz**	5.0/	-0.4/	31.37/	9.67/	4.74/	-2.52/
δ_K **/ kHz**	0.034/	-1.04/	0.032/	-0.18/	0.60/	0.15/
ΔG **/ kJ·mol^{-1}**	0.0/	2.2/	19.9/	28.5/	38.6/	42.2/
Δ(E+ZPE) / kJ·mol^{-1}	0.0 / 0.0	2.4 /	20.6/	30.8/	39.6/	44.0/

Therefore, and due to the much larger stability of the chair-chair configurations, we would expect to find transitions belonging to only those species in the rotational spectrum. The following figure represents the structure of the axial and equatorial chair-chair conformers. From now, we will use the name **axial** and **equatorial** to refer to these chair-chair structures.

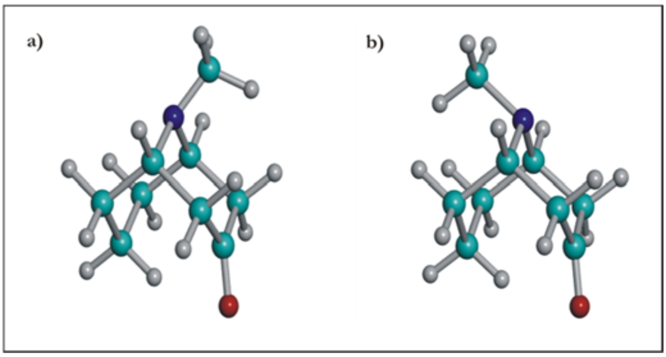

Figure: 2.4.- Most stable conformers according to ab initio and DFT calculations. **a)** Axial chair-chair conformer. **b)** Equatorial chair-chair conformer.

2.3. Results and Analysis.-

a. Assignment of the Rotational Spectrum.

As mentioned before, and considering the theoretical results of table 2.1), it is most probable that only the two less energetic structures could be detected with the MW spectrometer. The remaining conformers will possibly stay depopulated in the supersonic jet.[13]

For each conformation a prediction of the rotational spectrum was done. The equatorial species is a near-prolate assymetric rotor ($\kappa_{equatorial} \approx$ -0.98), while the axial species is much more asymmetric ($\kappa_{axial} \approx$ -0.11).[14] The predictions of the transitions for both conformers used the Watson's semi-rigid rotor Hamitonian and the theoretical parameters in table 2.1, implemented in Pickett's[15] SPCAT and Plusquellic´s JB95[16] programs.

The predicted dipole moments offer information on the intensities of the different rotational transitions. Both the axial and equatorial conformers belong to the C_s group point, so one component of the electric dipole moment, identified with the largest moment of inertia axis *c*, will be zero by symmetry. Among the remaining components, the electric dipole moment will be dominant along the direction between the two heteroatoms, identified as the *a* principal inertial axis. That means that the transitions with larger intensity will be the μ_a-type in both conformers.

An important difference between the axial and equatorial structures is found in the inertial moment oriented along the principal ***b***-axis. While in the axial conformer a non-zero value is found, the μ_b value for the equatorial conformer is negligible. As a consequence, μ_b-type transitions would eventually be detected only for the axial conformer and we will not detect the μ_b-type spectrum for the equatorial structure.

Therefore, for the spectrum assignment, transitions of the branch R (J+1 ← J) and μ_a–type are preferably predicted. For the axial conformer, μ_b–type lines were also predicted, despite if we compare the dipole components (μ_a= 2.53D >> μ_b=0.68D) it is probable that the intensities of the μ_b–type will be much weaker.

In the following figure, the experimental spectrum (in green) is shown compared with the theoretical predictions for the axial (in red) and equatorial (in blue) conformers.

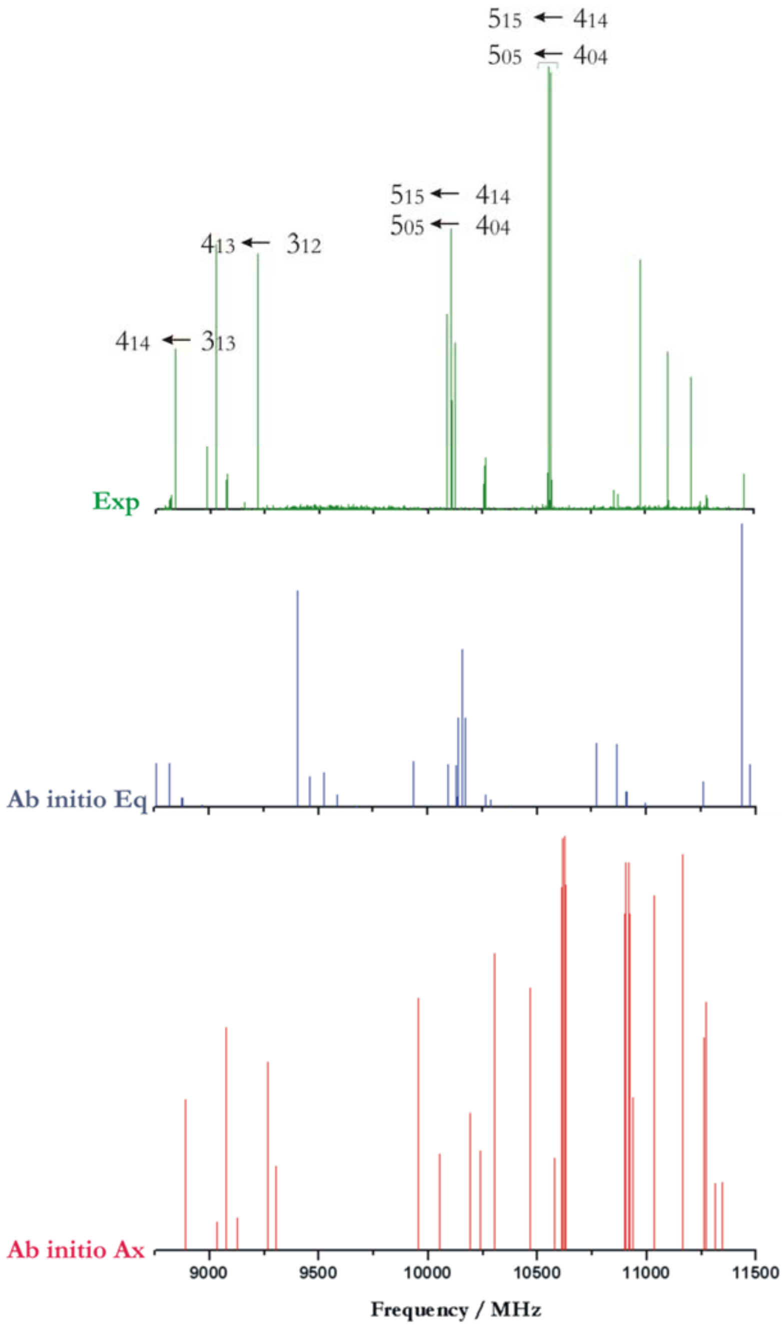

<u>Figure: 2.5.-</u> Section of the scan obtained for the pseudopelletierine molecule in which the assigned transitions of the most stable conformers can be identified. The differences between the intensities measured and predicted are due to the experimental conditions. The experimental spectrum is formed by the superposition of several short scans, which are not totally uniform because of the heating process and the need to replace periodically the sample.

b. Hyperfine effects: Nuclear Quadrupole Coupling.

The presence in pseudopelletierine of a ^{14}N nucleus with a nuclear spin (I=1) larger than one-half introduces in the molecule a nuclear quadrupole moment. This electric property can be visualized as originated by a nucleus with a non-spherical charge distribution.[16] The nuclear quadrupole interacts with the electric field gradient at the location of the quadrupolar nucleus, providing a mechanism for the coupling of the angular momenta from the nuclear spin and the molecular rotation. This effect splits the rotational levels, introducing new selection rules and resulting in detectable splittings in the observed transitions.[17,18]

In the case of pseudopelletierine, all transitions exhibited a small splitting into three more intense components. The magnitude of the splitting is larger than the instrumental Doppler effect (50-80 kHz), but typically smaller than $\Delta\nu \sim 0.5$ MHz so all the components can be easily resolved and recognized, as exemplified in figure 2.6.

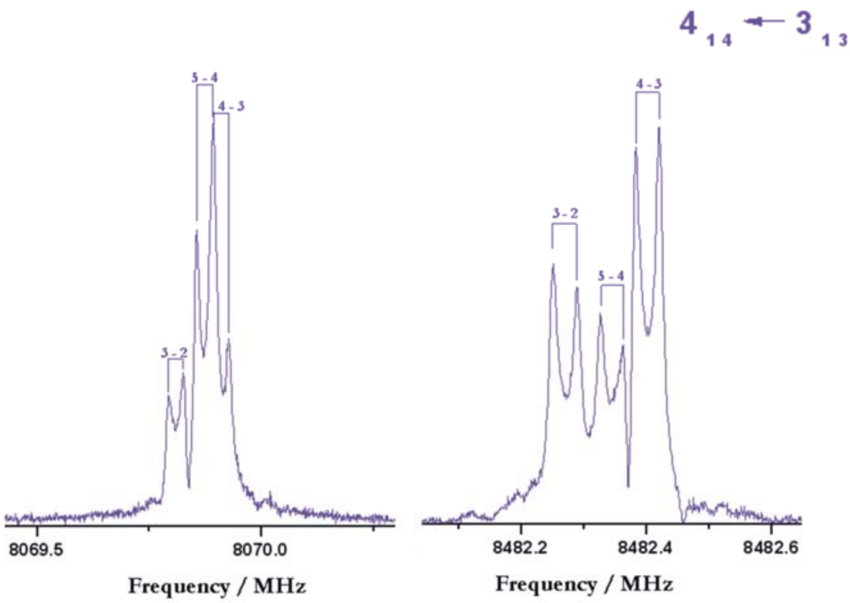

Figure: 2.6.- **(a)** The 41,4 ⟵ 31,3 transition for the axial conformer of pseudopelletierine. **(b)** The same transition for the equatorial conformer. The hyperfine components are labeled with the quantum number F ($\boldsymbol{F}=\boldsymbol{I}+\boldsymbol{J}$).

c. Determination of the spectroscopic parameters.

The search of the rotational spectrum produced two independent sets of rotational transitions, which were analysed separately. The carriers of the spectrum were assigned to the two axial and equatorial structures expected from the theoretical predictions.

The observed frequencies of the rotational transitions are shown in tables 2.3, 2.4 and 2.5). The transitions were fitted using the semi-rigid Watson Hamiltonian in the asymmetric reduction (A) and I^r representation,[14] with an extra term accounting for the nuclear quadrupole coupling interaction. As a result, the rotational and centrifugal constants, together with the diagonal elements of the nuclear quadrupole coupling tensor were accurately determined and reported in table 2.2.

Table: 2.2.- Experimental and theoretical rotational constants (*A*, *B* and *C*), diagonal elements of the quadrupole coupling tensor of the ^{14}N atom ($\chi_{aa}, \chi_{bb}, \chi_{cc}$) and centrifugal distortion constants ($\Delta_J, \Delta_{JK}, \Delta_K, \delta_J, \delta_K$) of axial and equatorial pseudopelletierine. The number of lines (*N*) and the rms deviation (σ) of the fit are also shown.

	Axial		**Equatorial**	
	Experiment	MP2 / M06-2X	Experiment	MP2 / M06-2X
***A* / MHz**	1391.70329 (70) [a]	1397.3 / 1393.9	1669.11 (16)	1678.1 / 1679.5
***B* / MHz**	1190.60002 (10)	1197.0 / 1198.7	1014.416063 (96)	1018.8 / 1020.0
***C* / MHz**	1032.058673(91)	1037.8 / 1038.1	1006.893694 (96)	1012.6 / 1014.1
Δ_J **/ kHz**	0.0360 (13)		0.04202 (92)	
Δ_{JK} **/ kHz**	0.3081 (90)		0.172 (16)	
Δ_K **/ kHz**	-0.324 (26)		[0.0][b]	
δ_J **/ kHz**	[0.0]		[0.0]	
δ_K **/ Hz**	-0.00415(46)		[0.0]	
χ_{aa} **/ MHz**	-3.4639 (51)	-3.21 / -3.91	1.935 (11)	2.02 / 2.10
χ_{bb} **/ MHz**	0.8658 (59)	0.60 / 1.10	-4.496 (36)	-4.66 / -4.91
χ_{cc} **/ MHz**	2.5982 (59)	2.61 / 2.81	2.561 (36)	2.65 / 2.81
$\lvert\mu_a\rvert$ **/ D**		2.53 / 2.78		3.35 / 3.56
$\lvert\mu_b\rvert$ **/ D**		0.68 / 0.73		0.02 / 0.07
$\lvert\mu_c\rvert$ **/ D**		0.00 / 0.00		0.00 / 0.00
$\lvert\mu_{TOT}\rvert$ **/ D**		2.62 / 2.87		3.35 / 3.56
N	94		54	
σ **/ kHz**	0.36		0.30	
ΔE **/ KJ·mol^{-1}**		0.0 / 0.0		2.42 / 1.86

[a] Standard errors in units of the last digit.
[b] Values in brackets fixed to zero.

The previous table compares also the experimental results for the detected conformers with the theoretical values. As can be observed by inspection of the rotational constants and coupling parameters, the detected conformers can be unambiguously identified with the two most stable axial and equatorial conformers of figure 2.4.

Four out of five quartic centrifugal distortion constants have been determined for the axial conformer, while only two were obtained for the equatorial. This issue is associated to the low quantum numbers of the transition dataset measured here.

Concerning the nuclear quadrupole coupling, only the diagonal elements of the tensor were determined, while the remaining off-diagonal terms were not needed to reproduce the experimental spectrum.

It is interesting to note that the accuracy in the determination of the spectroscopic parameters is better for the axial conformation. The main reason of this difference is the number and type of transitions measured for each conformer (axial vs equatorial = 94:54). This is especially noticeable in the *A* constant of the equatorial species, which is worse determined because of the presence for this conformer of only μ_a transitions. In any case, the standard deviation of the fit (< 1 kHz), is below the estimated uncertainty of the experimental frequencies (<3 kHz).

Table: 2.3.- Measured and calculated frequencies (MHz) for the μ_a-type transitions observed for the axial conformer of pseudopelletierine. The last column represents the difference $\Delta\nu = \nu_{OBS} - \nu_{CALC}$ (kHz) between the measured and calculated frequencies.

J'	*K'₋₁*	*K'₊₁*	*J''*	*K''₋₁*	*K''₊₁*	*F'*	*F''*	ν_{OBS} / MHz	ν_{CALC} / MHz	$\Delta\nu$ / kHz
4	1	3	3	1	2	4	3	9024.5061	9024.5056	0.5
						3	2	9024.6295	9024.6304	-0.9
						5	4	9024.6505	9024.6480	2.6
4	2	2	3	2	1	5	4	9215.2302	9215.2271	3.0
						4	3	9214.8269	9214.8242	2.7
						3	2	9215.3399	9215.3388	1.1
5	1	5	4	1	4	6	5	10555.6518	10555.6517	0.1
						5	4	10555.5527	10555.5527	0.0
						4	3	10555.6010	10555.6011	-0.1
5	0	5	4	0	4	6	5	10565.0752	10565.0756	-0.4
						5	4	10564.9926	10564.9910	1.5
						4	3	10565.0200	10565.0211	-1.1
4	1	4	3	1	3	5	4	8482.5999	8482.5999	0.0
						4	3	8482.4394	8482.4402	-0.8
						3	2	8482.5326	8482.5328	-0.2
4	0	4	3	0	3	5	4	8510.6798	8510.6790	0.8
						4	3	8510.5767	8510.5787	-2.0
						3	2	8510.5928	8510.5894	3.5
5	2	4	4	2	3	6	5	10973.9673	10973.9662	1.0
						5	4	10973.7079	10973.7073	0.5
						4	3	10973.9925	10973.9933	-0.9
5	1	4	4	1	3	5	4	11104.0953	11104.0953	0.0
						4	3	11104.1821	11104.1813	0.9
						6	5	11104.2013	11104.1989	2.4
5	3	3	4	3	2	6	5	11210.6923	11210.6896	2.7
						5	4	11210.1720	11210.1707	1.2
						4	3	11210.8185	11210.8186	-0.1
5	3	2	4	3	1	5	4	11453.5220	11453.5221	-0.1
						6	5	11454.0236	11454.0269	-3.3
						4	3	11454.1557	11454.1526	3.2
5	2	3	4	2	2	6	5	11492.9349	11492.9341	0.9
						5	4	11492.7485	11492.7482	0.3
						4	3	11492.9523	11492.9550	-2.7
6	1	6	5	1	5	7	6	12622.6818	12622.6809	0.9
						6	5	12622.6104	12622.6109	-0.5
						5	4	12622.6424	12622.6431	-0.7
6	0	6	5	0	5	7	6	12625.4517	12625.4511	0.6
						6	5	12625.3848	12625.3844	0.4
						5	4	12625.4118	12625.4126	-0.8
6	2	5	5	2	4	7	6	13076.8569	13076.8558	1.1
						6	5	13076.6912	13076.6914	-0.2

Table: 2.3 Continued.-

J'	K'_{-1}	K'_{+1}	J''	K''_{-1}	K''_{+1}	F'	F''	ν_{OBS} / MHz	ν_{CALC} / MHz	$\Delta\nu$ / kHz
6	1	5	5	1	4	7	6	13141.4193	13141.4172	2.2
						6	5	13141.3139	13141.3150	-1.0
						5	4	13141.4002	13141.4055	-5.3
6	3	4	5	3	3	7	6	13404.9648	13404.9657	-1.0
						6	5	13404.6636	13404.6644	-0.7
						5	4	13405.0141	13405.0138	0.3
6	4	3	5	4	2	7	6	13519.6482	13519.6475	0.8
						6	5	13519.1161	13519.1154	0.8
						5	4	13519.7626	13519.7630	-0.4
6	4	2	5	4	1	7	6	13630.3343	13630.3318	2.5
						6	5	13629.7864	13629.7882	-1.8
						5	4	13630.4471	13630.4490	-2.0
6	2	4	5	2	3	7	6	13676.4912	13676.4929	-1.7
						6	5	13676.3927	13676.3934	-0.7
6	3	3	5	3	2	7	6	13829.8508	13829.8537	-2.9
						6	5	13829.5926	13829.5935	-0.9
						5	4	13829.8941	13829.8949	-0.8
7	1	7	6	1	6	7	6	14687.5195	14687.5192	0.3
						6	5	14687.5441	14687.5432	0.9
						8	7	14687.5731	14687.5722	0.9
7	0	7	6	0	6	7	6	14688.2746	14688.2739	0.7
						6	5	14688.2978	14688.2970	0.7
						8	7	14688.3271	14688.3262	0.9

Table: 2.4.- Measured and calculated frequencies (MHz) for the μ_b-type transitions observed for the axial conformer of pseudopelletierine. The last column represents the difference $\Delta\nu = \nu_{OBS} - \nu_{CALC}$ (kHz) between the measured and calculated frequencies.

J'	K'_{-1}	K'_{+1}	J''	K''_{-1}	K''_{+1}	F'	F''	ν_{OBS} / MHz	ν_{CALC} / MHz	$\Delta\nu$ / kHz
5	0	5	4	1	4	5	4	10551.7633	10551.7649	-1.6
						4	3	10551.8198	10551.8183	1.5
						6	5	10551.8676	10551.8680	-0.4
5	1	5	4	0	4	5	4	10568.7817	10568.7789	2.7
						4	3	10568.8024	10568.8039	-1.5
						6	5	10568.8578	10568.8593	-1.5
4	4	1	3	3	0	5	4	10852.8468	10852.8478	-1.0
						4	3	10853.0543	10853.0588	-4.5
5	1	4	4	2	3	5	4	10872.1009	10872.0997	1.2
						6	5	10872.4497	10872.4496	0.1
						4	3	10872.4928	10872.4952	-2.4
4	4	1	3	3	0	5	4	10874.4050	10874.4031	1.9
						4	3	10874.6123	10874.6085	3.8
4	0	4	3	1	3	4	3	8469.2137	8469.2140	-0.4
						3	2	8469.3262	8469.3300	-3.8
						5	4	8469.3922	8469.3923	-0.1
4	1	4	3	0	3	3	2	8523.7865	8523.7922	-5.6
						4	3	8523.8068	8523.8049	2.0
						5	4	8523.8858	8523.8865	-0.8
6	0	6	5	1	5	6	5	12621.5962	12621.5965	-0.3
						5	4	12621.6294	12621.6298	-0.5
						7	6	12621.6684	12621.6675	1.0
6	1	6	5	0	5	6	5	12626.3993	12626.3988	0.5
						5	4	12626.4243	12626.4259	-1.6
						7	6	12626.4639	12626.4646	-0.7
6	1	5	5	2	4	6	5	13039.7073	13039.7073	0.0
						7	6	13039.9003	13039.9005	-0.2
						5	4	13039.9112	13039.9074	3.8
6	2	5	5	1	4	6	5	13178.2975	13178.2990	-1.5
						7	6	13178.3738	13178.3725	1.3

Table: 2.5.- Measured and calculated frequencies (MHz) for the μ_a-type transitions observed for the axial conformer of pseudopelletierine. The last column represents the difference $\Delta\nu = \nu_{OBS} - \nu_{CALC}$ (kHz) between the measured and calculated frequencies.

J'	K'_{-1}	K'_{+1}	J''	K''_{-1}	K''_{+1}	F'	F''	ν_{OBS} / MHz	ν_{CALC} / MHz	$\Delta\nu$ / kHz
5	1	5	4	1	4	4	3	10087.4063	10087.4068	-0.6
						6	5	10087.4456	10087.4448	0.8
						5	4	10087.4618	10087.4599	1.9
5	0	5	4	0	4	5	4	10105.2186	10105.2150	3.6
						6	5	10105.2410	10105.2407	0.4
						4	3	10105.2757	10105.2778	-2.1
5	2	4	4	2	3	4	3	10106.3212	10106.3247	-3.5
						6	5	10106.3409	10106.3379	3.0
						5	4	10106.4698	10106.4708	-0.9
5	2	3	4	2	2	4	3	10107.5973	10107.5977	-0.4
						6	5	10107.6160	10107.6149	1.2
						5	4	10107.7841	10107.7835	0.5
5	1	4	4	1	3	6	5	10125.0133	10125.0125	0.8
						5	4	10125.0635	10125.0643	-0.7
						4	3	10125.0949	10125.0956	-0.8
4	1	4	3	1	3	3	2	8069.9783	8069.9783	0.0
						5	4	8070.0563	8070.0543	2.1
						4	3	8070.0978	8070.0979	-0.2
4	0	4	3	0	3	4	3	8084.5593	8084.5639	-4.5
						5	4	8084.5785	8084.5775	1.0
						3	2	8084.6393	8084.6378	1.5
4	1	3	3	1	2	5	4	8100.0881	8100.0883	-0.2
						4	3	8100.1850	8100.1853	-0.2
						3	2	8100.2148	8100.2171	-2.3
6	1	6	5	1	5	5	4	12104.7266	12104.7289	-2.3
						6	5	12104.7532	12104.7536	-0.4
6	0	6	5	0	5	6	5	12125.5418	12125.5415	0.3
						7	6	12125.5770	12125.5773	-0.3
						5	4	12125.6041	12125.6033	0.8
6	2	5	5	2	4	5	4	12127.5018	12127.5004	1.4
						6	5	12127.5762	12127.5745	1.7
6	2	4	5	2	3	7	6	12129.7357	12129.7368	-1.1
						6	5	12129.8547	12129.8552	-0.5
6	1	5	5	1	4	7	6	12149.8401	12149.8395	0.7
						6	5	12149.8681	12149.8680	0.1
						5	4	12149.8966	12149.8976	-1.0
7	1	7	6	1	6	6	5	14121.9434	14121.9459	-2.4
						8	7	14121.9620	14121.9608	1.2
7	0	7	6	0	6	7	6	14145.4826	14145.4819	0.8
						8	7	14145.5257	14145.5266	-1.0
						6	5	14145.5475	14145.5463	1.3
7	2	6	6	2	5	8	7	14148.5843	14148.5840	0.3
						7	6	14148.6273	14148.6287	-1.4

Table: 2.5. Continued.-										
J'	*K'*$_{-1}$	*K'*$_{+1}$	*J''*	*K''*$_{-1}$	*K''*$_{+1}$	*F'*	*F''*	ν_{OBS} / MHz	ν_{CALC} / MHz	$\Delta\nu$ / kHz
7	2	5	6	2	4	6	5	14152.1634	14152.1634	0.0
						7	6	14152.2592	14152.2573	1.9
7	1	6	6	1	5	8	7	14174.5522	14174.5535	-1.3
						7	6	14174.5704	14174.5681	2.3
5	3	2	4	3	1	5	4	14174.5967	10106.9597	-3.4

d. Isotopic Substitutions: Structure Determination.

The structural information about gas-phase molecules provided by rotational spectroscopy is contained in the moments of inertia. In turn, those moments are closely related to the system masses and geometry, so at the end it could seem straightforward to derive the molecule structure. However, a molecular system is a quantum object with vibrational energy. In consequence the moments of inertia include vibrational contributions, and different procedures have been developed to take into account such contributions and to relate the determinable moments of inertia to the structure.

A detailed analysis of the structure requires information on several isotopic species of the sample, or isotopologues. As each isotopologue has different atomic masses, all of them produce totally independent spectra and need to be recorded separately. Isotopologues can be prepared by chemical synthesis, but very often it is possible to record the spectra using natural abundances, which range in the order of 0.2-1.1% for the common ^{18}O, ^{15}N and ^{13}C species present in organic compounds. In consequence, natural abundance isotopologues can be detected in favorable conditions, i.e., species with intense spectra (large populations and/or dipole moments).

In pseudopelleterine the conformational composition made possible to detect several isotopologues of the most abundant conformation. However, the second conformer was too weak for this kind of measurements. Axial pseudopelletierine additionally benefits from the plane-symmetric geometry of the complex, which makes equivalent the carbon positions symmetrically located with respect to this plane (1/5, 2/4 & 6/8 positions). In consequence the apparent abundance of the symmetric ^{13}C species is doubled with respect to normal carbon atoms.

Finally, we were able to detect all eight different monosubstituted isotopologues (six independent ^{13}C positions, and the ^{15}N and ^{18}O substitutions) for the axial conformer. In the following figure the transition $4_{1,4} \leftarrow 3_{1,3}$ is shown for five different isotopic substitutions of ^{13}C atoms and for the ^{15}N.

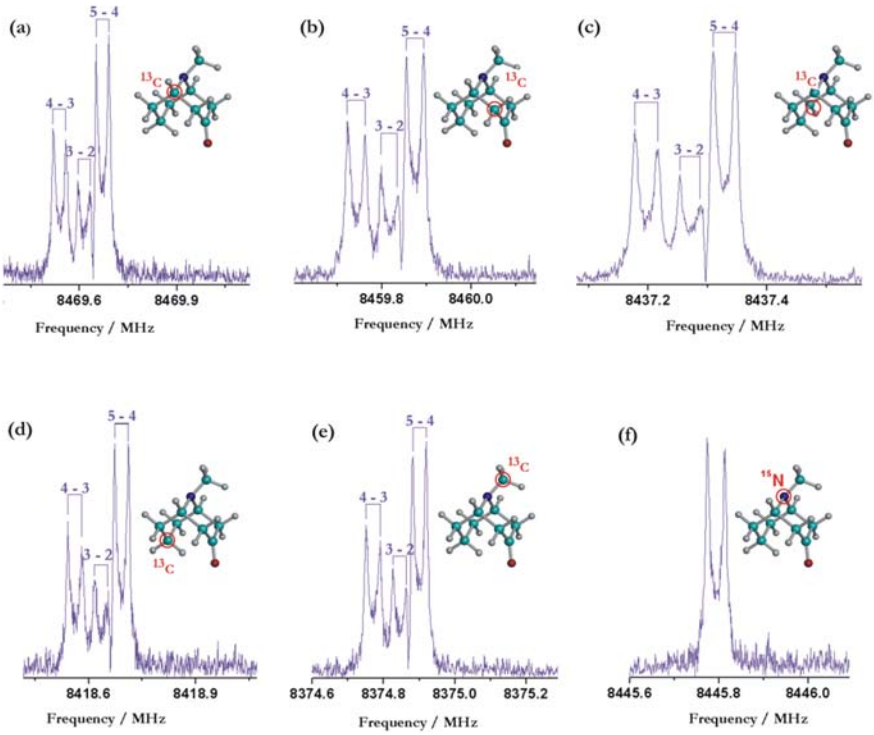

Figure: 2.10.- $4_{1,4} \leftarrow 3_{1,3}$ transitions of the isotopic substitutions for the axial conformer of pseudopelletierine. **(a)** $^{13}C_1$ -$^{13}C_5$ substitution. **(b)** $^{13}C_2$ -$^{13}C_4$ substitution. **(c)** $^{13}C_6$ -$^{13}C_8$ substitution. **(d)** $^{13}C_7$ substitution. **(e)** $^{13}C_{10}$ substitution. **(f)** $^{15}N_9$ substitution. The hyperfine interaction disappears in ^{15}N.

The rotational spectra from the pseudopelletierine isotopologues was analyzed similarly to the parent species. Because the number of transitions is smaller, and the isotopic substitution does not produce significant changes in the centrifugal distortion constants or the nuclear quadrupole coupling constants, these parameters were fixed in the fit to the values of the parent species. The results of the fits floating only the rotational constants are shown in the following table. (See the list of transitions in appendix I).

<u>Table: 2.6.-</u> Experimental rotational constants (*A*, *B* & *C*) of the monosubstituted species of the axial conformer. The quadrupole coupling tensor elements and the centrifugal distortion constant have been kept fixed and equal to the parent species. The number of transitions (*N*) and the standard deviation (*σ*) of the fit are given.

	^{13}C1 - ^{13}C5	^{13}C2 - ^{13}C4	^{13}C3	^{13}C6 - ^{13}C8	^{13}C7	^{15}N9	^{13}C10	^{18}O11
A/MHz	1386.1765(60)[a]	1383.7888(80)	1390.8713(39)	1378.0745(70)	1375.758 (10)	1390.703 (29)	1378.043 (12)	1391.676 (10)
B/MHz	1185.3084(12)	1184.4648(17)	1183.91241(61)	1184.9594(17)	1190.5801(30)	1185.2781(61)	1181.7848(31)	1150.7437(79)
C/MHz	1031.10525(19)	1029.86146(23)	1026.54803(18)	1026.67170(20)	1023.26907(30)	1027.48651(66)	1017.98885(37)	1001.3333(11)
Δ_J/kHz	[0.0360][a]	[0.0360]	[0.0360]	[0.0360]	[0.0360]	[0.0360]	[0.0360]	[0.0360]
Δ_{JK}/kHz	[0.3081]	[0.3081]	[0.3081]	[0.3081]	[0.3081]	[0.3081]	[0.3081]	[0.3081]
Δ_K/ kHz	[-0.324]	[-0.324]	[-0.324]	[-0.324]	[-0.324]	[-0.324]	[-0.324]	[-0.324]
δ_J / kHz	[0.0]	[0.0]	[0.0]	[0.0]	[0.0]	[0.0]	[0.0]	[0.0]
δ_K / Hz	[-0.00415]	[-0.00415]	[-0.00415]	[-0.00415]	[-0.00415]	[-0.00415]	[-0.00415]	[-0.00415]
χ_{aa}/MHz	[-3.4639]	[-3.4639]	[-3.4639]	[-3.4639]	[-3.4639]	[-3.4639]	[-3.4639]	[-3.4639]
χ_{bb}/MHz	[-3.4648]	[-3.4648]	[-3.4648]	[-3.4648]	[-3.4648]	[-3.4648]	[-3.4648]	[-3.4648]
χ_{cc}/MHz	[2.5982]	[2.5982]	[2.5982]	[2.5982]	[2.5982]	[2.5982]	[2.5982]	[2.5982]
σ / kHz	0.56	0.61	0.49	0.59	0.65	0.01	1.7	0.27
N	14	14	15	12	11	5	11	5

[a] Standard error in units of the last digit.

[b]Values in brackets fixed to the parent species.

The isotopic information produces structural information through different methods. The substitution method (or r_s coordinates) is based in the Kraitchmann equations[19,20] and provides absolute atomic coordinates for each substituted atom. In consequence a full substitution structure would require substituting all atoms in the molecule, which is impractical. More often, only the heavy atoms are substituted, which results in a partial substitution structure. The Kraitchman equations assume similar contributions of the molecular vibrations to the moments of inertia. In consequence, the differences between the experimental and equilibrium (r_e) moments of inertia (I_o-I_e) are expected to cancel the vibrational contributions, so the resulting coordinates approximate the equilibrium structure. The advantage of the substitution method is that it produces atomic coordinates without the need for any external data. However, this method is not valid for atoms close to the inertial axes, where it produces complex numbers.[21,22]

Alternatively, it is possible to select an appropriate set of structural parameters and to fit the best values reproducing the set of ground-state rotational constants. The resulting structure is known as effective (r_0) structure.[23,24] Different effective structure can be calculated for each vibrational state. This kind of structures are valid in cases where the rotational data are limited, since it is possible to constrain different parts of the molecule to theoretical values and adjust only selected parameters. On the other hand, the structural definition is purely operational and is not connected with the equilibrium structures.

There are several other methods for structural determination,[25] but I would like to mention the Watson's pseudo-equilibrium r_m method, which was attempted for pseudopelletierine. The r_m method introduces explicit mathematical models to express the difference between the ground-state and equilibrium moments of inertia. Different structures can thus be obtained when considering different fitting parameters. In the $r_m^{(1)}$ structures the vibrational contributions per inertial axis (I_o-I_e) are fitted to a monodimensional function on the square root of the masses. The $r_m^{(2)}$ is a more complex biparametric model. These models produce relatively accurate pseudo-equilibrium coordinates, but they require a large number of isotopic data. In pseudopelletierine the number of isotopologues was not enough for a good determination of r_m structure.

Table 2.7 shows the results for the substitution coordinates in pseudopelletierine. The derived molecular parameters (bond lengths, valence angles and torsion dihedrals) can be seen in the following table 2.8.

Table: 2.7.- Absolute values of the atomic coordinates in the principal axis system for the substituted species obtained from the Kraitchman equations.

	Isotopologues Coordinates (Å)		
	A	**b**	**C**
$^{13}C_1$ - $^{13}C_5$	0.6680 (0.0023)	0.053 (0.029)	1.2062 (0.0013)
$^{13}C_2$ - $^{13}C_4$	0.7572 (0.0021)	0.6751 (0.0024)	1.2805 (0.0013)
$^{13}C_3$	1.55035(0.00098)	0.4834 (0.0032)	0.00
$^{13}C_6$ - $^{13}C_8$	0.6915(0.0023)	1.4299 (0.0011)	1.2573(0.0013)
$^{13}C_7$	0.046 (0.036)	2.05359(0.00081)	0.072 (0.023)
$^{15}N_9$	1.3863 (0.0018)	0.5274 (0.0048)	0.00
$^{13}C_{10}$	1.72941(0.00097)	1.94904(0.00088)	0.00
$^{18}O_{11}$	2.73870(0.00058)	0.3227 (0.0051)	0.00

In order to determine an effective structure it is necessary to select which structural parameters can be fitted and which model and uncertainties can be given to the constrained parameters. Frequently a bad selection of structural parameters may produce bad convergence and ill-defined parameters. Moreover, a large experimental dataset is necessary to be able to adjust all independent parameters. In pseudopelletierine the symmetry of the molecule reduces the number of independent variables, so it was possible to fit a total of 15 different parameters, including 8 valence angles and 7 torsion dihedrals.

The following table 2.8 shows the results for the substitution and effective structures compared with the theoretical values.

To our knowledge no diffraction structure was available for pseudopelletierine so no comparison is possible with the solid state.

Table: 2.8.- Substituted and effective structure compared with the theoretical values for the equilibrium structure obtained for the axial conformer. The last column shows the equilibrium structure from the ab initio calculations for the equatorial conformer.

	Axial			**Equatorial**
	$\mathbf{r_s}$	$\mathbf{r_0}$	**Ab initio $\mathbf{r_e}$**	**Ab initio $\mathbf{r_e}$**
r (C_1-C_2) = r (C_4-C_5)/ Å	1.557 (17)	1.549 (14)	1.550	1.539
r (C_2-C_3) = r (C_3-C_4)/ Å	1.518 (19)	1.517 (17)	1.516	1.518
r (C_5-C_6) = r (C_1-C_8)/ Å	1.48 (3)	1.533 (9)	1.533	1.540
r (C_6-C_7) = r (C_7-C_8)/ Å	1.58 (2)	1.532 (22)	1.533	1.533
r (C_1-N) = r (C_5-N)/ Å	1.48 (2)	1.467 (18)	1.467	1.470
r (N-C_{10})/ Å	1.462 (6)	1.457 (7)	1.458	1.458
r (C_3-O)/ Å	1.199 (3)	1.222 (6)	1.221	1.222
(C_1-C_2-C_3) = (C_3-C_4-C_5) / deg	112.8 (9)	113.1 (12)	113.9	113.4
(C_2-C_3-O) = (O-C_3-C_4) / deg	122.3 (16)	122.2 (13)	122.9	112.1
(C_2-C_3-C_4) / deg	115.0 (3)	116.3 (9)	114.4	115.7
(C_4-C_5-C_6) = (C_8-C_1-C_2) / deg	114.3 (13)	112.5 (11)	112.0	112.3
(C_5-C_6-C_7) = (C_7-C_8-C_1) / deg	111.0 (6)	112.1 (12)	112.0	111.6
(C_6-C_7-C_8) / deg	104.9 (18)	109.7 (17)	110.4	110.2
(C_1-N-C_5) / deg	109.0 (14)	110.5 (9)	110.0	110.3
(C_1-N-C_{10}) = (C_5-N-C_{10}) / deg	115.1 (48)	113.6 (14)	113.1	113.1
τ(C_1-C_2-C_3-O)=-τ(C_5-C_4-C_3-O) / deg	-33.9 (18)	-37.1 (13)	140.8	144.4
τ(C_1-C_2-C_3-C_4)=-τ(C_5-C_4-C_3-C_2) / deg	139.1 (16)	142.8 (16)	-38.8	-37.7
τ(C_6-C_5-C_4-C_3)=-τ(C_8-C_1-C_2-C_3) / deg	-107.2 (17)	-105.4 (19)	73.7	73.9
τ(C_7-C_6-C_5-C_4)=-τ(C_7-C_8-C_1-C_2) / deg	116.4 (15)	113.2 (20)	-68.3	-67.8
τ(C_8-C_7-C_6-C_5)=-τ(C_1-C_8-C_7-C_6) / deg	124.1 (21)	128.7 (20)	-49.7	-51.0
τ(C_2-C_1-N-C_{10}) = τ(C_4-C_5-N-C_{10}) / deg	-112.5 (43)	-110.1 (19)	68.0	163.8
τ(C_3-C_2-C_1-N)=-τ(C_3-C_4-C_5-N) / deg	-128.0 (25)	-131.8 (15)	49.7	50.9
τ(C_8-C_1-N-C_{10}) = τ(C_6-C_5-N-C_{10}) / deg	14.8 (25)	14.5 (19)	-166.8	-71.4
τ(C_7-C_8-C_1-N)=-τ(C_7-C_6-C_5-N) / deg	118.3 (29)	123.2 (21)	-57.5	-55.2

e. Conformer Abundances: Estimation from Relative Intensities measurements.

To extract information about the conformer abundances, a study of the relative intensities (*I*) of the rotational transitions was carried out. In table 2.9 the intensity values of the selected transitions for both conformers are shown.

From these data, and using the following equation[26], which basically is a direct proportionality between populations and electric dipole moments, the conformational ratio can be approximated as

$$\frac{N_{axial}}{N_{equatorial}} \propto \frac{I_{axial}}{I_{equatorial}} \cdot \frac{\mu_{equatorial}}{\mu_{axial}}$$

This population ratio assumes that no conformational relaxation is occurring in the jet and that all populations have been frozen to the vibrational ground state within each conformational potential energy well.

We found with the previous equation that the approximated relation between the axial and the equatorial populations is: $N_{axial}/N_{equatorial} \sim 2/1$. Hence, the axial conformer population inside the sample is almost twice the equatorial population.

The conformational ratio is consistent with the predicted energy gap from the ab initio calculations. While the MP2 methods predict both axial and equatorial conformers isoenergetic, the relative intensity studies estimate the different about 0.1 kJ·mol^{-1}.

Table: 2.9.- Intensities (in arbitrary units) of the two conformational structures (axial and equatorial) for several μ_a & μ_b-type selected transitions.

Transition	I_{axial}	$I_{equatorial}$
$4_{04} \leftarrow 3_{03}$	4.00	3.18
$5_{15} \leftarrow 4_{14}$	6.17	2.83
$5_{05} \leftarrow 4_{04}$	6.29	2.82
$5_{24} \leftarrow 5_{23}$	3.75	1.96
$6_{25} \leftarrow 6_{24}$	5.03	2.24
$7_{17} \leftarrow 6_{16}$	1.90	1.69
$7_{07} \leftarrow 6_{06}$	1.71	1.15
$6_{15} \leftarrow 5_{14}$	2.49	1.56
$6_{24} \leftarrow 5_{23}$	4.19	2.54
$5_{23} \leftarrow 4_{22}$	2.67	2.34

2.4 Conclusions.-

The rotational spectrum of pseudopelletierine in gas phase led to the identification of two different conformers. The conformational assignment as chair-chair axial or equatorial species is consistent with the theoretical calculations which predict these structures as most stables (figure 2.4).

The analysis of the spectrum for the parent species could be extended to eight monosubstitued species in natural abundance. The detection of the weak ^{18}O species confirms the good sensitivity of the instrument. Rotational, centrifugal distortion and nuclear quadrupole coupling parameters were determined for all isotopologues.

Additionally, the structural analysis produced substitution and effective structures that were compared to the ab initio predictions.

Finally, a study about relative intensities was done, estimating the abundances of the two identified conformers. The population ratio shows that in the jet the axial population is approximately double than the equatorial conformer concentration.

Compared to tropinone we observe a population inversion associated to the addition of a methylene group in pseudopelletierine. In tropinone the most abundant species was the equatorial structure, while in pseudopelletierine the most stable structure is the chair-chair geometry with the methyl group in the axial orientation.

2.5 Appendix.-

In the followings tables we show the measured transitions for each isotopic substitution.

- ***Substitution $^{13}C_1 - {}^{13}C_5$.***

Table:2.10.- Measured and calculated frequencies in MHz for the μ_a-type transitions observed for the $^{13}C_1$ - $^{13}C_5$ substitution in the axial conformer of pseudopelletierine. The third column represents the difference (in kHz) between the calculated and the measured frequencies $\Delta\nu = \nu_{OBS} - \nu_{CALC}$.

J'	K'_{-1}	K'_{+1}	J''	K''_{-1}	K''_{+1}	F'	F''	ν_{OBS} / MHz	ν_{CALC} / MHz	$\Delta\nu$ / kHz
4	1	3	3	1	2	4	3	8999.7715	8999.7723	-0.8
						3	2	8999.8951	8999.8990	-3.9
						5	4	8999.9209	8999.9163	4.6
5	1	5	4	1	4	5	4	10541.0481	10541.0477	0.4
						4	3	10541.0958	10541.0961	-0.3
						6	5	10541.1469	10541.1467	0.2
5	0	5	4	0	4	6	5	10550.9633	10550.9632	0.2
						5	4	10550.8780	10550.8789	-0.9
4	1	4	3	1	3	4	3	8469.7021	8469.7025	-0.4
						3	2	8469.7938	8469.7953	-1.5
						5	4	8469.8644	8469.8624	2.0
4	0	4	3	0	3	4	3	8498.4401	8498.4439	-3.8
						3	2	8498.4589	8498.4538	5.1
						5	4	8498.5429	8498.5437	-0.8

- ***Substitution $^{13}C_2 - {}^{13}C_4$.***

Tabla:2.11.- Measured and calculated frequencies in MHz for the μ_a-type transitions observed for the $^{13}C_2$ - $^{13}C_4$ substitution in the axial conformer of pseudopelletierine. The third column represents the difference (in kHz) between the calculated and the measured frequencies $\Delta\nu = \nu_{OBS} - \nu_{CALC}$

J'	K'-1	K'+1	J''	K''-1	K''+1	F'	F''	ν_{OBS} / MHz	ν_{CALC} / MHz	$\Delta\nu$ / kHz
4	1	3	3	1	2	4	3	8990.2589	8990.2546	4.4
						3	2	8990.3731	8990.3805	-7.4
						5	4	8990.4014	8990.3979	3.5
5	1	5	4	1	4	5	4	10528.6382	10528.6370	1.2
						4	3	10528.6847	10528.6853	-0.7
						6	5	10528.7349	10528.7359	-1.0
5	0	5	4	0	4	5	4	10538.2357	10538.2359	-0.2
						6	5	10538.3213	10538.3203	1.1
						4	3	10538.2688	10538.2657	3.1
4	1	4	3	1	3	4	3	8459.9064	8459.9067	-0.3
						3	2	8459.9963	8459.9994	-3.2
						5	4	8460.0682	8460.0665	1.7
4	0	4	3	0	3	4	3	8488.1838	8488.1830	0.8
						5	4	8488.2792	8488.2829	-3.8

- ***Substitution $^{13}C_6 - {}^{13}C_8$.***

Tabla:2.12.- Measured and calculated frequencies in MHz for the μ_a-type transitions observed for the $^{13}C_6$ - $^{13}C_8$ substitution in the axial conformer of pseudopelletierine. The third column represents the difference (in kHz) between the calculated and the measured frequencies $\Delta\nu = \nu_{OBS} - \nu_{CALC}$.

J'	K'-1	K'+1	J''	K''-1	K''+1	F'	F''	ν_{OBS} / MHz	ν_{CALC} / MHz	$\Delta\nu$ / kHz
5	1	5	4	1	4	5	4	10499.1428	10499.1394	3.3
						4	3	10499.1857	10499.1878	-2.0
						6	5	10499.2380	10499.2383	-0.3
4	1	3	3	1	2	4	3	8974.2202	8974.2174	2.8
						5	4	8974.3547	8974.3574	-2.7
5	0	5	4	0	4	5	4	10507.6540	10507.6532	0.9
						6	5	10507.7372	10507.7383	-1.1
4	1	4	3	1	3	4	3	8437.3722	8437.3729	-0.8
						3	2	8437.4643	8437.4652	-0.9
						5	4	8437.5330	8437.5323	0.8
4	0	4	3	0	3	4	3	8463.5029	8463.4982	4.6
						5	4	8463.5945	8463.5993	-4.8

- ***Substitution $^{13}C_7$.***

Tabla:2.13.- Measured and calculated frequencies in MHz for the μ_a-type transitions observed for the $^{13}C_7$ substitution in the axial conformer of pseudopelletierine. The third column represents the difference (in kHz) between the calculated and the measured frequencies $\Delta\nu = \nu_{OBS} - \nu_{CALC}$.

J'	*K'₋₁*	*K'₊₁*	*J''*	*K''₋₁*	*K''₊₁*	*F'*	*F''*	ν_{OBS} / MHz	ν_{CALC} / MHz	$\Delta\nu$ / kHz
4	1	3	3	1	2	4	3	8974.2206	8974.2193	1.3
						3	2	8974.3332	8974.3333	-0.2
						5	4	8974.3514	8974.3526	-1.2
5	1	5	4	1	4	6	5	10472.8989	10472.8990	-0.1
5	0	5	4	0	4	5	4	10479.7406	10479.7401	0.5
						4	3	10479.7727	10479.7728	-0.1
						6	5	10479.8263	10479.8266	-0.3
4	1	4	3	1	3	4	3	8418.7283	8418.7281	0.2
						5	4	8418.8865	8418.8867	-0.2
4	0	4	3	0	3	4	3	8441.6330	8441.6352	-2.2
						5	4	8441.7405	8441.7384	2.2

- ***Substitution $^{15}N_9$.***

Tabla:2.14.- Measured and calculated frequencies in MHz for the μ_a-type transitions observed for the $^{15}N_9$ substitution in the axial conformer of pseudopelletierine. The third column represents the difference (in kHz) between the calculated and the measured frequencies $\Delta\nu = \nu_{OBS} - \nu_{CALC}$.

J'	*K'₋₁*	*K'₊₁*	*J''*	*K''₋₁*	*K''₊₁*	ν_{OBS} / MHz	ν_{CALC} / MHz	$\Delta\nu$ / kHz
4	1	3	3	1	2	8988.3100	8988.3100	0.0
5	1	5	4	1	4	10510.2388	10510.2388	-0.08
5	0	5	4	0	4	10520.2730	10520.2730	0.03
4	1	4	3	1	3	8445.9689	8445.9688	0.07
4	0	4	3	0	3	8475.2999	8475.3020	-2.0

- ***Substitution $^{18}O_{11}$.***

Tabla:2.15.- Measured and calculated frequencies in MHz for the μ_a-type transitions observed for the $^{18}O_{11}$ substitution in the axial conformer of pseudopelletierine. The third column represents the difference (in kHz) between the calculated and the measured frequencies $\Delta\nu = \nu_{OBS} - \nu_{CALC}$.

J'	*K'₋₁*	*K'₊₁*	*J''*	*K''₋₁*	*K''₊₁*	*F'*	*F''*	ν_{OBS} / MHz	ν_{CALC} / MHz	$\Delta\nu$ / kHz
4	0	4	3	0	3	5	4	8273.6352	8273.6336	1.6
						4	3	8273.5354	8273.5370	-1.6
4	1	4	3	1	3	4	3	8233.1333	8233.1333	0.0
5	1	5	4	1	4	6	5	10248.1476	10248.1461	1.5
						5	4	10248.0452	10248.0467	-1.5

- ***Substitution $^{13}C_{10}$.***

Tabla:2.16.- Measured and calculated frequencies in MHz for the μ_a-type transitions observed for the $^{13}C_{10}$ substitution in the axial conformer of pseudopelletierine. The third column represents the difference (in kHz) between the calculated and the measured frequencies $\Delta\nu = \nu_{OBS} - \nu_{CALC}$.

J'	K'_{-1}	K'_{+1}	J''	K''_{-1}	K''_{+1}	F'	F''	ν_{OBS} / MHz	ν_{CALC} / MHz	$\Delta\nu$ / kHz
4	1	3	3	1	2	5	4	8928.4958	8928.4796	1.6
5	1	5	4	1	4	5	4	10419.3717	10419.3737	-2.0
						6	5	10419.4741	10419.4726	1.6
5	0	5	4	0	4	5	4	10427.7724	10427.7743	-1.9
						6	5	10427.8648	10427.8596	5.2
4	1	4	3	1	3	4	3	8374.9414	8374.9398	1.6
						3	2	8375.0285	8375.0319	-3.5
						5	4	8375.0995	8375.0990	0.5
4	0	4	3	0	3	5	4	8401.1766	8401.1680	8.7

2.6 References.-

[1] G. Grynkiewicz, M. Gadzikowska, *Pharm. Rep.*, 60, 439, **2008**.

[2] F. J. Leeper, J. C. Vederas, in "Topics in Current Chemistry", ed. Springer-Verlag, Berlin-Heilderberg, vol. 209, pp. 175–206, **2000**.

[3] E. J. Cocinero, A. Lesarri, P. Écija, J.-U. Grabow, J. A. Fernández, F. Castaño, *Phys. Chem. Chem. Phys.*, 12, 6076, **2010**.

[4] P. Écija, E. J. Cocinero, A. Lesarri, F. J. Basterretxea, J. A. Fernández, F. Castaño, *ChemPhysChem*, 14, 1830, **2013**.

[5] R. J. Hrynchuk, R. J. Barton, B. E. Robertson, *Can. J. Chem.*, 61, 481, **1983**.

[6] A. M. Belostotskii, Z. Goren, H. E. Gottlieb, *J. Nat. Prod.*, 67, 1842, **2004**.

[7] R. J. Staples, Y. Qi, *Z. Kristallogr. – New Cryst. Struct.*, 222, 225, **2007**.

[8] R. Glasser, Q.-J. Peng, A. S. Perlin, *J. Org. Chem.*, 53, 2172, **1988**.

[9] G. S. Chappell, B. F. Grabowski, R. A. Sandmann, D. M. Yourtee, *J. Pharm. Sci.*, 62, 414, **1973**.

[10] L. Evangelisti, A. Lesarri, M. K. Jahn, E. J. Cocinero, W. Caminati, J.-U. Grabow, *J. Phys. Chem. A*, 115, 9545, **2011**.

[11] MAESTRO, version 9.2, Schrödinger, LLc, New York, NY, **2012**.

[12] M. J. Frisch, G. W. Trucks, H. B. Schlegel, G. E. Scuseria, M. A. Robb, J. R. Cheeseman, G. Scalmani, V. Barone, B. Mennucci, G. A. Petersson, H. Nakatsuji, M. Caricato, X. Li, H. P. Hratchian, A. F. Izmaylov, J. Bloino, G. Zheng, J. L. Sonnenberg, M. Hada, M. Ehara, K. Toyota, R. Fukuda, J. Hasegawa, M. Ishida, T. Nakajima, Y. Honda, O. Kitao, H. Nakai, T. Vreven, J. A. Montgomery, Jr., J. E. Peralta, F. Ogliaro, M. Bearpark, J. J. Heyd, E. Brothers, K. N. Kudin, V. N. Staroverov, R. Kobayashi, J. Normand, K. Raghavachari, A. Rendell, J. C. Burant, S. S. Iyengar, J. Tomasi, M. Cossi, N. Rega, J. M. Millam, M. Klene, J. E. Knox, J. B. Cross, V. Bakken, C. Adamo, J. Jaramillo, R. Gomperts, R. E. Stratmann, O. Yazyev, A. J. Austin, R. Cammi, C. Pomelli, J. W. Ochterski, R. L. Martin, K. Morokuma, V. G. Zakrzewski, G. A. Voth, P. Salvador, J. J. Dannenberg, S. Dapprich, A. D. Daniels, Ö. Farkas, J. B. Foresman, J. V. Ortiz, J. Cioslowski, and D. J. Fox, Gaussian, Inc., Wallingford CT, **2009**.

[13] D. H. Levy, *Science*, 214, 263, **1981**.

[14] W. Gordy, L. R. Cook, "Microwave Molecular Spectra", 3rd Edition, in Weissberger, A. (Ed.), Techniques of Chemistry, vol. XVIII, John Wiley & Sons Inc., New York, **1984**.

[15] H. M. Pickett, *J. Mol. Spectrosc.*, 148, 371, **1991**.

[16] http://physics.nist.gov/jb95 Retrieved 2014-01-30

[17] J-U. Grabow, W. Stahl, H. Dreizler. *Rev. Sci. Instrum.*, 67, num. 12, 4072, **1996**.

[18] E. J. Cocinero, Tesis Doctoral, Universidad de Valladolid, **2005**.

[19] J. Kraitchman, *Am. J. Phys.*, 21,17, **1953**.

[20] C. C. Costain, *J. Chem. Phys.*, 29, 864, **1958**.

[21] J. Demaison, H. D. Rudolph, *J. Mol. Spectr.* 215, 78, **2002**.

[22] B. P. Van Eijck, in 'Accurate molecular Structure', Domenicano, Hargitai Eds., Oxford University Press, **1992**, Chap. 3, pp.46.

[23] H. D. Rudolph, *Struct. Chem.,* 2, 581, **1991**.

[24] K. J. Epple, H. D. Rudolph, *J. Mol. Spectr.* 152, 355, **1992**.

[25] J. Demaison, J. E. Boggs, A. G. Csaszar, "Equilibrium Molecular Structures: from spectroscopy to Quantum chemistry", CRC Press, USA, **2011**.

[26] W. Caminati, *Microwave spectroscopy of large molecules and molecular complexes* in "Handbook of high resolution spectroscopy", Jonh Wiley & Sons, Inc., **1999**.

Chapter 3
Scopine

3.1. Introduction.-

Tropane alkaloids are natural products[1-4] sharing the common *N*-methyl 8-azabycicle structural motif. In the previous chapter we have mentioned their multiple pharmacological applications, like the anticholinergic and neurostimulant properties.[3-8] Previous structure-activity relationship studies in tropanes have established correlations between bioactivity and several aspects of ligand conformations and stereochemistry. It is thus interesting to examine progressively more complex structures containing this motif to understand the intramolecular properties and dynamics of this family of compounds.

This study follows previous investigations done in our group, which examined the conformational properties and intramolecular dynamics of tropinone[9] and scopoline[10]. In this work we extend the study of tropane alkaloids to the epoxytropanes with the aim to obtain information about the influence of the epoxy group on nitrogen inversion and ring conformation[11].

We started from the simplest epoxytropane, scopine, which is a tropine derivative where the epoxy group has been introduced in the C6-C7 position (see figure 3.1). Scopine is at the core of more complex compounds, in particular scopolamine.

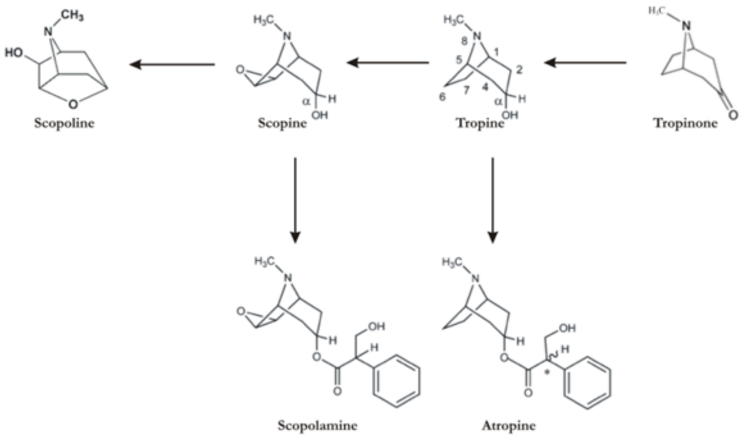

<u>Figure: 3.1.-</u> Some common hydroxy tropanes and ester derivatives.

However, it was known from previous solution studies that due to the high reactivity of the epoxy group and its strained three-membered ring, scopine and scopolamine can rearrange under alkaline conditions into scopoline.[12] This problem appeared also in the previous investigation of scopine in the gas-phase done by our group. Even at mild temperature conditions (90ºC), scopine was observed to suffer a fast spontaneous rearrangement reaction, breaking the epoxide group and cycling intramolecularly into scopoline. This gave us the opportunity to study scopoline, but information on scopine was still missing. The following figure shows this rearrangement reaction.

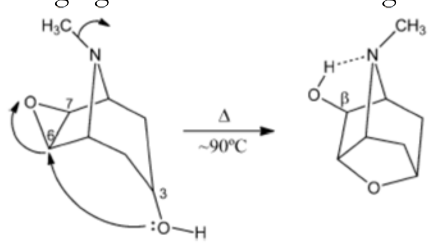

<u>Figure: 3.2.-</u> Scheme of the conversion of scopine into scopoline.

In consequence, in order to avoid this reaction we decided now to use a different heating technique to vaporize the sample. Since laser ablation has proved in the past to be very effective to bring intact molecules into the gas-phase with minor fragmentation, we decided to use a combination of laser ablation with FTMW spectroscopy[13-15] to obtain the rotational spectrum of scopine. The results are shown in following sections.

3.2. Computational Methods.-

Assuming that the epoxy group has no effects in the N-methyl inversion and following previous theoretical studies carried out for 8-azabycicles like tropinone, we can expect, in principle, two different configurations for the scopine molecule depending on the axial or equatorial methyl amino (N-CH_3) orientation. In tropinone the equatorial form was most stable, but in scopoline the distorted ring forces the methyl group to the axial position. In order to understand the intrinsic preferences of scopine we first explored the full conformational landscape of the molecule using molecular mechanics methods (implemented in Macromodel[16]). Six different structures were detected within an energy window of 20 kJ·mol^{-1}, including both axial and equatorial configurations. In figure 3.3, the six conformers are shown labelled from the most stable to the most energetic structure.

Full geometry optimizations were carried out later for the six conformers and vibrational frequency calculations were performed to obtain the spectroscopic parameters of each configuration. The ab initio calculations used the second-order Møller-Plesset (MP2) method with the Pople triple-ζ basis set 6-331++G(d,p). All the calculations were implemented in Gaussian 09.[17]

In the following table, the predicted rotational and centrifugal distortion constants, the electric dipole moments and the ^{14}N nuclear quadrupole coupling tensor elements are listed.

Table: 3.1.- Rotational constants (A, B, C), electric dipole moments (μ_α, α = a, b, c) and diagonal elements of the ^{14}N nuclear quadrupole coupling tensor ($\chi_{\alpha\beta}$, (α,β = a, b, c)) of the six most stable conformers. The five quartic centrifugal distortion constants (D_J, D_{JK}, D_K, d_1, d_2) and the relative energy, zero point corrected, are also given.

	Theory MP2, 6-311++G(d,p)					
	Conf I	**Conf II**	**Conf III**	**Conf IV**	**Conf V**	**Conf VI**
A/MHz	1866	1869	1519	2028	2029	1521
B/MHz	1117	1104	1319	931	927	1303
C/MHz	1014	1004	1032	888	884	1023
χ_{aa} / MHz	1.50	1.49	-4.71	-1.98	-2.14	-4.70
χ_{bb} / MHz	-4.27	-4.27	1.87	-0.87	-0.73	1.83
χ_{cc} / MHz	2.77	2.78	2.84	2.86	2.87	2.86
$\lvert\mu_a\rvert$ /D	1.82	0.55	2.45	0.69	0.26	0.26
$\lvert\mu_b\rvert$ /D	1.32	0.66	2.84	0.67	1.22	1.80
$\lvert\mu_c\rvert$ /D	1.06	0.00	1.07	1.09	0.00	0.00
$\lvert\mu_{TOT}\rvert$ /D	2.48	0.86	3.91	1.46	1.25	1.82
D_J / kHz	46.97	43.41	73.78	19.72	18.89	68.36
D_{JK} / kHz	-10.74	-10.71	-0.53	81.72	79.14	-8.29
D_K / kHz	83.17	88.01	-6.66	105.18	105.13	6.84
d_1 / kHz	6.18	5.44	18.66	1.08	1.08	16.94
d_2 / kHz	6.86	6.94	41.10	-24.11	-18.90	39.09
$\Delta(E+ZPE)$/ kJ·mol^{-1}	0.0	4.7	13.1	14.1	15.6	16.4

According to the theoretical results the epoxy and the hydroxy group enlarge the number of conformational possibilities. The most stable forms are still the equatorial form within a bridged piperidinic chair, but depending of the orientation of the hydroxy group two staggered (*gauche* and *trans*) conformers are predicted (the symmetry of the molecule makes the two gauche forms equivalent). The next conformation is the N-methyl axial (OH gauche) within a piperidinic chair. Then, two equatorial structures involving a piperidine chair are also predicted. Finally, the last structure is the axial N-methyl and OH *trans*. The axial configuration is relatively far away in energy (13.1 kJ mol^{-1}) and close to the boat arrangements (see table 3.2), so in principle we would expect to observe only the two lowest-lying structures.

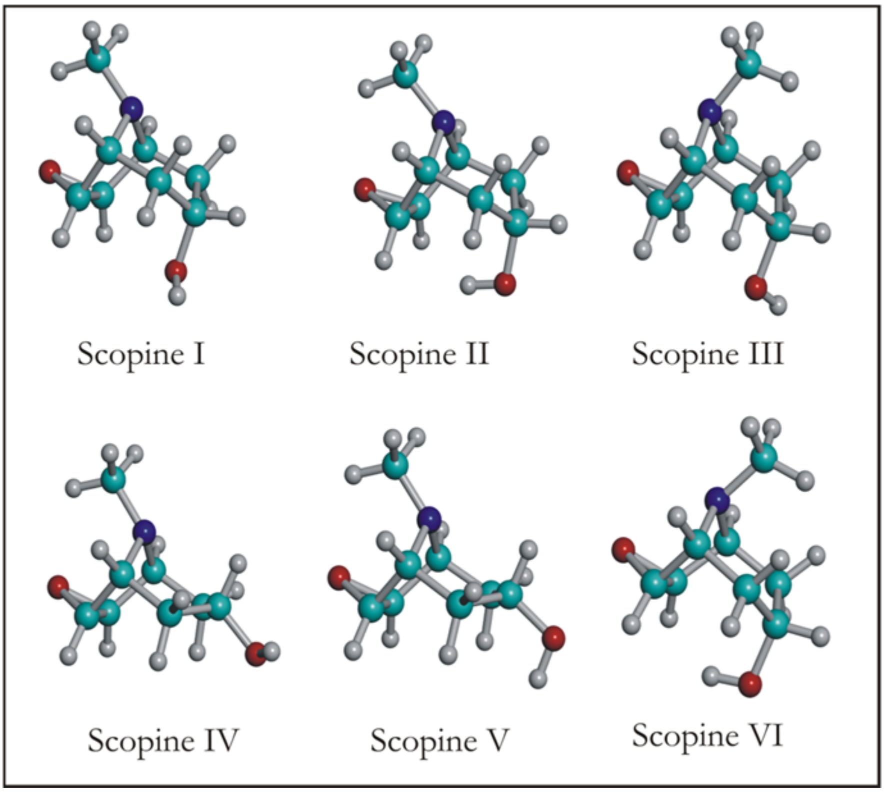

Figure: 3.3.- Geometry of the predicted stable conformers of scopine. Conformers I, II, IV and V are equatorial configurations while III and VI are conformers with the CH_3 group in the axial orientation.

3.3. Results and Analysis.-

a. Laser ablation.

The fast spontaneous rearrangement of scopine into scopoline when conventional heating systems are used to vaporize the solid sample makes impossible the detection of scopine. To avoid that reaction, the use of a different technique is needed. Since laser ablation has proved to bring intact molecules into the gas-phase with minor decomposition products, we decided to use it.

The combination of laser vaporization with MW spectroscopy requires the previous preparation of the sample as a cylindrical rod from the powder using a press. The sample is mixed with a binder to obtain a solid bar or eventually with a known compound and inserted in the instrument.

Scopine is very hygroscopic and it had to be mixed with a high quantity of glycine to estabilize the sample. As a consequence, the purity of the sample notably decreases (~30%) and the intensity of the rotational transitions decreased.

The laser beam is focused on the sample and the vaporized sample is diluted in a current of Ne as carrier gas. The fast vaporization process avoids the rearrangement of the epoxy group ledding to the detection of scopine in the rotational spectrum.

b. Assignment of the rotational spectra.

We predicted the rotational constants for the two most stable conformations of scopine. We should note that because of the symmetry plane in the *trans*-OH C_s conformation II this species would exhibit only μ_a- and μ_b-type spectra. On the other hand, the C_1 symmetry of *gauche*-OH conformation II would result in all three selections rules active. Both conformers I and II are near-prolate rotors ($\kappa_I \approx \kappa_{II} = -0.76$) respectively, and the rotational transitions were predicted using the Pickett's and JB95 programs.[18]

A progression corresponding to an ^{a}R-branch with J angular momentum quantum numbers running from 4 to 6 (K_{-1} from 0 to 2) was soon detected, but no μ_b and μ_c–type transitions were detected because of the lower intensity. We immediately noticed that each transition exhibited three different splittings: a) the instrumental Doppler effect, b) the ^{14}N nuclear quadrupole coupling interaction, and c) an additional fine interaction, not resolvable for all transitions. Since in scopine there are no possibilities for large-amplitude motions which might exchange equivalent conformations, the additional splitting must be attributed to the internal rotation of the N-methyl group. This effect was not expected, since we did not observe internal rotation in the related molecules of tropinone and scopoline.[10]

Later, we searched for a second conformation in the jet, but no other transitions could be identified. The reason is explained below.

b. Fine and Hyperfine effects: Nuclear quadrupole coupling and Internal rotation.

The presence of the ^{14}N nucleus in the molecule causes a electric interaction of the nuclear quadrupole moment with the electric field gradient at the nitrogen nucleus, providing a mechanism for the coupling of the spin and rotation angular momenta.[19] The consequences of this interaction are detected in the splitting of all the rotational transitions. As in other amines this splitting is relatively small (less than 1 MHz), so it is clearly distinguishable from the Doppler effect.

In the following figure, we show the nuclear quadrupole coupling splitting in a typical rotational transition. The additional internal rotation splitting is explained below.

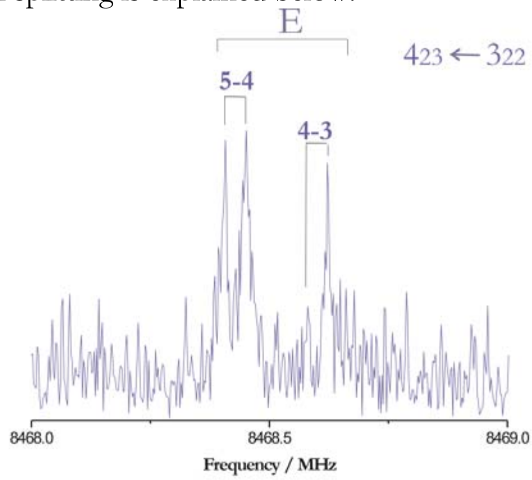

<u>Figure: 3.5.-</u> The $4_{2,3} \leftarrow 3_{2,2}$ rotational transition of scopine showing the nuclear quadrupole coupling effectsfor the E state.

The effects produced by the internal rotation of the methyl group are often detectable in the microwave spectrum when the torsion barriers are relatively small (<10-15 kJ mol^{-1}).

The methyl group is an internal rotor of three-fold (C_3) symmetry. In consequence the potential barrier for internal rotation has three equivalent minima and all energy levels are triply degenerated for infinite barriers. As the internal rotation barrier reduces, the degeneracy is partially lifted and quantum mechanical tunneling appears. The symmetry group of the internal rotor must be a subgroup of the molecular symmetry group, so the torsional levels are split into the irreducible representations A (totally symmetric) and E (doubly degenerated). The torsion Hamiltonian should be invariant to operations within the C_3 subgroup when they are carried on the methyl group. Since the molecular electric dipole moment is totally symmetric for the internal rotation, the transition moment $\langle\psi_j|\mu|\psi_i\rangle$ is finite when the transition connects torsional states of the same symmetry. In consequence, the selection rules are: A ← A or E ← E. In other words, the effect of quantum mechanical tunneling through the potential barrier is to split the triply degenerated energy states into two levels A and E. The magnitude of the splitting increases as the levels approach the top of the barrier, so these measurements allow an accurate determination of the internal rotation barriers.[20-24]

In order to analyze the experimental tunneling splittings, all the transition frequencies were fitted with the XIAM program. XIAM is a program using the Internal Axis Method (IAM) given by Woods,[25-28] which treats simultaneously the rotational Hamiltonian, the nuclear quadrupole coupling hyperfine interaction and the internal rotation. The results for scopine are shown in table 3.2. In cases of sufficient experimental data the analysis of the internal rotation specifically provides the barrier to internal rotation (V_3), the inertial moment of the internal top (I_α) and the orientation of the internal top in the principal inertial axes, given by the three angles between each principal axis and the internal rotation axis ($\sphericalangle(i,g)$, g=a, b, c). The rotational analysis used the Watson´s semi-rigid rotor Hamiltonian in the symmetric reduction and I^r representation. The results of the rotational constants, centrifugal distortion constants and nuclear quadrupole tensor parameters are shown in the following table.

Table: 3.2.- Experimental rotational constants (A, B, C), ^{14}N nuclear quadrupole coupling elements ($\chi_{aa}, \chi_{bb}, \chi_{cc}$), centrifugal distortion constants ($D_J, D_{JK}, D_K, d_1, d_2$) and internal rotation parameters (V_3, I_α and orientation of the internal rotor) for conformer I.

	Experiment Conformer I
A/MHz	1866.61 (6)[a]
B/MHz	1110.09969 (16)
C/MHz	1008.871 (2)
χ_{aa} / kHz	1.513 (98)
χ_{bb} / MHz	-0.03548 (21)
χ_{cc} / MHz	0.03397 (21)
D_J / kHz	0.0442 (27)
V_3 / kJ·mol^{-1}	6.249 (14)
I_α / kJ·mol^{-1}	3.275
∢(i,a) / deg[b]	174.01
∢(i,b) / deg	84.02
∢(i,c) / deg	90.36
N[c]	44
σ[d] / kHz	2.8

[a] Errors in parenthesis in units of the last digit.
[b] The label i denotes the axis of the internal rotor.
[c] Number of transitions (N) in the fit
[d] Standard deviation of the fit.

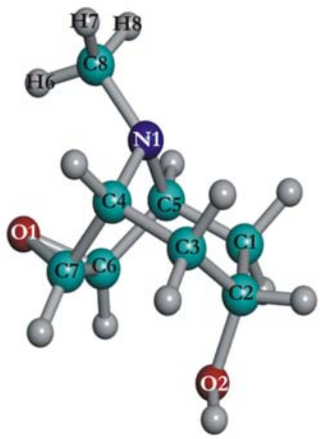

Figure: 3.6.- Molecular structure of Scopine and atom numbering..

c. Conformational assignment.

Once the rotational parameters were determined we could establish the conformational identity of the observed species. Four arguments were considered. If we check the rotational constants of conformers I and II we observe that they are very close. For both conformers, the difference respect to the experimental *A*, *B* and *C* is less than 1%. This is one of the cases in which the rotational constants alone do not provide enough basis for conformer identification. In these cases the nuclear quadrupole coupling constants are usually very effective, since they are sensitive to the electronic environment around ^{14}N and the orientation of the principal axes. However, in this case both conformers are practically identical and only differ in the orientation of a single H atom. In consequence the coupling parameters are also close and they are not useful. A third argument comes from the values of the electric dipole moment. While in conformer I μ_a is greater than μ_b, in conformer II the situation is reversed. As we did not observed μ_b-transitions we must admit that we observed the most stable conformer I of figure 3.6. A final argument comes from the conformational energies, which clearly argue in favor of conformer I by ca. 5 kJ mol^{-1}. In addition, the conversion of conformer I into II requires only a torsion around the C-O bond. Based on previous studies this barrier should be relatively low, so most probably conformer II relaxes conformationally into conformer I by collision with the carrier gas atoms. In conclusion, we can unambiguously identify the observed conformer in the jet as conformer I.

All the observed rotational transitions are listed in the following table.

Table: 3.3.- Measured and calculated frequencies in MHz for the transitions observed for conformer I of scopine. The last column represents the difference (in kHz) between the measured and calculated frequencies $\Delta\nu = \nu_{OBS} - \nu_{CALC}$.

J'	*K'₋₁*	*K'₊₁*	*J''*	*K''₋₁*	*K''₊₁*	*Sym.*	*F'*	*F''*	ν_{OBS} / MHz	ν_{CALC} / MHz	$\Delta\nu$ / kHz
4	0	4	3	0	3	A	4	3	8385.3826	8385.3810	1.6
							5	4	8385.6417	8385.6404	1.3
							3	2	8385.7178	8385.7201	-2.3
						E	4	3	8385.3826	8385.3826	0.0
							5	4	8385.6417	8385.6413	0.5
							3	2	8385.7178	8385.7213	-3.5
4	1	4	3	1	3	A	4	3	8255.9903	8255.9881	2.1
							5	4	8256.0174	8256.0176	-0.2
						E	4	3	8255.9903	8255.9903	0.0
							5	4	8256.0174	8256.0191	-1.7

Table: 3.3.- Continued.											
4	1	3	3	1	2	A	4	3	8657.5460	8657.5444	1.6
							5	4	8657.5460	8657.5426	3.4
							3	2	8657.6817	8657.6802	1.5
						E	4	3	8657.5460	8657.5427	1.5
							5	4	8657.5460	8657.6802	0.7
							3	2	8657.6817	8468.4700	1.6
4	2	3	3	2	2	A	5	4	8468.4297	8468.4293	0.5
							4	3	8468.5985	8468.5988	-0.3
						E	5	4	8468.4706	8468.4700	0.7
							4	3	8468.6426	8468.6410	1.6
4	2	2	3	2	1	A	5	4	8558.6154	8558.6183	-2.8
							4	3	8559.0573	8559.0583	-1.0
						E	5	4	8558.5779	8558.5786	-0.7
							4	3	8559.0198	8559.0203	-0.5
5	0	5	4	0	4	A	5	4	10425.6589	10425.6591	-0.2
							6	5	10425.9357	10425.9359	-0.2
							4	3	10425.9844	10425.9860	-1.6
						E	5	4	10425.6589	10425.6599	-1.0
							6	5	10425.9357	10425.9360	-0.4
							4	3	10425.9844	10425.9863	-1.8
5	1	5	4	1	4	A	5	4	10305.6315	10305.6314	0.1
							6	5	10305.6918	10305.6911	0.7
						E	5	4	10305.6315	10305.6323	-0.9
							6	5	10305.6918	10305.6915	0.2
5	1	4	4	1	3	A	5	4	10800.1961	10800.1962	-0.1
							6	5	10800.2690	10800.2660	3.0
							4	3	10800.3598	10800.3598	0.0
						E	5	4	10800.1961	10800.1962	-0.1
							6	5	10800.2690	10800.2655	3.5
							4	3	10800.3598	10800.3592	0.6
5	2	4	4	2	3	A	6	5	10573.7267	10573.7362	-9.5
							5	4	10573.7857	10573.7868	-1.2
						E	6	5	10573.7427	10573.7475	-4.8
							5	4	10573.8009	10573.7991	1.8
5	2	3	4	2	2	A	6	5	10742.4096	10742.4062	3.4
							5	4	10742.7423	10742.7402	2.1
						E	6	5	10742.3984	10742.3944	4.0
							5	4	10742.7287	10742.7289	-0.2
6	0	6	5	0	5	A	6	5	12446.1216	12446.1218	-0.2
							7	6	12446.3754	12446.3760	-0.5
							5	4	12446.4108	12446.4051	5.7
						E	6	5	12446.1216	12446.1210	0.6
							7	6	12446.3754	12446.3745	0.9
							5	4	12446.4108	12446.4037	7.1

Table: 3.3.- Continued.											
6	1	6	5	1	5	A	6	5	12348.2427	12348.2410	1.7
							5	4	12348.2908	12348.2937	-2.9
							7	6	12348.3155	12348.3135	2.0
						E	6	5	12348.2427	12348.2402	2.5
							5	4	12348.2908	12348.2927	-1.9
							7	6	12348.3155	12348.3123	3.2
6	2	5	5	2	4	A	6	5	12671.3160	12671.3201	-4.2
							7	6	12671.3290	12671.3294	-0.4
							5	4	12671.3386	12671.3386	0.0
						E	6	5	12671.3160	12671.3233	-7.4
							7	6	12671.3290	12671.3320	-2.9
							5	4	12671.3386	12671.3411	-2.5

3.4 Conclusions.-

The rotational spectrum of scopine has been analyzed to understand how the epoxy group affects the N inversion previously observed in several tropane alkaloids such as tropinone or scopoline.

The main difference between scopine and scopoline is the high reactivity of the epoxy group. Heating a sample of scopine results in the spectrum of scopoline. In order to observe the spectrum of scopine itself we combine three different techniques: laser vaporization of a solid sample, a supersonic jet expansion to stabilize the vapor products and FT-MW for obtaining the MW spectrum. The rotational study has revealed that the epoxy group does not affect the conformational equilibrium observed in tropinone, as again in scopine the equatorial conformer is the most stable species. However, while in tropinone we were able to detect both axial and equatorial species, in scopine only the most stable equatorial from was observed. Ab initio calculations are consistent with this description and offer reasonable predictions for the rotational parameters.

The rotational spectrum provided data not only on conformational equilibrium and molecular structure, but also on the potential barrier hindering the internal rotation of the methyl group. In particular, the value of the V_3 barrier was found to be 6.249 $kJ \cdot mol^{-1}$.

We can compare the value of the experimental barrier with that calculated theoretically using ab initio methods. In the following figure we estimated the periodic monodimensional potential barrier for the internal rotation. The value was found to be V_3~6 kJ·mol^{-1} which is in good agreement with the experimental value.

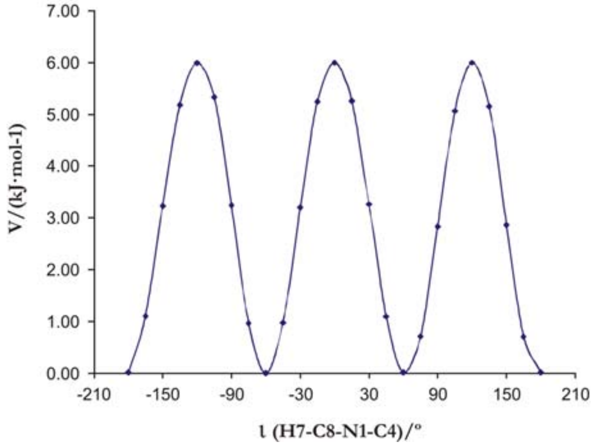

Figure: 3.7.- Theoretical energy potential curve of the internal rotor CH_3. The value of the barrier was found to be V_3~6 kJ·mol^{-1}.

Extra information on the orientation of the internal rotor with respect to the principal axes was found. They are in good agreement with the values of the angles predicted theoretically (see table below).

Table: 3.4.- Ab initio and experimental angles between the internal rotor and the principal inertial axes.

	$\measuredangle(i,a)$ / deg	$\measuredangle(i,b)$ / deg	$\measuredangle(i,c)$ / deg
Experimental	174 (1)	84.0 (7)	90.4 (3)
Ab initio	173.99	84.10	89.65

3.5 References.-

[1] M. Lounasmaa, T. Tamminen, "The tropane alkaloids" in The Alkaloids: Chemistry and Pharmacology, Vol. 44, Ed.: G. A. Cordell, Academic Press, New York, **1993**, pp. 1– 114.

[2] D. O'Hagan, *Nat. Prod. Rep.*, 17, 435, **2000**.

[3] G. Fodor, R. Dharanipragada, *Nat. Prod. Rep.*, 11, 443, **1994**.

[4]G. Fodor, R. Dharanipragada, *Nat.Prod. Rep.*, 8, 603, **1991** and references therein.

[5] P. Christen, Studies in Natural Products Chemistry, part 3, Vol. 22 (Ed.A.-U. Rahman). Elsevier, Amsterdam, **2000,** pp. 717– 749.

[6] A. Wee, F. I. Carroll, L. Woolverton, *Neuropsychopharmacology*, 31, 351, **2006**.

[7] M. Appell, W. J. Dunn III, M. E. Reith, L. Miller, J. L. Flippen-Anderson, *Bioorg. Med. Chem.*, 10, 1197, **2002**.

[8] T. Hemscheidt in *Topics in Current Chemistry*, vol. 209, Eds.: Leeper, F. J.; Vederas, J. C.

[9] E. J. Cocinero, A. Lesarri, P. Écija, J.-U. Grabow, J. A. Fernández, F. Castaño, *Phys. Chem. Chem. Phys.*, 12, 6076, **2010**.

[10] P. Écija, E. J. Cocinero, A. Lesarri, F. J. Basterretxea, J. A. Fernández, F. Castaño. *ChemPhysChem.*, 14, 1830, **2013**.

[11] A. M. Belostotskii, Z. Goren, H. E. Gottlieb, *J. Nat. Prod.*, 67, 1842, **2004**.

[12] W. Caminati, J. U. Grabow in Frontiers of Molecular Spectroscopy (Ed. J.Laane). Elsevier, Amsterdam, chap. 15, **2009**.

[13] A. Lesarri, S. Mata, E. J. Cocinero, S. Blanco, J. C. López, J. L. Alonso, *Angew. Chem. Int. Ed.*, 41, 4673, **2002**.

[14] A. Lesarri, S. Mata, J. C. López, J. L. Alonso, *Rev. Sci. Instrum.*, 74, 4799, **2003**.

[15] J. L. Alonso, E. J. Cocinero, A. Lesarri, M. E. Sanz, J. C. López, *Angew. Chem. Int. Ed.*, 45, 3471, **2006**.

[16] Macromodel, Version 9.2, Schrödinger LLc., New York, NY, **2012**.

[17] M. J. Frisch et al., Gaussian Inc., Wallingford CT, **2009**.

[18] H.M. Pickett, *J. Mol. Spectrosc.*, 148, 371, **1991**.

[19] W. Gordy, L.R. Cook, 'Microwave Molecular Spectra', 3rd Edition, in: A.Weissberger (Ed.), Techniques of Chemistry, vol. XVIII, John Wiley & SonsInc., New York, **1984**.

[20] C. C. Lin, J. D. Swalen, *Rev. Mod. Phys.*, 31, 841, **1959**.

[21] D. G. Lister, J. N. McDonald, N. L. Owen, 'Internal rotation and inversion', Academic Press Inc., New York, **1978**.

[22] K. W. Kroto, 'Molecular rotation spectra', Dover publications Inc., New York, **1992**.

[23] J. E. Wollrab, 'Rotational spectra and molecular structure', Academic Press Inc., New York & London, **1967**.

[24] I. Kleiner, *J. Mol. Spectrosc.,* 260, 1, **2010**.

[25] H. Hartwing, H. Dreizler, *Z. Naturforsh., A: Phys. Sci.*, 51, 923, **1996**.

[26] R. C. Woods, *J. Mol. Spectrosc.,* 21, 4, **1966**.

[27] R. C. Woods, *J. Mol. Spectrosc.,* 22, 49, **1967**.

[28] K. N. Rao, C. W. Mathews, in 'Molecular spectroscopy: modern research', New York, **1972**.

Chapter 4
Isobutamben

4.1. Introduction.-

The need for drugs causing sensory and motor paralysis in local areas soon attracted interest in several families of compounds with action properties different to those of general anesthetics. Generally speaking, local anesthetics bind in a reversible way to specific receptors in the Na^+ channels of the central nervous system,[1] blocking the ion potentials responsible of the nerve conduction.

One of the most common molecular families of local anesthetics is that which combines aminoester or aminoamide groups. Both are used in deontology and in solar creams as active UV absorbents.

Some examples of this kind of anesthetics include benzocaine (BZC), butamben (BTN), isobutamben (BTI), procaine (novocaine) and lidocaine, among others. Apart from several electronic spectroscopy studies on BZC,[2] both BZC and BTN have been studied by our group using microwave spectroscopy,[3,4] so we found reasonable to extend this work here to BTI.

BZC, BTN and BTI share a general formula hydr-ester-lip, where lip represents the aliphatic lipofilic ending group and hydr is a hydrophilic amine group. The particular properties of these drugs depend on the different combination of the two subunits. While the lipofilic moiety apparently acts on the action time, the hydrophilic part can also affect the action power of those anesthetics. That would imply that the acceptors sites in the Na^+ channels are mostly hydrophobic. This affinity can be understood by studying the molecular properties and binding affinities of these compounds.[1]

In the three anesthetics BZC, BTN and BTI the hydrophilic tail of the chain is always a p-aminophenyl group, while the lipophilic head is an aliphatic chain made of two or four carbons skeleton, i.e., an ethyl group in BZC, a n-butyl chain in BTN and a isopropyl group in isobutamben.[5] In all of them, the head and tail are connected by an ester group.

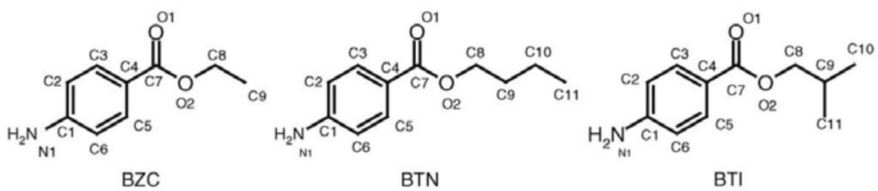

Figure: 4.1.- Chemical formulas of three local aminoester anesthetics: a) Benzocaine. b) Butamben. c) Isobutamben.

Previous molecular studies have revealed some of the structural properties of these molecules using different spectroscopic (infrared spectroscopy,[1] UV-Visible[2,4,5] or Raman[4]) and X ray-diffraction techniques.[4] Moreover, other analyses have tried to explain the interaction mechanism in anesthetic-receptor binding either theoretically[6] or experimentally.[7]

Within the experimental techniques the role of gas-phase methods is remarkable. Despite the fact that the gas phase does not represent the anesthetic in the biological environment, these studies allow determining the intrinsic molecular properties often hindered in condensed phases, making possible to compare the experimental data with the theoretical results.

In the present work we extend rotationally-resolved studies to BTI. Previous information from electronic spectroscopy in supersonic expansion for benzocaine[2] have shown two stable conformations in which the aminobenzoate skeleton is nearly planar, whereas the ethyl group (corresponding to the ending C9) can adopt, depending on the torsion angle, two alternative *anti* or *gauche* orientations which lead to two different conformations.

Since in BTI the hydrophilic moiety is the same as in the BZC and the molecules differ in the lipophilic chain, we would expect, in principle, that we could find different configurations depending on the orientations of the C9 carbon. Additionally, for each configuration we could achieve different orientations of the isopropyl terminal carbons, which depend on the torsion angles $\tau(C10 - C9 - C8 - O2)$ and $\tau(C11 - C9 - C8 - O2)$.

It is thus clear that the increment of the number of carbons in the aliphatic chain cause some additional degrees of freedom in the conformational space compare to the simpler BZC. This fact gives more complexity to the Potential Energy Surface (PES), where several local minima must be analyzed within the ground vibronic state (only accessible in the jet expansion).

The methodology followed in the study of BTI starts with a theoretical part which includes the conformational search and calculations of the structural and electric properties of the detected conformers, followed by a second experimental part recording the microwave spectra and the most characteristic rotational transitions of the molecule. The conformational landscape of BTI was first explored using molecular mechanics (MM). MM is able to quickly predict the most stables structures according to an empirical molecular force field. Despite classical mechanics does not offer a good prediction of conformational energies, this initial screening is very convenient to provide a systematic search of molecular structures. Once the conformational search is over, ab-initio and DFT calculations were performed in order to obtain accurate calculations for each stationary point of the PES, including the global and local minima. The molecular orbital study is completed with vibrational frequency calculations, which characterize the stationary points and provide vibrational energy corrections and thermodynamic properties (in particular the Gibbs free energy).

In the case of BTI, both the first principle calculations and the density functional theory provided us with five different conformations within an energy window of ca. 2 kJ mol^{-1}. Despite the small energy gap, which in principle makes all these conformations thermally accessible, not all of them could be populated because of collisional relaxation in the jet. Populations in a supersonic expansion are kinetically modulated by molecular collisions between the sample and the carrier gas[8], so frequently some of the expected conformations are not detected in the experimental spectrum revealing that interconversion barriers are low. In this work, only the two most stable structures were found with the FTMW spectrometer described in chapter 1. The energy gap between the observed species is about 0.1kJ mol^{-1}., making those structures practically isoenergetic. The next figure shows the geometry of the detected structures.

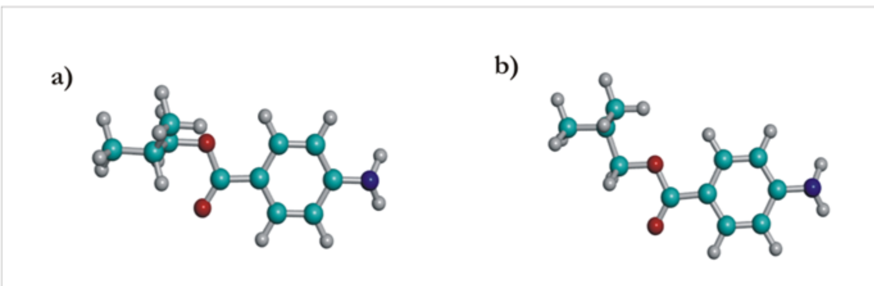

Figure: 4.2.- (a) Most stable conformer of isobutamben (Conformer 1, E~ -631.7892 Hartree). **(b)** Conformer 2, 0.1 kJ mol^{-1} higher in energy than conformer 1.

4.2. Computational Methods.-

The computational procedure was described in previous chapters (Chap. 1). The theoretical calculations are required to describe the PES and to determine several relevant properties for the rotational study of the molecule, such as structural properties (moment of inertia or rotational constants) and electric properties (molecular dipole moments, nuclear quadrupole coupling constants). This information is needed for the initial predictions of the rotational transitions of the molecule, helping to clarify the most convenient frequency regions and most intense transitions.

In the case of BTI, we first started a conformational search using MM calculations. The force field used was MMFF. The conformational search used both Monte-Carlo and large-scale low-mode vibrational frequency calculations. Optimization and conformational search were carried out with Hyperchem,[9] Macromodel and Maestro[10] programs. The less energetic structures were identified and a first list of conformers was made. The selected structures received full geometry reoptimization, including vibrational frequency calculations with ab initio (MP2) and DFT (B3LYP and M06-2X) methods. Several Pople basis sets were used in the calculations, including double- and triple-ζ functions with polarization and diffuse functions (6-31G and 6-311++G(d,p)). All the theoretical calculations were implemented in Gaussian 09.[11] The latter basis set has demonstrated that provides satisfactory results for the spectroscopic parameters in similar organic molecules.

4.3. Results and Analysis.-

a. Assignment of the Rotational Spectrum.

Once the MP2 and M06-2X calculations were performed for all the conformers found with MM, we selected the less energetic structures as plausible conformers to be detected in the experimental spectra.

According to the results in table 4.1, we can expect in the isobutamben spectrum transitions belonging to the five most stable structures shown in figure 4.3. The remaining structures obtained with MM are not interesting in our rotational analysis due to the high energy gap (> 10 kJ mol^{-1}) with respect to the predicted global minimum.

For the five structures the aminobenzoate moiety is nearly planar (the pyramidal configuration of the NH_2 amino group would displace its hydrogen atoms slightly out of the plane). However, the carbon chain associated to the C10 and C11 atoms results in several non-planar skeletons for the isopropyl group. (See figure 4.1 for atom numbering).

Due to the structural similarity in the lipophilic moiety of the molecule, we have defined each conformation by the torsion angles $\tau_1(C_9 - C_8 - O_2 - C_7)$ and $\tau_2(H - C_9 - C_8 - O_2)$, which are the torsion angles associated with the C_β carbon and the H_β hydrogen, respectively.

Table: 4.1.- Rotational Constants (*A*, *B* and *C*), electric dipole moments (μ_a, α = a, b, c) and diagonal elements of the nuclear quadrupole tensor for ^{14}N ($\chi_{\alpha\beta}$, α,β = a, b, c) of the most stable conformers optimized with the MP2 and M06-2X methods. Centrifugal distortion constants (Δ_J, Δ_{JK}, Δ_K, δ_K and δ_K) are also shown. The ΔE value indicates the energy gap between each conformer with respect the energy of the less energetic conformer (zero point energy corrected, ZPE). ΔG calculated at 298K and 1 atm.

Theory MP2 / M06-2X	BTI 1 (RG-)	BTI 2 (TG+)	BTI 3 (TT)	BTI 4 (RT)	BTI 5 (RG+)
***A* / MHz**	1994.8 / 1999.0	1829.9 / 1838.1	1501.9 / 1508.0	1602.9 / 1615.1	2023.2 / 2053.5
***B* / MHz**	287.2 / 289.2	281.6 / 284.1	314.6 / 317.4	323.0 / 326.3	285.3 / 286.7
***C* / MHz**	267.7 / 268.9	250.7 / 252.4	276.2 / 278.4	295.0 / 298.0	271.3 / 272.5
χ_{aa} / MHz	2.7 / 2.7	2.5 / 2.5	2.4 / 2.4	2.7 / 2.7	2.7 / 2.7
χ_{bb} / MHz	1.1 / 1.3	1.6 / 1.9	2.0 / 2.2	1.4 / 1.7	1.8 / 2.1
χ_{cc} / MHz	-3.8 / -4.0	-4.1 / -4.5	-4.4 / -4.7	-4.1 / -4.4	-4.5 / -4.8
$\|\mu_a\|$ / D	2.0 / 2.4	1.5 / 1.9	1.3 / 1.7	1.8 / 2.3	1.9 / 2.3
$\|\mu_b\|$ / D	1.5 / 1.8	2.2 / 2.6	2.4 / 2.8	1.8 / 2.1	1.9 / 2.2
$\|\mu_c\|$ / D	1.0 / 0.8	1.4 / 1.2	1.0 / 0.89	0.87 / 0.69	0.71 / 0.46
$\|\mu_{TOT}\|$ / D	2.7 / 3.1	3.0 / 3.4	2.9 / 3.4	2.7 / 3.2	2.8 / 3.2
Δ_J / kHz	0.012 / 0.010	0.004 / 0.005	0.007 / 0.007	0.023 / 0.026	0.013 / 0.010
Δ_{JK} / kHz	-0.18 / -0.14	-0.04 / -0.06	-0.03 / 0.08	-0.18 / -0.25	-0.16 / -0.14
Δ_K / kHz	2.9 / 2.3	0.84 / 0.90	0.42 / 0.31	1.8 / 1.9	3.6 / 2.6
δ_J / kHz	0.001 / 0.001	0.001 / 0.001	0.001 / 0.002	0.002 / 0.002	0.000 / 0.000
δ_K / kHz	0.13 / 0.03	0.06 / 0.05	0.12 / -0.17	0.77 / -0.1	0.53 / -0.25
ΔG / kJmol^{-1}	0.0 / 0.0	0.3 / -5.0	-1.0 / -5.2	0.7 / -1.6	-0.2 / -1.0
Δ (E+ZPE)/ kJ mol^{-1}	0.0 / 0.0	1.5 / 0.7	2.1 / 0.9	2.4 / 2.0	2.5 / 1.9

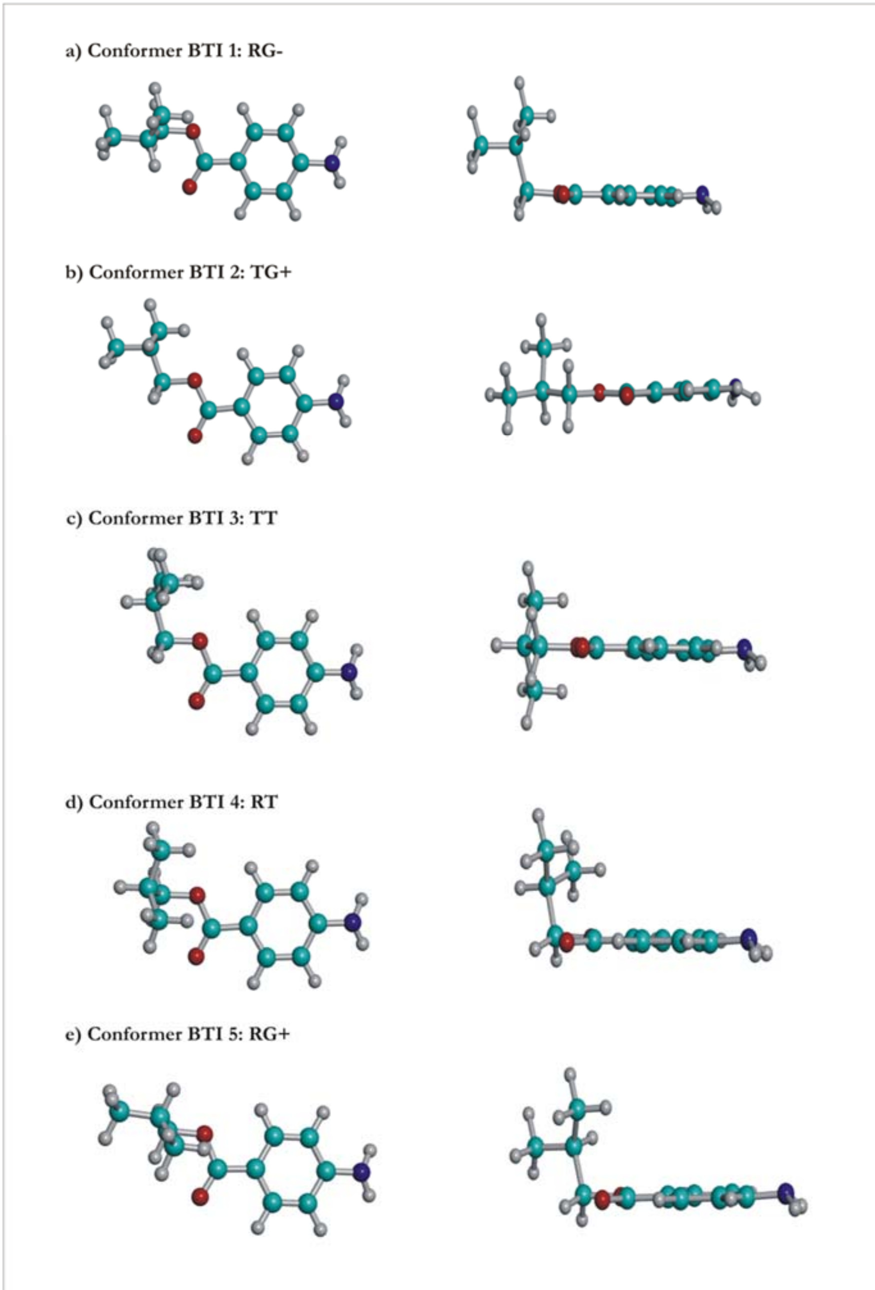

Figure: 4.3.- Molecular structure of the five most stable conformers of isobutamben (BTI) in two different views (plane of the aminobenzoate group, left; and in its perpendicular plane, right). **a)** Less energetic conformer E~ -631.7892 Hartree (Conformer 1). **b)** Conformer 2, with energy 0.7kJ mol^{-1} higher than the conformer 1. c) Conformer 3 ($\Delta E = 0.9\mathrm{kJ} \cdot \mathrm{mol}^{-1}$). d) Conformer 4 ($\Delta E = 0.9\mathrm{kJ} \cdot \mathrm{mol}^{-1}$. e) Conformer 5 ($\Delta E = 0.9\mathrm{kJ} \cdot \mathrm{mol}^{-1}$).

Attending to the C_β dihedral angle, we can distinguish two different families. One in which the torsion is close to the right angle R ($\tau_1 \sim 90°$), that includes conformers 1, 4 and 5. The second family is formed by the conformers 2 and 3, in which the C_β carbon of the isopropyl group is in *trans* position (T, $\tau_2 \sim 180°$).

Within each of these families, we can also sort the conformers depending on the H_β orientation. Hence, for the R family we have one *trans* (conformer 4, RT) and two *gauche* species (conformer 1, RG-, $\tau_2 \sim -60°$, and 5, RG+, $\tau_2 \sim +60°$).

In the particular case of conformers 2 and 3, we find $\tau_2 \sim +60°$ or $\tau_2 \sim 180°$, so we name these two structures as TG+ and TT respectively.

We predicted the rotational spectrum for each conformation using the theoretical parameters for the center frequencies and hyperfine effects. For this objective, we considered the types of rotor for this molecule, all of them near-prolate asymmetric rotors ($\kappa \approx$ -0.98 for the first conformer, $\kappa \approx$ -0.94 to -0.98 for the other species). The spectrum predictions used the Watson's semi-rigid rotor Hamiltonian[12] and provided the frequencies and intensities of the spectral lines at the estimated temperature in the supersonic jet ($T_{rot} \sim 2K$). The predictions used both Pickett's SPCAT program[13] and graphical NIST's JB95 simulations.[14]

All the most stable conformers of BTI are rotors with non-zero electric dipole moment components (μ_a, μ_b, μ_c) along the three principal inertial axes. In conformer 1 (RG-) μ is dominant in the *a* –axis, less intense in *b*-axis and even smaller in the *c* –axis. For the remaining conformers μ is dominant in the *b*-axis, followed by the *a*-axis and less intense in the *c*-axis. Therefore, to carry out the assignment of the experimental data, we predicted and measured preferentially R branch (J+1 $\leftarrow$ J) transitions of type μ_a and μ_b in both cases. The μ_c-type lines intensity is much lower compared with the other two.

The figure below shows a simulation of the ^{a}R type spectrum predicted for the most stable conformer, in which we can see the characteristic pattern of near-prolate asymmetric rotors. This pattern shows groups of lines belonging to transitions $(J+1) \leftarrow J$, each angular momentum quantum number separated from the previous one by a distance approximately equal to the value of $B+C$.[12]

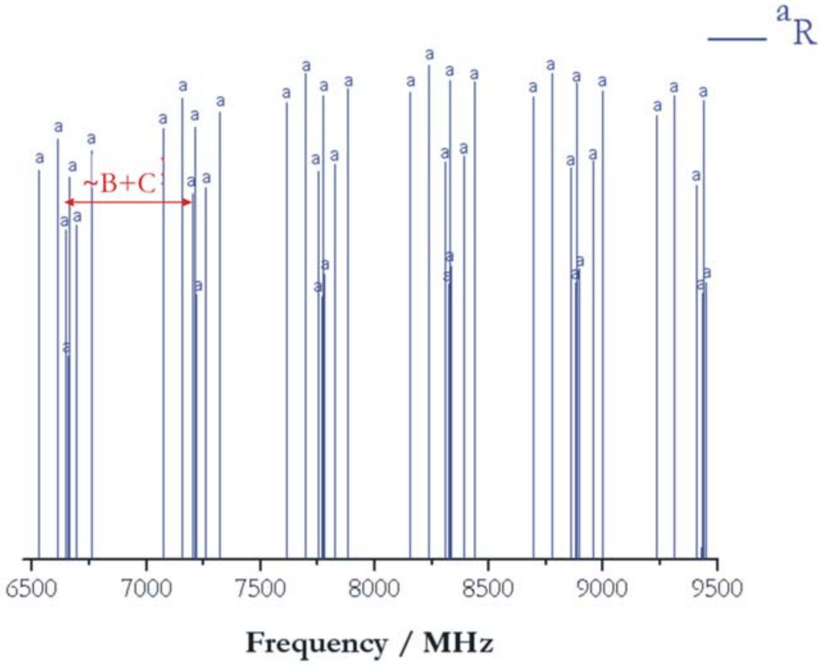

Figure: 4.4.- ^{a}R-type spectrum predicted for the less energetic conformer.

For BTI the values of $(B+C)$ are about 550 MHz, and the different series are relatively close to each other.

For each ^{a}R series, the prediction gives us the frequency of all the transitions originated by the different values of the pseudo quantum numbers K_a and K_c. Because of the asymmetry doubling there are two transitions for each K_a (except for $K_a = 0$) for a given series $J+1 \leftarrow J$. This fact explains the $2J+1$ group of lines found for each J value. Within each series the asymmetry splitting reduces progressively, so the lines with the larger values of the pseudo quantum number K_a become closer and eventually colapse. The intensities of the transitions within a given series decrease as the K_{1} value increase due to the Boltzmann factor.

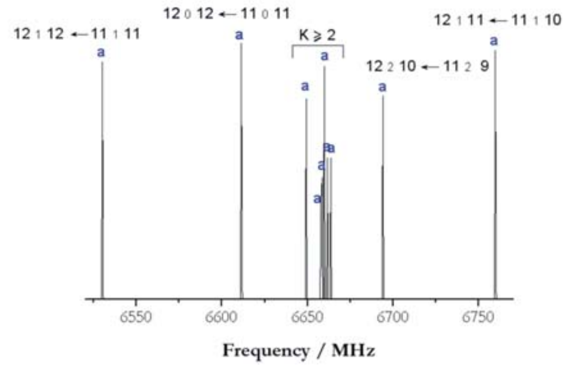

Figure: 4.5.- The J+1= 12 ⟵J =11 series of the μ_a–type spectrum simulated for the less energetic conformer (RG-).

For the *b* and *c* type there are no such characteristic patterns which can be useful for the assignment. Even so, the prediction with the ab initio rotational constants helps us to establish a range of interest where series of μ_b–type lines can be found and therefore the measurement is optimized. In our case, this area or region of interest is located in the frequency range 7700 - 9500 MHz as reflected in the following picture.

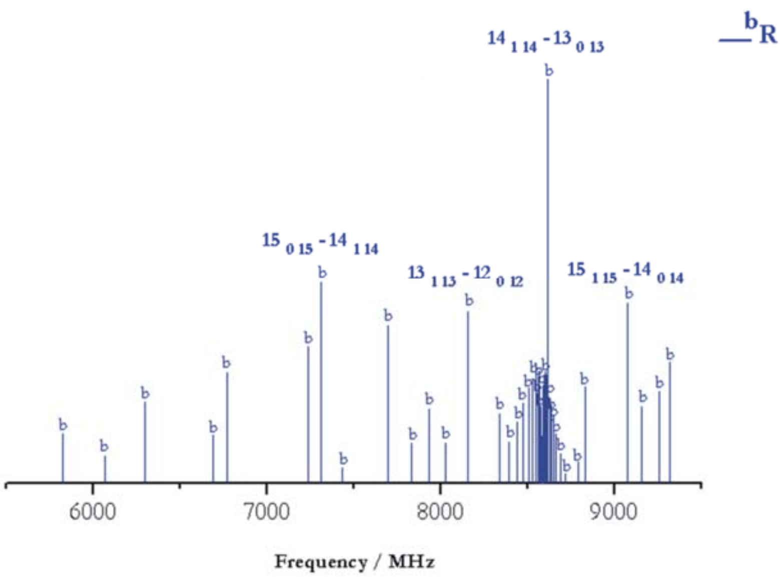

Figure: 4.6.- Part of the μ_b spectrum predicted for the most stable conformer RG-.

Following the predictions we scan the spectrum in the range 6800-8000 MHz, part of which is shown in the following figure.

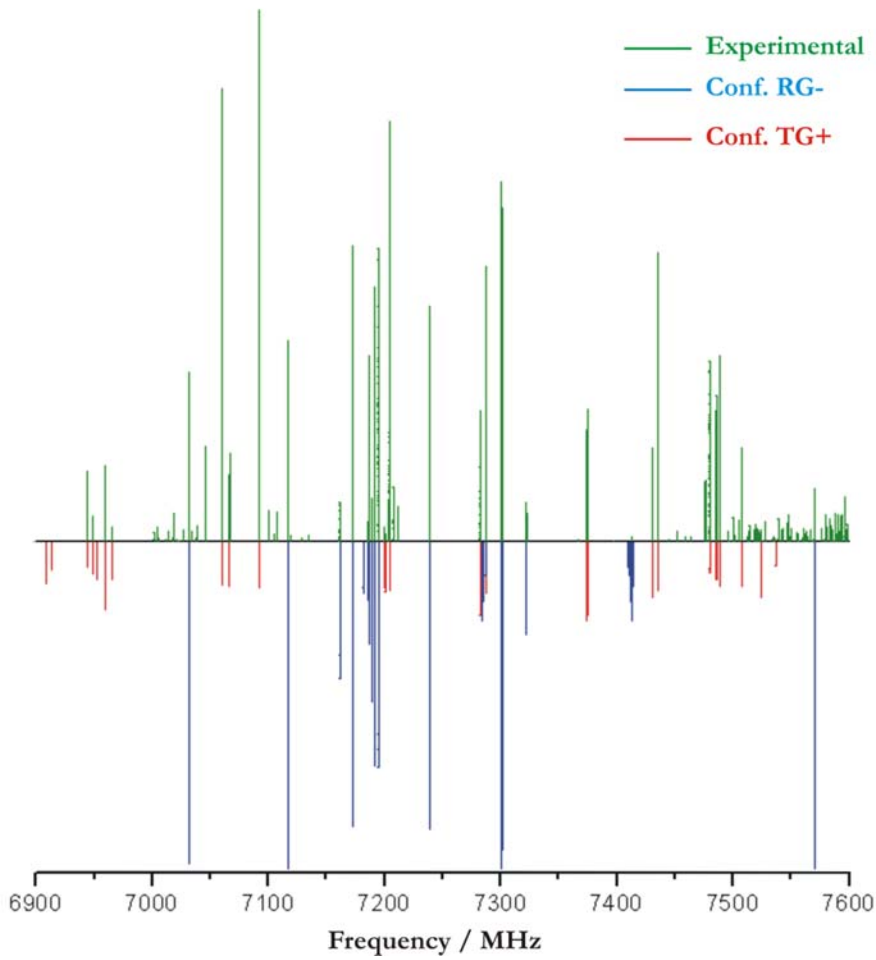

Figure: 4.7.- Section of the initial scan made for the BTI anesthetic, showing the assigned transitions for the most stable conformers. It is important to notice that there are some differences between the intensities of the experimental spectrum and the fitted ones, because of the superposition of short scans in which the conditions are not uniform due to the heating process used to vaporize the sample.

Once we collected the experimental frequency data of the sample in the range of interest, we started the analysis of the spectrum.

b. Hyperfine effects: Nuclear quadrupole coupling.

BTI has a ^{14}N nucleus with a nuclear spin larger than one half: I=1. This means that the atom has a non-spherical distribution of the nuclear charge and in consequence it is characterized by a quadrupolar nuclear moment (Q= 20,44(3)mb). The electric interaction between the nuclear quadrupole and the molecular electric field gradient at the nucleus site provides a mechanism for the angular momentum coupling between the nuclear spin (***I***) and the molecular rotational angular moment (***J***), resulting in a total momentum of ***F***=***I***+***J*** (=|I+J|,… |I-J|) (See chap. 1). As a consequence, a splitting in the rotational transitions appears, whose magnitude depends on the quadrupolar moment. In general, Q will depend on the nuclear charge and can change up to five orders of magnitude depending of the considered atom. The splitting will also depend on the number of quadrupolar nuclei. In BZI, and due to the small quadrupolar moment of ^{14}N the transition splittings are also small (< 1MHz), as can be seen in the following figures. These pictures are an example of the transition $15_{1,15} \leftarrow 14_{1,14}$ observed for the RG- and TG+ conformers, respectively.

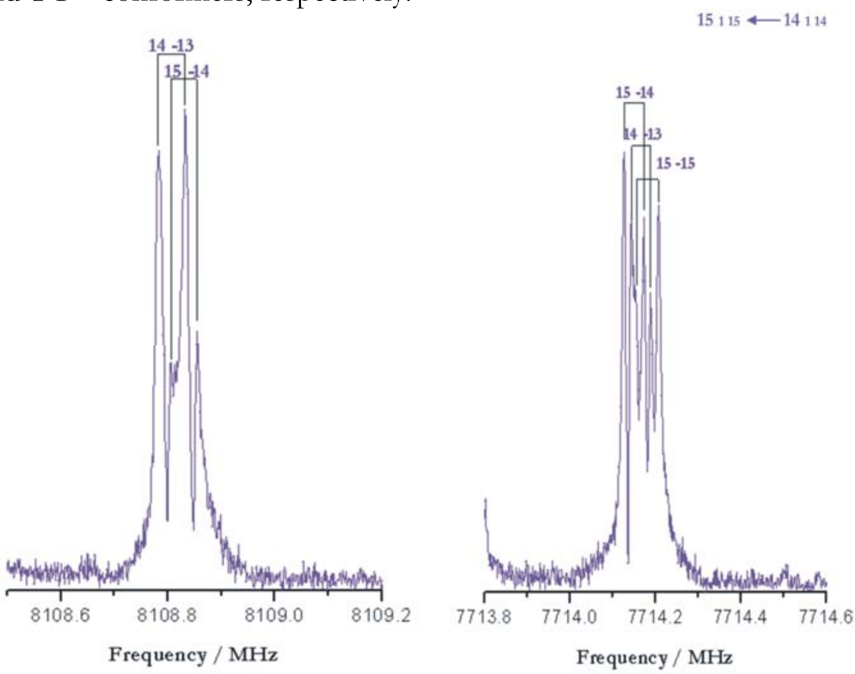

Figure: 4.8..- **(a)** The $15_{1,15} \leftarrow 14_{1,14}$ transition of conformer 1 (RG-). **(b)** The same transition for the second conformer TG+. The hyperfine components have been labeled with quantum numbers F´←F´´.

The hyperfine effects let us calculate the coupling tensor elements $\chi_{\alpha,\beta}(\alpha, \beta = a, b, c)$ and to obtain some information about the electronic environment in the proximities of the quadrupolar atom, since the tensor $\boldsymbol{\chi}$ is directly proportional to the electric field gradient at the nucleus according to $\boldsymbol{\chi}=eQ\boldsymbol{q}$ (Chap. 1). This strong dependency with the electronic environment, together with the dependence with the orientation of the principal inertial axes, allows the identification and discrimination of the different conformers in the sample, especially when the rotational constants of them are very similar (i.e. conformer 1 and 2).

c. Determination of spectroscopic parameters.

Despite the predicted small energy gap between the five low-lying conformers, experimentally we were only able to identify transitions belonging to the two most stable structures (conformers RG- and TG+). This 'conformer loss' in the supersonic expansions is due to the collisional relaxation of the more energetic structures into the less energetic conformers when energy barriers are affordable. In other words, the more energetic conformers collide with the carrier gas atoms (Ar, Ne), and interconvert in other more stable structures. Hence, in the jet-cooled spectrum we cannot always detect transitions related with all the conformers predicted to be thermally accessible.[15]

To observe this relaxation phenomenon, the interconversion barrier between conformers must be lower than a threshold value, which empirically depends on the number of structural degrees of freedom and on the energy difference between confromations. For this reason it is convenient to know the interconversion paths and to calculate the barrier heights using theoretical methods.

For conformational interconversion involving only one degree of freedom several studies[16] point to a barrier threshold of about ~ 400 cm^{-1}, while this value increases till about 1000 cm^{-1} in the case of conversions in which there are more torsions involved.[17, 18]

For BTI we can conceive monodimensional relaxation processes between conformer 3 and the second conformation, and between conformers 4 and 5 into the less energetic one. Theoretical calculations can then be applied to investigate the magnitude of the interconversion barriers.

The experimental rotational transitions (see table 4.3 and 4.4) for the observed conformers were fitted using the semi-rigid Watson Hamiltonian in the asymmetric reduction (A) and in the I^r representation, with an additional term which takes into account the nuclear quadrupole interaction. The I^r representation is suitable for prolate rotors[12] like the molecule we are analyzing, while the A and S reductions are in principle adapted to symmetric or asymmetric rotors respectively. The results of the fit for the rotational constants, centrifugal distortion and nuclear quadrupole tensor parameters are shown in the following table.

Table: 4.2.- Experimental rotational constants *A*, *B* and *C*, nuclear quadupole coupling elements of ^{14}N ($\chi_{aa}, \chi_{bb}, \chi_{cc}$) and centrifugal distortion constants ($\Delta_J, \Delta_{JK}, \Delta_K$) for the conformers found in the spectrum. Besides, the number of transitions used in the fit (N^t) and the standard deviation (σ) are shown.

	Experiment	
	BTI 1 (RG-)	BTI 2 (TG+)
A **/ MHz**	1988.564 (10)[a]	1831.7140 (54)
B **/ MHz**	286.80483 (15)	282.57210 (20)
C **/ MHz**	265.83394 (15)	251.02624 (30)
Δ_J **/ kHz**	0.01044 (37)	0.00378 (71)
Δ_{JK} **/ kHz**	-0.1608 (54)	-0.0480 (14)
Δ_K **/ kHz**	-26. (10)	-2.35 (39)
χ_{aa} **/ MHz**	2.73 (26)	2.256 (51)
χ_{bb} **/ MHz**	0.38 (14)	0.969 (39)
χ_{cc} **/ MHz**	-4.47 (14)	-4.353 (39)
N	43	40
σ **/ kHz**	2.4	1.9

[a] Standard error in parenthesis in units of the last digit.

Table: 4.3.- Observed (ν_{obs}) and calculated (ν_{calcs}) frequencies (MHz) of the transitions detected for the RG- conformer. The third column represents the difference (kHz) between measured and calculated frequencies ($\Delta\nu = \nu_{OBS} - \nu_{CALC}$).

J'	K'_{-1}	K'_{+1}	J''	K''_{-1}	K''_{+1}	F'	F''	ν_{OBS} / MHz	ν_{CALC} / MHz	$\Delta\nu$ / kHz
13	1	13	12	1	12	14	13	7032.2815	7032.2838	-2.3
						12	11	7032.2945	7032.2946	-0.1
						13	12	7032.3095	7032.3059	3.6
13	0	13	12	0	12	12	11	7117.8541	7117.8602	6.0
						13	12	7117.9174	7117.9181	-0.7
11	1	11	10	0	10	12	11	7161.9787	7161.9794	-0.8
						11	10	7162.6358	7162.6313	0.5
13	2	12	12	2	11	14	13	7173.1215	7173.1204	1.1
						12	11	7173.1215	7173.1231	-1.6
						13	12	7173.1462	7173.1458	0.4
13	5	9	12	5	8	12	11	7187.6535	7187.6516	1.9
						14	13	7187.6535	7187.6536	0.0
13	3	11	12	3	10	14	13	7191.8768	7191.8773	-0.5
13	3	10	12	3	9	14	13	7195.1703	7195.1680	2.3
						12	11	7195.1703	7195.1718	-1.4
						13	12	7195.1811	7195.1823	-1.1
13	2	11	12	2	10	13	12	7239.3802	7239.3806	-0.5
						14	13	7239.4136	7239.4157	-2.1
13	1	12	12	1	11	12	11	7301.6175	7301.6164	1.1
						14	13	7301.6175	7301.6167	0.7
						13	12	7301.6440	7301.6407	3.3
15	0	15	14	1	14	15	14	7322.0961	7322.0946	1.6
14	0	14	13	0	13	15	14	7655.3328	7655.3324	0.4
						13	12	7655.3328	7655.3336	-0.8
						14	13	7655.3984	7655.3945	3.9
14	2	12	13	2	11	14	13	7804.2319	7804.2301	1.8
						15	14	7804.2703	7804.2680	2.3
						13	12	7804.2703	7804.2737	-3.4
14	1	13	13	1	12	13	12	7859.5903	7859.5900	0.3
						15	14	7859.5903	7859.5907	-0.4
						14	13	7859.6123	7859.6163	-4.0
13	1	13	12	0	12	12	11	8071.0995	8071.0979	1.6
						13	12	8071.7072	8071.7111	-3.9
15	1	15	14	1	14	14	13	8108.8076	8108.8101	-2.5
						15	14	8108.8301	8108.8253	4.9
15	0	15	14	0	14	14	13	8191.2216	8191.2229	-1.3
						15	14	8191.2848	8191.2842	0.6
15	2	14	14	2	13	14	13	8272.1909	8272.1939	-3.1
						15	14	8272.2142	8272.2130	1.1
15	2	13	14	2	12	15	14	8370.2067	8370.2029	3.7
						14	13	8370.2449	8370.2473	-2.5
15	1	14	14	1	13	14	13	8416.6298	8416.6312	-1.5
						15	14	8416.6603	8416.6595	0.8

Table: 4.4.- Observed (ν_{obs}) and calculated (ν_{calcs}) frequencies (MHz) of the transitions detected for the TG+ conformer. The third column represents the difference (kHz) between measured and calculated frequencies ($\Delta\nu = \nu_{OBS} - \nu_{CALC}$).

J'	K'_{-1}	K'_{+1}	J''	K''_{-1}	K''_{+1}	F'	F''	ν_{OBS} / MHz	ν_{CALC} / MHz	$\Delta\nu$ / kHz
13	0	13	12	0	12	14	13	6785.3093	6785.3108	-1.5
						12	11	6785.3172	6785.3170	0.2
13	2	12	12	2	11	14	13	6909.3553	6909.3533	2.0
						12	11	6909.3553	6909.3552	0.0
						13	12	6909.3873	6909.3854	1.9
13	7	7	12	7	6	14	13	6941.4441	6941.4454	-1.3
						13	12	6941.5513	6941.5521	-0.8
13	5	9	12	5	8	12	11	6945.0749	6945.0711	3.8
						14	13	6945.0749	6945.0726	2.3
						13	12	6945.1282	6945.1241	4.1
13	4	10	12	4	9	14	13	6949.2621	6949.2609	1.1
						13	12	6949.2861	6949.2900	-3.9
13	4	9	12	4	8	14	13	6949.6621	6949.6624	-0.3
						13	12	6949.6885	6949.6906	-2.1
13	3	11	12	3	10	14	13	6953.2628	6953.2665	-3.6
						12	11	6953.2746	6953.2732	1.3
						13	12	6953.2895	6953.2853	4.2
12	1	12	11	0	11	11	10	6959.6103	6959.6089	1.3
						13	12	6959.6396	6959.6422	-2.6
13	3	10	12	3	9	13	12	6966.4764	6966.4801	-3.7
						12	11	6966.4879	6966.4879	0.0
13	2	11	12	2	10	14	13	7060.3836	7060.3828	0.9
13	1	12	12	1	11	12	11	7092.2809	7092.2790	1.9
						14	13	7092.2809	7092.2821	-1.3
						13	12	7092.3257	7092.3256	0.1
15	3	12	15	2	13	15	15	7200.9431	7200.9422	0.9
14	1	14	13	1	13	13	12	7205.1930	7205.1929	0.1
						14	13	7205.2201	7205.2175	2.6
15	0	15	14	1	14	14	13	7283.0890	7283.0910	-2.0
14	0	14	13	0	13	15	14	7288.3014	7288.3020	-0.6
						13	12	7288.3014	7288.3030	-1.6
14	3	11	14	2	12	13	13	7322.5078	7322.5068	1.0
						15	15	7322.5367	7322.5373	-0.6
						14	14	7322.9622	7322.9635	-1.3
13	1	13	12	0	12	12	11	7374.9151	7374.9161	-0.9
						14	13	7374.9423	7374.9416	0.6
14	2	13	13	2	12	15	14	7435.9334	7435.9324	1.0
						13	12	7435.9334	7435.9349	-1.5
						14	13	7435.9638	7435.9637	0.2
15	0	15	14	0	14	14	13	7789.5810	7789.5801	0.9

The spectroscopic parameters (rotational constants and the nuclear quadrupole parameters) match unambiguously with the theoretical predictions. If the fit values are compared with those predicted ab initio (table 4.1), it is easy to note that the observed conformers are RG- and TG+ respectively, predicted theoretically as the most stable ones.

Apart from the transitions belonging to the identified conformers, in the experimental spectrum there are some transitions (see figure 4.7) which apparently do not belong to them or to the higher energy conformers (TT, RT or RG+). Those lines might correspond to impurities of the sample or to decomposition products generated in the vaporization process.

On the other hand, it is possible to see in figure 4.7 that the transition intensities of the measured lines are not exactly the same as those predicted theoretically in some regions of the scan. The reason is the way of acquisition of the spectrum. The whole scan for BTI is made by the superposition of several small scans and the conditions are not exactly the same along all the experiment: different sample quantity, different heating, different valve apertures, etc.

As we can notice looking at table 4.2, we are able to fit only 3 out of 5 quartic centrifugal distortion constants for the observed conformers. The reason is the kind of transitions measured, since all of them have relatively low quantum numbers. A more detailed treatment of the centrifugal distortion would require measurements of the spectrum in the millimeter wave region.

Concerning the nuclear quadrupole tensor we fitted only its diagonal terms. The remaining non-diagonal terms are not sensitive to the transitions measured. Generally it is not possible to fit the whole tensor for amine groups unless a large set of transitions is determined.

The rotational constants *B* and *C* are determined with larger accuracy than for the *A* constant. This is due to the kind of transitions used in the fit, because the number of ^{a}R transitions is much larger than those of μ_b- or μ_c-type. Despite this consideration, the fit quality is high, as its rms deviation (2.4 kHz) is below the estimated accuracy of the experimental frequencies (<3 kHz).

d. Conformer Abundances: Estimation from relative intensity measurements.

To achieve information about the abundances of the detected conformers in the supersonic jet, we can study the relative intensities (*I*) of the rotational transitions. This can be done because there is a direct relation between the intensities and the numerical density of each conformer in the jet (N_j). The relation between them also includes the dipole moment along each axis (μ_i) according to the following expression:

$$\frac{N_j}{N_1} \propto \frac{I_j \omega_1 \Delta\nu_j \mu_i^2(1) \gamma_1 \nu_1^2}{I_1 \omega_j \Delta\nu_1 \mu_i^2(j) \gamma_j \nu_j^2} \propto \frac{I_j}{I_1} \cdot \frac{\mu_i(1)}{\mu_i(j)}$$

where ω is the conformational degeneration, $\Delta\upsilon$ the line width at half height and γ the line strength.[19]

In this way, if the transition intensities are well-known for the different conformers, it is possible to estimate the abundance of each conformer respect to the most stable.

It is important to remark that this analysis assumes that the supersonic expansion populates only the ground vibrational within each conformer well, and that there is no conformational relaxation between conformers.

However, in our case, some conformational relaxation takes place in the jet: conformer 4 and 5 may convert to conformer 1 and conformer 3 to the second stable. As a consequence, we will overestimate the population of the RG- and TG+ conformers.

Another important fact is that the calculation of relative intensities strongly depends on several experimental factors, so this is an approximate method and its accuracy respect to the frequency precision is much lower.

We show in Table 4.5 a set of relative intensity measurements for a set of 10 transitions from the two observed RG- and TG+ conformations of BTI. From these measurements we estimated the relation between the two populations as $N(Conf.TG+)/N(Conf.RG-) = 0.38 \pm 0.05$. This result supports the fact that the conformer predicted as most stable (RG-) is the most abundant in the supersonic jet.

Tabla: 4.5.- Intensities (in arbitrary units) of the two conformers 1 and 2 for each μ_a and μ_b type transitions selected.

Transition	***I* (RG-)**	***I* (TG+)**
$7_{1\,6} \leftarrow 6_{0\,6}$	0.21	0.21
$13_{0\,13} \leftarrow 12_{0\,12}$	0.48	0.30
$13_{1\,12} \leftarrow 12_{1\,12}$	0.75	0.30
$14_{2\,12} \leftarrow 13_{2\,11}$	0.85	0.46
$15_{0\,15} \leftarrow 14_{1\,14}$	0.19	0.19
$13_{1\,13} \leftarrow 12_{0\,12}$	0.29	0.18
$13_{6\,8} \leftarrow 12_{6\,7}$	0.29	0.12
$13_{3\,10} \leftarrow 12_{3\,9}$	0.69	0.35
$13_{5\,9} \leftarrow 12_{5\,8}$	0.69	0.18
$13_{2\,12} \leftarrow 12_{2\,11}$	0.98	0.31

4.4 Conclusions.-

A rotational analysis has been completed for BTI. While theoretically five low energetic conformations could be populated, only two of them (the two most stable: RG- and TG+) were found in the experimental measurements due to the interconversion process that takes place in the jet.

All rotational, centrifugal distortion and diagonal elements of the nuclear tensor parameters have been accurately determined. An estimation of the populations of the conformers found in the sample was done using relative intensities of the microwave transitions. As a result we found that the RG- conformer is much more abundant than the TG+ structure. However, this is an estimated calculation because the plausible presence of conformational relaxation in the jet. This fact produces an unequal overestimation of the population of both conformers.

The experiment also let us check the validity of the theoretical results provided by the MP2 and M06-2X methods. We observe from Tables 4.1 and 4.2 that the theoretical calculations are able to reproduce satisfactorily the experimental results in the gas phase.

4.5 References.-

[1] L. L. Brunton, J. S. Lazo, K. L. Parker, Goodman & Gilman´s. *The Pharmacological Basis of Therapeutics*, 11th ed.; McGraw Hill: New York, **2006**.

[2] E. Aguado, A. Longarte, E. Alejandro, J. A. Fernández, F. Castaño. *J. Phys. Chem. A*, 110, 6010, **2006**.

[3] M. K. Jahn, D. Dewald, J.-U. Grabow, W. Caminati, E. J. Cocinero, A. Lesarri. In publication.

[4] A. Lesarri, S. T. Shipman, G. G. Brown, L. Alvarez-Valtierra, R. D. Suenram, B. H. Pate, 63rd International Symposium on Molecular Spectroscopy, Comm. RH07, **2008**.

[5] I. León, E. Aguado, A. Lesarri, J.A. Fernández, F. Castaño. *J. Phys. Chem. A*, 113, 982, **2009**.

[6] M. Remko, K. R. Liedl, B. M. Rode. *Chem Papers*, 51, 234, **1997**.

[7] E. Aguado, I. León, E. J. Cocinero, A. Lesarri, J. A. Fernández, F. Castaño. *Phys. Chem. Chem. Phys.*, 11, 11608, **2009**.

[8] D. H. Levy. *Science*, 214, num.4518, 263, **1981**.

[9] HyperChem(TM) Professional 7.51, Hypercube, Inc., 1115 NW 4th Street, Gainesville, Florida 32601, USA.

[10] F. Mohamadi, N. G. J. Richards, W. C. Guida, R. Liskamp, M. Lipton, C. Caufield, G. Chang, T. Hendrickson, W. C. Still, *Journal of Computational Chemistry*, 11, num.4, 440-467, **1990**.

[11] M. J. Frisch, G. W. Trucks, H. B. Schlegel, G. E. Scuseria, M. A. Robb, J. R. Cheeseman, G. Scalmani, V. Barone, B. Mennucci, G. A. Petersson, H. Nakatsuji, M. Caricato, X. Li, H. P. Hratchian, A. F. Izmaylov, J. Bloino, G. Zheng, J. L. Sonnenberg, M. Hada, M. Ehara, K. Toyota, R. Fukuda, J. Hasegawa, M. Ishida, T. Nakajima, Y. Honda, O. Kitao, H. Nakai, T. Vreven, J. A. Jr. Montgomery, J. E. Peralta, F. Ogliaro, M. Bearpark, J. J. Heyd, E. Brothers, K. N. Kudin, V. N. Staroverov, R. Kobayashi, J. Normand, K. Raghavachari, A. Rendell, J.

C. Burant, S. S. Iyengar, J. Tomasi, M. Cossi, N. Rega, N. J. Millam, M. Klene, J. E. Knox, J. B. Cross, V. Bakken, C. Adamo, J. Jaramillo, R. Gomperts, R. E. Stratmann, O. Yazyev, A. J. Austin, R. Cammi, C. Pomelli, J. W. Ochterski, R. L. Martin, K. Morokuma, V. G. Zakrzewski, G. A. Voth, P. Salvador, J. J. Dannenberg, S. Dapprich, A. D. Daniels, Ö. Farkas, J. B. Foresman, J. V. Ortiz, J. Cioslowski, D. J. Fox, GAUSSIAN09, Revision **D.01**, Gaussian, Inc., Wallingford CT, **2009**.

[12] W. Gordy, L.R. Cook, 'Microwave Molecular Spectra', 3rd Edition, in: A. Weissberger (Ed.), *Techniques of Chemistry*, vol. XVIII, John Wiley & Sons Inc., New York, **1984**.

[13] M. Pickett, *J.Mol. Spectrosc.,*148, 371, **1991**.

[14] http://www.nist.gov/pml/div686/sources_detectors/jb95.cfm Retrieved 2014-01-30.

[15] P. D. Godfrey, R.D. Brown, F.M. Rodgers. *J. Mol. Struc.*, 376, 65-81, **1996**.

[16] R. S. Ruoff, T. D. Klots, H. S. Gutowsky, *J. Chem. Phys.*, 93, 3142-3150, **1990**.

[17] G. M. Florio, R. A. Christie, K. D. Jordan, T. S. Zwier. *J. Am. Chem. Soc.*, 124, 10236-10247, **2002**.

[18] P. D. Godfrey, R. D. Brown, *J. Am. Chem. Soc.*, 12, 10724-10732, **1998**.

[19] J.-U. Grabow, W. Caminati, *Microwave Spectroscopy: Experimental Techniques*. In Frontiers of Molecular Spectroscopy; Laane, J., Ed.; Elsevier: Amsterdam, The Netherlands, , Chapter 14, 383-454, **2008**.

Chapter 5
Lupinine

5.1. Introduction.-

Lupinine is an alkaloid with bitter taste which is synthesized naturally in leguminous plants. Lupinine was first extracted from seeds and herbs of the *Lupinus luteus* species and its structure was later established by chemical methods.

This work started because of our interest to examine the structural properties of bicyclic decanes based on decalin derivatives. Bicyclic decanes appear as the molecular core of different biochemical products, like alkaloids and steroids, so a knowledge of its structure was a requisite to study different families containing this structural building block.

In particular, lupinine belongs to the family of *quinolizidine alkaloids*, well known because of its toxicity in humans and animals. Those types of alkaloids have in common a structural motif based in the azabycicle quinolizidine, which is shown in the following figure. In quinolizidine, the bridgehead atom of decalin has been replaced by a nitrogen atom, forming a heterocycle.[1]

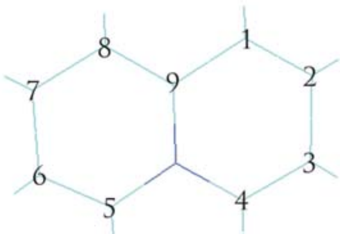

<u>Figure: 5.1.-</u> Structural motif of all the quinolizidine alkaloids.

All quinolizidine alkaloids contains this bicyclic motif, either with different substitutents like lupinine, or, in occasions, enlarged with additional fused rings, like esparteine or citisine. Some of them are shown in figure 5.2:

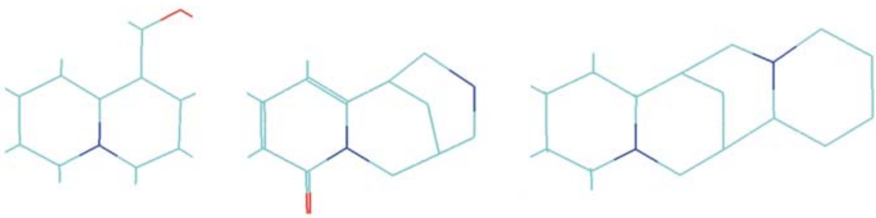

Lupinina **Citisina** **Esparteina**

<u>Figure: 5.2.-</u> Molecular formulas of some quinolizidine derivatives: Lupinine, Citisine and Esparteine.

The important biological interest of alkaloids is due to their multiple pharmacological properties. Some of them can act on the central nervous system (CNS), causing the inhibition of some functions responsible of the muscular coordination. This is the case, for example, of cocaine[2] or citisine,[3] which have been previously studied and several works are available in gas phase and solid state.

Other alkaloid molecules, like the tropanes[4-7], have been also studied in this thesis, like pseudopelletierine (chapter 2) and scopine (chapter 3).[8]

There were several previous studies on the chemical properties of the quinolizidine alkaloids.[9,10,11] However, the absence of vibrational and rotational information on these molecules moved us to examine some compounds with rotational resolution, starting by lupinine.

The lupinine structure is that of the quinolizidine bicycle with a hydroxymethyl substituent next to the carbon bridgehead, or [(1R,9R)-Octahydro-1H-quinolizin-1-yl]methanol. The introduction of the nitrogen atom and the side chain creates two chiral centers. In consequence two diastereoisomers can be formed, denoted epilupinine and lupinine. For each diastereoisomer there are two enantiomers, like (-)-lupinine and (+)-lupinine, shown below.

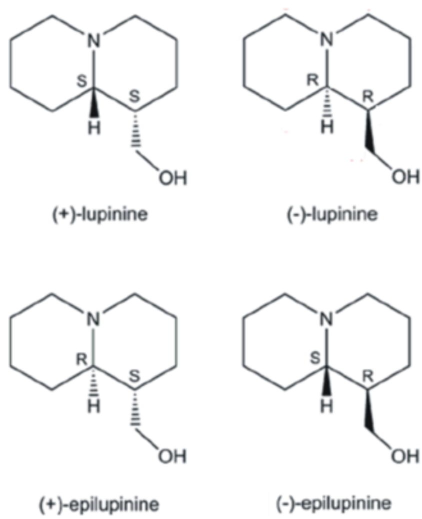

Figure: 5.3.- Diastereoisomers of lupinine.

In this study we have examine the structural properties of the biologically active form of (-)-lupinine, shown in Figure 5.4.

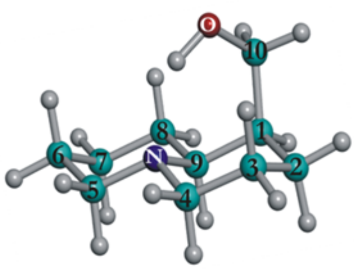

Figure: 5.4.- A conformer of lupinine ($C_{10}H_{19}NO$).

5.2. Computational Methods.-

First, a conformational search was made to obtain the plausible conformers of lupinine. Molecular mechanics were performed using the Merck Molecular Force Field[12] and implemented in Macromodel+Maestro.[13] This program uses a mixed Montecarlo and "large-scale low-modes" procedure in the conformational search providing hundreds of initial conformational structures of the molecule. Hence, a set of 57 structures within an energy window of 20 $kJ \cdot mol^{-1}$ was selected.

According to the geometry of the molecule, lupinine can adopt different configurations attending to the diverse degrees of freedom of the rings and the orientation of the methoxy group.

First of all and due to the bicycle arrangement, each ring can display some characteristic configurations like chair, twist or boat. These configurations can be specified by the $\tau_1(C_6 - C_5 - N \quad - C_9)$ and $\tau_2(N \quad - C_4 - C_3 - C_2)$ torsions. The structures obtained in the conformational search adopt the chair-chair, boat-chair, chair-boat, boat-boat or twist structures.

The most stable chair-chair structure can display two different isomers depending of the relative position of the two rings. We call the structure *trans*- when the decalin ring arrangement exhibits a C_{2h} symmetry. It is important to note that *trans* isomers are chiral, but they cannot invert. Conversely, when the two chairs belong to the point group C_2, a *cis*- conformation is found. The *cis*- isomers are also chiral and they can double-invert, so they might generate new conformations depending on the substitutents. The figure 5.5 illustrates both configurations in lupinine.

For all geometries, and depending on the methoxy group orientation, we will obtain different conformers, increasing the complexity of the molecule. Hence, for the most stable *trans* chair-chair structure three preferred staggered geometries are found depending on the hidroxyl group, like the Gauche$^-$ (G^- : $\tau_3(O - C_{10} - C_1 - C_2) \sim \quad -70°$), Anticlinal ($A^+$: $\tau_3(O - C_{10} - C_1 - C_2) \sim 170°$) o Gauche$^+$ (G^+: $\tau_3(O - C_{10} - C_1 - C_2) \sim 50°$).

Despite the calculation methods based on MM are very fast, in order to determine with high accuracy the spectroscopic properties, (such as rotational constants) and the conformational energetics, more sophisticated methods like ab initio or DFT should be used. These calculations used Gaussian09[14].

Full geometry optimizations and frequency calculations were thus performed for the predicted conformers with energies below 25 kJ·mol^{-1}. The theoretical methods used here were the ab initio MP2 perturbation method and the DFT M06-2X. These methods have been proved to be appropriate for spectroscopic purposes in organic molecules. The relative energies and molecular properties of the eight most stable conformations of lupinine are collected in table 5.1.

The basis set used in the geometry optimization, as well as in the frequency calculations, was always the Pople triple-ζ with polarization and diffuse functions (6-311++G(d,p)).

As expected, all the lowest-energy structures of (−)-lupinine are predicted in a double-chair configuration (both MP2 and M06-2X). Among the chair−chair structures, both *cis*- and *trans*-quinolizidine skeletons were detected, but the *trans* form is much more stable, and the first *cis* form is observed only at conformational free energies above ΔG = 17.3−21.7 kJ mol^{-1} (electronic energies of 18.8−23.1 kJ mol^{-1}). For this reason, most of the lowest lying conformations are generated by the two internal rotation axes of the hydroxyl-methyl group (bonds C1−C10 and C10−O in figure 5.4) in a *trans* configuration.

Trans skeletons sharing boat and twist configurations, expected at relatively higher energies, were first encountered around ΔE = 20.2−21.0 kJ mol^{-1} (ΔG =20.4−21.2 kJ mol−1), that is, slightly below the first *cis* form.

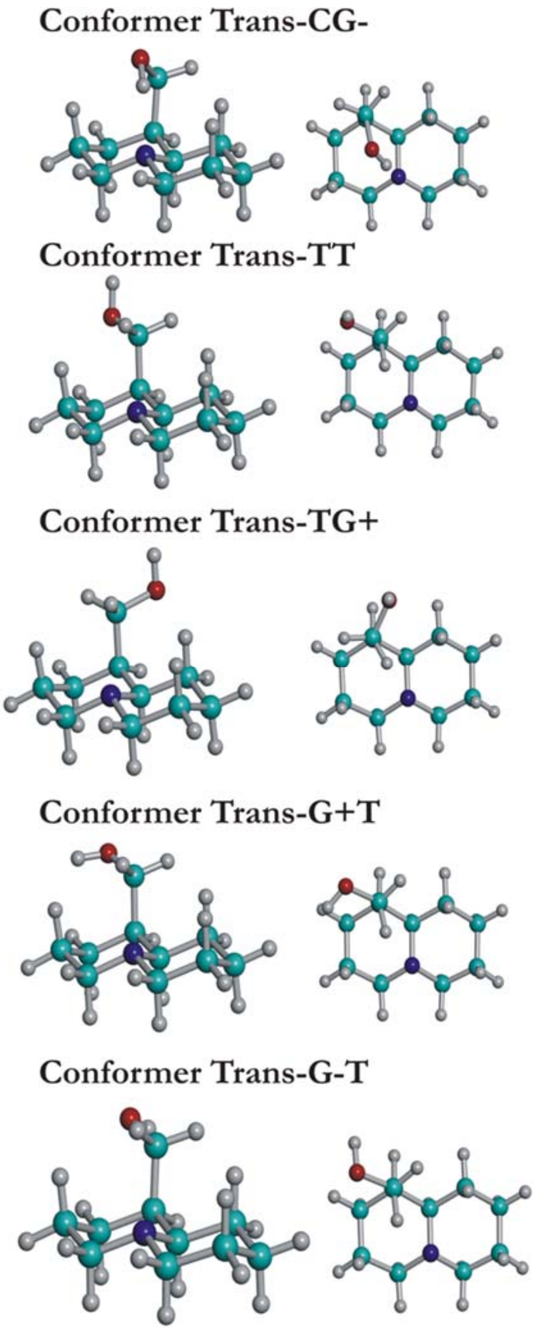

Figure: 5.5.- Molecular structures of the six lowest-lying conformers in two different views: perspective (left), where the chair-chair structure is shown, and above (right) showing the bicycle ring.

<u>Table: 5.1.-</u> Rotational constants (*A*, *B*, *C*), [14]N nuclear cuadrupole tensor ($\chi_{\alpha\beta}$, (α,β = a, b, c)) and electric dipole moments (μ_a, α = a, b, c) for the most stable conformers of lupinine. The quartic centrifugal distortion constants (Δ_J, Δ_{JK} , Δ_K, δ_K and δ_K) were also shown, just like the energy difference Δ*E* between each conformer and the most stable one (zero point energy, ZPE, corrected). ΔG at 298K and 1 atm.

Theory MP2 / M06-2X	***trans*-CG-**	***trans*-TT**	***trans*-TG+**	***trans*-G+T**	***trans*-G-T**	***trans*-G+G+**	***twist*-CG-**	***cis*-G+G+**
A/MHz	1425.8/1422.5	1503.3/1504.9	1213.0/1212.9	1485.9/1490.0	1485.1/1212.9	1208.7/1209.1	1388.1/1383.4	1246.6/1245.1
B/MHz	815.1 / 815.7	719.2 / 720.6	869.6 / 871.7	720.3 / 721.8	718.1 / 871.7	869.7 / 872.8	878.9 / 880.0	827.6 / 834.7
C/MHz	677.1 / 672.2	559.9 / 560.6	583.0 / 583.0	559.6 / 561.2	556.6 / 583.0	585.0 / 584.3	721.0 / 718.5	586.7 / 586.0
χ_{aa} **/ MHz**	2.0 / 2.2	2.1 / 2.2	2.1 / 2.3	2.0 / 2.2	2.0 / 2.3	2.0 / 2.3	2.3 / 2.5	1.9 / 2.2
χ_{bb} **/ MHz**	1.1 / 1.1	1.7 / 1.8	1.6 / 1.7	1.7 / 1.8	1.7 / 1.7	1.5 / 1.7	0.2 / 0.2	1.7 / 1.8
χ_{cc} **/ MHz**	-3.1 / -3.4	-3.8 / -4.0	-3.7 / -4.0	-3.7 /-4.0	-3.7 / -4.0	-3.6 /-4.0	-2.5 / -2.8	-3.6 / -3.9
Δ_J **/ Hz**	22.62 / 24.06	17.94 / 17.91	27.75 / 26.31	18.37 / 17.33	18.66 / 18.96	26.71 / 25.99	28.08 / 29.02	45.28 / 46.68
Δ_k **/ Hz**	2.16 / 1.41	94.04 / 85.12	-13.51 / -9.93	100.61 / 92.75	94.37 / 78.76	-10.79 / -12.55	5.91 / 11.68	131.78/131.14
Δ_{Jk} **/ Hz**	64.87 / 68.13	70.60 / 77.47	44.66 / 39.75	66.34 / 58.72	81.53 / 85.51	43.23 / 44.72	51.49 / 51.88	-102.92/-105.91
δ_J **/ Hz**	2.65 / 2.75	0.12 / -0.2	6.31 / 5.75	0.15 / 0.17	-0.29 / -0.64	5.67 / 5.00	2.99 / 3.25	16.59 / 17.23
δ_k **/ Hz**	19.53 / 18.89	74.17 / 76.64	61.59 / 57.46	71.41 / 66.66	80.98 / 82.63	58.64 / 60.95	23.34 / 20.74	33.59 / 33.22
$\lvert\mu_a\rvert$ **/D**	1.3 / 1.3	1.1 / 1.1	0.29 / 0.25	1.4 / 1.4	1.3 /0.25	0.70/0.72	0.92 / 0.99	0.28 / 0.26
$\lvert\mu_b\rvert$ **/D**	1.1 / 1.1	0.48 / 0.48	0.83 / 0.80	1.7 / 1.7	0.46 / 0.80	1.2 / 1.1	1.4 / 1.3	1.3 / 1.2
$\lvert\mu_c\rvert$ **/D**	2.4 / 2.3	0.64 / 0.63	0.83 / 0.83	0.45/0.46	1.6 / 0.83	1.4 / 1.5	2.3 / 2.2	0.20 / 0.08
$\lvert\mu_{TOT}\rvert$ **/D**	2.9 / 2.9	1.4 / 1.3	1.2 / 1.2	2.2 / 2.2	2.1 / 1.2	2.0 / 2.0	2.8 / 2.8	1.3 / 1.3
ΔE / kJ·mol^{-1}	0.0 / 0.0	14.8 / 14.6	16.5 / 15.7	17.0/16.0	17.7 / 16.1	18.2/16.6	20.4/20.2	22.0/25.0
Δ(E+ZPE) / kJ·mol^{-1}	0.0 / 0.0	17.0 / 12.1	13.5 / 12.5	14.7 / 14.1	15.1 / 13.5	15.9 / 13.3	21.0 / 20.2	23.1 / 18.8
ΔG / kJ·mol^{-1}	0.0 / 0.0	10.4 / 10.4	11.5 / 11.1	12.2 / 13.0	13.3 / 11.6	13.6 / 11.8	21.2 / 20.4	21.7 /17.3

Observing the results in the previous table, we can conclude that only one of six most stable conformers is expected to be populated in the rotational spectrum.

5.3. Results and Analysis.-

a. Assignment of the Rotational Spectrum.

Initially, a prediction of the rotational spectral of the five structures shown in figure 5.5 was made. All structures are near- prolate asymmetric tops ($\kappa\approx$ -0.63 to $\kappa\approx$ -0.66) except conformers 3 and 6, which have a much larger asymmetry degree ($\kappa_3\approx$ -0.09 and $\kappa_6\approx$ -0.09). The predictions were carried out with the Pickett[15] and JB95[16] programs, that use the Watson semi-rigid rotor Hamiltonian to give the frequencies and intensities of the spectral transitions at the temperature of the supersonic jet ($T_{rot}\sim 2K$).

For all conformers found in the 20 kJ/mol energy window, all the electric dipole moment components are non-zero along the three principal inertial axes. For instance, in the case of the most stable conformer (1) the dipole moment is dominant along the *c* axis, less intense along *a* and smaller along *b*. So, for the assignment of the spectrum, we predicted initially transitions belonging to the R branch ($J+1 \leftarrow J$) μ_c-type. Following a search of the spectrum in the region 14900-15300 MHz a set of $J=6 \leftarrow J=5$ μ_c- and μ_b-type transitions were readily identified, which enable the further detection of other $J=10 \leftarrow J=9$ μ_a-type lines in the region. After a sequence of successive fits the rotational spectrum was totally identified. The search was extended to other conformations, but only a single species could be detected.

In the following figure the experimental spectrum (violet) is compared with the fitted (including μ_c, μ_a and μ_b–type transitions). Several transitions appeared in the spectrum which could not be assigned (see for example in figure 5.8 the transition at $\upsilon\sim$14995 MHz). Considering that lupinine was vaporized by heating methods this probably indicates the presence of minor decomposition or fragmentation products.

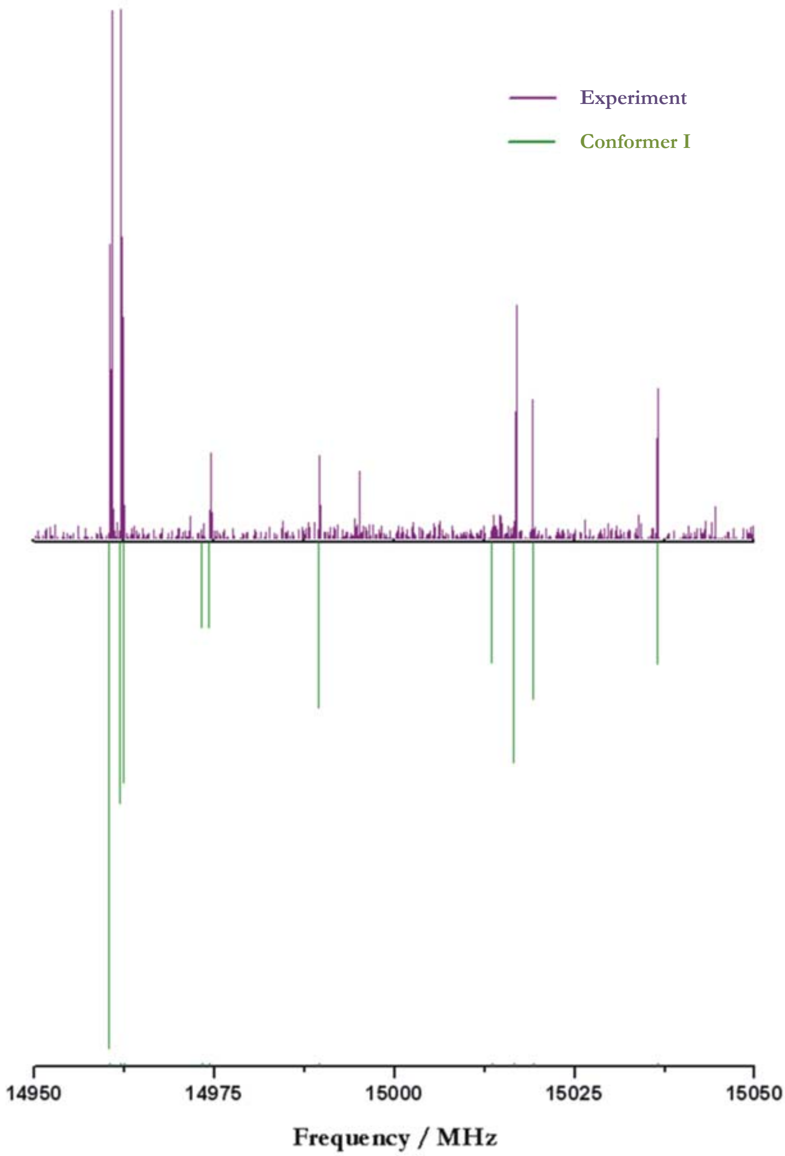

Figure: 5.8.- Scan section for the lupinine molecule with transitions belonging to the most stable conformer. Intensity fluctuations are due to the different conditions in the successive scans (temperature, sample, etc).

b. Hyperfine effects: Nuclear Quadrupole Coupling.

The bicyclic structure of lupinine contains a nitrogen atom. The presence of the ^{14}N isotope (nuclear spin I=1) introduces a nuclear quadrupole coupling interaction (also observed in other molecules in this thesis), which splits the rotational transition into several components in addition to the instrumental Doppler effect.[17]

The ^{14}N splitting in amines is rather small, typically $\Delta\nu \sim 200 kHz$, which makes it easily recognizable in comparison with the smaller Doppler effect, as can be seen in the following figure. In that figure, an example transition belonging to the experimentally identified conformer is shown, clearly distinguishing between the Doppler and the quadrupole coupling effects.

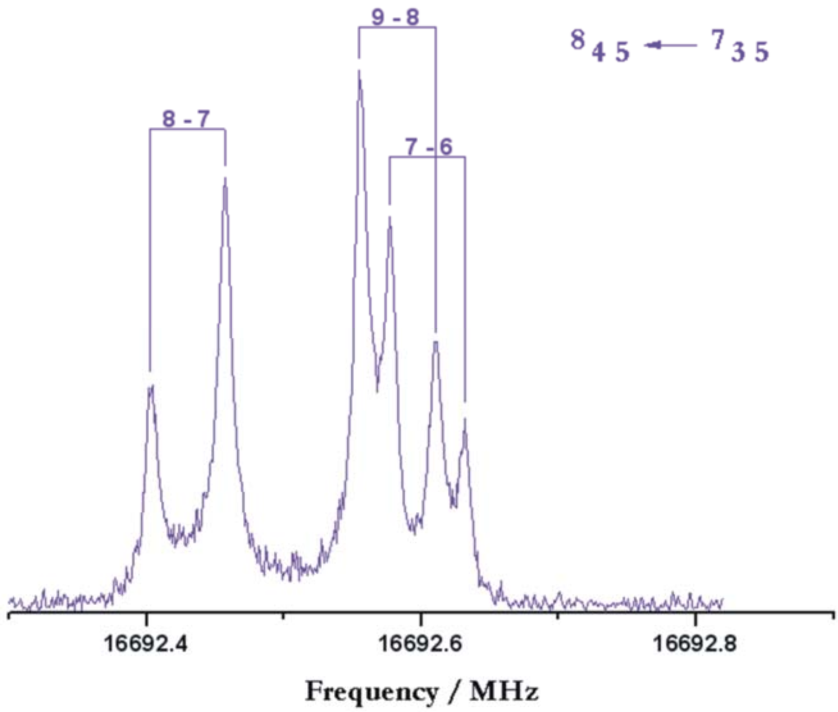

Figure: 5.9.- $8_{4,5} \leftarrow 7_{3,5}$ transition of the most stable conformer of lupinine. The hyperfine components are marked with quantum numbers $F' \leftarrow F''$ ($\boldsymbol{F}=\boldsymbol{I}+\boldsymbol{J}$).

c. Determination of Spectroscopic Parameters.

The experimental transitions (shown in table 5.3) were fitted using the asymmetric reduction (A) of the Watson semi-rigid rotor Hamiltonian in the I^r representation (appropriate for near prolate tops[17]) with an additional term that takes into account the quadrupolar interactions. The fit results for the rotational properties of lupinine are shown in the following table.

Table: 5.2.- Experimental values for the rotational constants (*A*, *B*, *C*), elements of the nuclear quadrupole coupling tensor of the ^{14}N atom ($\chi_{aa}, \chi_{bb}, \chi_{cc}$) and quartic centrifugal distortion constants ($\Delta_J, \Delta_{JK}, \Delta_K, \delta_J, \delta_K$) of the observed conformer of lupinine.

	Conformer I
	Experiment
***A* / MHz**	1414.12628(11)[a]
***B* / MHz**	811.67165(12)
***C* / MHz**	671.52998(13)
Δ_J / kHz	0.02520(49)
Δ_{JK} / kHz	0.0665(15)
Δ_K / kHz	---
δ_J / kHz	0.00313(16)
δ_{JK} / kHz	0.0272(31)
$\|\mu_a\|$ / D	observed
$\|\mu_b\|$ / D	observed
$\|\mu_c\|$ / D	observed
χ_{aa} / MHz	2.007 (9)
χ_{bb} / MHz	1.0601 (87)
χ_{cc} / MHz	-3.0671 (87)
N[b]	72
σ[c] / kHz	0.41

[a]Standard error in units of the last digit.
[b]Number of lines used in the fit.
[c] Root-mean-square deviation of the fit.

The quality of the fit was good, according to the rms value (~0.41 kHz), one order of magnitude below the estimated resolution of the spectrometer, and acceptable correlations. We could not determine the quartic centrifugal distortion Δ_K, as well as the out of diagonal elements of the nuclear quadrupole coupling tensor. A larger set of experimental transitions would be needed to improve the centrifugal distortion values. The determination of only the diagonal elements of the quadrupole coupling tensor is common in amines.

The comparison of the theoretical predictions with the experimental rotational constants and nuclear quadrupole coupling hyperfine parameters led to the unambiguous identification of the detected conformer of lupinine, which clearly identifies as the most stable species in the theoretical ab initio calculations (first column of table 5.1).

The non-observation of additional conformers is also consistent with the predictions for the conformational energies.

Table: 5.3.- Measured and calculated frequencies (in MHz) for the observed transitions of the most stable conformer of lupinine. The last column is the difference between the observed and calculated frequencies in kHz $\Delta\nu = \nu_{OBS} - \nu_{CALC}$.

J'	K'_{-1}	K'_{+1}	J"	$K"_{-1}$	$K"_{+1}$	F'	F"	ν_{OBS} / MHz	ν_{CALC} / MHz	$\Delta\nu$ / kHz
6	4	2	5	3	3	6	5	13646.0543	13646.0558	-1.5
						7	6	13646.2419	13646.2424	-0.4
						5	4	13646.2712	13646.2721	-0.9
6	5	2	5	4	1	6	5	14960.5273	14960.5282	-0.9
6	5	1	5	4	1	6	5	14960.6690	14960.6675	1.5
						7	6	14960.7876	14960.7865	1.2
6	5	2	5	4	2	6	5	14962.0743	14962.0750	-0.6
10	6	4	9	6	3	11	10	14974.4507	14974.4559	-5.1
						10	9	14974.5826	14974.5825	0.1
11	0	11	10	1	10	12	11	15094.3975	15094.3987	-1.2
						10	9	15094.4127	15094.4120	0.7
						11	10	15094.4361	15094.4365	-0.4
11	1	11	10	1	10	12	11	15096.0657	15096.0670	-1.4
						10	9	15096.0819	15096.0802	1.7
						11	10	15096.1056	15096.1058	-0.2
7	4	4	6	3	4	7	6	15152.9464	15152.9478	-1.4
						8	7	15153.1251	15153.1226	2.5
						6	5	15153.1490	15153.1507	-1.7
12	3	9	11	4	7	13	12	15187.1450	15187.1449	0.1
						12	11	15187.2060	15187.2071	-1.1
10	2	8	9	2	7	9	8	15227.7940	15227.7927	1.3
						11	10	15227.8063	15227.8064	-0.1
						10	9	15227.9530	15227.9534	-0.4
8	3	6	7	2	6	8	7	15872.2949	15872.2941	0.8
						9	8	15872.7320	15872.7286	3.4
						7	6	15872.7951	15872.7975	-2.3
8	4	4	7	3	4	7	6	16395.0932	16395.0978	-4.6
						9	8	16395.1141	16395.1084	5.7
						8	7	16395.1777	16395.1782	-0.5
12	0	12	11	0	11	13	12	16440.3603	16440.3609	-0.6
						11	10	16440.3739	16440.3722	1.7
						12	11	16440.3932	16440.3947	-1.5

Table: 5.3.Continued.-

J'	K'$_{-1}$	K'$_{+1}$	J"	K"$_{-1}$	K"$_{+1}$	F'	F"	ν_{OBS} / MHz	ν_{CALC} / MHz	$\Delta\nu$ / kHz
12	0	12	11	0	11	13	12	16440.3603	16440.3609	-0.6
						11	10	16440.3739	16440.3722	1.7
						12	11	16440.3932	16440.3947	-1.5
11	6	5	10	6	4	10	9	16498.2353	16498.2385	-3.2
						12	11	16498.2527	16498.2478	4.9
						11	10	16498.3353	16498.3347	0.7
11	4	8	10	4	7	12	11	16514.7613	16514.7613	-0.1
						11	10	16514.8195	16514.8203	-0.8
11	5	7	10	5	6	12	11	16540.4403	16540.4382	2.0
						11	10	16540.4932	16540.4941	-0.9
11	2	9	10	2	8	10	9	16580.5501	16580.5487	1.3
						12	11	16580.5624	16580.5614	1.0
						11	10	16580.7238	16580.7240	-0.2
11	5	6	10	5	5	12	11	16593.9249	16593.9262	-1.2
						11	10	16593.9511	16593.9517	-0.6
8	4	5	7	3	5	8	7	16692.5248	16692.52450	0.3
						9	8	16692.7110	16692.71037	0.6
						7	6	16692.7365	16692.73818	-1.7
12	1	11	11	1	10	13	12	17107.9625	17107.96198	0.5
						12	11	17108.0537	17108.05412	-0.4
12	3	10	11	3	9	13	12	17650.8770	17650.87718	-0.2
						12	11	17650.9654	17650.96586	-0.5
9	4	5	8	3	5	10	9	17728.3792	17728.37556	3.7
						9	8	17728.4929	17728.49124	1.7
12	4	9	11	4	8	13	12	17993.7272	17993.72721	0.0
						12	11	17993.7873	17993.78736	-0.5
12	5	8	11	5	7	13	12	18067.1131	18067.11368	-0.5
						12	11	18067.1601	18067.15643	3.6
12	5	7	11	5	6	12	11	18178.9404	18178.94159	-1.2
						13	12	18178.9509	18178.94911	1.8
						11	10	18178.9509	18178.94991	1.0
9	4	6	8	3	6	9	8	18269.1641	18269.16424	-0.2
						10	9	18269.3726	18269.37133	1.3
						8	7	18269.3971	18269.39928	-2.2
12	4	8	11	4	7	12	11	18526.3665	18526.36781	-1.3
						11	10	18526.4152	18526.41727	-2.1
10	2	8	9	1	8	11	10	18707.7763	18707.77391	2.4
7	7	0	6	6	0	7	6	19128.6980	19128.69905	-1.0
						6	5	19128.7203	19128.72209	-1.8
						8	7	19128.7411	19128.74340	-2.3
7	7	1	6	6	1	7	6	19128.6980	19128.69987	-1.9
						6	5	19128.7203	19128.72291	-2.6
						8	7	19128.7411	19128.74422	-3.1
8	6	2	7	5	2	8	7	19277.7870	19277.78438	2.6
						9	8	19277.8838	19277.88502	-1.3
						7	6	19277.8932	19277.89135	1.9

5.4 Conclusions.-

The rotational spectrum of the alkaloid lupinine was measured in the gas phase. The experimental results reveal only one conformational structure which was unambiguously identified. As predicted, no signals belonging to the higher-energy conformers (see table 5.1) were detected.

The experimental measurements allowed an accurate determination of the rotational parameters for the most stable species of the molecule. At the same time, the agreement with the theoretical methods, both ab initio (MP2) and DFT (M06-2X) was satisfactory, as previously observed for spectroscopic predictions of other organic compounds.

The predicted preference for the *trans* chair-chair configuration was confirmed by the experimental data. The detected conformer characteristically exhibits a stabilizing intramolecular hydrogen bond between the electron lone-pair at the nitrogen atom and the hydroxyl group: O-H···N. It should be noted that this hydrogen bond is not noticeable in the X-ray crystalline structure, probably due to crystal packing effects. In order to estimate computationally the stabilizing effect of this moderate hydrogen bond,[18-21] we compared the Gibbs free energies of the *cis* and *trans* configurations of decalin and two derivatives: epilupinine and lupinine (see table 5.4). The energy gap of the cis form of lupinine (21.7 kJ mol^{-1}) turns out to be nearly double that in the epilupinine (11.6 kJ mol^{-1}) and decalin (11.8 kJ mol^{-1}) configurations. At the same time decalin and epilupinine, where the hydrogen bonding is not possible, show basically the same energy gap between the *cis* and *trans* structures. Both arguments point to a contribution of the intramolecular O-H···N in lupinine stabilization of ca. 10 kJ mol^{-1}, outlining the important role of intramolecular hydrogen bonding in isolated molecules.

Table: 5.4.- Relative Gibbs free and electronic energies of decalin and its derivatives lupinine and epilupinine.

	Decalin		Lupinine		Epilupinine	
	trans	**cis**	**trans**	**cis**	**trans**	**Cis**
ΔE (kJ·mol^{-1})	0.0	9.3	0.0	25.0	0.0	9.3
ZPE (H)	0.265887	0.266553	0.289253	0.288546	0.287937	0.288356
Δ(E+ZPE) (kJ·mol^{-1})	0.0	11.05	0.0	23.14	0.0	10.4
ΔG (kJ·mol^{-1})	0.0	11.84	0.0	21.7	0.0	11.55

5.5 References.-

[1] E. L. Eliel, S. H. Wilen, "Stereochemistry of Organic Compounds", Wiley: New York, **1994**.

[2] R. J. Hrynchuk, R. J. Barton, B. E. Robertson, *Can. J. Chem.*, 61, 481, **1983**.

[3] J. P. Michael, *Nat. Prod. Rep.*, 25, 139, **2008**.

[4] A. Krunic, D. Pan, W. J. Dunn III, S. V. S. Mariappan, *Bioorg. Med. Chem.*, 17, 811, **2009**.

[5] E. J. Cocinero, A. Lesarri, P. Écija, J.-U. Grabow, J. A. Fernández, F. Castaño, *Phys. Chem. Chem. Phys.*, 12, 6076, **2010**.

[6] L. Evangelisti, A. Lesarri, M. K. Jahn, E. J. Cocinero, W. Caminati, J.-U. Grabow, *J. Phys. Chem. A*, 115, 9545, **2011**.

[7] A. M. Belostotskii, Z. Goren, H. E. Gottlieb, *J. Nat. Prod.*, 67, 1842, **2004**.

[8] G. Grynkiewicz, M. Gadzikowska, *Pharm. Rep.*, 60, 439, **2008**.

[9] R. Greinwald, J. H. Ross, L. Witte. F.-C. Czygan, Alkaloids of Templetonia incana in "Biochemical Systematics and Ecology", Vol. 24, Elsevier Science, U. K., **1996**.

[10] R. Greinwald, C. Henrichs, G. Veen, J. H. Ross, L. Witte. F.-C. Czygan, A survey of alkaloids in Templetonia biloba in "Biochemical Systematics and Ecology", Vol. 23, Elsevier Science, U. K., **1995**.

[11] A. Sparatore, A. Cagnotto, F. Sparatore, *Il farmaco*, 54, 248, **1999**.

[12] T. A. Halgren, *J. Comput. Chem.*, 20, 730, **1999**.

[13] MAESTRO, version 9.2, Schrödinger, LLc, New York, NY, **2012**.

[14] M. J. Frisch et al., Gaussian, Inc., Wallingford CT, **2009**.

[15] H. M. Pickett, *J. Mol. Spectrosc.*, 148, 371, **1991**.

[16] http://physics.nist.gov/jb95 Retrieved 2014-01-30

[17] W. Gordy and L. R. Cook, "Microwave Molecular Spectra", 3rd Edition, in Weissberger, A. (Ed.), Techniques of Chemistry, vol. XVIII, John Wiley & Sons Inc., New York, **1984**.

[18] G. A. Jeffrey, "An Introduction to Hydrogen Bonding", Oxford Univ. Press: Oxford, U.K., **1997**.

[19] J. A. Jeffrey, W. Saenger, "Hydrogen bonding in biological structures", Springer, Berlin, **1991**.

[20] M. J. Tubergen, R.L. Kuczkowski, *J. Am. Chem. Soc.* 115, 9263, **1993**.

[21] T. Herbine and T.R. Dyke, *J. Chem. Phys.* 83, 3768, **1985**.

Water Complexes

Chapter 6

Tropinone···water

6.1. Introduction.-

Tropinone is a synthetic precursor of tropane alkaloids. All these compounds share an eight-membered bicycle with a nitrogen bridge, or 8-azabicycle[3.2.1]octane. Several examples of tropane derivatives have been presented in chapter 2, together with some of their structural characteristics. Many of these compounds are synthesized because of their therapeutical properties[1,2]. As an example, studies of phenyltropanes have revealed that this kind of substances can improve neurotransmission in the brain.[1] These properties make interesting the study of both the structural properties and the biochemical mechanisms.

The biochemical properties of most molecules are exerted in the physiological medium or in solution. In consequence, it is interesting to know not only the structural properties of the bare molecule, but also how the conformational landscape can be affected by solvation. For this purpose the physical-chemistry approach is based on the controlled addition of a limited number of water molecules. These *microsolvated clusters* cannot represent the full solvation process, but on the other hand they serve to locate the preferred binding sites at the solvated molecule, the competition between molecular groups for water and the strength of the different intermolecular interactions.

As a continuation of our previous studies on tropane molecules (tropinone,[3] scopine, scopoline[4]) we decided to examine here the interactions between tropinone and a single water molecule. Tropinone exhibits two plausible binding sites at the amino and carbonyl groups, so this study can examine how they react to the presence of a water molecule. At the same time, and since the structure of the isolated structure is well known[5], we can check if monohydration can affect the conformational equilibrium of the N-methyl inversion. In the bare molecule the dominant species is the equatorial form.[6-10] The population ratio in the jet of ca. Eq:Ax ≈ 2:1 would correspond to a relative energy of ca. 2 kJ mol^{-1}. The barrier between the axial and equatorial species was calculated to be ca. 40 kJ mol^{-1}. The different conformations of tropinone are shown in the following figure.

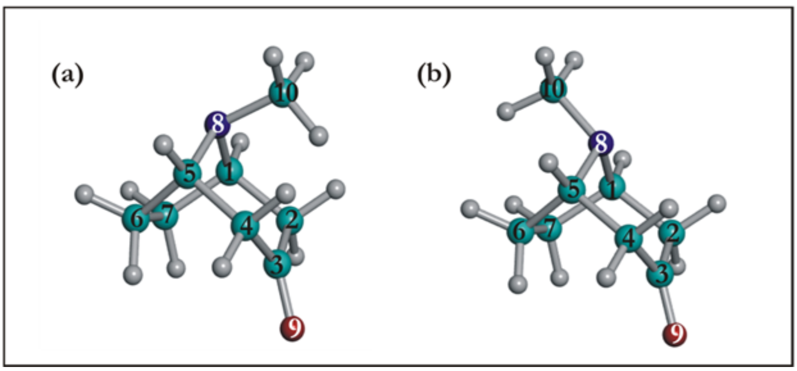

Figure:6.2.- Tropinone molecule structure. The IUPAC notation for the heavy atoms is used. **(a)** Equatorial configuration. **(b)** Axial conformer.

Since the tropane motif is relatively rigid the structure of the monomer can be described with a short number of dihedral angles, i.e.,

$\tau_1(C_{10} - N_8 - C_1 - C_2)$ for the N-methyl orientation and $\tau_2(N_8 - C_1 - C_2 - C_3)$ for the piperidine ring conformation.

Once the stable structures of tropinone molecule are known, the plausible ways of interaction between this molecule and water can be studied. The H_2O molecule can interact in different ways, playing the role of either proton donor (hydrogen bond O-H···B) or acceptor (A-H···O).[11] In tropinone the carbonyl and amino group may link also through different hydrogen bonds.[10] The nitrogen group is a tertiary amine, so it operates as proton acceptor through the electron lone pair, giving rise to moderate A-H···N hydrogen bonds.[12,13] The carbonyl group works also as proton acceptor, either through the oxygen lone pairs[14] or the π electron system.

Additional weak hydrogen bonds might be established between the two subunits of the complex such as C-H···O_w contributing to the stabilization of the system.

Using this hypotheses, a conformational search of tropinone···water was started.

6.2. Computational Methods.-

First of all a conformational search based on a molecular mechanics calculations was done using MACROMODEL-MAESTRO.[15] This method gave us the less energetic conformers shown in figure 6.3. As expected, we obtained two different types of interaction between water and tropinone: either through the nitrogen (N8) or through the oxygen (O9) atoms. Since tropinone additionally adopts two axial or equatorial conformations, the following four conformations were detected for the complex:

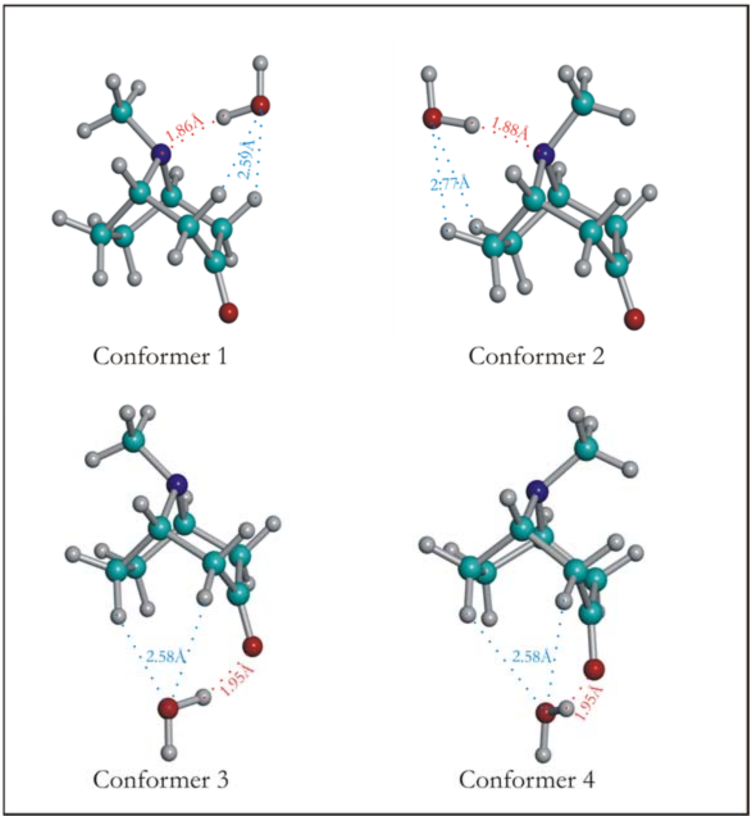

Figure: 6.3.- Plausible conformational structures for the tropinone···water complex depending on the N inversion (τ_1 torsion) and the water molecule bonding site with tropinone: O-H···N or O-H···O.

Starting from these geometries, later theoretical studies of the structures were done using DFT methods and ab initio calculations to know which one is the most stable conformers.

Once the plausible structures associated to the PES minima were identified, more sophisticated and more expensive computational methods were performed in order to obtain with higher accuracy the system energies and the structural and electrical properties characterizing the different stacionary states.

In particular, for the complex we are analyzing, geometry optimizations for each of the structures in figure 6.3 were carried out using second order perturbation calculations (MP2) and hybrid methods based on the Density Functional Theory (DFT), such as M06-2X. The basis set used in both cases was the Popple triple zeta with polarization and diffuse functions: 6-311++G(d,p). All the theoretical calculations were implemented in Gaussian 09[16].

Apart from the geometry optimizations, vibrational frequency calculations of the complex were also done, both to characterize the stationary points of the PES and to obtain vibrational corrections to the electronic energy, thermodynamic parameters and the vibrational force field, from which the centrifugal distortion constants were derived.

Electric dipole moments and other different electric properties like the nuclear quadrupole coupling constants were also obtained. The hyperfine effect appears as a consequence of the presence of the ^{14}N nucleus (I=1) in tropinone, which can be represented with a non-spherical nuclear charge. All the theoretical results are summarized in the following table.

Table: 6.1.- Rotational constants (A, B, C), electric dipole moments (μ_α, α = a, b, c) and nuclear quadrupole tensor diagonal elements of ^{14}N ($\chi_{\alpha\beta}$, (α,β = a, b, c)) found with MP2 and M06-2X methods. Centrifugal distortion constants (Δ_J, Δ_{JK}, Δ_K, δ_K, δ_K) are also calculated. ΔE represents the energy difference with respect to the global minimum (zero point energy corrected: ZPE). Gibbs free energy differences ΔG calculated at 298K and 1 atm.

	Theory MP2			
	Conf. 1	**Conf. 2**	**Conf. 3**	**Conf. 4**
A / MHz	1289.9	1807.3	1757.1	1676.8
B / MHz	1094.8	828.7	818.4	822.9
C / MHz	808.7	765.6	724.3	772.8
χ_{aa} / MHz	2.4	-4.4	2.6	0.68
χ_{bb} / MHz	-4.7	2.0	-0.66	-2.7
χ_{cc} / MHz	2.3	2.4	-2.0	2.0
$\|\mu_a\|$ / D	4.2	1.2	1.9	1.9
$\|\mu_b\|$ / D	3.1	3.4	0.0	0.9
$\|\mu_c\|$ / D	0.0	0.0	0.55	-0.16
$\|\mu_{TOT}\|$ / D	5.2	3.6	2.0	2.1
Δ_J / Hz	115.8	83.4	152.9	153.4
Δ_{JK} / Hz	521.4	280.2	-164.2	96.4
Δ_K / Hz	-388.1	-150.2	485.6	56.5
δ_J / Hz	32.4	14.0	27.3	26.1
δ_K / Hz	83.2	-120.7	-165.2	198.9
ΔG / kJ·mol^{-1}	0.0	2.0	8.4	10.7
Δ(E+ZPE) / kJ·mol^{-1}	0.0	3.2	8.9	11.0

It is easy to see from the results of table 6.1 that the two most stable structures have in common the O-H···N interaction between tropinone and the water molecule, which correspond to the equatorial (conformer 1) and axial (conformer 2) configurations of tropinone.

The third and fourth conformers are more energetic structures and, hence, they are expected with smaller equilibrium populations and, eventually, not detectable in the jet-cooled expansion.

6.3. Results and Analysis.-

a. Assignment of the Rotational Spectra.

According to the results in table 6.1 we searched first for the experimental transitions belonging to the two lowest-lying O-H···N conformations. The spectral simulations used the Watson semi-rigid rotor Hamiltonian, as implemented in the Pickett's[17] program and in the graphical simulator JB95.[18]

To carry out the predictions, the starting point is the determination of the Ray parameter indicating the degree of asymmetry in the complex and the specification of the appropriate selection rules.[19] Here the axial and equatorial conformers differ noticeably, as the equatorial form ($\kappa_{equatoral} \approx 0.19$) is oblate and much more asymmetric that the prolate axial ($\kappa_{axial} \approx -0.88$). In both structures, both the axial and equatorial species have the dipole moment mainly oriented along the two principal inertial axes *a* and *b*, while the projection along the *c* axis is negligible (μ_c=0). In consequence, only the μ_a and μ_b–type spectra transitions were predicted for the two conformers. The following figures 6.4 and 6.5) show, respectively, some of these transitions (μ_a and μ_b) for the most stable conformer (conformer 1).

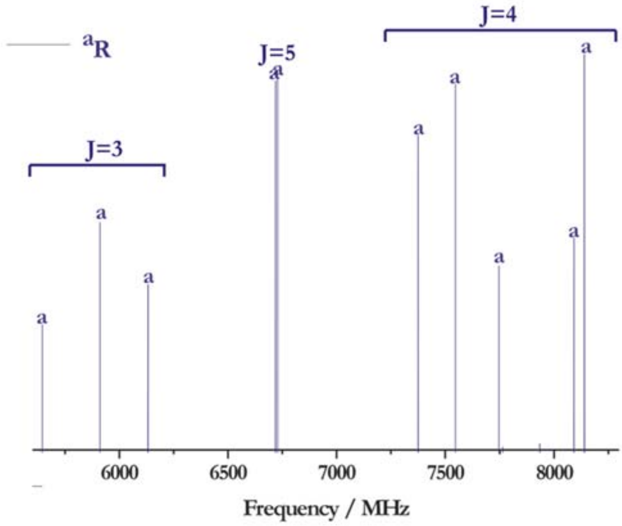

Figure: 6.4.- An example of ^{a}R-type series predicted for the equatorial conformer (most stable conformer).

In the previous ^{a}R type spectra the characteristic spacing between successive J+1 ← J series is approximately $B + C \approx 1880MHz$. We show a similar prediction of the μ_b–transitions in the same frequency region:

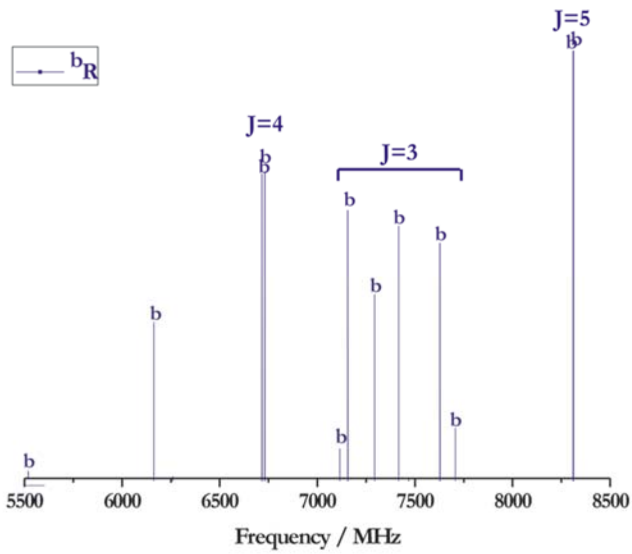

Figure: 6.5.- Example of ^{b}R-type spectrum simulations for conformer 1 (equatorial).

This kind of predictions give useful information for the experimental data acquisition because it also informs where the spectral density is higher (rotational temperatures of 2 K are used for the prediction of intensities). Later, this information let us test the computational calculations for weakly-bound clusters.

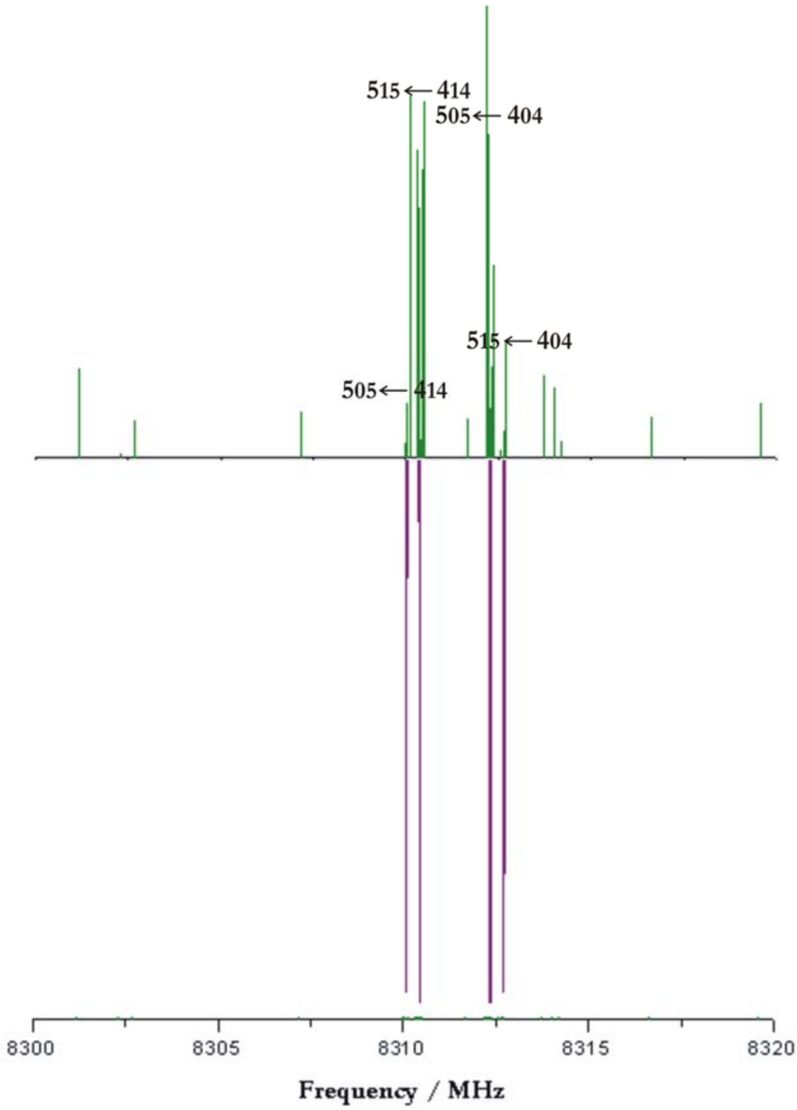

Figure: 6.6.- A section of the experimental scan obtained for the complex tropinone···water. Some of the assigned transitions belonging to the most stable equatorial conformer have been identified. The variation of the experimental intensities is due to the non-uniform conditions during the scans.

We show in figure 6.6 above a section of the experimental scan for the system tropinone···water. The transitions for the most stable equatorial conformer were easily distinguished and assigned accordingly. The signals for the axial species were not identified. The search for less stable species did not provide also any result.

b. Hyperfine effects: Nuclear Quadrupole Coupling.

Due to the presence in tropinone of an atom with a non-spherical nuclear charge distribution (^{14}N, I=1) which can interact with the local electric fields, the angular momentum of the molecular rotation couples to the nuclear spin. As a result, a splitting in the rotational transitions is observed in the spectrum.

We show some typical transitions in Figure 6.7, where we observe both the instrumental Doppler effect (ca. 50-70 kHz) and the larger nuclear quadrupole coupling hyperfine effects.[20,21] The transition nuclear quadrupole splittings are relatively small ($<\Delta\nu\sim 1.0 MHz$).

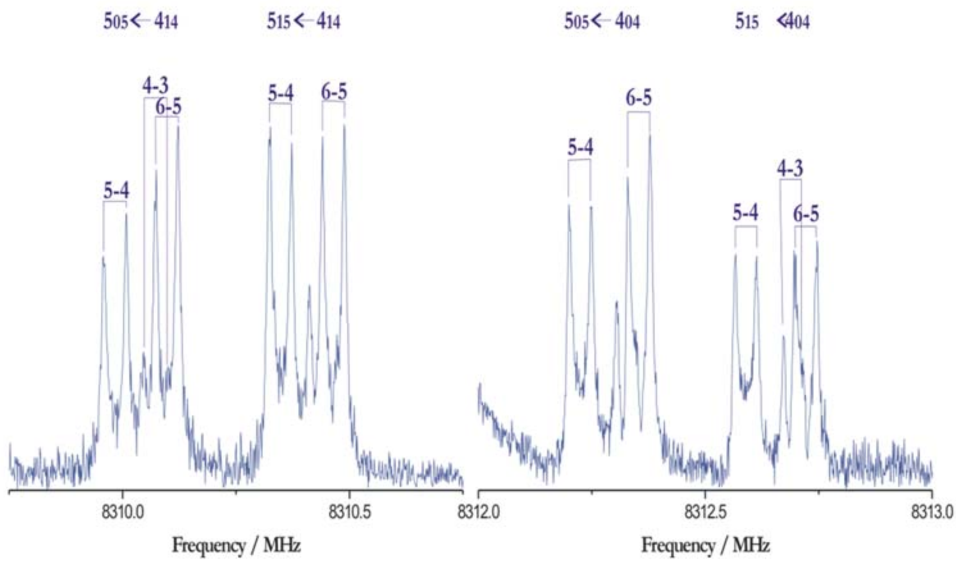

Figure: 6.7.- **(a)** $5_{0,5} \leftarrow 4_{1,4}$ and $5_{1,5} \leftarrow 4_{1,4}$ rotational transitions for the most stable conformer of the complex tropinone···water. **(b)** $5_{0,5} \leftarrow 4_{0,4}$ and $5_{1,5} \leftarrow 4_{0,4}$ transitions for the same conformer. Hyperfine components are labeled with quantum numbers ***J*=*I*+*F***.

c. Determination of the Spectroscopic Parameters.

The transition frequencies in Table 6.3 and were fitted to derive the rotational parameters shown in table 6.2. The fit was carried out using the semi-rigid rotor Watson Hamiltonian in the Symmetric reduction (S) and in the I^r representation (suitable to prolate tops[19]). An extra term that takes in account the nuclear quadrupole coupling interactions was also added to the Hamiltonian.

As observed in table 6.2, four out of five quartic centrifugal distortion constants were determined. All rotational parameters were obtained with high accuracy thanks to the good number and different types of transitions observed (μ_a and μ_b). The diagonal elements of the nuclear quadrupole coupling tensor were also obtained. These matrix elements were sufficient to reproduce the small experimental splittings, so no out-of-diagonal elements were determined.

A total of 89 different transitions were measured leading to a good accuracy of the spectroscopic parameters. According to the correlations coefficients between parameters we detected some high values for the correlations between some centrifugal distortion constants such as D_J and D_{JK}. More transitions should be measured in order to improve this problem. However, the low intensity of them and the frequency range makes difficult the detection.

Table: 6.2.- Experimental rotational parameters and comparison with the MP2 values for the observed conformation of tropinone···water.

	Conformer 1 (equatorial)	
	Experiment	Theory MP2
A **/ MHz**	1260.2583 (11)[a]	1290
B **/ MHz**	1087.39092 (50)	1095
C **/ MHz**	794.12498 (19)	809
D_J / kHz	0.1341 (69)	0.10
D_{JK} /kHz	-0.719 (33)	-0.52
D_K / kHz	0.671 (50)	0.39
d_1 / Hz	-35.0 (36)	-32.4
d_2 / Hz	---	83.2
χ_{aa} / MHz	2.450 (11)	2.4
χ_{bb} / MHz	-4.7368 (91)	-4.7
χ_{cc} / MHz	2.2868 (91)	2.3
$\|\mu_a\|$ / D		4.2
$\|\mu_b\|$ / D		3.1
$\|\mu_c\|$ / D		0.0
$\|\mu_{TOT}\|$ / D		5.2
N[b]	89	
σ / kHz[c]	0.58	

[a] Standard errors in parenthesis in units of the last digit.
[b] Number of fitted transitions.
[c] Standard deviation of the fit.

Table: 6.3.- Experimental frequencies and calculated values (MHz) for the μ_a-transitions of the equatorial conformer of the complex tropinone···water. The last column is the difference (kHz) between the measured and calculated frequencies ($\Delta\nu = \nu_{OBS} - \nu_{CALC}$).

J'	K'_{-1}	K'_{+1}	J''	K''_{-1}	K''_{+1}	F'	F''	ν_{OBS} / MHz	ν_{CALC} / MHz	$\Delta\nu$ / kHz
4	1	4	3	1	3	4	3	6718.3594	6718.3582	1.3
						3	2	6718.4633	6718.4630	0.3
						5	4	6718.5000	6718.5013	-1.2
4	0	4	3	0	3	4	3	6728.5315	6728.5311	0.4
						5	4	6728.7584	6728.7576	0.8
4	2	3	3	2	2	5	4	7374.9312	7374.9254	5.8
						4	3	7374.9676	7374.9668	0.8
4	1	3	3	1	2	4	3	7546.0573	7546.0537	3.6
						5	4	7546.7598	7546.7583	1.4
4	2	2	3	2	1	5	4	8140.0984	8140.0952	3.2
						3	2	8140.2061	8140.2000	6.0
						4	3	8140.2395	8140.2370	2.4

Table: 6.3 Continued.-

5 1 5	4 1 4	5	4	8310.3452	8310.3482	-3.0
		6	5	8310.4635	8310.4653	-1.8
5 0 5	4 0 4	5	4	8312.2230	8312.2254	-2.3
		6	5	8312.3547	8312.3553	-0.6
5 2 4	4 2 3	5	4	9026.5537	9026.5542	-0.4
		6	5	9026.7235	9026.7214	2.1
		4	3	9026.7556	9026.7576	-1.9
5 1 4	4 1 3	5	4	9088.3230	9088.3215	1.4
		6	5	9088.7740	9088.7756	-1.5
		4	3	9088.8890	9088.8903	-1.2
5 3 3	4 3 2	4	3	9575.7495	9575.7526	-3.0
		6	5	9575.7905	9575.7953	-4.8
		5	4	9576.0478	9576.0491	-1.2
6 1 6	5 1 5	6	5	9899.1873	9899.1895	-2.2
		5	4	9899.2530	9899.2552	-2.1
		7	6	9899.2779	9899.2776	0.3
6 0 6	5 0 5	6	5	9899.4976	9899.4986	-1.0
		5	4	9899.5659	9899.5664	-0.4
		7	6	9899.5893	9899.5884	0.8
5 2 3	4 2 2	5	4	9925.6484	9925.6494	-0.9
		6	5	9926.1163	9926.1157	0.5
		4	3	9926.2988	9926.2998	-1.0
5 3 2	4 3 1	4	3	10252.5776	10252.5759	1.6
		6	5	10252.6267	10252.6308	-4.1
		5	4	10253.2077	10253.2139	-6.1
6 2 5	5 2 4	6	5	10634.8378	10634.8353	2.4
		7	6	10635.0243	10635.0240	0.2
		5	4	10635.0540	10635.0514	2.5
6 1 5	5 1 4	6	5	10650.2523	10650.2488	3.5
		7	6	10650.5060	10650.5063	-0.2
		5	4	10650.5470	10650.5483	-1.2
6 3 4	5 3 3	6	5	11302.4128	11302.4145	-1.6
		7	6	11302.4733	11302.4748	-1.4
		5	4	11302.4980	11302.4997	-1.6
7 1 7	6 1 6	7	6	11487.4507	11487.4490	1.7
		6	5	11487.4941	11487.4974	-3.3
		8	7	11487.5176	11487.5162	1.3
7 0 7	6 0 6	7	6	11487.4941	11487.4965	-2.4
		8	7	11487.5659	11487.5639	1.9

Table: 6.4.-. Experimental frequencies and calculated values (MHz) for the μ_b-transitions of the equatorial conformer of the complex tropinone···water. The last column is the difference (kHz) between the measured and calculated frequencies ($\Delta\nu = \nu_{OBS} - \nu_{CALC}$).

J'	K'_{-1}	K'_{+1}	J''	K''_{-1}	K''_{+1}	F'	F''	ν_{OBS} / MHz	ν_{CALC} / MHz	$\Delta\nu$ / kHz
4	1	4	3	0	3	4	3	6730.7735	6730.7729	0.6
						5	4	6731.0140	6731.0143	-0.2
5	0	5	4	1	4	5	4	8309.9846	8309.9836	1.0
						4	3	8310.0714	8310.0712	0.2
						6	5	8310.0980	8310.0986	-0.6
5	1	5	4	0	4	5	4	8312.5912	8312.5900	1.1
						4	3	8312.6962	8312.6989	-2.6
						6	5	8312.7227	8312.7220	0.6
5	1	4	4	2	3	5	4	9007.2709	9007.2667	4.2
						6	5	9007.3486	9007.3494	-0.8
						4	3	9007.3754	9007.3684	7.0
5	2	4	4	1	3	5	4	9107.6064	9107.6090	-2.6
						6	5	9108.1461	9108.1475	-1.4
						4	3	9108.2775	9108.2795	-1.9
4	4	1	3	3	0	4	3	9738.9054	9738.9034	1.9
						5	4	9739.4289	9739.4249	3.9
						3	2	9739.5257	9739.5256	0.0
4	4	0	3	3	1	3	2	9854.1726	9854.1731	-0.5
						5	4	9854.2579	9854.2552	2.7
						4	3	9854.2929	9854.2951	-2.1
5	4	2	4	3	1	5	4	11434.7550	11434.7601	-5.1
						6	5	11435.8333	11435.8364	-3.0
6	2	4	5	2	3	6	5	11494.7998	11494.8018	-1.9
						7	6	11495.3719	11495.3736	-1.7
						5	4	11495.5150	11495.5122	2.8
7	2	6	6	1	5	7	6	12231.3119	12231.3131	-1.2
						8	7	12231.4896	12231.4893	0.2
						6	5	12231.5116	12231.5073	4.2
7	1	6	6	2	5	7	6	12226.7409	12226.7375	-3.0
						8	7	12226.8928	12226.8953	-2.4
						6	5	12226.9134	12226.9103	3.0
7	2	6	6	2	5	7	6	12227.4407	12227.4391	1.5
						8	7	12227.5971	12227.5996	-2.4
						6	5	12227.6227	12227.6149	7.7
7	1	6	6	1	5	7	6	12230.6128	12230.6114	1.3
						8	7	12230.7834	12230.7850	-1.5
						6	5	12230.8059	12230.8026	3.2

6.4 Conclusions.-

The experimental study of the complex of tropinone···water in gas phase led to the identification of the equatorial conformer predicted as most stable, with the water molecule bound through a O-H···N hydrogen bond. This observation is consistent with the theoretical calculations in Table 6.1.

No other conformers were detected in the jet despite the axial structure was predicted relatively close in energy (ca. 3 kJ mol^{-1}).

Since the main interaction O-H···N hydrogen bond is very similar in both conformers, we can consider the role played by the weak C-H···O_w secondary interactions in the hydrated environment controlling the conformational balance. Those weak hydrogen bond interactions attached the water molecule to tropinone avoiding any intramolecular dynamics in the complex.

The unambiguous identification of the conformer predicted as most stable allows the check of the validity of the ab initio MP2 calculations to reproduce with high accuracy the intramolecular interactions as well as intramolecular force of the complex in gas phase.[20] Moreover, these theoretical calculations let us test the poor results obtained with the methods based on the Density Functional Theory when the system is formed by more than one molecule and the intermolecular interactions are important.

It is important to point out that, as in the tropinone case, the most stable conformer is associated to the equatorial chair structure. This is different from the pseudopelletierine molecule, where the less energetic state for the 8-membered ring, was the chair-chair axial structure (see chapter 2).

6.5 Referencias.-

[1] G. Grynkiewicz, M. Gadzikowska, *Pharm. Rep.*, 60, 439, **2008**.

[2] T. Hemscheidtt, in *Topics in Current Chemistry*, ed. F. J. Leeper and J. C. Vederas, Springer-Verlag, Berlin-Heilderberg, **2000**, vol.209, pp.175-206.

[3] E. J. Cocinero, A. Lesarri, P. Écija, J.-U. Grabow, J. A. Fernández, F. Castaño, *Phys. Chem. Chem. Phys.*, 12, 6076, **2010**.

[4] P. Écija, E. J. Cocinero, A. Lesarri, F. J. Basterretxea, J. A. Fernández, F. Castaño, *ChemPhysChem*, 14, 1830, **2013**.

[5] R. Glasser, Q.-J. Peng, A. S. Perlin, *J. Org. Chem.*, 53, 2172, **1988**.

[6] G. S. Chappel, B. F. Grabowski, R. A. Sandman, D. M. Yourtee, *J. Pharm. Sci.*, 62, 414, **1973**.

[7] R. Glasser, J.-P. Charland, A. Michel, *J. Chem. Soc.*, Pekin Trans. 2, 1875, **1989**.

[8] L. Evangelisti, A. Lesarri, M. K. Jahn, E. J. Cocinero, W. Caminati, J.-U. Grabow, *J. Phys. Chem. A*, 115, 9545-9551, **2011**.

[9] E. Zwart, J. J. ter Meulen, W.L. Meerts, L.H. Coudert, *J. Mol. Spectrosc.*, 147, 27, **1991**.

[10] G. A. Jeffrey, "An introduction to hydrogen bonding", Oxford University Press, New York, **1997**.

[11] J. A. Jeffrey, W. Saenger, "Hydrogen bonding in biological structures", Springer, Berlin, **1991**.

[12] M. J. Tubergen, R.L. Kuczkowski, *J. Am. Chem. Soc.* 115, 9263, **1993**.

[13] T. Herbine, T.R. Dyke, *J. Chem. Phys.* 83, 3768, **1985**.

[14] L.B. Favero, L. Evangelisti, A. Maris, A. Vega-Toribio, A. Lesarri, W. Caminati, *J. Phys. Chem. A*, 115, 9493-9497, **2011**.

[15] Macromodel, version 9.2, Schrödinger, LLc, New York, NY, **2012**.

[16] M. J. Frisch et al. GAUSSIAN09, Revision **D.01**, Gaussian, Inc., Wallingford CT, **2009**.

[17] M. Pickett, *J.Mol. Spectrosc.,*148, 371, **1991**.

[18] http://www.nist.gov/pml/div686/sources_detectors/jb95.cfm Retrieved 2014-01-30.

[19] W. Gordy, L.R. Cook, 'Microwave Molecular Spectra', 3rd Edition, in: A. Weissberger (Ed.), *Techniques of Chemistry*, vol. XVIII, John Wiley & Sons Inc., New York, **1984**.

[20] Y. Zhao, D. G. Truhlar, *Acc. Chem. Res.*, 41, num. 2, 157, **2008**.

Chapter 7

2-Fluoropyridine···water

7.1. Introduction.-

Pyridine is an aromatic heterocycle widely used in the pharmaceutical and chemical industry.[1] The fluorination of that molecule causes different chemical behavior depending on the site of the ring where the halogen atom is attached. This phenomenon has been revealed in previous studies in both 2-fluoropyridine and 3-fluoropyridine.[2] According to the structural parameters obtained from the rotational spectrum, it has been proved that the fluorine substitution at the ortho position has a larger effect in the electronic structure than the fluorination in the meta position. Different bond lengths and angles were determined in order to demonstrate the structural changes of the fluoropyridines respect to the pyridine molecule: while the distance N-C2 in the 2-fluoropyridine is 1.310Å, it is found to be 1.336Å for 3-

fluoropyridine (see figure 1 for atom labeling) and 127º and 122º are the values found for the N-C2-C3 angle, respectively. Comparing those values with the bond lengths in the case of the pyridine molecule (see table 7.1) we can easily notice that the distortion in 2-fluoropyridine is larger than the structural distortion found when fluorination occurs in the meta position.

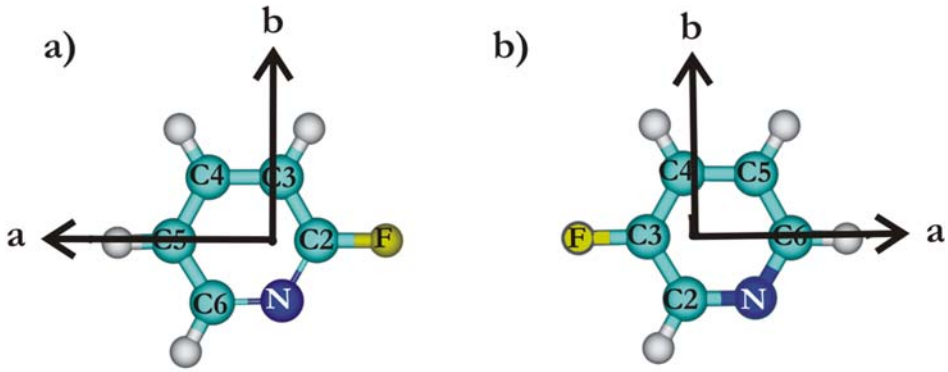

Figure: 7.1.- a) 2-Fluoropyridine b) 3-Fluoropyridine in its respective principal axis orientation. All the heavy atoms are labeled.

Studies of the nuclear charge distribution confirm that the position of the fluorine atom in the ring dramatically affects the charge density and in consequence the chemical properties and behavior of the molecule. It is clear the interest of the effects of these fluorinations due to the widely used of molecules with fluorine substitutions in pharmacokinetic studies as a way to alter the rate of the reaction.[3]

Table: 7.1.- Structural parameters of fluoro substituted pyridines compared with the pyridine values.

	Pyridine	**2-Fluoropyridine**	**3-Fluoropyridine**
N-C2 / Å	1.340	1.310	1.336
N-C2-C3 /º	123.8	127	122

In this work we are interested to explore the microsolvation of 2-fluoropyridine with a single water molecule, to establish the effect of the fluorination in the weak interactions between pyridine and water. We are thus particularly interested to check whether there are different binding sites or interactions depending on the fluorination site.

7.2. Computational Methods.-

In order to understand the possible ways of interaction between the ring and water, we first considered the electronegative nitrogen nucleus. We can expect the interaction of the two subunits through a hydrogen bond between the nitrogen of the ring and the hydrogens of water in interactions O-H···N.[4-7] On the other hand, we could also consider other weak hydrogen bonds where the ring links to water via a proton acceptor oxygen, as in C-H···O interactions. Finally, weak interactions involving the C-F···H bond might also be possible.[8-10] In order to fully explore the conformational landscape of the complex we used computational tools that are able to obtain the rotational properties of the molecule and its energies.

First of all, we used Molecular Mechanics[11] to quickly identify the structures of the most stable conformers. Four different structures were identified in a window energy of about 15 kJ·mol^{-1}, and their geometries are shown in figure 7.2.

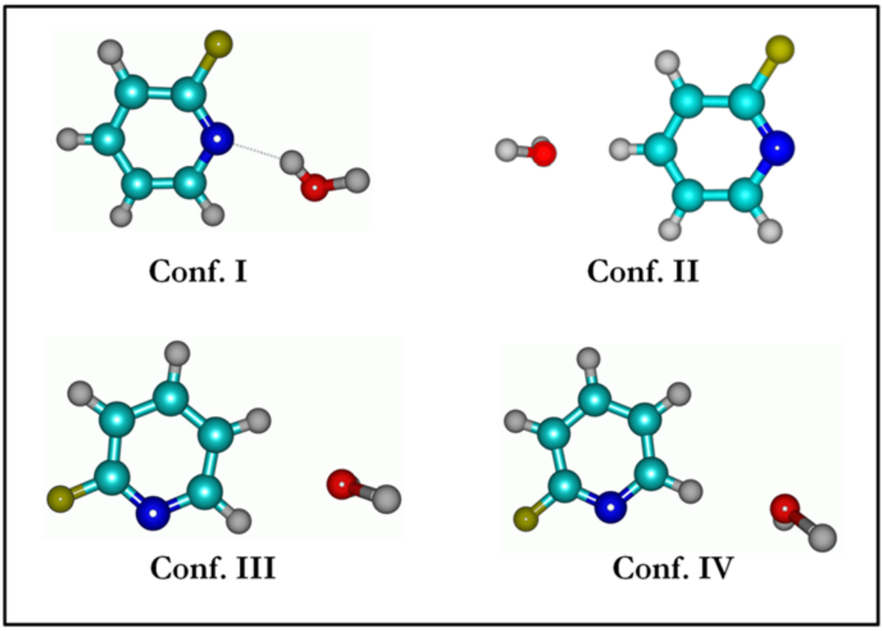

Figure: 7.2.- Structures of the four most stable conformers of the complex 2-fluoropyridine···water.

The obtained geometries were later fully optimized using ab initio methods. In particular, second-order Møller-Plesset calculations were used with the Pople triple-ζ basis set with diffuse and polarization functions (6-311++G(d,p)). This kind of ab initio methods were proved to be appropriate for spectroscopic purposes for this type of complexes.

In order to distinguish the conformers which are real minima within the four detected structures, vibrational harmonic frequency calculations were carried out and the dissociation energy of each complex was calculated using the counterpoise procedure. All the computations were implemented in Gausian09.[12]

In the following table, the predicted rotational constants, the electric dipole moments of the system, as well as several rotational parameters are listed.

Table: 7.2.- Rotational constants (*A*, *B*, *C*), dipole moments (μ_a, α = a, b, c) and diagonal elements of the quadrupole tensor of the ^{14}N nucleus ($\chi_{\alpha\beta}$, (α,β = a, b, c)) for the four plausible conformers. The five quartic centrifugal distortion constants (Δ_J, Δ_{JK}, Δ_K, δ_K and δ_K) and the relative energy, zero point corrected, are also given. The dissociation energy (BSSE corrected) was also calculated.

	Theory MP2, 6-311++G(d,p)			
	Conf I (1)	**Conf II (4)**	**Conf III (6)**	**Conf IV (10)**
***A*/MHz**	2704	3483	4684	3437
***B*/MHz**	1474	944	950	968
***C*/MHz**	956	745	793	758
χ_{aa} / MHz	-3.50	-4.17	1.52	1.35
χ_{bb} / MHz	0.94	1.40	-4.33	-4.17
χ_{cc} / MHz	2.56	2.77	2.80	2.82
$\|\mu_a\|$ /D	3.70	5.97	4.58	2.70
$\|\mu_b\|$ /D	0.82	0.40	2.29	1.95
$\|\mu_c\|$ /D	0.78	0.01	0.02	0.00
$\|\mu_{TOT}\|$ /D	3.87	5.98	5.12	3.33
D_J / kHz	0.05	0.31	0.26	0.16
D_{JK} / kHz	9.98	29.30	1.27	29.60
D_K / kHz	-8.55	12.83	14.75	37.86
d_1 / kHz	-0.17	-0.17	-61.92	-0.19
d_2 / kHz	-0.21	-0.09	-10.80	-0.18
$\Delta(E+ZPE)$ / kJ·mol^{-1}	0.0	11.2	11.8	13.2
E_d / kJ·mol^{-1}	15.7	4.7	4.2	2.6

7.3. Results and Analysis.-

a. Assignment of the Rotational Spectrum.

According to the ab initio calculations, it is most probable that only the conformer predicted as most stable could be detected in the jet due to the large energy difference of other geometries with the global minimum (>10 kJ·mol^{-1}). The large dissociation energy of conformer I is also indicative of its stability.

We predicted the rotational spectrum of the asymmetric prolate top ($\kappa \approx$ -0.40) conformer 1 using the Pickett[13] programs. This program uses the semi-rigid rotor Watson Hamiltonian[14] to calculate the transition frequencies and intensities at the jet temperature (ca. 2 K). Looking at the theoretical predictions for conformer I, we observe that the electric dipole moments along the three principal axis are different from zero ($\mu_a >> \mu_b \approx \mu_c$), so we can expect that the three selection rules will be active.

The large value of the electric dipole along the a-axis suggests that the spectrum search could start by the characteristic μ_a-type R-branch pattern, which was soon identified. This pattern consists of (J+1) $\leftarrow J$ progressions separated by a distance close to the value of $B + C$. We measured several transitions with angular momentum J running from 3 to 8 and K_{-1} from 0 to 4.

Some weaker μ_b–type and μ_c–type lines were later detected. The experimental spectra were analyzed using the semi-rigid Watson´s Hamiltonian in the symmetric reduction and I^r representation with an additional term that takes into account the ^{14}N nuclear quadrupole coupling effect.[15] This effect can be described as an electrical interaction resulting from the non-spherical charge distribution in the ^{14}N nucleus. As a consequence of that hyperfine effect, each transition is split into different resolvable components. The observed conformer was identified as the most stable structure predicted by the ab initio calculations. It the next figure, we can see the experimental spectrum compared with the final simulation for conformer 1. No other species were detected in the jet.

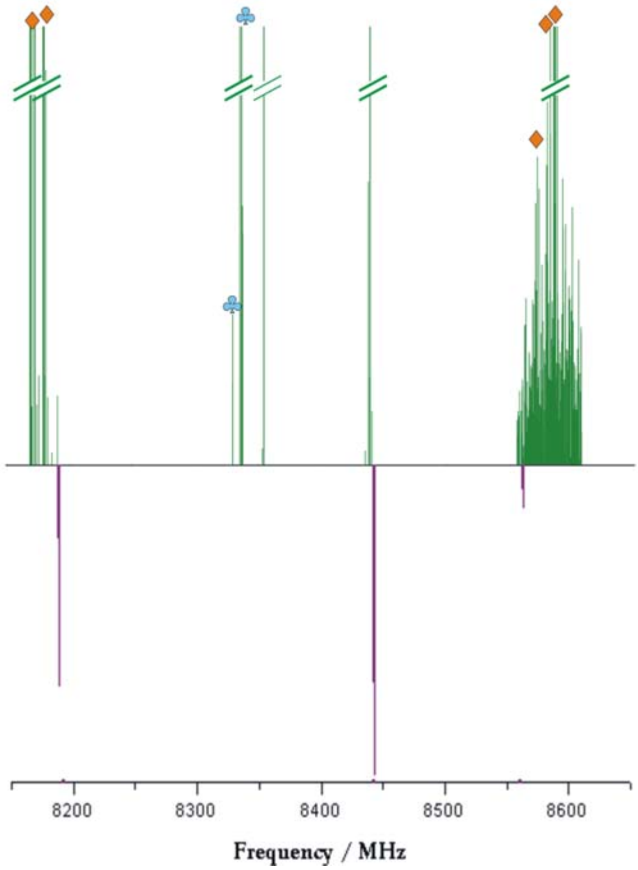

Figure: 7.3.- A section of the experimental spectrum of the complex 2-Fluoropyridine···water (green) compared with the predicted (violet). Some transitions to isotopic species (♣) and to the monomer (♦) were also detected.

b. Hyperfine effects: Nuclear quadrupole coupling.

The electric interactions between the charge distribution of a nucleus with non-zero nuclear spin and the molecular electric field gradient cause the splitting of the rotational transitions. This hyperfine effect is characterized by the quantum number F associated to the angular momentum coupling of the nuclear spin and molecular rotation ($\boldsymbol{F} = \boldsymbol{J}+\boldsymbol{I}$), with selection rules $\Delta F = 0, \pm 1$. The most intense transitions are those with $\Delta F = \Delta J$.

In the 2-fluoropyridine···water system, and due to the small quadrupole moment of ^{14}N, the transition splittings are rather small, i.e., less than 1 MHz in all cases. An example of a rotational transition showing the hyperfine components can be seen in figure 7.4.

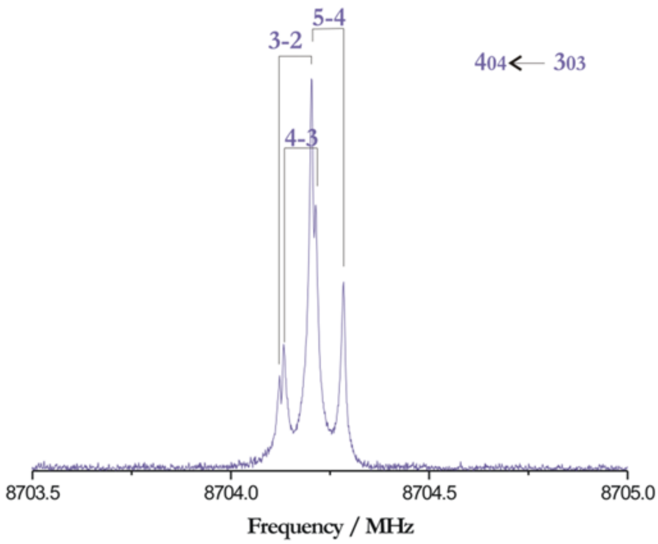

Figure: 7.4.- $4_{0,4} \leftarrow 3_{0,3}$ transition of conformer 1. The hyperfine components are labeled as $F' \leftarrow F''$.

The nuclear quadrupolar components can give information on the electronic environment around the ^{14}N nucleus, since the tensor elements ($\chi_{\alpha\beta}$) are linearly related to the electric field gradient ($\boldsymbol{q}$) and the quadrupolar moment (Q) through $\boldsymbol{\chi} = eQ\boldsymbol{q}$. Since the quadrupole coupling constants are also sensitive to the orientation of the principal inertial axes they can also serve to discern between the different conformations.

c. Determination of the spectroscopic parameters.

The experimental measurements (see table 7.4) were fitted using the semi-rigid Watson Hamiltonian in the asymmetric reduction (A) and in the I^r representation, with an additional term which accounts for the quadrupole interactions. The I^r representation is suitable for prolate rotors.[14] The results of the fit are shown in the following table.

Table: 7.3.- Experimental rotational constants (A, B, C), ^{14}N nuclear quadrupole coupling elements ($\chi_{aa}, \chi_{bb}, \chi_{cc}$) and centrifugal distortion constants ($D_J, D_{JK}, D_K, d_1, d_2$) for the conformer found in the spectrum.

	Experiment	**Theory**
A/MHz	2738.1777 (7)[a]	2704
B/MHz	1462.5221 (2)	1474
C/MHz	953.0579 (1)	956
χ_{aa} / MHz	-3.570 (6)	-3.50
χ_{bb} / MHz	1.00 (2)	0.94
χ_{cc} / MHz	2.57 (2)	2.56
D_J / kHz	0.029 (4)	0.05
D_{JK} / kHz	-11.24 (1)	-8.55
D_K / kHz	9.62 (7)	9.98
d_1 / kHz	-0.179 (1)	-0.17
d_2 / kHz	-0.224 (1)	-0.21
N[b]	102	---
σ[c] / kHz	3.63	--

[a] Standard error in parentheses in units of the last digit.
[b] Number of transitions in the fit.
[c] Standard deviation of the fit.

All the transitions are listed in the following tables. No other conformers were detected in the spectrum.

Table: 7.4.- Measured and calculated frequencies in MHz for each transition observed for the complex 2-fluoropyridine···water. The last column represents the difference (in kHz) between the measured and calculated frequencies $\Delta\nu = \nu_{OBS} - \nu_{CALC}$.

J'	K'_{-1}	K'_{+1}	J''	K''_{-1}	K''_{+1}	F'	F''	ν_{OBS} / MHz	ν_{CALC} / MHz	$\Delta\nu$ / kHz
3	1	2	2	1	1	4	3	7920.8592	7920.8614	2.2
						3	2	7920.5319	7920.5297	-2.6
						2	1	7920.8960	7920.8885	-7.5
3	2	2	2	2	1	4	3	7246.7460	7246.7431	2.9
						3	2	7245.5945	7245.5963	-1.8
						2	1	7247.3765	7247.3798	-3.8
3	2	1	2	2	0	4	3	7702.9236	7702.9189	4.7
						3	2	7701.8262	7701.8248	1.4
						2	1	7703.5456	7703.5453	0.3
4	0	4	3	0	3	3	2	8704.3269	8704.3276	-0.7
						4	3	8704.3380	8704.3384	-0.4
						5	4	8704.4250	8704.4244	0.6
4	1	4	3	1	3	4	3	8442.1218	8442.1231	-1.3
						3	2	8442.2204	8442.2105	0.9
						5	4	8442.2847	8442.2858	-1.1

Table: 7.4 continued.-

J'	K'_{-1}	K'_{+1}	J''	K''_{-1}	K''_{+1}	F'	F''	ν_{OBS} / MHz	ν_{CALC} / MHz	$\Delta\nu$ / kHz
4	1	3	3	1	2	4	3	10366.3591	10366.3596	-0.4
						3	2	10366.5005	10366.4994	1.1
						5	4	10366.5152	10366.5183	-3.1
4	2	3	3	2	2	4	3	9563.2399	9563.2390	0.9
						3	2	9563.8629	9563.8618	1.1
						5	4	9563.7334	9563.7344	-1.0
4	2	2	3	2	1	4	3	10518.5227	10518.5220	0.7
						5	4	10518.9627	10518.9589	3.8
						3	2	10519.0852	10519.0793	5.9
4	3	2	3	3	1	4	3	9861.8269	9861.8259	1.0
						3	2	9863.2790	9863.2781	-0.9
						5	4	9862.8736	9862.8718	1.8
4	3	1	3	3	0	4	3	9975.3531	9975.3544	-1.3
						3	2	9976.7965	9976.7987	-2.2
						5	4	9976.3917	9976.3924	-0.7
5	0	5	4	0	4	5	4	10561.8157	10561.8144	1.3
						4	3	10561.8278	10561.8301	-2.3
						6	5	10561.8876	10561.8880	-0.4
5	1	5	4	1	4	4	3	10420.7241	10420.7251	-1.0
						5	4	10420.6755	10420.6775	-2.0
						6	5	10420.7771	10420.7761	1.0
5	1	4	4	1	3	4	3	12606.8432	12606.8371	6.1
						5	4	12606.7547	12606.7514	3.3
						6	5	12606.8600	12606.8582	1.8
5	2	4	4	2	3	5	4	11801.7618	11801.7642	-2.4
						6	5	11802.0364	11802.0331	3.3
						4	3	11802.0580	11802.0612	-3.2
5	2	3	4	2	2	4	3	13297.7422	13297.7495	-7.3
						5	4	13297.5069	13297.5098	-2.9
						6	5	13297.7219	13297.7244	-2.5
5	3	3	4	3	2	4	3	12340.6542	12340.6505	3.7
						5	4	12339.9744	12339.9765	-2.1
						6	5	12340.5158	12340.5164	-0.6
5	3	2	4	3	1	4	3	12701.3968	12701.3946	2.2
						5	4	12700.7469	12700.7400	6.9
						6	5	12701.2690	12701.2633	5.7
5	4	2	4	4	1	5	4	12350.9699	12350.9694	0.5
						4	3	12352.1992	12352.2014	-2.2
						6	5	12351.9176	12351.9169	0.7
6	0	6	5	0	5	7	6	12428.8336	12428.8323	1.3
						5	4	12428.7933	12428.7924	0.9
						6	5	12428.7644	12428.7755	-7.7
6	1	6	5	1	5	7	6	12363.9338	12363.9343	-0.5
						6	5	12363.8661	12363.8663	-0.2
						5	4	12363.8949	12363.8960	-1.1

Table: 7.4 continued.-										
J'	***K'$_{-1}$***	***K'$_{+1}$***	***J''***	***K''$_{-1}$***	***K''$_{+1}$***	***F'***	***F''***	**ν_{OBS} / MHz**	**ν_{CALC} / MHz**	**$\Delta\nu$ / kHz**
6	1	5	5	1	4	7	6	14613.6649	14613.6599	5.0
						6	5	14613.5712	14613.5713	-0.1
						5	4	14613.6385	14613.6431	-4.6
6	2	5	5	2	4	7	6	13954.1892	13954.1869	2.3
						6	5	13954.0177	13954.0178	-0.1
						5	4	13954.1892	13954.1887	0.5
6	2	4	5	2	3	7	6	15932.4423	15932.4420	0.3
						6	5	15932.3239	15932.3170	6.9
						5	4	15932.4423	15932.4432	-0.9
6	3	4	5	3	3	7	6	14774.2528	14774.2556	-2.8
						5	4	14774.3117	14774.3062	5.5
						6	5	14773.9269	14773.9379	-11.0
6	3	3	5	3	2	7	6	15578.0139	15578.0162	-2.3
						6	5	15577.7217	15577.7249	-3.2
8	0	8	7	0	7	9	8	16210.5452	16210.5436	1.6
						8	7	16210.4995	16210.5044	-4.9
						7	6	16210.5193	16210.5201	-0.8
8	1	8	7	1	7	9	8	16199.8160	16199.8170	-1.0
						8	7	16199.7770	16199.7771	-0.1
						7	6	16199.7994	16199.7938	5.6
3	3	0	2	2	1	4	3	14988.3109	14988.3097	1.2
						3	2	14988.6591	14988.6626	-3.5
						2	1	14988.4283	14988.4218	6.5
3	2	2	2	1	1	4	3	11073.3355	11073.3374	-1.9
						3	2	11073.6612	11073.6582	3.0
						2	1	11073.1597	11073.1592	0.5
3	2	1	2	1	2	4	3	13182.4247	13182.4238	0.9
						3	2	13183.3360	13182.3384	-2.4
						2	1	13181.9304	13182.9337	-3.3
4	0	4	3	1	3	3	2	8191.9242	8191.4254	-1.2
						4	3	8191.7841	8191.7836	0.5
						5	4	8191.9807	8191.9824	-1.7
4	1	4	3	0	3	3	2	8954.6250	8954.6218	3.2
						4	3	8954.6774	8954.6780	-0.6
						5	4	8954.7269	8954.7277	-0.8
4	3	2	3	2	1	5	4	17003.8596	17003.8619	-2.3
						4	3	17004.2211	17004.2246	-3.5
						3	2	17003.7792	17003.7816	2.4
5	0	5	4	1	4	6	5	10311.5850	10311.5847	0.3
						5	4	10311.4746	10311.4748	-0.2
						4	3	10311.5329	10311.5360	-3.1
5	1	5	4	0	4	6	5	10671.0799	10671.0795	0.4
						5	4	10671.0186	10671.0172	1.4
						4	3	10671.0186	10671.0192	-0.6

Table: 7.4 continued.-										
J'	***K'*$_{-1}$**	***K'*$_{+1}$**	***J''***	***K''*$_{-1}$**	***K''*$_{+1}$**	***F'***	***F''***	ν_{OBS} / **MHz**	ν_{CALC} / **MHz**	$\Delta\nu$ / **kHz**
6	1	6	5	0	5	7	6	12473.1252	12473.1257	-0.5
						6	5	12473.0704	12473.0691	1.3
						5	4	12473.0928	12473.0852	7.6

The number and diversity of transitions resulted in a satisfactory fitting, with the root-mean square (rms) deviation under 4 kHz and acceptable correlation coefficients. Besides, all the centrifugal distortion constants were determined, as well as the diagonal elements of the nuclear quadrupole coupling tensor.

The conformational assignment of the experimental observations was unambiguous from a comparison between the experimental rotational constants and the predictions for conformer I (see table 7.3), with differences below 2%. So, the final fit unequivocally identifies the conformer detected in the jet as the predicted theoretically as most stable.

Concerning the preferred binding sites of this system, it was proved that the most stable configuration is obtained when the water hydrogen acts as a proton donor and the complex is linked through a moderate O-H···N hydrogen bond to the lone pair at the nitrogen atom. The alternative structures with water acting as proton acceptor from pyridine hydrogens are considerably less stabilized.

To obtain more information about the structure and bonding of the complex we studied the rotational spectra of different isotopic species. Starting from the rotational constants of the isotopologues we determined the substitution and effective structures and from that we estimated the dissociation energy of the complex. The results are explained in the next section.

d. Isotopic Substitution: Structure Determination.

The changes in the atomic masses dramatically affect and modify the moments of inertia of the system. Consequently, the rotational constants become slightly different respect to the parent species, allowing the calculation of the experimental structure of the observed conformer. To evaluate the bonding parameters of the complex, as well as some interesting magnitudes such as the dissociation energy, we analyzed the rotational spectra of several isotopically substituted species. However, the low intensity of the complex signals made it impossible to measure isotopologues in natural abundance, so we used chemically marked samples in order to obtain a measurable rotational spectrum of the $C_5H_4FN\cdots H_2{}^{18}O$, $C_5H_4FN\cdots DOH$, $C_5H_4FN\cdots HOD$ and $C_5H_4FN\cdots D_2O$ species.

Following the same procedure used for the parent species, we fitted μ_a, μ_b and μ_c-type transitions for all the considered isotopologues. Despite the reduced number of transitions in these cases, we obtained the rotational constants with good accuracy. In all of the fits, the values of the quartic centrifugal distortion constants were fixed to its parent value for convenience (see table 7.3). The results are summarized in table 7.5 and an example of the measured rotational transitions for each substituted species is shown in figure 7.5.

The rotational constants and errors allowed obtaining the substitution[16,17] (r_s) and effective[18,19] (r_0) structures. The substitution structure is obtained replacing each atom for another isotopic species. From the rotational constants of all the isotopologues and the variation of the inertial moments with respect to the parent, we calculate the absolute atomic coordinates of the substituted atom in the principal inertial axes system using the Kraitchman equations. Depending on the number of substituted coordinates we can derive some interesting structural parameters such as bond lengths or dihedral angles relevant to the stability of the complex. However, a full substitution structure requires substitution for all atoms, which is impractical for this complex since we observed only substitutions in the water dimer. We show in Table 7.6 the atomic coordinates for the substituted atoms.

Table: 7.5.- Experimental rotational constant (*A*, *B*, *C*) for all the substituted species. The centrifugal distortion constants and the ^{14}N nuclear quadrupole coupling elements were fixed to the parent species.

	$C_5H_4FN\cdots H_2{}^{18}O$	$C_5H_4FN\cdots DOH$	$C_5H_4FN\cdots HOD$	$C_5H_4FN\cdots D_2O$
***A*/MHz**	2739.992 (4) [a]	2733.395 (8)	2735.231 (7)	2734.371 (2)
***B*/MHz**	1436.4305 (5)	1397.4351 (5)	1374.2075 (5)	1369.5822 (5)
***C*/MHz**	942.1313 (3)	924.6685 (4)	914.666 (3)	912.2303 (2)
χ_{aa} **/ MHz**	[-3.570][b]	[-3.570]	-3.75 (5)	-3.49 (6)
χ_{bb} **/ MHz**	[1.00]	[1.00]	1.07 (15)	0.947 (1)
χ_{cc} **/ MHz**	[2.57]	[2.57]	2.69 (15)	2.539 (1)
D_J **/ kHz**	[0.029]	[0.029]	[0.029]	[0.029]
D_{JK} **/ kHz**	-11.2 (2)	-11.3 (3)	-11.4 (3)	[11.24]
D_K **/ kHz**	[9.62]	[9.62]	[9.62]	[9.62]
d_1 **/ kHz**	[-0.179]	[-0.179]	[-0.179]	-0.169 (1)
d_2 **/ kHz**	[-0.224]	[-0.224]	[-0.224]	[-0.223]
N[c]	35	33	33	64
σ[d] **/ kHz**	4.7	3.0	2.7	5.0

[a] Standard error in parenthesis in units of the last digit.

[b] Values in brackets fixed to the parent species.

[c] Number of transitions in the fit.

[c] Standard deviation of the fit.

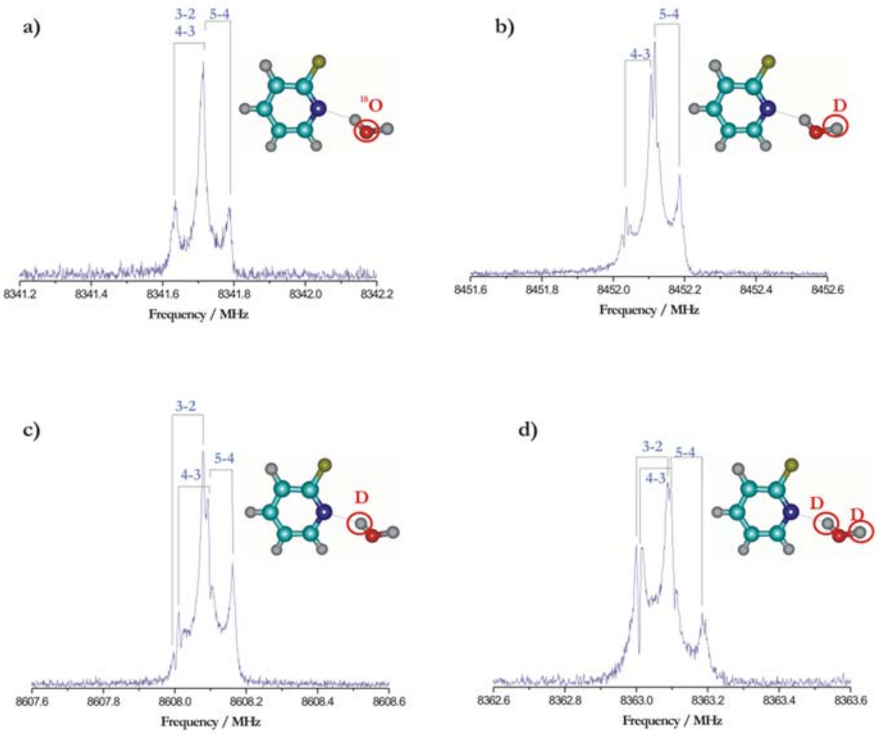

Figure: 7.5.- $4_{0,4} \leftarrow 3_{0,3}$ transition for the substituted species: a) $C_5H_4FN\cdots H_2{}^{18}O$, b) $C_5H_4FN\cdots HOD$, c) $C_5H_4FN\cdots DOH$ and d) $C_5H_4FN\cdots D_2O$.

The effective structure (r_0) is the geometry which better reproduces the experimental rotational constants of the complex for the ground-vibrational state. The calculation of the effective structure ideally requires a good number of isotopic species to avoid ill-conditioned fits and careful selection of the fitting parameters. In the case of 2-fluoropyridine$\cdots H_2O$ we got 15 inertial data (3 moment of inertia per species) which we decided to fit to only two key structural parameters, the hydrogen bond length (R) and the angle (α) giving the orientation of the water molecule with respect to the pyridine ring (See figure 7.6).

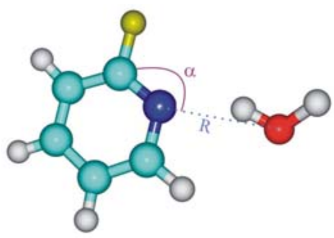

Figure: 7.6.- Effective structure calculation, showing the fitting parameters R and α.

The values of the resulting structural parameters are listed in the following table and compared with the ab initio equilibrium structure.

Table: 7.6.- R and α structure parameters obtained from the r_0 structure determination compared with the equilibrium geometry.

	R / Å	**α / º**
r_0 - exp.	2.95 (3)	144 (5)
r_e - theory	2.91	149.9

Several parameters of interest such as bond lengths and the non linearity of the hydrogen bond can be derived from the obtained structure. Hence it was found the value <(N-H-O)~ 145º for the angle of the non linearity of the bond and d (H_W-N) = 2.01 (2)Å which is within the range of hydrogen bonds where the water acts as a proton donor and the N as acceptor[20].

Apart from the geometry characterization, we can roughly estimate the dissociation energy of the complex from the r_0 structure. When the intermolecular stretching motion leading to dissociation is almost parallel to the a-axis of the complex, it is possible to derive the corresponding force constant within the pseudo-diatomic approximation, through the equation:[21]

$$k_s = 16\pi^4(\mu R_{CM})^2[4B^4 + 4C^4 - (B-C)^2(B+C)^2]/\left(hD_J\right)$$

where μ is the pseudo-diatomic reduced mass, R_{CM} is the distance between the centers of the mass of the two subunits, D_J is the centrifugal distortion constant and A, B and C the rotational constants. The validity of the pseudo-diatomic approximation is limited. However, it is useful for comparison with similar systems in which this approximation was also used.

Moreover, assuming a Lennard–Jones type potential, the zero-point dissociation energy of the complex can be derived applying the approximate expression:[22]

$$E_D = 1/72 k_s R_{CM}^2$$

Hence, the dissociation energy of the complex was found to be 239 kJ mol^{-1}. This value is about one order-of-magnitude larger than the predictions obtained from the ab initio calculations (15.7 kJ mol^{-1}), despite the distance between the centers of mass which is reasonable for that kind of systems. The pseudo-diatomic dissociation value is also larger than the bonding energies found for other complexes involving water. The reason of that phenomenon is the low value of the quartic centrifugal distortion constant D_J. This fact is surprising and reveals the failure of the pseudo-diatomic approximation. In the pyridine···H_2O complex the water molecule is bound through a single O-H bond and the second hydrogen bond could be relatively free to move in the complex. A plausible explanation could be related also to a bad determination of D_J, which would require examining a much larger set of experimental data at higher frequencies.

7.4 Conclusions.-

The rotational spectrum of the complex formed by the 2-Fluoropyridine molecule with water has been analyzed in gas phase. The conformational structure of the most stable configuration was predicted by the ab initio calculations to be an adduct where water acts as a proton donor to the electron lone pair at the nitrogen atom. This hypothesis was later confirmed by the experimental data. Taking into account the structural data an additional secondary weak interaction C-H···O might be established between the aromatic ring and the oxygen atom in the water molecule as the distances are 2.01Å.

No signals belonging to other conformers were detected in the spectrum, as had been suggested by the theory (energy gaps larger than 10 $kJ\cdot mol^{-1}$). The rotational spectrum of the observed conformer corresponds to a rigid rotor, without any tunneling effects associated to large-amplitude motions of the water molecule. The only hyperfine effect was due to electric nuclear quadrupole interactions associated to the ^{14}N nucleus.

In order to obtain structural information of the complex we also studied the rotational spectra of some substituted species. Due to the weak transition intensities of the parent species, it was not possible to detect other isotopologues in natural abundance. However, commercial samples were used to measure rotational transitions of the $C_5H_4FN\cdots H_2{}^{18}O$, $C_5H_4FN\cdots DOH$, $C_5H_4FN\cdots HOD$ and $C_5H_4FN\cdots D_2O$ species.

We determined substitution coordinates and the effective structure of the complex from the moments of inertia of the observed isotopologues. The O-H···N hydrogen bond length turned out to be 2.01 (2)Å, which is consistent with the equilibrium value (2.01Å).

Finally, we estimated the dissociation energy of the complex from the partial r_0 structure and the centrifugal distortion. We found a value about one order of magnitude larger than expected for a complex involving one water molecule.

7.5 Appendix.-

The followings tables contain all the measured transition frequencies for each isotopic species.

• ***Substitution*** $\mathbf{C_5H_4FN\cdots H_2{}^{18}O}$.

Tabla: 7.7.- Measured and calculated frequencies in MHz for the $C_5H_4FN\cdots H_2{}^{18}O$ species. The last column represents the difference (in kHz) between the calculated and the measured frequencies $\Delta\nu = \nu_{OBS} - \nu_{CALC}$.

J'	K'_{-1}	K'_{+1}	J''	K''_{-1}	K''_{+1}	F'	F''	ν_{OBS} / MHz	ν_{CALC} / MHz	$\Delta\nu$ / kHz
4	0	4	3	0	3	4	3	8341.8384	8341.8419	-3.5
						3	2	8341.8384	8341.8337	4.7
						5	4	8341.9313	8341.9324	-1.1
4	1	4	3	1	3	4	3	8051.6816	8051.6810	0.6
						3	2	8051.7739	8051.7781	1.8
						5	4	8051.8470	8051.8452	-2.1
4	1	3	3	1	2	4	3	9804.2508	9804.2669	-16.1
						3	2	9804.4139	9804.4106	3.3
5	0	5	4	0	4	5	4	10128.1789	10128.1742	4.7
						4	3	10128.1903	10128.1924	-2.1
						6	5	10128.2486	10128.2504	-1.8
5	1	5	4	1	4	5	4	9953.8874	9953.8870	0.4
						4	3	9953.9334	9953.9355	-2.1
						6	5	9953.9852	9953.9868	-1.6
5	1	4	4	1	3	5	4	11989.9875	11989.9921	-4.6
						4	3	11990.0806	11990.0824	-1.8
						6	5	11990.0950	11990.1024	-7.4
6	0	6	5	0	5	6	5	11911.0618	11911.0615	0.3
						5	4	11911.0824	11911.0832	-0.8
						7	6	11911.1215	11911.1234	-1.9

Tabla: 7.7.- Continued										
J'	***K'$_{-1}$***	***K'$_{+1}$***	***J''***	***K''$_{-1}$***	***K''$_{+1}$***	***F'***	***F''***	**ν_{OBS} / MHz**	**ν_{CALC} / MHz**	***Δν* / kHz**
6	1	6	5	1	5	6	5	11821.9388	11821.9389	-0.1
						5	4	11821.9701	11821.9696	0.6
						7	6	11822.0081	11822.0081	0.0
6	1	5	5	1	4	6	5	13980.2158	13980.2125	3.3
						5	4	13980.2812	13980.2891	-7.9
						7	6	13980.3112	13980.3051	6.2
7	0	7	6	0	6	7	6	13709.6321	13709.6329	-0.8
						6	5	13709.6522	13709.6524	-0.2
						8	7	13709.6841	13709.6825	1.6
7	1	7	6	1	6	7	6	13668.3668	13668.3643	2.5
						6	5	13668.3861	13668.3865	-0.4
						8	7	13668.4121	13668.4162	-4.1
7	1	6	6	1	5	7	6	15801.1395	15801.1268	12.7
						6	5	15801.1971	15801.1983	-1.2
						8	7	15801.2249	15801.2108	14.13
8	0	8	7	0	7	8	7	15520.7984	15520.8007	-2.3
						7	6	15520.8229	15520.8171	5.8
						9	8	15520.8361	15520.8407	-4.6
8	1	8	7	1	7	8	7	15502.8530	15502.8522	0.8
						7	6	15502.8752	15502.8694	5.8
						9	8	15502.8901	15502.8929	-2.8
8	1	7	7	1	6	8	7	17543.3689	17543.3630	5.9
						7	6	17543.4256	17543.4285	-2.9
						9	8	17543.4448	17543.4387	6.1
9	0	9	8	0	8	9	8	17338.9112	17338.9148	-3.6
						10	9	17338.9457	17338.9475	-1.8
4	0	4	3	1	3	4	3	7716.6135	7716.6076	5.9
						3	2	7716.7472	7716.7478	-0.6
						5	4	7716.8088	7716.8061	2.7
4	1	4	3	0	3	3	2	8676.8637	8676.8640	-0.3
						4	3	8676.9086	8676.9153	-6.7
						5	4	8676.9651	8676.9715	-6.4
5	0	5	4	1	4	5	4	9793.1046	9793.1008	3.8
						4	3	9793.1642	9793.1621	2.1
						6	5	9793.2132	9793.2113	1.9
5	1	5	4	0	4	5	4	10288.9528	10288.9604	-7.6
						6	5	10289.0232	10289.0260	-2.8
6	0	6	5	1	5	6	5	11750.2745	11750.2753	-0.8
						5	4	11750.3070	11750.3098	-2.8
						7	6	11750.3489	11750.3478	1.1
6	1	6	5	1	5	6	5	11982.7288	11982.7251	3.7
						5	4	11982.7388	11982.7429	-4.1
						7	6	11982.7802	11982.7837	-3.5

• ***Substitution*** **$C_5H_4FN\cdots HOD$.**

Tabla: 7.8.- Measured and calculated frequencies in MHz for the $C_5H_4FN\cdots HOD$ species. The last column represents the difference (in kHz) between the calculated and the measured frequencies $\Delta\nu = \nu_{OBS} - \nu_{CALC}$.

J'	*K'*$_{-1}$	*K'*$_{+1}$	*J''*	*K''*$_{-1}$	*K''*$_{+1}$	*F'*	*F''*	ν_{OBS} / MHz	ν_{CALC} / MHz	$\Delta\nu$ / kHz
3	1	2	2	1	1	3	2	7600.5404	7600.5392	1.2
						4	3	7600.8614	7600.8618	-0.4
						2	1	7600.9128	7600.9086	4.2
4	0	4	3	0	3	3	2	8452.2423	8452.2327	9.6
						4	3	8452.2423	8452.2436	-1.3
						5	4	8452.3262	8452.3295	-3.3
4	1	4	3	1	3	4	3	8170.3535	8170.3533	0.2
						3	2	8170.4454	8170.4498	-4.4
						5	4	8170.5182	8170.5162	2.0
4	1	3	3	1	2	4	3	9974.5919	9974.5924	-0.5
						3	2	9974.7376	9974.7329	4.7
						5	4	9974.7480	9974.7517	-3.7
5	0	5	4	0	4	5	4	10259.6709	10259.6699	1.0
						4	3	10259.6855	10259.6853	0.2
						6	5	10259.7423	10259.7433	-1.0
5	1	5	4	1	4	5	4	10095.9056	10095.9085	-2.9
						4	3	10095.9584	10095.9562	2.2
						6	5	10096.0079	10096.0071	0.8
5	1	4	4	1	3	5	4	12178.4925	12178.4951	-2.6
						4	3	12178.5841	12178.5816	2.5
						6	5	12178.5988	12178.6026	-3.8
6	0	6	5	0	5	6	5	12067.8968	12067.8927	4.1
						5	4	12067.9082	12067.9126	-4.4
						7	6	12067.9530	12067.9527	0.3
6	1	6	5	1	5	6	5	11986.8328	11986.8335	-0.7
						5	4	11986.8662	11986.8633	3.0
						7	6	11986.9041	11986.9015	2.6
4	0	4	3	1	3	4	3	7863.6085	7863.6081	0.4
						3	2	7863.7484	7863.7511	-2.7
						5	4	7863.8087	7863.8079	0.8

- ***Substitution* $C_5H_4FN\cdots DOH$.**

Tabla: 7.9.- Measured and calculated frequencies in MHz for the $C_5H_4FN\cdots DOH$ species. The last column represents the difference (in kHz) between the calculated and the measured frequencies $\Delta\nu = \nu_{OBS} - \nu_{CALC}$.

J'	*K'₋₁*	*K'₊₁*	*J''*	*K''₋₁*	*K''₊₁*	*F'*	*F''*	ν_{OBS} / MHz	ν_{CALC} / MHz	$\Delta\nu$ / kHz
3	1	2	2	1	1	3	2	7793.5645	7793.5668	-2.3
						4	3	7793.8919	7793.8893	2.6
						2	1	7793.9389	7793.9361	2.8
4	0	4	3	0	3	3	2	8608.2054	8608.2120	-6.6
						4	3	8608.2204	8608.2228	-2.4
						5	4	8608.3178	8608.3087	9.1
4	1	4	3	1	3	4	3	8336.8211	8336.8197	1.4
						3	2	8336.9128	8336.9162	-3.4
						5	4	8336.9836	8336.9826	1.0
4	1	3	3	1	2	4	3	10212.5092	10212.5143	-5.1
						3	2	10212.6568	10212.6546	2.2
						5	4	10212.6745	10212.6735	1.0
5	0	5	4	0	4	5	4	10446.3541	10446.3517	2.4
						4	3	10446.3648	10446.3673	-2.5
						6	5	10446.4251	10446.4253	-0.2
5	1	5	4	1	4	5	4	10295.3529	10295.3544	-1.5
						4	3	10295.3984	10295.4020	-3.6
						6	5	10295.4581	10295.4529	5.2
5	1	4	4	1	3	5	4	12441.3998	12441.3999	-0.1
						4	3	12441.4875	12441.4861	1.4
						6	5	12441.5054	12441.5071	-1.7
6	1	6	5	1	5	6	5	12218.7111	12218.7106	0.5
						5	4	12218.7407	12218.7404	0.3
						7	6	12218.7829	12218.7786	4.3
7	0	7	6	0	6	7	6	14152.2439	14152.2459	-2.0
						8	7	14152.2941	14152.2942	-0.2
4	0	4	3	1	3	4	3	8062.8019	8062.8011	0.8
						3	2	8062.9431	8062.9436	-0.5
						5	4	8062.9989	8063.0006	-1.7
4	1	4	3	0	3	3	2	8882.1819	8882.1845	-2.6
						4	3	8882.2399	8882.2414	-1.5
						5	4	8882.2945	8882.2907	3.8

• ***Substitution*** **$C_5H_4FN\cdots D_2O$.**

Tabla: 7.10.- Measured and calculated frequencies in MHz for the $C_5H_4FN\cdots D_2O$ species. The last column represents the difference (in kHz) between the calculated and the measured frequencies $\Delta\nu = \nu_{OBS} - \nu_{CALC}$.

J'	*K'-1*	*K'+1*	*J''*	*K''-1*	*K''+1*	*F'*	*F''*	ν_{OBS} / MHz	ν_{CALC} / MHz	$\Delta\nu$ / kHz
3	1	2	2	1	1	3	2	7486.2365	7486.2379	-1.4
						4	3	7486.5787	7486.5768	1.9
						2	1	7486.6207	7486.6249	-4.2
4	0	4	3	0	3	3	2	8363.0493	8363.0421	7.3
						4	3	8363.0662	8363.0557	10.5
						5	4	8363.1362	8363.1448	-8.6
4	1	4	3	1	3	4	3	8073.9435	8073.9437	-0.2
						3	2	8074.0360	8074.0450	-9.0
						5	4	8074.1132	8074.1144	-1.2
4	1	3	3	1	2	4	3	9833.9536	9833.9587	-5.1
						3	2	9834.1154	9834.1050	10.4
						5	4	9834.1266	9834.1254	1.2
5	0	5	4	0	4	5	4	10153.7020	10153.7034	-1.4
						4	3	10153.7120	10153.7184	-6.4
						6	5	10153.7752	10153.7794	-4.2
5	1	5	4	1	4	5	4	9980.8335	9980.8406	-7.1
						4	3	9980.8923	9980.8903	2.0
						6	5	9980.9535	9980.9437	9.8
5	1	4	4	1	3	5	4	12023.8055	12023.8080	-2.5
						4	3	12023.9011	12023.8972	3.9
						6	5	12023.9153	12023.9197	-4.4
6	0	6	5	0	5	6	5	11941.5084	11941.5028	5.6
						5	4	11941.5157	11941.5231	-7.4
						7	6	11941.5667	11941.5651	1.6
6	1	6	5	1	5	6	5	11853.5079	11853.5049	3.0
						5	4	11853.5385	11853.5359	2.6
						7	6	11853.5781	11853.5760	2.1
4	0	4	3	1	3	4	3	7742.8315	7742.8300	1.5
						3	2	7742.9780	7742.9814	-3.4
						5	4	7743.0414	7743.0406	0.8

7.6. References.-

[1] S. Shimizu, N. Watarabe, T. Kataoka, T. Shoji, N. Abe, S. Morishita, H. Ichinura, *Pyridine and Pyridine derivation*, in "Ullmann´s encyclopedia of industrial chemistry", Wiley, **2000**.

[2] C. W. van Dijk, M. Sun, J. van Wijngaarden, *J. Phys. Chem. A*, 116, 4082, **2012**.

[3] F. Dollé, *Curr. Pharm. Des.*, 11, 3221, **2005**.

[4] F. T. Fraser, R. D. Suenram, *J. Chem. Phys.*, 96, 7287, **1992**.

[5] D. Consalvo, W. Stahl, *J. Mol. Spectrosc.*, 174, 520, **1995**.

[6] W. Caminati, A. Dell'Erba, G. Maccaferr, P. G. Favero, *J. Am. Chem. Soc.*, 120, 2616, **1998**.

[7] P. Écija, M. Vallejo-López, L. Evangelisti, J. A. Fernández, F. Castaño, A. Lesarri, W. Caminati, E. J. Cocinero, *ChemPhysChem*, DOI: 10.1002/cphc.201301213, **2014**.

[8] L. Spada, Q. Gou, M. Vallejo-López, A. Lesarri, E. J. Cocinero, W. Caminati, *Phys. Chem. Chem. Phys.*, 16, 2149, **2014**.

[9] M. Vallejo-López, L. Spada, Q. Gou, A. Lesarri, E. J. Cocinero, W. Caminati, *Chem. Phys. Lett.*, 591, 216, **2014**.

[10] L. B. Favero, B. M. Giuliano, A. Maris, S. Melandri, P. Ottaviani, B. Velino, W. Caminati, *Chem. Eur. J.*, 16, 1761, **2010**.

[11] MAESTRO, version 9.2, Schrödinger, LLc, New York, NY, **2012**.

[12] M. J. Frisch, G. W. Trucks, H. B. Schlegel, G. E. Scuseria, M. A. Robb, J. R. Cheeseman, G. Scalmani, V. Barone, B. Mennucci, G. A. Petersson, H. Nakatsuji, M. Caricato, X. Li, H. P. Hratchian, A. F. Izmaylov, J. Bloino, G. Zheng, J. L. Sonnenberg, M. Hada, M. Ehara, K. Toyota, R. Fukuda, J. Hasegawa, M. Ishida, T. Nakajima, Y. Honda, O. Kitao, H. Nakai, T. Vreven, J. A. Montgomery, Jr., J. E. Peralta, F. Ogliaro, M. Bearpark, J. J. Heyd, E. Brothers, K. N. Kudin, V. N. Staroverov, R. Kobayashi, J. Normand, K. Raghavachari, A. Rendell, J. C. Burant, S. S. Iyengar, J. Tomasi, M. Cossi, N. Rega, J. M. Millam, M. Klene, J. E. Knox, J. B. Cross, V. Bakken, C. Adamo, J. Jaramillo, R. Gomperts, R. E. Stratmann, O. Yazyev, A. J. Austin, R. Cammi, C. Pomelli, J. W. Ochterski, R. L. Martin, K. Morokuma, V. G. Zakrzewski, G. A. Voth, P. Salvador, J. J. Dannenberg, S. Dapprich, A. D. Daniels, Ö. Farkas, J. B. Foresman, J. V. Ortiz, J. Cioslowski, and D. J. Fox, Gaussian, Inc., Wallingford CT, **2009**.

[13] H. M. Pickett, *J. Mol. Spectrosc.*, 148, 371, **1991**.

[14] W. Gordy and L. R. Cook, "Microwave Molecular Spectra", 3rd Edition, in Weissberger, A. (Ed.), Techniques of Chemistry, vol. XVIII, John Wiley & Sons Inc., New York, **1984**.

[15] G. Scoles, "Atomic and molecular beam methods", Vol.1, Oxford University Press, New York, **1988**.

[16] J. Kraitchman, *Am. J. Phys.*, 21,17, **1953**.

[17]C. C. Costain, *J. Chem. Phys.*, 29, 864, **1958**.

[18] H. D. Rudolph, *Struct. Chem.*, 2, 581, **1991**.

[19] K. J. Epple, H. D. Rudolph, *J. Mol. Spectr.* 152, 355, **1992**.

[20] T. Steiner, *Angew. Chem. Int. Ed.,* 41, 48, **2002**.

[21] D. Millen, *Can. J. Chem.*, 63, 1477, **1985**.

[22] S.E. Novick, S.J. Harris, K.C. Janda, W. Klemperer, *Can. J. Phys.*, 53, 2007, **1975**.

Formaldehyde Complexes

Chapter 8

$CH_2F_2\cdots$ Formaldehyde

8.1. Introduction.-

The study of intermolecular complexes is a large and interesting field for multiple reasons.[1-13] First of all, the analysis of weakly-bound clusters illustrates the magnitude of the intermolecular forces linking two or several monomers. In many cases intermolecular complexes can be generated specifically to investigate a particular interaction, i.e. hydrogen bonds (HB) and dispersive interactions[4-6] or certain functional groups,[7-9] for example hydration. [10-13] In a second place, intermolecular complexes serve as small-scale models of the interactions occurring in larger systems, like protein binding, providing a description of the local forces involved in biochemical forces. Finally, intermolecular clusters may be difficult to model theoretically, so the availability of structural data can be used as a benchmark for theoretical studies. This is particularly useful for weak interactions, like dispersion forces or weak hydrogen bonds, which can be difficult to model by some theoretical methods,[14] for example, some DFT calculations.

Hence, several works on homodimers and heterodimers (clusters involving the same or different molecules) have been done in the course of this work. At the beginning of this work we were particularly interested in the analysis of clusters of anesthetics to reproduce specific anesthetic-receptor interactions, but the size of these systems moved us to first examine smaller molecules with relevant interactions, many involving halocarbons.

Several of these clusters involved the use of difluoromethane (DFM). DFM is a well-known molecule with a simple near-tetrahedral structure, and where both the isolated molecule and several clusters[7, 15-24] have been studied by rotational spectroscopy.

In the present work we investigated the cluster with formaldehyde (FA) or DFM···FA, following previous studies of complexes with formaldehyde like clorofluoromethane···formaldehyde. Formaldehyde contains a carbonyl group with a π electron system and electron lone pairs at the oxygen atom. In consequence several interactions are possible, both as proton donor or acceptor. In DFM we have both C-H and C-F bonds. The C-H bond is in principle a weak donor, but the activation with vicinal electronegative atoms can result occasionally in relatively intense hydrogen bonds. On the other hand the C-F, sometimes called "organic fluorine", is recognized as a weaker proton acceptor. Examples of plausible interactions include the C-H···F interaction or the intermolecular halogen···oxygen bond (F···O).[25,26]

The conformational search started on the usual assumption that the structures of the monomers are not distorted upon complexation for moderate or weak hydrogen bonds. We then performed an exhaustive conformational search including the different interaction paths found in other systems with this freon. In particular, systems where the two subunits of the conformer are linked by weak hydrogen bonds and by halogen links were considered and optimized. Finally, we found that the only stable conformers are those where intermolecular WHBs are revealed (both C-H···F or C-H···O) as it can be observed in figure 8.1. The energy of the halogen type complexes is much higher, as those of the complexes bound to the π system of the carbonyl group.

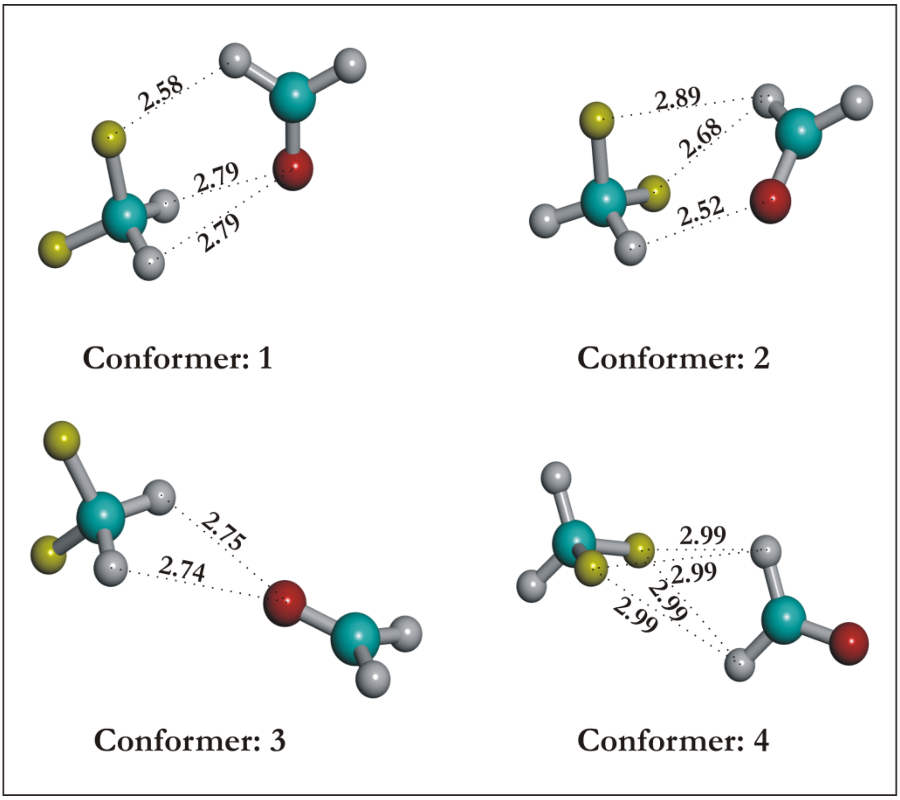

Figure: 8.1.- Stable conformational structures for the DFM···FA complex. WHBs were revealed for all the conformers. Two families were found according to the different C-H···O and C-H···F bonds.

8.2. Computational Methods.-

The calculations proceeded in two steps, as described in other chapters. First the conformational search was accomplished using molecular mechanics (MMMF).[27] Later, more accurate ab initio methods were used in order to obtained electric and structural properties of our complex (DFM···formaldehyde). Frequency calculations followed the optimization of the most stable structures, using MP second-order perturbation theory (Chap. 1). As in other systems, we used the Pople triple-ζ basis set with diffusion and polarization functions, or

6-311++G(d,p). All the theoretical calculations were implemented in Macromodel [28] and Gaussian.[29]

The results of these theoretical calculations gave information about the inertial moments of the complex and in consequence, the rotational constants. Besides, electric dipole moments and centrifugal distortion constants were also determined and they are summarized in the following table.

Table: 8.1.- Rotational constants (*A*, *B* and *C*), electric dipole moments (μ_a, α = a, b, c) and centrifugal distortion constants (Δ_J, Δ_{JK} , Δ_K, δ_K and δ_K) of the theoretical conformers. The Δ*E* value indicate the energy difference between each conformer respect to the most stable. This energy is corrected with the zero point energy (ZPE). ΔG is calculated at 298K and 1 atm.

	Conf. 1	Conf. 2	Conf. 3	Conf. 4
***A* / MHz**	13891.9	7523.2	10168.2	10176.9
***B* / MHz**	1766.3	2465.8	1307.6	1495.4
***C* / MHz**	1583.5	2192.8	1176.2	1327.4
$\lvert\mu_a\rvert$ / D	2.54	0.08	3.86	4.80
$\lvert\mu_b\rvert$ / D	0.42	0.14	0.03	0.00
$\lvert\mu_c\rvert$ / D	0.02	0.29	3.09	0.02
$\lvert\mu_{TOT}\rvert$ / D	2.57	0.33	4.94	4.80
D_J / kHz	1.86	8.16	-1.28	3.76
D_{JK} / kHz	13.41	90.56	-1.71	165.17
D_K / MHz	0.389	-0.090	1.82	-0.155
d_1 / kHz	-0.198	-1.04	-0.19	-0.49
d_2 / kHz	-0.019	-0.11	-0.16	-0.19
ΔG / kJ·mol^{-1}	0.0	-0.5	-10.8	-0.2
Δ(*E*+ZPE) / kJ·mol^{-1}	0.0	0.4	2.0	5.9

According to the previous results we could find in principle in the experimental spectrum transitions belonging to the three most stable conformers, for which the energy difference is less than 5 kJ·mol^{-1}. However, as explained in the results section, only conformer 1 was finally detected in the jet for two different torsional states: the ground and the first excited state.

8.3. Results and Analyses.-

a. Assignment of the Rotational Spectrum.

We did a prediction of the rotational spectrum for each predicted structure. The three most stable conformers are asymmetric rotors close to the near-prolate limit ($\kappa \approx$ -0.97 / -0.90 / -0.97).[30] We used the conventional Watson's semi-rigid rotor Hamiltonian using Pickett's[31] and JB95[32] programs to predict the frequencies and intensities of the rotational transitions.

We can get estimations about the transition intensities of each structure from the values of the dipole moments obtained with the theoretical calculations (see table 8.1). The dipole moments are linearly related to the transition intensities in the FT-MW technique. Obviously, transitions with very small or zero dipole moment will not be detectable. In the three most stable conformers the behavior is very different. For conformer 1, the dipole moment is practically fully oriented along the principal axis *a*, so the strongest signals would be the μ_a-type transitions though some μ_b-type transitions might be detected. In conformer 2 the electric dipole moment is much smaller, mostly though the *c* inertial axis. Finally, conformer 3 has very intense electric dipole components along the *a* and *b* axes.

For this reason, we predicted for conformer 1 the frequencies of the μ_a and μ_b R-branch (J+1$\leftarrow$ J) transitions. The following figure shows the spectral simulation of the predicted spectrum for conformer 1. In the figure the characteristic pattern of the μ_a-type lines can be identified. In particular, for the DFM···FA complex, the distance between the successive (J+1) $\leftarrow$ J series was predicted to be at B+C ~ 3350 MHz.[30] This quite large value makes a spectrum with relatively low transitions density and in the 6-18 GHz spectrometer range we could only find three different series. Similar predictions were made for the other conformers.

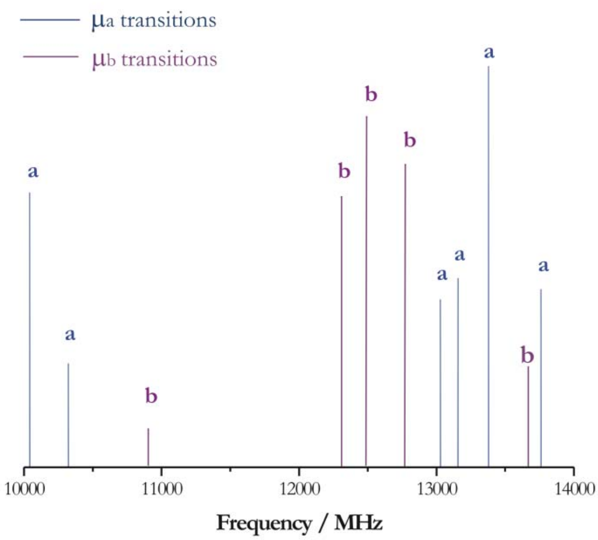

Figure: 8.2.- ^{a}R and ^{b}R predicted spectra for the most stable conformer 1.

Once we acquired the experimental spectrum the comparison of the observed transitions with the previous theoretical predictions allowed a conformational assignment, identifying the structure of the most stable conformer in the jet. This process requires iterative trial and error assignment of different sets of lines till the full dataset of observations can be reproduced.

The following figure 8.3 shows some of the assigned transitions. Apart from the instrumental Doppler splitting, we can see that the transitions are additionally split into two different components. The identification of this splitting was done on the basis of several arguments. First of all the magnitude of the splitting is relatively large (> 2 MHz), which probably excludes the possibility of hyperfine effects other than nuclear quadrupolar interactions, which are not possible in the molecule. Other hyperfine effects would be smaller in magnitude. Interestingly, the two components have an intensity ratio of ca. 1:3. This suggests that the two components are due to the internal rotation of formaldehyde around its C_{2v} internal axis. The exchange of the two hydrogen atoms (fermions with spin ½) would produce a nuclear spin statistics ratio consistent with the observations. In consequence we can safely associate the transition doublings to the distinct rotational ladders of two torsional vibrational levels. We have labelled the torsional states as 0^+ and 0^-. The selection rules involving the vibrational states depend on the symmetry of the electric dipole moment. For a symmetric electric dipole the transition moment $\langle\psi_{vib}^{final}|\mu|\psi_{vib}^{inicial}\rangle$ will be non-zero for torsional states of the same symmetry, i.e., $0^+\leftarrow 0^+$ or $0^-\leftarrow 0^-$. Conversely, if the dipole moment is antisymmetric the selection rules require a change of symmetry in the torsional states, i.e. $0^+\leftarrow 0^-$. Since the electric dipole moment is symmetric for the internal rotation the only allowed transitions are within each vibrational level, i.e. $0^+\leftarrow 0^+$ or $0^-\leftarrow 0^-$. The transitions $0^+\leftarrow 0^-$ are thus forbidden.

According to the theoretical calculations (table 8.1), two other predicted conformers have relative energies below 2.0 kJ mol^{-1}. However, only transitions belonging to the most stable conformer were finally found (table 8.2).

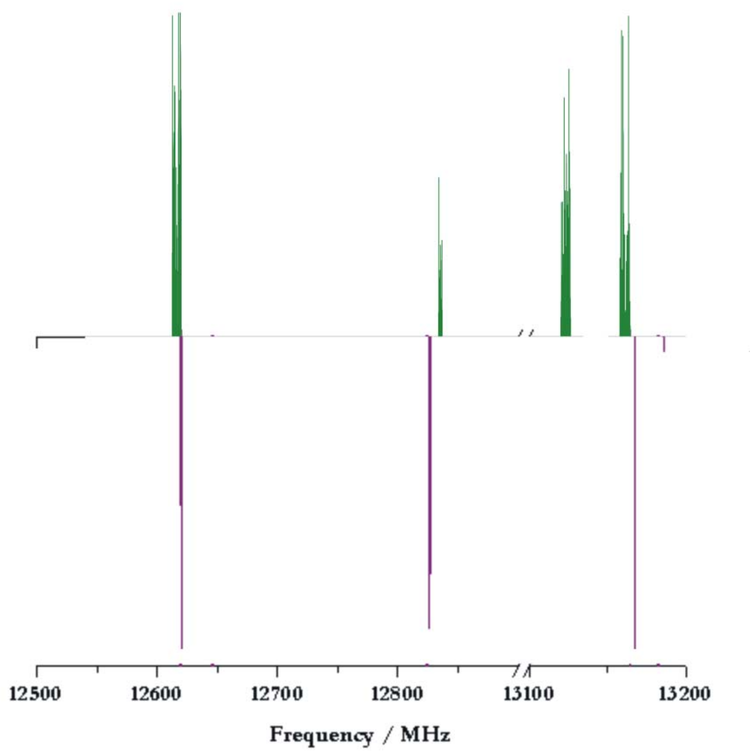

Figure: 8.3.- Section of a frequency scan for the DFM···FA complex where the assigned transitions of the most stable conformer can be identified. The difference between the experimental (green) and predicted (purple) spectra is due to the internal rotation motion that has not been taken into account in the predictions.

In the next figure the $3_{0,3} \leftarrow 2_{0,2}$ rotational transition is shown for both states.

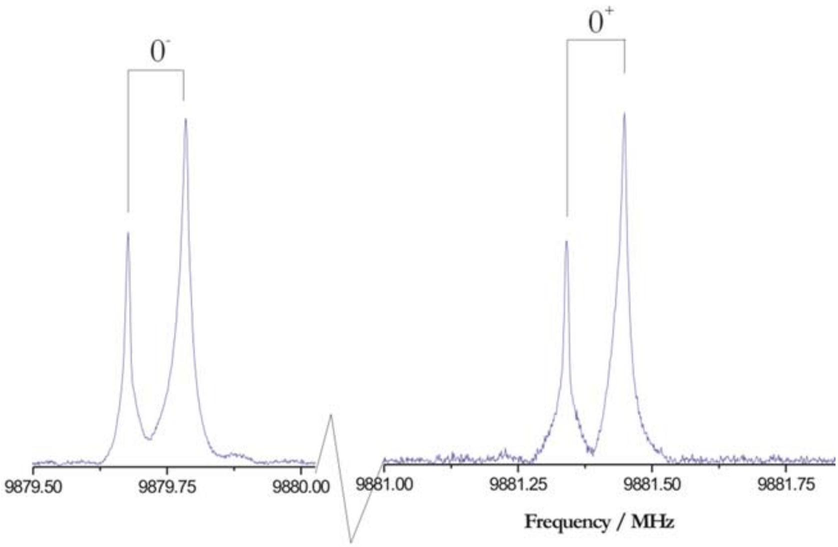

Figure: 8.4.- Transition $3_{0,3} \leftarrow 2_{0,2}$ for the 0^+ and 0^- states of conformer 1 of the complex DFM···FA.

b. Determination of the spectroscopic parameters.

Since we detected two different torsional states for the observed conformer we considered fitting both states together with a two-state Hamiltonian[30]

$$\boldsymbol{H} = \begin{pmatrix} H_{rot}^{0^+0^+} & H_{coupling} \\ H_{coupling} & H_{rot}^{0^-0^-} + \Delta E^{0^+0^-} \end{pmatrix}$$

However, we observed no interactions between the two sets of lines shown in table 8.3), so each of them could be fitted independently without any coupling terms. The rotational analysis used the Watson´s semi-rigid rotor Hamiltonian in the symmetric reduction (S) and in the I^r representation. As a result, several different parameters were determined and summarized in the following table.

Table: 8.2.- Experimental and theoretical rotational and centrifugal distortion constants (*A*, *B*, *C*, $D_J, D_{JK}, D_K, d_1, d_2$), number of lines used in the fit (*N*) and root-mean-square deviation (*σ*).

	Theory	Experiment	
		State 0^-	State 0^+
A **/ MHz**	13892	13725.3980(30)[a]	13719.3512(30)
B **/ MHz**	1766	1737.2577(10)	1736.7195(10)
C **/ MHz**	1584	1559.24713(95)	1559.21789(95)
D_J **/ kHz**	1.86	2.330(12)	2.333(12)
D_{Jk} **/ kHz**	13.41	21.252(50)	20.776(50)
D_k **/ MHz**	0.389	[0.0]	[0.0]
d_1 **/ kHz**	-0.198	-0.236(12)	-0.231(12)
d_2 **/ kHz**	-0.0188	-0.0288(65)	-0.0216(65)
μ_a **/ D**	-2.54	---	---
μ_b **/ D**	0.42	---	---
μ_c **/ D**	-0.02	---	---
μ_{TOT} **/ D**	2.57	---	---
Δ(*E*+ZPE) / kJ·mol^{-1}	0.0		
σ / kHZ		0.57	0.57
N		23	23

[a] Standard errors in units of the last digit.

The previous table contains the experimental parameters obtained from the rotational transitions of the 0^+ and 0^- states of the most stable conformer. They are compared with the theoretical values and we could unambiguously identify the detected conformer with the predicted conformer 1(figure 8.1).

For the two states the rotational constants and four out of five quartic centrifugal distortion constants have been fitted and the results are pointed out in table 8.2. Despite the D_K parameter couldn´t be fitted with the variety of transitions measured, the other constants were obtained with enough accuracy.

The root-mean-square deviation is, in both cases, less than 1 kHz which is a value lower than the error in the measurements. It means that the fit quality is high and the number of different types of transitions used in the fit is acceptable. The low correlation values reinforce this fact.

Table: 8.3.- Measured and calculated frequencies (MHz) for the most stable conformer of the complex DFM···FA. The last column is the difference between the observed and measured frequencies: $\Delta\nu = \nu_{OBS} - \nu_{CALC}$ in kHz.

J'	K'_{-1}	K'_{+1}	J''	K''_{-1}	K''_{+1}	υ_i	υ_f	ν_{OBS} / MHz	ν_{CALC} / MHz	$\Delta\nu$ / kHz
3	1	3	2	1	2	1	1	9619.9886	9619.9915	-2.9
						0	0	9620.9220	9620.9221	-0.1
3	0	3	2	0	2	1	1	9879.7330	9879.7330	0.0
						0	0	9881.3947	9881.3947	0.0
3	2	2	2	2	1	1	1	9887.0600	9887.0637	-3.7
						0	0	9888.7558	9888.7558	0.0
3	2	1	2	2	0	1	1	9894.8891	9894.8869	2.2
						0	0	9896.6124	9896.6187	-6.3
3	1	2	2	1	1	1	1	10152.4327	10152.4330	-0.3
						0	0	10154.8923	10154.8895	2.8
1	1	0	1	0	1	1	1	12160.9878	12160.9908	-3.0
						0	0	12166.1094	12166.1076	1.8
2	1	1	2	0	2	1	1	12339.4587	12339.4593	-0.6
						0	0	12345.9939	12345.9933	0.6
3	1	2	3	0	3	1	1	12612.1598	12612.1595	0.3
						0	0	12619.4851	12619.4881	-3.0
4	1	4	3	1	3	1	1	12824.1695	12824.1680	1.5
						0	0	12825.3980	12825.3980	0.0
4	1	3	4	0	4	1	1	12982.5378	12982.5386	-0.8
						0	0	12990.9604	12990.9621	-1.7
4	0	4	3	0	3	1	1	13163.5946	13163.5962	-1.6
						0	0	13165.7636	13165.7643	-0.7
4	2	3	3	2	2	1	1	13180.9757	13180.9705	5.2
						0	0	13183.2209	13183.1998	1.1
4	2	2	3	2	1	1	1	13200.5158	13200.5160	-0.2
						0	0	13202.8641	13202.8647	-0.6
5	1	4	5	0	5	1	1	13456.3314	13456.3302	1.2
						0	0	13466.1796	13466.1781	1.5
4	1	3	3	1	2	1	1	13533.9748	13533.9753	-0.5
						0	0	13537.2428	13537.2373	4.5
1	1	1	0	0	0	1	1	15278.5222	15278.5192	3.0
						0	0	15284.5950	15284.5944	0.6
5	1	5	4	1	4	1	1	16026.2548	16026.2533	1.5
						0	0	16027.7759	16027.7736	2.3
5	0	5	4	0	4	1	1	16439.4532	16439.4559	-2.7
						0	0	16442.0865	16442.0901	-3.6
5	2	4	4	2	3	1	1	16473.3519	16473.3511	0.8
						0	0	16476.1514	16476.1518	-0.4
5	3	3	4	3	2	1	1	16483.2343	16483.2366	-2.3
						0	0	16486.0720	16486.0765	4.5
5	3	2	4	3	1	1	1	16483.5185	16483.5181	-0.6
						0	0	16486.3478	16486.3519	-4.1
5	2	3	4	2	2	1	1	16512.3964	16512.3941	2.3
						0	0	16515.3949	16515.3930	1.9
5	1	4	4	1	3	1	1	16913.2474	16913.2475	-0.1
						0	0	16917.3041	16917.3060	-1.9

c. Isotopic Substitutions: Structure determination.

From rotational spectroscopy we can obtain information on the structure of the molecules in gas phase based on its strong dependence with the inertial moments. In turn, these moments are linked to the system masses and geometry and, at the end, connected to the structure of the complex.

Because of the large number of independent structural parameters, the structural determinations require observing several isotopic species. Once the rotational spectra are resolved for the different isotopologues (species with different atomic numbers) we can obtain the structural parameters of the parent species through different procedures.

In the complex DFM···FA the fluorine atoms are monoisotopic (^{19}F), so the search of isotopologues in natural abundance is restricted to the carbon and oxygen atoms (natural abundances of 1.1% and 0.20% respectively) in both difluoromethane and formaldehyde (the abundance of the deuterium atoms is smaller: 0.015%). Due to the small proportion of the isotopes respect to the parent species, the transition intensities are much weaker, making difficult its acquisition. In particular, for the system we are studying, we were able to detect only transitions belonging to the ^{13}C species.

Since in the DFM···FA there are two different carbon atoms we observed two ^{13}C species, depending if the substitution was done in the formaldehyde or the DFM moiety. The following picture displays the $3_{1,3} \leftarrow 2_{1,2}$ transition of both ^{13}C substitutions.

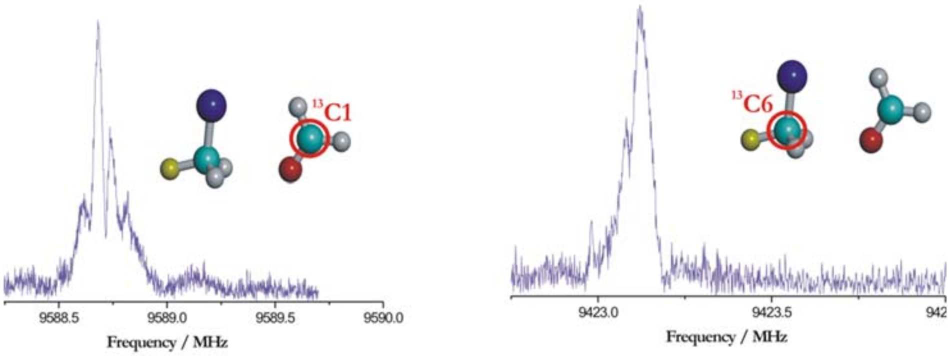

Figure: 8.5.- Transition $3_{1,3}$←$2_{1,2}$ for the isotopologues of conformer 1 of DFM···FA. **(a)** Substitution in the carbon $^{13}C_1$. **(b)** Substitution in the carbon $^{13}C_6$.

The analysis of these transitions was similar to the parent species. Using the Watson semi-rigid rotor Hamiltonian, we fitted the rotational and the D_J centrifugal distortion constant. All the other parameters were fixed to the values of the parent species. The transitions for the substituted species are list in appendix I and the values obtained for the spectroscopic parameters are the following:

Table: 8.4.- Experimental rotational constants for the two substituted species of the most stable conformer of DFM···FA.

	^{13}C(1)	^{13}C(6)
***A* / MHz**	13675.01 (76)[a]	13671.0 (23)
***B* / MHz**	1731.06574 (30)	1698.77633 (83)
***C* / MHz**	1554.16235 (35)	1528.07409 (94)
D_J / kHz	2.3146 (69)	2.228 (18)
D_{JK} / kHz	[21.252][b]	[21.252]
d_1 / kHz	[-0.2363]	[-0.2363]
d_2 / kHz	[-0.0288]	[-0.0288]
σ / kHz	0.36	0.66
***N*[c]**	9	9

[a] Standard error in units of the last digit.
[b] The centrifugal distortion constants were fixed to the parent species except the D_J parameter.
[c] Number of transitions used in the fit.

Because there are only three isotopic species a full substitution structure (r_s) is not possible, so we limited ourselves to the determination of the atomic coordinates of the two substituted carbon atoms.

In order to obtain the substitution coordinates we applied the Kraitchman[33] equations, which relate this information to the difference between the inertial moments of the parent and the substituted species. The following table shows the absolute values obtained for the coordinates of the two carbon atoms.

Table: 8.5.- Kraitchman values for coordinates in the principal axes orientation of the substituted species compared with the ab initio structure.

	Isotopologues Coordinates (Å)		
	a	**b**	**C**
$\mathbf{C_{1\ (exp)}}$	1.05234 (49)[a]	0.3883 (54)	0.00[b]
$\mathbf{C_{6\ (exp)}}$	2.55829(71)	0.2946 (62)	0.00[b]
$\mathbf{C_{1\ (theor)}}$	0.98689	-0.33454	0.00217
$\mathbf{C_{6\ (theor)}}$	-2.56439	0.33258	-0.00693

[a] Standard error in units of the last digit.
[b] Fixed to zero by symmetry.

From these coordinates we can determine the value of the distance between the two carbon atoms which results to be:

$$\mathbf{d\ (C_1 - C_6)} = (3.6314 \pm 0.0033)\text{Å}$$

Additionally, we calculated an effective structure (r_0) intended to reproduce the experimental rotational constants of the system in the ground vibrational state (we consider that there are no structural changes between the first two torsional levels). In this calculation we fit a set of structural parameters to the experimental rotational constants by the least-squares method. As initial structure we used the ab initio geometry, which is also used to constrain the non-determinable structural parameters.

For the DFM···FA cluster we floated only two structural variables defining the relative orientation of both units: the distance between DFM and FA (d=r (C_1-C_6)), and the angle giving the orientation of the two units. We preserved in the calculations the C_s symmetry of the complex.

In the following table the results for the substituted and the effective structures[34,35] are compared with the values predicted from the ab initio calculations.

Table: 8.6.- Derived parameters of the substitution and effective structures compared with the theoretical predictions for the most stable conformer.

	Conformer 1 (0^- State)		
	r_s	**r_0**	**Ab initio r_e**
d (C_1-C_6) / Å	3.6314(33)[a]	3.6290(85)	3.613
α (C_1-C_6-O_9)/deg	---	54.31(63)	52.09

[a] Standard error in units of the last digit.

8.4 Conclusions.-

The rotational spectrum of DFM···formaldehyde was assigned and a single conformation was detected. The observed species is unambiguously identified with the predicted most stable conformer (figure 8.1).

Two different rotational states were detected according to the exchange of the two hydrogen atoms (fermions with spin ½) would produce a nuclear spin statistics ratio consistent with the observations (1:3).

From the partial r_0 structure the distance between the carbon atoms could be estimated. A value of 3.6314 Å was obtained which is consistent with the predicted value for the ab initio calculations (3.613Å). This result let us check the validity of the theoretical MP2 methods to reproduce the behavior of complex in gas phase.

Only transitions belonging to the most stable conformer were experimentally observed. This effect can be explain from the so-called phenomenon 'conformer interconversion'[39-41] that takes places in the jet as a consequence of the collisions between the system with the carrier gas. It could also happened that the intensity of the second and third structures are not enough to be detected with our experimental set up.

No lines belonging to the ^{18}O substitution could be measured due to the weak intensity spectrum. Despite the high sensitivity of the spectrometer, the quite small dipole moment value makes impossible the detection of that isotopologue.

8.5 Appendix.-

The following tables show the rotational transitions measured for the substituted species of the 0^- state of conformer 1.

- ***Substitution*** $^{13}C_1$.

Table: 8.7.- Measured and calculated frequencies (MHz) of the μ_a-type transitions observed for the $^{13}CH_2F_2 \cdots CH_2O$ substituted species. The last column is the difference between the observed and measured frequencies: $\Delta\nu = \nu_{OBS} - \nu_{CALC}$ in kHz.

J'	K'_{-1}	K'_{+1}	J''	K''_{-1}	K''_{+1}	ν_{OBS} / MHz	ν_{CALC} / MHz	$\Delta\nu$ / kHz
3	1	3	2	1	2	9588.7496	9588.7673	-17.7
3	0	3	2	0	2	9847.6324	9847.6344	-2.0
3	1	2	2	1	1	10119.4174	10119.4146	2.8
4	1	4	3	1	3	12782.5447	12782.5456	-0.9
4	0	4	3	0	3	13120.8331	13120.8338	0.7
4	1	3	3	1	2	13489.9604	13489.9612	-0.8
5	1	5	4	1	4	15976.2420	15976.2410	1.0
5	0	5	4	0	4	16386.0559	16386.0559	0.0
5	1	4	4	1	3	16858.2461	16858.2468	-0.7

- ***Substitution*** $^{13}C_6$.

Table: 8.8.- Measured and calculated frequencies (MHz) of the μ_a-type transitions observed for the $CH_2F_2 \cdots {}^{13}CH_2O$ substituted species. The last column is the difference between the observed and measured frequencies: $\Delta\nu = \nu_{OBS} - \nu_{CALC}$ in kHz.

J'	K'_{-1}	K'_{+1}	J''	K''_{-1}	K''_{+1}	ν_{OBS} / MHz	ν_{CALC} / MHz	$\Delta\nu$ / kHz
3	1	3	2	1	2	9423.0362	9423.0311	5.1
3	0	3	2	0	2	9673.0600	9673.0631	-3.1
3	1	2	2	1	1	9935.0735	9935.0762	-2.7
4	1	4	3	1	3	12561.7259	12561.7314	-5.5
4	0	4	3	0	3	12888.7225	12888.7231	-0.6
4	1	3	3	1	2	13244.3525	13244.3509	1.6
5	1	5	4	1	4	15698.4859	15698.4882	-2.3
5	0	5	4	0	4	16096.9643	16096.9634	0.9
5	1	4	4	1	3	16551.5191	16551.5181	1.0

8.6 References.-

[1] L. F. Elmuti, R. A. Peebles, S. A. Peebles, A. L. Steber, J. L. Neil, H. B. Pate, *Phys. Chem. Chem. Phys.*, 13, 14043, **2011**.

[2] G. Feng, L. Evangelisti, L. B. favero, J.-U. Grabow, Z. Xia, W. Caminati, *Phys. Chem. Chem. Phys.*, 13, 14092, **2011**.

[3] P. Ottaviani, W. Caminati, J.-U. Grabow, *J. Chem. Phys.*, 125, 19, **2006**.

[4] W. Caminati, S. Melandri, P. Moreschini, P. G. Favero, *Angew. Chem. Int. Ed.*, 38, 2924, **1999**.

[5] P. Ottaviani, S. Melandri, W. Caminati, J. C. López, *J. Mol. Spect.*, 239, 24, **2006**.

[6] S. Blanco, S. Melandri, P. Ottaviani, W. Caminati, *J. Am. Chem. Soc.*, 129, 2700, **2007**.

[7] M. Vallejo-López, L. Spada, Q. Gou, A. Lesarri, E. J. Cocinero, W. Caminati, *Chem. Phys. Lett.*, 591, 216, **2014**.

[8] L. B. Favero, B. M. Giuliano, A. Maris, S. Melandri, P. Ottaviani, B. Velino, W. Caminati, *Chem. Eur. J.*, 16, 1761, **2010**.

[9] L. Spada, Q. Gou, M. Vallejo-López, A. Lesarri, E. J. Cocinero, W. Caminati, *Phys. Chem. Chem. Phys.*, 16, 2149, **2014**.

[10] P. Écija, F. J. Basterretxea, A. Lesarri, J. Millán, F. Castaño, E. J. Cocinero, *J. Phys. Chem. A*, 116, 10099, **2012**.

[11] L. B. Favero, L. Evangelisti, A. Maris, A. Vega-Toribio, A. Lesarri, W. Caminati, *J. Phys. Chem. A*, 115, 9493, **2011**.

[12] W. Caminati, S. Melandri, M. Schnell, D. Banser, J.-U. Grabow, J. L. Alonso, *J. Mol. Struc.*, 742, 87, **2005**.

[13] P. Écija, m. Vallejo-López, L. Evangelisti, J. A. Fernández, F. Castaño, A. Lesarri, W. Caminati, E. J. Cocinero, *ChemPhysChem*, DOI: 10.1002/cphc.201301213.

[14] Y. Zhao, D. G. Truhlar, *Acc. Chem. Res.*, 41, 157, **2008**.

[15] G. Feng, L. Evangelisti, I. Cacelli, L. Carbonaro, G. Prampolini, W. Caminati, *Chem. Comm.*, 50, 171, **2014**.

[16] Q. Gou, G. Feng, L. Evangelisti, M. Vallejo-López, A. Lesarri, E. J. Cocinero, W. Caminati, *Phys. Chem. Chem. Phys.*, 15, 6714, **2013**.

[17] S. Y. Tang, L. Evangelisti, W. Caminati, *J. Mol. Spectr.*, 258, 71, **2009.**

[18] S. Blanco, S. Melandri, P. Ottaviani, W. Caminati, *J. Am. Chem. Soc.*, 129, 2700, **2007**

[19] P. Ottaviani, S. Melandri, W. Caminati, J. C. López, *J. Mol. Spectr.*, 239, 24, **2006**.

[20] W. Caminati, *J. Phys. Chem. A*, 110, 4359, **2006**.

[21] W. Caminati, S. melandri, M. Schnell, D. Banser, J.-U. Grabow, J. L. Alonso, *J. Mol. Struct.*, 742, 87, **2005.**

[22] A. Maris, S. Melandri, W. Caminati, I. Rossi, *Chem. Phys. Lett.*, 407, 192, **2005**.

[23] S. Blanco, J. C. López, A. Lesarri, W. Caminati, J. l. Alonso, *ChemPhysChem*, 5, 1779, **2004**.

[24] J. C. López, P. G. Favero, A. Dell´Erba, W. Caminati, *Chem. Phys. Lett.*, 316, 81, **2000**.

[25] M. M. Serafin, S. A. Peebles, *J. Phys. Chem. A*, 110, 11938, **2006**.

[26] E. J. Cocinero, R. Sánchez, S. Blanco, A. Lesarri, J. C. López, J. L. Alonso, *Chem. Phys. Lett.*, 402, 4, **2005**.

[27] T. A. Halgren, MMFF VII. Characterization of MMFF94, MMFF94s, and Other Widely Available Force Fields for Conformational Energies and for Intermolecular-Interaction Energies and Geometries. *J. Comput. Chem.*, 20, 730, **1999**.

[28] Macromodel, version 9.2, Schrödinger, LLc, New York, NY, **2012**.

[29] M. J. Frisch et al., Gaussian, Inc., Wallingford CT, **2009**.

[30] W. Gordy and L. R. Cook, "Microwave Molecular Spectra", 3rd Edition, in Weissberger, A. (Ed.), Techniques of Chemistry, vol. XVIII, John Wiley & Sons Inc., New York, **1984**.

[31] H. M. Pickett, *J. Mol. Spectrosc.*, 148, 37, **1991**.

[32] http://physics.nist.gov/jb95, retrieved: 2014/01/31

[33] J. Kraitchman, *Am. J. Phys.*, 21, 17, **1953**.

[34] H. D. Rudolph, *Struct. Chem.*, 2, 581, **1991**.

[35] K. J. Epple, H. D. Rudolph, *J. Mol. Spectr.* 152, 355, **1992**.

Chapter 9

$CH_2ClF\cdots$ Formaldehyde

9.1. Introduction.-

As in the DFM$\cdots$formaldehyde complex, the two monomers that form the chlorofluoromethane$\cdots$formaldehyde complex ($ClFCH_2\cdots CH_2O$) have been studied previously using microwave spectroscopy. Also, several complexes that involve chlorofluoromethane[1-11] or formaldehyde monomers have been characterized (see chapter 8), offering an opportunity to compare the binding sites and strength in $ClFCH_2\cdots CH_2O$ with previous reports.

$ClFCH_2$, and in general all chlorofluorocarbons (CFC's), are interesting from the atmospheric point of view, since detection or monitoring by spectroscopic means requires a detailed knowledge of the spectrum.

The chlorofluorocarbons or CFC´s[12] are organic compounds obtained from the saturated hydrocarbons in which some of the hydrogen atoms have been substituted by chlorine and/or fluorine atoms. These substances, volatiles in all cases, were widely used in refrigeration systems and as propellant in aerosols. However, the emissions of these particles were found to be the cause of the ozone (O_3) layer destruction in the 80's. When CFC´s reach the top layers in the atmosphere, in particular, the stratosphere, the ultraviolet radiation impacts with those molecules and the CFC dissociation takes place, liberating Cl^- radicals. Those ions react with the ozone particles destroying the O_3 molecules and generating chlorine monoxide (ClO) and molecular oxygen (O_2).[13,14]

Apart from the atmospheric interest, ClFM is interesting because of the presence of two different halogen atoms: F and Cl. In consequence we can compare the strength of the interactions involving those atoms. In particular, we can compare the possibility that C-F or C-Cl bonds act as proton acceptors in C-F···H or C-Cl···H hydrogen bonds.

The most important part of this work is thus the investigation of the possible binding sites and dominant interactions in CFM··· CH_2O. The study is relevant in connection with the role of weak hydrogen bonding and halogen bonding, for which the structural information available is much reduced compared to moderate hydrogen bonds. At the same time the comparison with other formaldehyde···$Cl_xF_yCH_{4-x-y}$ intermolecular complexes[15-17] involving CFC, like difluoromethane, trifluoromethane or chlorotrifluoromethane, may give a perspective of the general trends controlling clustering of these systems.

The study of the CFM···CH_2O complex represents in this way an intermediate step in the knowledge of systems with higher complexity such as isoflurane···formaldehyde. (See chapter 12 for further details).

9.2. Computational Methods.-

Concerning the conformational landscape of the system, we started this study considering all conceivable interactions between the two monomers of ClFM and formaldehyde, in particular different hydrogen and halogen bonds. In order to distinguish which of the structures were real minima on the potential energy surface theoretical calculations were performed. This method has been discussed in the previous chapter and gives some interesting structural and electrical properties, such as the dipole moments, that let us know which structures might be populated and could be expected in the supersonic jet using rotational spectroscopy.

Finally, all the structures predicted as stable conformers exhibit several simultaneous hydrogen bonds. The plausible geometries for the system are shown in the following figure, where the hydrogen bond lengths are indicated for each structure.[18-24] As observed in the picture formaldehyde acts as proton donor through one or two of its hydrogen atoms, and at the same time the oxygen atom behaves as proton acceptor through its lone pairs (except in conformer 4). There are no direct interactions with the π system of the carbonyl group among the most stable conformers.

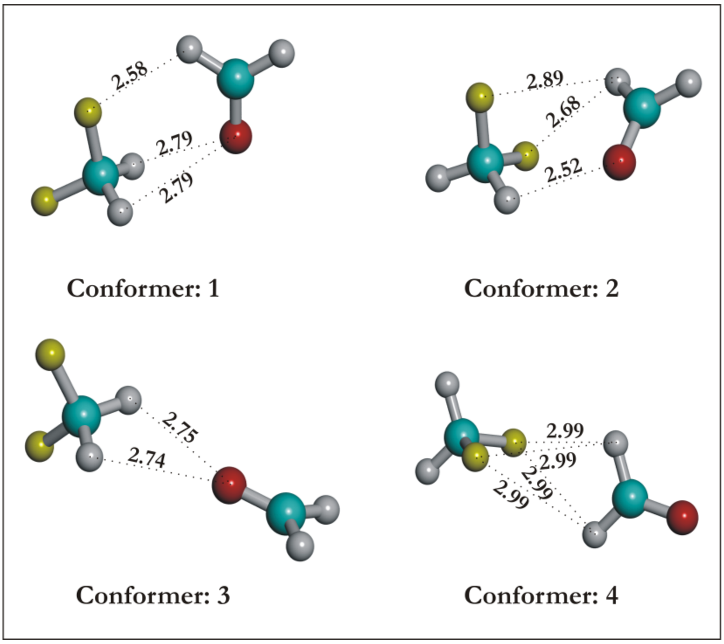

<u>Figure: 9.1.-</u> Plausible conformational configurations for the complex ClFM···formaldehyde depending on the different interacting hydrogen bonds.

The theoretical characterization of the molecule included several calculation methods. First of all, Molecular Mechanics were used, in particular, in combination with algorithms that use Monte Carlo Multiple minimizations and Large-scale Low-Mode procedures, [25] assuring a reliable conformational search. In order to obtain more accurate values of the spectroscopic parameters and relevant properties such as bonding energies or inertial moments, some ab initio calculations were later performed. Following this procedure, the stationary points on the potential energy surface minima were identified and the most important interactions between the two subunits of the complex were detected.

For the ClFM···CH_2O geometry optimizations we used second-order perturbation methods: MP2 with Pople´s triple-ζ basis set: 6-311++G(d,p). Harmonic vibrational frequency calculations were also done following optimization. All the calculations were implemented in Gaussian 03 and Gaussian 09[26] and the results of the spectroscopic parameters for the four most stable conformers are summarized in the following table.

Table: 9.1.- Rotational Constants (A, B and C), dipole moments (μ_a, α = a, b, c) and diagonal elements of the quadrupolar coupling tensor of the ^{35}Cl nucleus ($\chi_{\alpha\beta}$, (α,β = a, b, c)) for the predicted conformers. The centrifugal distortion constants are also shown (D_J, D_{JK}, D_K, d_1 and d_2). The ΔE relative energies are computed between each structure and the most stable one, zero point energy corrected (ZPE). ΔG is calculated at 298K and 1 atm.

	Conf. 1	Conf.2	Conf.3	Conf.4
***A* / MHz**	4976	6021	13397	5970
***B* / MHz**	1995	1625	1196	1254
***C* / MHz**	1635	1290	1106	1051
χ_{aa} / MHz	28.21	30.10	-67.34	28.89
χ_{bb} / MHz	-43.65	-66.21	30.43	-66.42
χ_{cc} / MHz	15.43	36.11	36.91	37.53
$\lvert\mu_a\rvert$ / D	0.26	3.20	2.28	3.61
$\lvert\mu_b\rvert$ / D	0.05	0.75	0.38	1.30
$\lvert\mu_c\rvert$ / D	0.39	0.00	0.00	2.52
$\lvert\mu_{TOT}\rvert$ / D	0.47	3.29	2.31	4.59
D_J / kHz	6.86	1.29	0.66	
D_{JK} / kHz	14.69	13.14	1.57	
D_K / kHz	6.52	28.96	636.32	
d_1 / kHz	-1.86	-0.27	-0.06	
d_2 / kHz	-0.25	-0.07	0.00	
ΔG / kJ·mol^{-1}	0.0	1.4	1.7	
Δ(E+ZPE) / kJ·mol^{-1}	0.0	-0.3	-0.7	

Considering the relative energies of all the predicted conformers, we might expect in principle to detect in the rotational spectrum transitions belonging to the three more stables conformers, as the energy difference is rather low (< 2 kJ mol^{-1}).

9.3. Results and Analysis.-

a. Assignment of the rotational spectrum.

For all the predicted conformational structures, we simulated the expected rotational spectra based on different arguments. The Ray parameter is used to quantify the rotor asymmetry. Here, all the plausible conformers are asymmetric near-prolate tops (κ≈ -0.78 to κ≈ -0.98).[27] We predict the rotational transitions the Pickett[28] and JB95[29] programs. These predictions are based on the Watson semirigid rotor Hamiltonian[27] and starting from the initial rotational constants obtained from the quantum mechanics calculations (table 9.1), they are used later to fit the rotational spectra.

Apart from the rotational constants, the ab initio calculations give other properties of interest for the rotational studies such as dipole moments. The value of these magnitudes let us distinguish which kind of selection rules are active.

In particular, for the conformer 2, the μ_c component is zero so no μ_c-type rotational transitions could be measured. On the other hand, the dipole moment is mainly oriented along the *a* and b inertial axes and, in consequence, transitions μ_a and μ_b could be identified. We thus first predicted the most intense R-branch (*J*+1 ← *J*) μ_a and μ_b transitions for this conformer.

The following figure shows the simulated ^{a}R and R^{b} spectrum for conformer 2. In the first one we can identify the typical progression where the lines appear in groups separately approximately by the value $B + C \approx 2900MHz$.[27] No pattern is found for the μ_b spectrum.

Figure: 9.2.- [a]R and [b]R predicted spectrum for conformer 2.

The previous predictions let us fix the interesting region where the most intense transitions are found. However, that prediction is made with the theoretical values of the rotational constants and small errors can cause large shifts (>100-300 MHz usually) between the predictions relative to the experimental measurements.

In this way, the comparison of the experimental and theoretical results let us check the validity of the computational methods used for clusters formed by several molecules in the gas phase.

The following figure shows the experimental rotational spectrum obtained for the complex. In the experimental spectrum, only transitions corresponding to the second most stable conformer (ΔE~1.5 kJ·mol^{-1}) were detected. The dipole moment along the principal axis c is zero by symmetry. The measured transitions are all μ_a and μ_b-type. In the following section, the dynamics associated to all internal motions of the complex are explained.

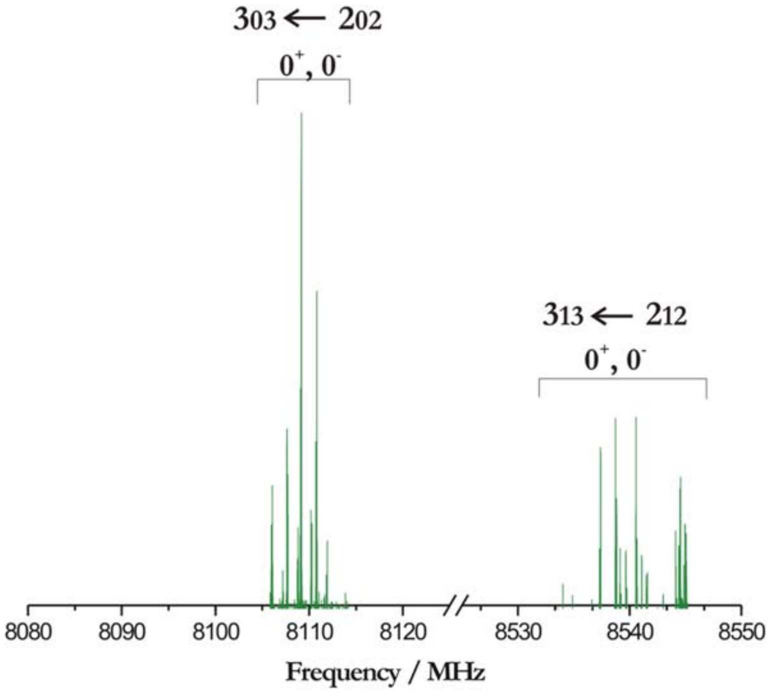

Figure: 9.3.- Section of the experimental scan measured for the ClFM···formaldehyde complex. The observed conformer was unambiguously identified and assigned as conformer 2.

b. Fine and Hyperfine effects: Nuclear quadrupole coupling and proton tunneling.

In the ClF···CH_2O complex, we observed three different kinds of frequency splittings in all the measured rotational transitions. Apart from the characteristic Doppler splitting due to the coaxial arrangement in the FTMW spectrometer,[30,31] and the expected hyperfine components associated to the coupling between the quadrupole moment of the ^{35}Cl nucleus of ClFM and the molecular electric gradient, we noticed an additional frequency doubling. These doublets must be produced by a quantum tunneling effect between equivalent conformations. In consequence, the only molecular mechanism which can give rise to the doublings is the exchange of the hydrogen atoms of the formaldehyde subunit, which can be described as an internal rotation of the formaldehyde molecule around its C_2 axis.

The coupling between the nuclear spin angular momentum of the ^{35}Cl nucleus ($I = {}^3/_2$)[32, 33] with the rotational angular moment of the complex is a well known phenomenon, previously observed in this thesis for the ^{14}N atom. As a consequence, each rotational transition is split according to the new quantum number F ($\boldsymbol{F}=\boldsymbol{I}+\boldsymbol{J}$) and selection rules $\Delta F=0, \pm 1$, increasing the complexity of the spectrum.

In particular, for the ClFM···formaldehyde complex, the splitting of the transitions due to this hyperfine effect is much larger than for nitrogen-containing molecules because of the larger quadrupole moment of the Cl atom (-8.11 vs 2.01 fm^2). As an example the splitting of the $1_{1,1} \leftarrow 0_{0,0}$ transition is more than 30 MHz (i.e., hundreds of times the linewidth). In the following figure the $3_{0,3} \leftarrow 2_{0,2}$ transition of the second conformer is represented and the quadrupole coupling components are distinguished. Furthermore, it is important to note that for each $F \leftarrow F'$ hyperfine component there is a doubling into two transitions because of the internal rotation of formaldehyde. The two components of the internal rotational doubling have been labeled as two torsional states 0^- and 0^+. Because the internal rotation of formaldehyde around its internal symmetry axes will not invert the sign of electric dipole moment of this monomer the torsional selection rules must imply vibrational states of the same symmetry. In consequence, the fine components should correspond to rotational transitions within the same torsional state, or $0^- \leftarrow 0^-$ and $0^+ \leftarrow 0^+$.

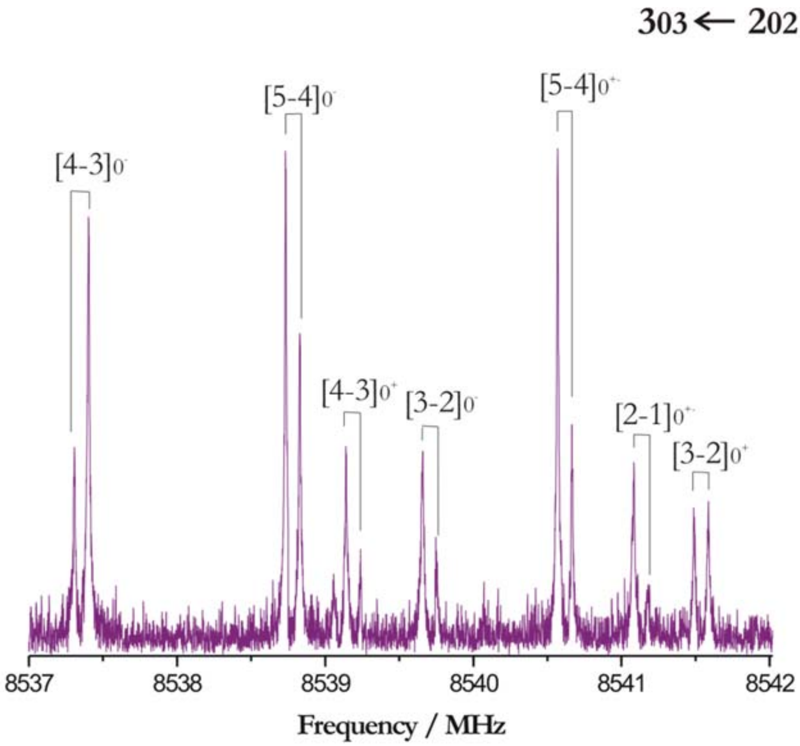

Figure: 9.4.- $3_{0,3} \leftarrow 2_{0,2}$ transition of conformer 2 of the chlorofluoromethane···formaldehyde complex. The hyperfine components are labelled for each torsional states.

c. Determination of the spectroscopic parameters.

Although the theoretical results suggest the coexistence of three different conformers, experimentally only one was detected in the jet, corresponding to that predicted as second in energy. The small dipole moment value in the global minimum (<0.4 D) may cause the absence of these transitions in the experimental spectrum.

From the measured rotational spectrum, relevant spectroscopic parameters for the conformational characterization of the complex were determined. In order to obtain those parameters, the experimental transitions (shown in table 9.3) were assigned and fitted using the Watson semi-rigid Hamiltonian in the asymmetric reduction and within the I^r representation (convenient for prolate tops[27]) with an additional term that considers the nuclear quadrupole coupling hyperfine effects. The two torsional states were fitted independently, except for the centrifugal distortion constants, which were constrained to the same values in the two states. Because the symmetry of the complex does not allow observing interstate transitions $0^- \leftarrow 0^+$ it was not possible to fit the energy difference between the torsional states.

Table: 9.2.- Experimental values for the rotational constants *A*, *B*, *C*, diagonal elements of the ^{35}Cl nuclear quadrupole coupling tensor ($\chi_{aa}, \chi_{bb}, \chi_{cc}$) and centrifugal distortion constants ($\Delta_J, \Delta_{JK}, \Delta_K, \delta_J, \delta_K$) for each state. The results are compared with the MP2 theoretical calculations. The number of lines used in the fit (N^c) and the root-mean-square deviation of the fit (σ) are also listed in the table.

	Theory* MP2	Experiment	
		State 0⁺	**State 0⁻**
A / MHz	6021	5982.6779 (11)[a]	5984.5910 (14)
B / MHz	1625	1597.43184 (26)	1598.08391 (25)
C / MHz	1290	1271.98947 (24)	1272.02736 (23)
μ_a / D	3.20	---	---
μ_b / D	0.75	---	---
μ_c / D	0.00	---	---
μ_{TOT} / D	3.29	---	---
χ_{aa} / MHz		31.1347 (48)	31.116 (10)
χ_{bb} / MHz		-76.2593 (93)	-76.255 (11)
χ_{cc} / MHz		29.5572 (93)	29.581 (11)
D_J / kHz	1.29	1.5947 (15)	
D_{Jk} / kHz	13.14	17.773 (23)	
D_k / MHz	28.96	---	
d_1 / kHz	-0.27	-0.3290 (20)	
d_2 / kHz	-0.07	-0.0864 (14)	
σ / kHZ		0.64	
N		88	62

[a] Standard error in parentheses in units of the last digit.

No transitions belonging to other conformers were detected in the acquired spectrum.

The rms deviation in both cases is under 1 kHz, below the estimated accuracy for the experimental measurements. Also the correlation coefficients are acceptably small. This means that the fit quality is good for this experimental data ser. The accuracy of the rotational constants is almost the same for both torsional states, though it is slightly worse for the quadrupole coupling constants in the excited state 0^- (probably because of the different number of transitions measured in each case: 88 for the 0^+ instead of 62 for the 0^-).

Four out of five quartic centrifugal distortion constants were determined for the two vibrational states. No results were obtained for the D_k constants and transitions with higher J values would be required to get a good fitting for this parameter.

Concerning the quadrupolar coupling moment, only the diagonal elements of the tensor were obtained but not the out of diagonal elements. Additional F'←F transitions would be needed to obtain these magnitudes, which (unlike the ^{14}N tensor) are sometimes determinable from the rotational spectrum.

Looking at the results we can also conclude that the ab initio method MP2, can reproduce reasonably the interactions and the internal motion of the complex in gas phase.

Table: 9.3.- Measured and calculated frequencies for the μ_a and μ_b type transitions of the 0^+ and 0^- torsional states for the observer conformer of the complex ClFM···formaldehyde. The last column represents the difference in kHz between the measured and calculated frequencies: $\Delta\nu = \nu_{OBS} - \nu_{CALC}$.

$J'\ K'_{-1}\ K'_{+1}$	$J''K''_{-1}\ K''_{+1}$	F'	F''	$\upsilon_1\ \upsilon_2$	ν_{OBS} / MHz	ν_{CALC} / MHz	$\Delta\nu$ / kHz
1 1 1	0 0 0	2	2	1 1	7240.9448	7240.9439	0.9
				0 0	7242.8924	7242.8902	2.2
		3	2	1 1	7258.0559	7258.0559	0.0
				0 0	7260.0064	7260.0069	-0.5
		1	2	1 1	7271.7614	7271.7619	-0.5
				0 0	7273.7129	7273.7131	-0.2
4 0 4	3 1 3	6	5	1 1	7654.1296	7654.1310	-1.4
				0 0	7656.3294	7656.3271	2.3
3 1 3	2 1 2	2	1	1 1	8106.0208	8106.0215	-0.7
				0 0	8107.1426	8107.1445	8.1
		3	2	1 1	8107.6739	8107.6751	-1.2
				0 0	8108.7865	8108.7865	0.0
		5	4	1 1	8109.1265	8109.1226	3.9
				0 0	8110.2362	8110.2359	0.3
		4	3	1 1	8110.7724	8110.7726	-0.2
				0 0	8111.8867	8111.8844	2.3
3 0 3	2 0 2	3	3	1 1	8534.8404	8534.8450	-4.6
		4	3	1 1	8537.3562	8537.3562	0.0
				0 0	8539.1865	8539.1875	-1.0
		5	4	1 1	8538.7793	8538.7786	0.7
				0 0	8540.6164	8540.6139	2.5
		3	2	1 1	8539.7040	8539.7075	-3.5
				0 0	8541.5385	8541.5385	0.0
		2	1	1 1	8541.1298	8541.1312	-1.4
				0 0	8542.9601	8542.9645	-4.4
		4	4	1 1	8544.1798	8544.1792	0.6

Table: 9.3 Continued.-								
J' K'₋₁ K'₊₁	*J''K''₋₁ K''₊₁*	*F'*	*F''*	υ_1 υ_2	ν_{OBS} / MHz	ν_{CALC} / MHz	$\Delta\nu$ / kHz
3 2 2	2 2 1	5	4	1 1	8605.4568	8605.4556	1.2
				0 0	8607.5257	8607.5267	-1.0
		3	2	1 1	8607.6770	8607.6785	-1.5
				0 0	8609.7527	8609.7585	4.2
		4	3	1 1	8613.2374	8613.2390	-1.6
				0 0	8615.3083	8615.3057	2.6
3 2 1	2 2 0	5	4	1 1	8674.3832	8674.3801	3.1
				0 0	8676.6919	8676.6976	4.3
		3	2	1 1	8677.5967	8677.5935	3.2
				0 0	8679.9039	8679.9014	2.5
		4	3	1 1	8683.5848	8683.5864	-1.6
				0 0	8685.8925	8685.8917	0.8
3 1 2	2 1 1	5	4	1 1	9083.5442	9083.5443	-0.1
				0 0	9086.4984	9086.4972	1.2
		4	3	1 1	9085.1789	9085.1785	0.4
				0 0	9088.1320	9088.1295	2.5
		2	1	1 1	9087.0206	9087.0176	3.0
				0 0	9089.9726	9089.9712	1.4
		3	2	1 1	9088.6604	9088.6601	0.3
				0 0	9091.6156	9091.6120	3.6
2 1 2	1 0 1	3	2	1 1	9785.6341	9785.6301	4.0
		2	2	1 1	9792.3050	9792.3132	-8.2
		3	3	1 1	9793.4146	9793.4157	-1.1
		4	3	1 1	9802.7276	9802.7273	0.3
				0 0	9804.7569	9804.7545	2.4
		2	1	1 1	9806.3221	9806.3227	-0.6
		1	1	1 1	9815.6685	9815.6674	1.1
4 1 4	3 1 3	3	2	1 1	10792.2039	10792.2054	-1.5
				0 0	10793.6242	10793.6258	-1.6
		4	3	1 1	10792.5686	10792.5683	0.3
				0 0	10793.9907	10793.9876	3.1
		6	5	1 1	10793.2326	10793.2318	0.8
				0 0	10794.6538	10794.6525	1.3
		5	4	1 1	10793.5860	10793.5871	-1.1
				0 0	10795.0064	10795.0067	-0.3
5 0 5	4 1 4	7	6	1 1	10873.2327	10873.2313	1.4
				0 0	10876.3469	10876.3507	-3.8
		5	4	1 1	10879.0126	10879.0119	0.7
		6	5	1 1	10881.9636	10881.9652	-1.6
4 0 4	3 0 3	4	4	1 1	11303.1772	11303.1798	-2.6
		5	4	1 1	11304.4150	11304.4156	-0.6
				0 0	11306.5934	11306.5944	-1.0
		4	3	1 1	11305.6899	11305.6909	-1.0
				0 0	11307.8714	11307.8699	1.5
		6	5	1 1	11306.2486	11306.2493	-0.7
				0 0	11308.4308	11308.4311	-0.3
		3	2	1 1	11307.5120	11307.5155	-3.5
				0 0	11309.6905	11309.6973	-6.8
		5	5	1 1	11309.8178	11309.8148	3.0

Table: 9.3 Continued.-							
J' K'$_{-1}$ K'$_{+1}$	***J''K''$_{-1}$ K''$_{+1}$***	***F'***	***F''***	υ_1 υ_2	ν_{OBS} / MHz	ν_{CALC} / MHz	$\Delta\nu$ / kHz
4 2 3	3 2 2	6	5	1 1	11462.1066	11462.1069	-0.3
		4	3	1 1	11463.9822	11463.9842	-2.0
				0 0	11466.7035	11466.6969	6.6
		5	4	1 1	11464.9860	11464.9863	-0.3
				0 0	11467.6956	11467.6981	-2.5
4 2 2	3 2 1	6	5	1 1	11632.8306	11632.8352	-4.6
				0 0	11636.1242	11636.1274	-3.2
		4	3	1 1	11636.1684	11636.1736	-5.2
				0 0	11639.4603	11639.4667	-6.4
		5	4	1 1	11637.5465	11637.5503	-3.8
				0 0	11640.8396	11640.8431	-3.5
4 1 3	3 1 2	4	4	1 1	12084.1549	12084.1536	1.3
		6	5	1 1	12090.5560	12090.5569	-0.9
				0 0	12094.4193	12094.4169	2.4
		5	4	1 1	12090.8358	12090.8381	-2.3
				0 0	12094.6987	12094.6968	1.9
		3	2	1 1	12092.6271	12092.6310	-3.9
				0 0	12096.4912	12096.4913	-0.1
		4	3	1 1	12092.9162	12092.9175	-1.3
				0 0	12096.7769	12096.7765	0.4
3 1 3	2 0 2	4	3	1 1	12176.4089	12176.4139	-5.0
		3	3	1 1	12180.0063	12179.9997	6.6
		5	4	1 1	12190.8982	12190.8983	-0.1
				0 0	12192.7179	12192.7179	0.0
5 1 5	4 1 4	5	4	1 1	13461.8702	13461.8697	0.5
				0 0	13463.5517	13463.5505	1.2
		4	3	1 1	13461.9871	13461.9855	1.6
				0 0	13463.6670	13463.6672	-0.2
		6	5	1 1	13462.3401	13462.3389	1.2
				0 0	13464.0186	13464.0198	-1.2
		7	6	1 1	13462.4623	13462.4596	2.7
				0 0	13464.1414	13464.1416	-0.2
5 0 5	4 0 4	6	5	1 1	14010.1938	14010.1946	-0.8
				0 0	14012.5369	14012.5360	0.9
		5	4	1 1	14011.0458	14011.0438	2.0
				0 0	14013.3865	14013.3851	1.4
		7	6	1 1	14012.3323	14012.3320	0.3
				0 0	14014.6777	14014.6763	1.4
		4	3	1 1	14013.1660	14013.1674	-1.4
				0 0	14015.5082	14015.5117	-3.5
5 1 4	4 1 3	6	5	1 1	15076.3539	15076.3507	3.2
				0 0	15081.0442	15081.0416	2.6
		7	6	1 1	15076.6359	15076.6381	-2.2
				0 0	15081.3308	15081.3307	0.1
		5	4	1 1	15077.7387	15077.7389	-0.2
				0 0	15082.4312	15082.4302	1.0
		4	3	1 1	15078.0279	15078.0226	5.3
				0 0	15082.7194	15082.7153	4.1

Table: 9.3 Continued.-								
***J' K'*$_{-1}$ *K'*$_{+1}$**	***J''K''*$_{-1}$ *K''*$_{+1}$**	***F'***	***F''***	υ_1 υ_2	ν_{OBS} **/ MHz**	ν_{CALC} **/ MHz**	$\Delta\nu$ **/ kHz**
6 1 6	5 1 5	6	5	1 1	16114.5297	16114.5242	5.5
				0 0	16116.4166	16116.4179	-1.3
		7	6	1 1	16114.7832	16114.7822	1.0
		5	4	1 1	16114.8570	16114.8691	-12.1
		8	7	1 1	16115.1382	16115.1305	7.7
				0 0	16117.0271	16117.0254	1.7
6 0 6	5 0 5	7	6	1 1	16651.7236	16651.7221	1.5
				0 0	16654.0655	16654.0645	1.0
		6	5	1 1	16652.3433	16652.3420	1.3
		8	7	1 1	16654.0112	16654.0084	2.8
				0 0	16656.3507	16656.3531	-2.4
		5	4	1 1	16654.5823	16654.5820	0.3
				0 0	16656.9238	16656.9267	-2.9
6 2 5	5 2 4	8	7	1 1	17132.7616	17132.7712	-9.6
		5	4	1 1	17135.8662	17135.8653	0.9
		7	6	1 1	17135.9365	17135.9330	3.5
6 2 4	5 2 3	5	4	1 1	17695.9199	17695.9179	2.0
		8	7	1 1	17696.0810	17696.0818	-0.8
		6	5	1 1	17698.6201	17698.6171	3.0
		7	6	1 1	17698.7764	17698.7769	-0.5
6 1 5	5 1 4	7	6	1 1	18033.9397	18033.9397	0.0
				0 0	18039.3516	18039.3584	-6.8
		8	7	1 1	18034.5950	18034.5909	4.1
				0 0	18040.0101	18040.0114	-1.3
		6	5	1 1	18034.9530	18034.9499	3.1
				0 0	18040.3661	18040.3687	-2.6
		5	4	1 1	18035.5983	18035.5980	0.3

d. Isotopic Substitutions: Structural Determination.

We can obtain relevant information about the structure of the complex such as bond lengths, valence angles and dihedrals from the rotational spectra of additional isotopologues.

The moments of inertia, and in consequence the rotational constants, are quantities directly connected to the masses and geometries of the molecular system. Although moments of inertia include contributions from molecular vibrations, several procedures can be used to derive near-equilibrium or effective structural information from the ground-state constants. This calculations rely on the changes in the rotational constants following a change in the atomic masses such as those originated from isotopic substitutions (or isotopologues in natural abundance).

In our case, the system we are studying is formed by carbon, hydrogen, chlorine, fluorine and oxygen atoms. All of them have different isotopes in different natural abundances. For the ^{37}Cl, ^{13}C and ^{18}O the natural abundances are 24.23%, 1.1% and 0.20%,[32,33] respectively. This makes it quite easy to detect the ^{37}Cl species, while for the latter two the concentration is quite low and in consequence it is more difficult to detect signals in the experimental spectrum due to their transitions.

The intensity of the isotopologues can increase when the system involves equivalent atoms, but this is excluded in ClFM···CH_2CO. In the present study, only transitions belonging to the ^{37}Cl isotopologue were finally detected in the spectrum.

The rotational transitions of the substituted species (see appendix I) were fitted similarly to the parent species. The spectroscopic parameters for the two vibrational states of the $CH_2{}^{37}ClF$ complex are shown in table 9.4. They can be compared with the fitting results of the parent species in table 9.2.

Table: 9.4.- Experimental rotational constants *A*, *B* and *C* of the two states of the substituted species $CH_2{}^{37}ClF\cdots CH_2CO$. The diagonal elements of the nuclear quadrupole coupling tensor were fitted while the centrifugal distortion constants values were fixed to the values in the parent species. The number of transition fitted *N* and the root-mean-square deviation (σ) are also given.

	$CH_2{}^{37}ClF$		
	State 0^-		State 0^+
A / MHz	5817.1958 (35) [a]		5818.9265 (36)
B / MHz	1592.83764 (25)		1593.48776 (29)
C / MHz	1261.42423 (18)		1261.46024 (21)
χ_{aa} / MHz	24.541 (31)		24.590 (42)
χ_{bb} / MHz	-60.184 (27)		-60.207 (33)
χ_{cc} / MHz	23.372 (27)		23.322 (33)
D_J / kHz		[1.5947][b]	
D_{Jk} / kHz		[17.773]	
D_k / MHz		---	
d_1 / kHz		[1.5947]	
d_2 / kHz		[17.773]	
σ / kHZ	0.90		0.90
N	41		29

[a] Standard error in parentheses in units of the last digit.
[b] Fixed to the parent species value.

Once the spectroscopic parameters are determined, we can obtain the substituted (r_s) and the effective (r_0) structures for the identified conformer.

The substituted structure is a good approximation to the unmeasurable equilibrium structure. To obtain the coordinates of the substituted atom in the principal axis orientation we use the Kraitchman[34] equations, that give the absolute values of the coordinates for the substituted atoms. This method uses the differences between the inertial moments of the parent and the isotopologues. Since in this complex only the Cl atom was substituted, the resulting structural information is limited to one atom.

Table: 9.5.- Absolute values of the atomic coordinates in the principal axis orientation for the chlorine atom in the complex compared with the ab initio.

	Isotopologue Coordinates (Å)		
	a	b	c
Cl (exp)	0.6814 (22)[a]	1.1118 (14)	0.00[b]
Cl (theor)	-0.66939	1.11743	0.00089

[a] Errors in parentheses in units of the last digit.
[b] Zero by symmetry.

Alternatively, the effective structure is that which best reproduces the rotational constants of the system in a given vibrational state. To determine this effective structure, as well as in the substituted structure determination, the rotational constants values and its errors (see the fitting results in table 9.4) are fitted to a structural model. Since we have in this case six experimental data the determinable parameters should be smaller. The method requires a careful selection of the fitting parameters. In the ClFM···CH_2O system, three key parameters (shown in figure 9.5) were selected: one angle (α), one distance (R) and a dihedral angle (τ). All other parameters were fixed to the ab initio geometry.

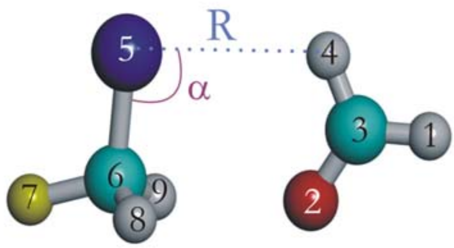

Figure: 9.4.- Effective structure calculation, showing the fitting parameters R and α.

In the following table the results of those parameters are compared with the ab initio values.

Table: 9.6.- Effective structure compared with the theoretical equilibrium structure for the detected conformer (see figure 9.4 for atom numbering).

	$\mathbf{r_0}$	**Ab initio $\mathbf{r_e}$**
r (Cl_5-H_4)/ Å	3.116 (11)	3.086
< (C_6-Cl_5-H_4) / deg	96.31 (33)	96.311
τ(C_6-Cl_5-H_4-C_3) / deg	-5.14 (27)	-0.24
r (H_9- O)/ Å	2.75 (6) [a]	2.70
r (H_8- O)/ Å	2.78 (7) [a]	2.72

[a] Derived parameters.

We found no other spectroscopic studies on the CH_2ClF···CH_2CO complex, so no comparison is possible with other experimental data.

9.4 Conclusions.-

The rotational spectrum of the ClFM···formaldehyde complex was observed using time-domain microwave spectroscopy. The spectrum revealed the presence of a single conformer, which was identified as the second most stable isomer (conformer 2) in the ab initio calculations (figura 9.1). No other species were detectable.

The absence of conformer 1 can be rationalized either because of its small dipole moment, or, eventually, by a collisional relaxation to conformer 2 (which would imply that the ab initio prediction is reversed).

In the plausible conformers of the complex ClFM··· FA, different C-H, C-F and C-Cl bonds can be found and several hydrogen bonds are established between the two subunits of the complex. According to the experimental measurements, the most stable configuration presents three hydrogen bonds: two moderate C=O···H-C and an extra hydrogen bond with the Cl halogen of the ClFM.

Comparing conformers II and III, we can notice the low energy gap between those configurations. Despite they have similar dipole moments, only the first one was detected in the jet, which can suggest that the C-Cl···H-C interaction is more favourable than the C-F···H-C bond.

In the detected configuration, three different kinds of interactions were involved. As expected, this conformer was found to be more stable than the one in which the two subunits are linked by only two weak hydrogen bonds (conformer IV).

The structure determination let us characterize the bond length of the complex. It was found to be 3.116 Å, which is within the range of the values obtained in freon complexes link by these weak hydrogen bonds.

9.5 Appendix.-

The following tables show the measured transitions for the monosubtituted species $CH_2{}^{37}ClF$.

- ***^{37}Cl substitution.***

Table: 9.7.- Measured and calculated frequencies (in MHz) for the μ_a and μ_b–type transitions of the substituted $^{37}ClFCH_2\cdots COH_2$. The third column is the difference (in kHz) between the observed and the calculated frequencies $\Delta\nu = \nu_{OBS} - \nu_{CALC}$.

J' K'₋₁ K'₊₁	*J''K''₋₁ K''₊₁*	*F'*	*F''*	υ_1 υ_2	ν_{OBS} / MHz	ν_{CALC} / MHz	$\Delta\nu$ / kHz
1 1 1	0 0 0	2	2	1 1	7067.7755	7067.7773	-1.8
				0 0	7069.5406	7069.5416	-1.0
		3	2	1 1	7081.2857	7081.2853	0.4
				0 0	7083.0533	7083.0526	0.7
3 1 3	2 1 2	2	1	1 1	8051.4956	8051.5014	-5.8
		3	2	1 1	8052.7914	8052.7929	-1.5
		5	4	1 1	8053.9360	8053.9419	-5.9
				0 0	8055.0377	8055.0396	-1.9
		4	3	1 1	8055.2307	8055.2311	-0.4
				0 0	8056.3296	8056.3316	-2.0
3 0 3	2 0 2	4	3	1 1	8486.9917	8486.9924	-0.7
				0 0	8488.7998	8488.7978	2.0
		5	4	1 1	8488.1736	8488.1771	-3.5
		3	2	1 1	8488.8632	8488.8646	-1.4
		2	1	1 1	8490.0436	8490.0490	-5.4
3 1 2	2 1 1	5	4	1 1	9046.4584	9046.4618	-3.4
				0 0	9049.4000	9049.3989	1.1
		4	3	1 1	9047.7336	9047.7348	-1.2
				0 0	9050.6770	9050.6746	2.4
		2	1	1 1	9049.2052	9049.2116	-6.4
				0 0	9052.1501	9052.1482	1.9
		3	2	1 1	9050.4853	9050.4899	-4.6
				0 0	9053.4314	9053.4292	2.2
4 1 4	3 1 3	3	2	1 1	10717.4607	10717.4635	-2.8
				0 0	10718.8616	10718.8625	-0.9
		4	3	1 1	10717.7318	10717.7317	0.1
				0 0	10719.1331	10719.1315	1.6
		6	5	1 1	10718.2672	10718.2685	-1.3
				0 0	10719.6653	10719.6664	-1.1
		5	4	1 1	10718.5305	10718.5319	-1.4
				0 0	10719.9287	10719.9306	-1.9

Table: 9.7 Continued.-

J' K'_{-1} K'_{+1}	$J''K''_{-1}$ K''_{+1}	F'	F''	υ_1 υ_2	ν_{OBS} / MHz	ν_{CALC} / MHz	$\Delta\nu$ / kHz
4 0 4	3 0 3	5	4	1 1	11231.6284	11231.6296	-1.2
				0 0	11233.7611	11233.7600	1.1
		4	3	1 1	11232.6438	11232.6473	-3.5
				0 0	11234.7762	11234.7793	-3.1
		6	5	1 1	11233.1456	11233.1497	-4.1
				0 0	11235.2777	11235.2816	-3.9
		3	2	1 1	11234.1585	11234.1613	-2.8
				0 0	11236.2913	11236.2950	-3.7
4 1 3	3 1 2	6	5	1 1	12039.1731	12039.1757	-2.6
				0 0	12043.0105	12043.0107	-0.2
		5	4	1 1	12039.3685	12039.3730	-4.5
				0 0	12043.2078	12043.2087	-0.9
		3	2	1 1	12040.8097	12040.8200	-10.3
				0 0	12044.6486	12044.6554	-6.8
		4	3	1 1	12041.0199	12041.0207	-0.8
				0 0	12044.8554	12044.8567	-1.3
5 1 5	4 1 4	5	4	1 1	13366.3256	13366.3237	1.9
		4	3	1 1	13366.4322	13366.4348	-2.6
		6	5	1 1	13366.6907	13366.6912	-0.5
				0 0	13368.3358	13368.3409	-5.1
		7	6	1 1	13366.8027	13366.8055	-2.8
				0 0	13368.4544	13368.4550	-0.6
5 0 5	4 0 4	6	5	1 1	13911.4043	13911.4022	2.1
				0 0	13913.6678	13913.6666	1.2
		5	4	1 1	13912.0817	13912.0808	0.9
		7	6	1 1	13913.1604	13913.1606	-0.2
				0 0	13915.4253	13915.4265	-1.2
		4	3	1 1	13913.8310	13913.8286	2.4
5 1 4	4 1 3	6	5	1 1	15009.0694	15009.0653	4.1
				0 0	15013.7230	15013.7174	5.6
		7	6	1 1	15009.3261	15009.3265	-0.4
				0 0	15013.9784	15013.9788	-0.4
		5	4	1 1	15010.1703	15010.1677	2.6
		4	3	1 1	15010.4300	15010.4264	3.6
6 1 6	5 1 5	8	7	1 1	15997.8796	15997.8702	9.4
				0 0	15999.7284	15999.7212	7.2
6 0 6	5 0 5	8	7	1 1	16526.2601	16526.2541	6.0
				0 0	16528.4990	16528.4943	4.7
6 1 5	5 1 4	8	7	1 1	17948.9840	17948.9645	19.5

9.6 References.-

[1] S. Blanco, A. Lesarri, J. C. López, J. L. Alonso, A. Guarnieri, *J. Mol. Spect.*, 174, 397, **1995**.

[2] S. Blanco, A. Lesarri, J. C. López, J. L.Alonso, A. Guarnieri, *J. Mol. Spect.*, 175, 267, **1996**.

[3] R.N. Nandi, A. Chatterji, *Spectrochim. Acta A*, A31, 603, **1975**.

[4] L. F. Elmuti, R. A. Peebles, S. A. Peebles, A. L. Steber, J. L. Neil, B. H. Pate, *Phys. Chem. Chem. Phys.*, 13, 14043, **2011**.

[5] G. Feng, L. Evangelisti, L. B. Favero, J.-U. Grabow, Z. Xia. *Phys. Chem. Chem. Phys.*, 13, 14092, **2011**.

[6] T. Liu, M. B. Huang, *Mol. Phys.*, 105, 2279, **2007**.

[7] P. Ottaviani, W. Caminati, J.-U. Grabow, *J. Chem. Phys.*, 125, **2006**.

[8] O. S. Binbrek, B. H. Torrie, I. P. Swaison, *Acta Crystallogr. C*, 58, o672-o674, **2002**.

[9] S. A. Schlueler, A. Anderson, *J. Raman Spectrosc.*, 25, 429, **1994**.

[10] E. K. Plyler, M. A. Lamb, *J. Res. Nat. Bur. Stand*, 45, 204, **1950**.

[11] A. Baldacci, P. Stoppa, S. Giorgianni, R. Visioni, A. Baldan, *J. Mol. Spect.*, 183, 388, **1997**.

[12] A. Perrin, J.M. Flaud, H. Burger, G. Pewelke, S. Sander, H. Willner, *J. Mol. Spect.*, 209, 122-132, **2001**.

[13] L. Wachowski, P. Kirszensztejn, Z. Foltynowicz, *Pol. J. Environ. Stud.*, 10, 415, **2001**.

[14] A. J. Miller, S. M. Hollandsworth, L. E. Flynn et al, *J. Geophys. Res. - atmos*, 101, 9017, **1996**.

[15] Z. Kisiel, E. Bialkowska, L. Pszczo´łkowski, A. Milet, C. Struniewicz, R. Moszynski, J. Sadlej, *J. Chem. Phys.*, 112, 5767, **2000**.

[16] Z. Kisiel, B. A. Pietrewicz, O. Desyatnyk, L. Pszczo´łkowski, I. Struniewicz, J. Sadlej, *J. Chem. Phys.*, 119, 5907, **2003**.

[17] Trifluoroacetona con formaldehido.

[18] L. B. Favero, L. Evangelisti, A. Maris, A. Vega-Toribio, A. Lesarri, W. Caminati, *J. Phys. Chem. A*, 115, 9493, **2011**.

[19] W. Caminati, S. Melandri, M. Schnell, D. Banser, J-U. Grabow, J. L. Alonso, *J. Mol. Struct.*, 742, 87, **2005**.

[20] L. Evangelisti, G. Feng, P. Écija, E. J. cocinero, F. Castaño, W. Caminati. *Angew. Chem. Int.*, 50, 7807, **2011**.

[21] M. Goswami, E. Arunan, *Phys. Chem. Chem. Phys.*, 13, 14153, **2011**.

[22] L. Evangelisti, W. Caminati. *Phys. Chem. Chem. Phys.*, 12, 14433, **2010**.

[23] W. Caminati, J. C. López, S. Blanco, S. Mata, J. L. Alonso. *Phys. Chem. Chem. Phys.*, 12, 10230, **2010**.

[24] W. Caminati, S. Melandri, P. Moreschini, P. G. Favero. *Angew. Chem. Int.* 38, No.19, **1998**.

[25] Macromodel, version 9.2, Schrödinger, LLc, New York, NY, **2012**.

[26] M. J. Frisch et al., Gaussian, Inc., Wallingford CT, **2009**.

[27] W. Gordy and L. R. Cook, "Microwave Molecular Spectra", 3rd Edition, in Weissberger, A. (Ed.), Techniques of Chemistry, vol. XVIII, John Wiley & Sons Inc., New York, **1984**.

[28] H. M. Pickett, *J. Mol. Spectrosc.*, 148, 37, **1991**.

[29] http://physics.nist.gov/jb95 Retrieved: 2014/01/31

[30] J.-U. Grabow, W. Stahl, H. Dreizler. *Rev. Sci.Instrum*, 67, num. 12, 4072, **1996**.

[31] E. J. Cocinero, Tesis Doctoral, Universidad de Valladolid, **2005**.

[32] E.R. Cohen, T. Cvitas, J.G. Frey, B. Holmström, K. Kuchitsu, R. Marquardt, I. Mills, F. Pavese, M. Quack, J. Stohner, H.L. Strauss, M. Takami, and A.J. Thor, "Quantities, Units and Symbols in Physical Chemistry", IUPAC Green Book, Third Edition, Second Printing, IUPAC & RSC Publishing, Cambridge, **2008**.

[33] http://goldbook.iupac.org/PDF/goldbook.pdf, retrieved 2014-01-30.

[34] J. Kraitchman, *Am. J. Phys.*, 21, 17, **1953**.

[35] A. Maris, L. B. Favero, B. Velino, W. Caminati, *J. Phys. Chem. A*, Publication Date (Web): October 18, 2013, DOI: 10.1021/jp409173v.

Other Studies

Journal of Molecular Spectroscopy 297 (2014) 32–34

Contents lists available at ScienceDirect

Journal of Molecular Spectroscopy

journal homepage: www.elsevier.com/locate/jms

The shape of trifluoromethoxybenzene

Lu Kang [a], Stewart E. Novick [b], Qian Gou [c], Lorenzo Spada [c], Montserrat Vallejo-López [c,1], Walther Caminati [c,*]

[a] Department of Biology, Chemistry and Physics, Southern Polytechnic State University, Marietta, GA 30060, USA
[b] Department of Chemistry, Wesleyan University, Middletown, CT 6549, USA
[c] Dipartimento di Chimica "G. Ciamician" dell'Università, Via Selmi 2, I-40126 Bologna, Italy

ARTICLE INFO

Article history:
Received 23 December 2013
In revised form 17 January 2014
Available online 30 January 2014

Keywords:
Trifluoroanisole
Molecular conformation
Molecular structure
Rotational spectra

ABSTRACT

The rotational spectra of trifluoroanisole (trifluoromethoxybenzene, $C_6H_5OCF_3$) and of its ^{13}C and ^{18}O isotopologues in natural abundance have been measured in a supersonic expansion with pulsed-jet Fourier transform microwave spectroscopy. The spectrum is consistent with a perpendicular conformation of the CF_3 group with respect to the phenyl ring.

1. Introduction

Several molecules in which a phenyl ring is attached to a short chain have been investigated by rotational spectroscopy. It has been found that even very short chemical chains consisting of two (C, O, N or S) atoms, present an interesting variety of conformational features. These two atoms chains generate, indeed, quite different configurations. The prototype compound of the series, ethyl benzene, has a perpendicular shape [1], while in anisole the side chain is in the plane of the aromatic ring [2]. The same is true for thioanisole [3], but benzyl amine has a perpendicular shape. In this case, the orientation of the amino group generates two different conformers [4]. Finally, benzyl alcohol adopts a *gauche* shape that exists in 4 degenerate energy minima, involving severe Coriolis interactions which made assignment of the rotational spectrum quite challenging [5].

In the case of anisole, the rotational spectrum of its 1:1 complex with water has also been investigated, and an interesting result was reported: the conformational change upon $H_2O \rightarrow D_2O$ substitution [6]. For this reason we considered it interesting to investigate how the fluorination of the CH_3 group would change the features of the complex with water, that is, to study the rotational spectrum of the adduct trifluoroanisole -water. Since the paper on the MW spectrum of trifluoroanisole (from now on TFA) available in the literature [7], did not report an experimental value of the rotational constant *A*, the first step towards the investigation of TFA-H_2O was to precisely assign the rotational spectrum of TFA. The results are reported below.

2. Experimental methods

A commercial sample of TFA ($\geqslant$99.5%, Aldrich) was used without further purification. The spectra of the mono-substituted ^{13}C or ^{18}O isotopologues were measured in natural abundance.

The rotational spectra have been measured with pulsed jet Fourier-transform microwave (FT-MW) spectrometers [8], in a coaxially oriented beam-resonator arrangement-(COBRA)-type [9] at the Wesleyan and Bologna Universities, with the experimental setups described below:

(1) Wesleyan University: Gas tanks were prepared with 0.1–0.3% TFA in argon. The TFA with the argon carrier gas were expanded through a 0.5 mm diameter pulsed jet nozzle with a total backing pressure of ~1 atm (0.1 MPa). The supersonically cooled TFA then flowed through a hole in one mirror of the cavity of a Fourier transform microwave (FTMW) spectrometer, operating between 3.7 and 26.5 GHz. This spectrometer has been described elsewhere [10]. Many modifications of the spectrometer have been made since the initial publication, including automatic scanning for ease of use, coaxial expansion of the gas along the cavity axis for increased sensitivity and resolution, changes in the microwave circuit to minimize microwave noise, and the use of

* Corresponding author. Fax: +39 051 2099456.
E-mail address: walther.caminati@unibo.it (W. Caminati).
1 Permanent address: Departamento de Química Física y Química Inorgánica, Universidad de Valladolid, E-47011 Valladolid, Spain.

http://dx.doi.org/10.1016/j.jms.2014.01.011

multiple microwave pulses for each gas pulse to speed data collection. Scans of TFA were performed with 1 k data points in the time domain; however, selected transitions were also measured at 4 k data points for enhanced resolution.

(2) Bologna University: The rotational spectrum in the 6–18 GHz frequency region was measured using the spectrometer described elsewhere [11], and recently updated with the FTMW++ set of programs [12]. Helium, as carrier gas, was passed over the TFA at room temperature, at a backing pressure of about 0.2 MPa, and expanded through the pulsed valve (General valve, series 9, nozzle diameter 0.5 mm) into the Fabry–Perot cavity to about 1×10^{-3} Pa. The spectral line position was determined after Fourier transformation of the 8 k data point time domain signal, recorded at intervals of 100 ns. Each rotational transition is split by Doppler effect as a result of the coaxial arrangement of the supersonic jet and resonator axes in the COBRA-FTMW spectrometer. The rest frequency is calculated as the arithmetic mean of the Doppler components. The estimated accuracy of frequency measurements is better than 3 kHz and lines separated by more than 7 kHz are resolvable.

3. Computational calculations

Ab initio computations at the MP2/6-311++G(d,p) level were carried out, using the Gaussian03 program package [13], to explore the structural landscape of TFA. We found two stationary points, one with the CF_3 group perpendicular to and other with the CF_3 group in the plane of the aromatic ring. The second one was 345 cm^{-1} higher in energy, and according to the frequency calculations it is not a minimum (we found one negative frequency). The obtained shape of the stable form is shown in Fig. 1, where the atom numbering used through the text and the principal axes system are also indicated. The calculated rotational constants and dipole moment components are given at the bottom of the Figure. A very strong μ_a-type spectrum is expected.

4. Rotational spectra

Following the *B* and *C* values from Ref. [7] and the prediction from the model calculation, a scan has been first performed to search for the μ_a-*R*-type $J = 6 \leftarrow 5$ band, where the most intense transitions were expected. It was easy to assign some very strong lines, corresponding to $K_a = 0$ and 1. Later on, transitions with *J* up to 20 and K_a up to 8 and some much weaker μ_c-type transitions have been measured. No μ_b-type transitions were observed.

All measured transitions could be fit, with Watson's semirigid Hamiltonian (*S*-reduction; I^r-representation) [14], obtaining the rotational constants reported in the first row of Table 1. The centrifugal distortion constants have been fitted to $D_J = 44.22(7)$, $D_{JK} = 816(1)$, $D_K = -560(20)$, $d_1 = -2.67(5)$, $d_2 = 4.35(3)$ Hz, respectively.

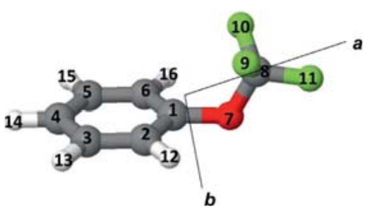

A, *B*, *C*/MHz	2703, 704, 633
μ_a, μ_b, μ_c/D	-2.6, 0.0, -0.2

Fig. 1. *Ab initio* molecular sketch of TFA with the principal axes system, atom numbering, rotational constants and dipole moment components.

Table 1
Experimental spectroscopic parameters of all measured isotopologues of TFA.

	A/MHz	*B*/MHz	*C*/MHz	σ^c/kHz	N^d
Parent[a]	2722.2146(3)[b]	702.94305(5)	632.39743(5)	1.2	270
^{13}C1	2719.08(2)	702.4407(1)	632.1685(1)	1.8	97
^{13}C2 (or ^{13}C6)	2699.67(2)	701.4093(1)	630.0584(1)	1.7	121
^{13}C3 (or ^{13}C5)	2701.13(2)	696.5417(1)	626.0986(1)	3.5	112
^{13}C4	2720.96(2)	692.7716(1)	624.2234(1)	7.0	118
^{13}C8	2722.36(2)	700.1550(1)	630.1396(1)	2.4	128
^{18}O	2697.82(2)	700.2992(1)	631.5824(1)	3.6	79

[a] For the parent species, quartic centrifugal distortion constants have been determined: $D_J = 44.22(7)$, $D_{JK} = 816(1)$, $D_K = -560(20)$, $d_1 = -2.67(5)$, $d_2 = 4.35(3)$ Hz, respectively. These parameters have been fixed to the parent species values in the fittings of all other isotopologues.
[b] Standard error in parentheses in units of the last digit.
[c] Standard deviation of the fit.
[d] Number of fitted transitions.

After empirical corrections of the rotational constants, it has been possible to assign the spectra of all the ^{13}C and ^{18}O isotopologues in natural abundance with the same procedure. In the portion of the spectrum presented in Fig. 2, one can see the transition 6_{06}–5_{05} for the parent and all mono-^{13}C species. Few transitions have been measured for each isotopic species, and for this reason the centrifugal distortion constants have been fixed, in the fits, to the values of the parent species. The determined spectroscopic parameters of all isotopologues are also listed in Table 1.

From the rotational constants it has been easy to calculate the planar moments of inertia, P_{gg}, $g = a, b, c$. The values of P_{bb} ($=\sum_i m_i b_i^2$) were the same, within 132.919 and 132.925 uÅ^2, for the normal, ^{13}C1, ^{13}C4, ^{13}C8 and ^{18}O isotopologues, showing that the four substituted atoms all lie in the *ac* plane, which is then a plane of symmetry of the molecule. As a consequence, the CF_3 group is perpendicular to the aromatic ring. This is in agreement with the failure to observe the μ_b-type transitions.

5. Molecular structure

We used the rotational constants of the seven isotopic species to determine the substitution coordinates of the heavy atoms frame (apart from the F atoms) with Kraitchman's equations [15]. The obtained values are given in Table 2 and there compared to the *ab initio* values. From these coordinates it has been possible

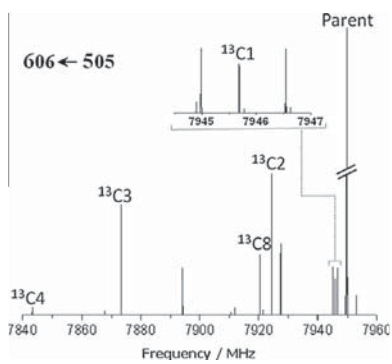

Fig. 2. Survey scan of the J $6 \leftarrow 5$ μ_a-*R*-type band. The 6_{06}–5_{05} transitions of the parent and of the various isotopologues are labeled.

Table 2
Substitution coordinates (r_s) of the carbon and oxygen atoms in the principal axes system of parent TFA (C2 is equivalent to C6 and C3 is equivalent to C5).

	a/Å		b/Å		c/Å	
	r_s	r_e	r_s	r_e	r_s	r_e
C1	±0.544(3)[a]	−0.577	0.0[b]	0.0	±0.468(4)	0.471
C2	±1.222(2)	−1.232	±1.216(2)	1.223	±0.283(7)	0.292
C3	±2.569(1)	−2.573	±1.209(1)	1.210	±0.09(2)	−0.107
C4	±3.239(1)	−3.240	0.0[b]	0.0	±0.301(6)	0.302
O7	±0.723(2)	0.753	0.0[b]	0.0	±0.921(2)	0.932
C8	±1.696(1)	1.698	0.0[b]	0.0	0.0[c]	−0.033

[a] Errors in parenthesis are expressed in units of the last digit.
[b] Fixed to zero by symmetry.
[c] Imaginary value, fixed to zero.

Table 3
The theoretical (r_e, MP2/6-311++G(d,p)) and the heavy atoms r_s geometries of TFA are compared to each other.

	r_e	r_s
Bond lengths/Å		
C1–C2	1.394	1.404(3)[a]
C2–C3	1.399	1.398(6)
C3–C4	1.400	1.399(3)
C1–O7	1.407	1.346(4)
O7–C8	1.351	1.340(2)
C8–F11	1.327	
C8–F9	1.343	
C2–H12	1.085	
C3–H13	1.086	
C4–H14	1.086	
Valence angles/°		
C2C1C6	122.2	119.9(3)
C1C2C3	118.6	119.7(2)
C2C3C4	120.3	120.4(2)
C2C1O7	118.8	119.9(2)
O7C1C6	118.8	119.9(2)
C1O7C8	115.2	116.9(2)
F9C8O7	112.6	
F11C8O7	107.7	
H12C2C1	119.7	
H13C3C2	119.5	
Dihedral angles/°		
C4C3–C2C1	0.9	
C5C4–C3C2	−0.3	
C6C5–C4C3	0.3	
O7C1–C6C2	177.1	174.9(7)
C8O7–C1C6	93.0	92.5(4)
F9C8–O7C1	60.5	
H12C2–C1C3	−179.5	
H13C3–C2C1	−179.8	
H14C4–C3C2	179.8	

[a] Errors in parenthesis are expressed in units of the last digit.

to calculate the r_s geometry of the mainframe of the molecule, constituted by the C and O atoms. This structure is reported in Table 3, and compared to the *ab initio* (r_e) geometry of the molecule.

6. Conclusions

The rotational spectrum of TFA shows that the fluorination of the methyl group of anisole causes a dramatic change of the molecular conformation, from a planar to a perpendicular shape of the heavy atoms mainframe. This conformational change appears, at a first sight, unexpected, because two electronegative fluorine atoms are oriented towards the aromatic π system cloud. However, in such an arrangement, two weak C–H···F hydrogen bond linkages are formed between the CF_3 group fluorine atoms and two adjacent phenyl hydrogens. The H···F distances are 2.84 Å, typical of weak hydrogen bonds [16].

Acknowledgments

We acknowledge Italian MIUR (PRIN project 2010ERFKXL_001) and the University of Bologna (RFO) for financial support. Q.G. also thanks the China Scholarships Council (CSC) for financial support. M.V.L. gratefully acknowledges a FPI grant from the MICINN.

Appendix A. Supplementary material

Supplementary data for this article are available on ScienceDirect (www.sciencedirect.com) and as part of the Ohio State University Molecular Spectroscopy Archives (http://library.osu.edu/sites/msa/jmsa_hp.htm). Supplementary data associated with this article can be found, in the online version, at http://dx.doi.org/10.1016/j.jms.2014.01.011.

References

[1] W. Caminati, D. Damiani, G. Corbelli, B. Velino, C.W. Bock, Mol. Phys. 74 (1991) 885–895.
[2] B. Velino, S. Melandri, W. Caminati, P.G. Favero, Gazz. Chim. Ital. 125 (1995) 373–376.
[3] M. Onda, A. Toda, S. Mori, I. Yamaguchi, J. Mol. Struct. 144 (1986) 47–51.
[4] S. Melandri, A. Maris, P.G. Favero, W. Caminati, ChemPhysChem 2 (2001) 172–177.
[5] K.A. Utzat, R.K. Bohn, J.A. Montgomery Jr., H.H. Michels, W. Caminati, J. Phys. Chem. A 114 (2010) 6913.
[6] B.M. Giuliano, W. Caminati, Angew. Chem. Int. Ed. 44 (2005) 603–605.
[7] D. Federdel, A. Herrmann, D. Christen, S. Sander, H. Willner, H. Oberhammer, J. Mol. Struct. 567 (568) (2001) 127–136.
[8] T.J. Balle, W.H. Flygare, Rev. Sci. Instrum. 52 (1981) 33.
[9] J.-U. Grabow, W. Stahl, H. Dreizler, Rev. Sci. Instrum. 67 (1996) 4072.
[10] A.R. Hight Walker, W. Chen, S.E. Novick, B.D. Bean, M.D. Marshall, J. Chem. Phys. 102 (1995) 7298.
[11] W. Caminati, A. Millemaggi, J.L. Alonso, A. Lesarri, J.C. López, S. Mata, Chem. Phys. Lett. 392 (2004) 1.
[12] J.-U. Grabow, Habilitationsschrift, Universität Hannover, Hannover 2004; <http://www.pci.uni-hannover.de/~lgpca/spectroscopy/ftmw>.
[13] M.J. Frisch et al., Gaussian 03, Revision B.01, Gaussian Inc, Pittsburgh PA, 2003.
[14] J.K.G. Watson, in: J.R. Durig (Ed.), Vibrational Spectra and Structure, vol. 6, Elsevier, New York, 1977, p. 1.
[15] J. Kraitchman, Am. J. Phys. 21 (1953) 17.
[16] G. Feng, L. Evangelisti, I. Cacelli, L. Carbonaro, G. Prampolini, W. Caminati, Chem. Commun. 50 (2014) 171. and refs therein.

THE JOURNAL OF PHYSICAL CHEMISTRY A

Article

pubs.acs.org/JPCA

Fluorination Effects on the Shapes of Complexes of Water with Ethers: A Rotational Study of Trifluoroanisole−Water

Qian Gou,[†] Lorenzo Spada,[†] Montserrat Vallejo-López,[†] Lu Kang,[‡] Stewart E. Novick,[§] and Walther Caminati*,[†]

[†]Dipartimento di Chimica, "G. Ciamician" dell'Università, Via Selmi 2, I-40126 Bologna, Italy

[‡]Department of Biology, Chemistry and Physics, Southern Polytechnic State University, Marietta, Georgia 30060, United States

[§]Department of Chemistry, Wesleyan University, Middletown, Connecticut 6549, United States

Supporting Information

ABSTRACT: The rotational spectra of five isotopologues of the 1:1 complex trifluoroanisole−water have been investigated with pulsed jet Fourier transform microwave spectroscopy. The triple fluorination of the methyl group greatly affects the features of the rotational spectrum of the complex with water, with respect to those of the related complex anisole−water. The shape, the internal dynamics, and the isotopic effects turned out to be quite different from those of the anisole−water adduct (Giuliano, B. M.; Caminati, W. *Angew. Chem., Int. Ed.* **2005**, *44*, 603−606). However, as in anisole−water, water has the double role as a proton donor and proton acceptor, and it is linked to trifluoroanisole through two, O−H···O and C−H···O hydrogen bonds.

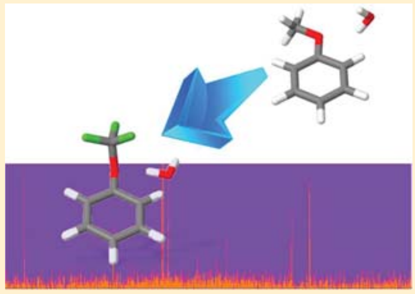

INTRODUCTION

Water adducts of organic molecules have been widely studied to help in understanding the solvation processes in aqueous environments and the effects of the molecular interactions on gas-phase reactions.[1−4] The typology of the complexes of water with organic molecules has been described and classified in a recent paper.[5] Generally speaking, with ethers,[6−9] aliphatic amines,[10] diazines,[11−13] and alcohols,[5,14] water acts as a proton donor to form relatively strong (15−25 kJ mol^{-1}) hydrogen bonds such as O−H···O, O−H···N, or N−H···O interactions. When forming an adduct with phenols[15] and with an N-heteroaromatic ring molecule,[16,17] water takes the role of a proton acceptor. In the water adducts of amides[18] and amino acids,[19] a ring structure with two hydrogen bonds is formed with water as both a proton donor and a proton acceptor.

With hydrogen-containing freons, water forms weak (4−6 kJ mol^{-1}) OH···X (X = F and Cl) hydrogen bonds.[20−22] When the Cl and F atoms coexist in a freon molecule, the OH···Cl linkage[21] or the OH···F bond[22] is preferred depending on the different cases. However, when an aliphatic freon molecule is perhalogenated and no hydrogen atom is present in the molecule, then a halogen bond (6−10 kJ mol^{-1}) rather than a hydrogen bond is formed.[23,24] One can notice that the halogenation will greatly change the way that the organic molecule interacts with water. In its adduct with isoflurane, a highly fluorinated anesthetic ether, water acts as a proton acceptor, and it is linked to the anesthetic molecule through a C−H···O hydrogen bond.[25] The configurations observed in adducts of water with molecules containing a π-electron system, such as ethylene−water[26] and benzene−water,[27] have been found to be stabilized by OH···π interactions. Finally, an oxygen lone pair−π interaction is the linking interaction found in the complex chlorotrifluoroethylene−water.[28]

α,α,α-Trifluoroanisole (trifluoromethoxybenzene, $C_6H_5OCF_3$, TFA from now on) is a halogenated ether with an electronic π system. Water can interact with this molecule in several ways. It has been found that in the isolated molecule, the substitution of the three methyl hydrogens with fluorine atoms changes the position of the side chain from the in-plane configuration of anisole[29] to a perpendicular shape.[30,31] In the 1:1 complex anisole−water, water acts mainly as a proton donor, but the deuteration of water produces a conformational change, as shown in Figure 1. The value of the θ angle decreases from 138 to 128°, while the secondary interaction O···H_{Me} is replaced by the O···H_{Ph} one.[32]

It is interesting to investigate how the fluorination of the CH_3 group of anisole will change these features of the complex with water. The different shape of TFA (perpendicular) with respect to anisole (coplanar) can change the accessibility of the ether oxygen lone pairs, and the presence of electronegative fluorine atoms can represent a competitive electron-rich site. Thus, we studied the rotational spectrum of the adduct TFA−water with the pulsed jet Fourier transform microwave technique. The results are presented below.

Received: December 27, 2013
Revised: January 22, 2014
Published: January 23, 2014

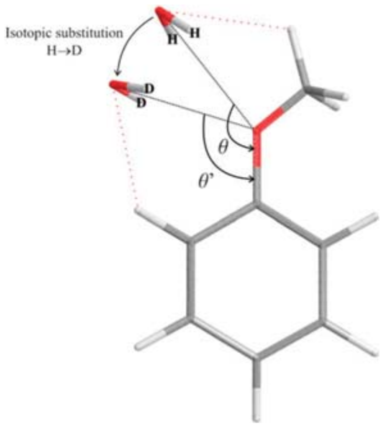

Figure 1. The deuteration of water produces a conformational change in the anisole–water complex.[5,32]

■ EXPERIMENTAL SECTION

Molecular clusters were generated in a supersonic expansion, under conditions optimized for the molecular adduct formation. Details of the Fourier transform microwave spectrometer[33] (COBRA-type[34]), which covers the range of 6.5–18 GHz, have been described previously.[35]

Helium at a stagnation pressure of ~0.3 MPa was passed over a 1:1 mixture of TFA (commercial sample) and water (at 0 °C) and expanded through a solenoid valve (General Valve, Series 9, nozzle diameter 0.5 mm) into the Fabry–Pérot cavity. The spectral line positions were determined after Fourier transformation of the time domain signal with 8k data points, recorded with 100 ns sample intervals. Each rotational transition appears as doublets due to the Doppler Effect. The line position was calculated as the arithmetic mean of the frequencies of the Doppler components. The estimated accuracy of the frequency measurements was better than 3 kHz. Lines separated by more than 7 kHz were resolvable.

■ THEORETICAL CALCULATION

We preliminarily explored the conformational space of the complex by molecular mechanics using conformational search algorithms implemented in MacroModel 9.2 within the MMFFs force field.[36] We found 100 different geometries within an energy window of 13 kJ mol^{-1}, which, at the MP2/6-311++G(d,p) level,[37] converged to six plausible conformers. Further vibrational frequency calculations at the same level proved the four conformers, shown in Table 1, to be real minima and provide additional centrifugal distortion constants. All of these conformers are characterized by hydrogen bonds, with water acting as a proton donor (conformers II and III) or having the double role of proton donor and proton acceptor (conformers I and IV).

In order to have a better estimation of the energy differences, all intermolecular binding energy values were counterpoise corrected for the basis set superposition error (BSSE).[38] This resulted in conformer I, with O–H···O and C–H···O hydrogen bonds, being the global minimum. The dissociation energies have been estimated, inclusive of BSSE corrections. All of the theoretical parameters are reported in Table 1.

Table 1. MP2/6-311++G(d,p) Calculated Energies and Spectroscopic Parameters of the Plausible Conformers of TFA–Water

	I	II
	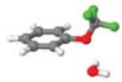	
A,B,C/MHz	1309,662,505	1502,620,571
μ_a,μ_b,μ_c/D	1.1,-0.6,-0.3	-2.1,-2.4,-0.6
D_J,D_{JK},D_K/kHz	0.035,0.62,0.53	0.053,0.64, 0.10
d_1,d_2/Hz	-2.65,-6.17	1.87,3.90
$\Delta E,\Delta(E+\text{ZPE}),\Delta E_{\text{BSSE}}$/kJ·mol^{-1}	0.0,^{a} 0.5,0.0^b	0.5,0.0,^{c} 3.4
$E_D{}^d$/kJ·mol^{-1}	12.2	8.8
	III	IV
		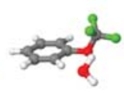
A,B,C/MHz	1224,627,531	1239,673,482
μ_a,μ_b,μ_c/D	2.8,-2.9,0.0	0.6,0.3,-0.3
D_J,D_{JK},D_K/kHz	0.049,1.70,-1.08	0.053,0.18,1.40
d_1,d_2/Hz	-2.37,10.07	-10.33,0.78
$\Delta E,\Delta(E+\text{ZPE}),\Delta E_{\text{BSSE}}$/kJ·mol^{-1}	2.0,0.1,3.7	2.7,2.3,2.1
E_D/kJ·mol^{-1}	8.5	10.1

^{a}Absolute energy: −719.396479 E_h. ^{b}Absolute energy: −719.3754723 E_h. ^{c}Absolute energy: −719.267205 E_h. ^{d}Calculated dissociation energy with BSSE correction.

■ ROTATIONAL SPECTRA

We started our search with frequency scans for μ_a-type R-branch transitions belonging to conformer I, which, according to the theoretical calculations, is the most stable species. We could first identify the $J = 8 \leftarrow 7$, $K_{-1} = 0$ and 1 transitions. Then, the assignment was extended to many R-type transitions with J_{upper} from 7 to 11 and with K_{-1} up to 5. Later on, some much weaker μ_b and μ_c transitions could be measured. Each transition appeared as a doublet, with a relative intensity ratio of the two component lines about 1:3, as shown in Figure 2 for the $8_{18} \leftarrow 7_{17}$ transition. This ratio corresponds to the statistical weight expected for the internal rotation of water around its C_{2v} axis, which implies the exchange of a pair of equivalent hydrogen atoms (fermions with $I = 1/2$). We could assign the weaker line of the two components to the ground state (0^+).

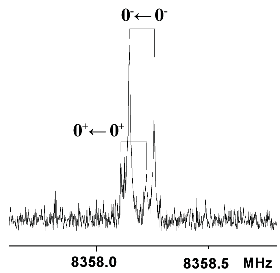

Figure 2. 0^+ and 0^- component lines of the $8_{18} \leftarrow 7_{17}$ transition of TFA–H_2O. Each component is further split by an instrumental Doppler effect.

Table 2. Spectroscopic Parameters of the 0^+ and 0^- Substates of the Parent Species and Its $H_2{}^{18}O$ Isotopologue of the Observed Conformer of TFA−Water

	TFA−H_2O		TFA−$H_2{}^{18}O$	
	0^+	0^-	0^+	0^-
A/MHz	1291.6717(6)[a]	1292.6534(6)	1233.72(1)	1233.70(1)
B/MHz	656.3183(2)	656.3193(2)	652.709(4)	652.713(4)
C/MHz	500.8509(2)	500.8532(2)	490.0453(2)	490.0479(2)
D_J/kHz	0.0385(7)		[0.0385][b]	
D_{JK}/kHz	0.901(8)		[0.901]	
D_K/kHz	0.64(2)		[0.64]	
d_1/Hz	−5.0(3)		[−5.0]	
d_2/Hz	−8.2(2)		[−8.2]	
σ^c/kHz	2.5		2.7	
N^d	96		18	

[a]Errors in parentheses are in units of the last digit. [b]Fixed at the values of the parent species. [c]RMS error of the fit. [d]Number of lines in the fit.

The splitting is quite smaller than that of anisole−water, implying a higher barrier to internal rotation.

Using Pickett's SPFIT program,[39] the 96 rotational transition frequencies were fitted by the following Hamiltonian

$$H = H_R(0^+) + H_R(0^-) + H_{CD} \quad (1)$$

$H_R(0^+)$ and $H_R(0^-)$ represent the rigid rotational parts of the Hamiltonian for the 0^+ and 0^- states, respectively. The centrifugal distortion contributions are represented by H_{CD}. Watson S-reduction and I^r-representation have been adopted.[40] The transition frequencies of the two tunneling components did not show any appreciable interaction between the two states; thus, it was not possible to determine parameters such as ΔE (the energy difference between the two states) or Coriolis's coupling terms. The fitted rotational and centrifugal distortion constants are reported in the first two columns of Table 2. The centrifugal distortion constants have been forced to have common values for both substates. The differences between the rotational constants of the 0^+ and 0^- states can, in principle, allow the estimation of the barrier to internal rotation of water, as in the cases, for example, of phenol−water[15] or chlorofluoromethane−water.[21] A knowledge of the associated structural relaxations is required for this purpose because it strongly affects the reduced mass of the motion. However, in the case TFA−H_2O, we could not determine these structural relaxations because we did not succeed in finding, by ab initio calculations, the pathway of the motion.

After an empirical adjustment to the molecular structure, the spectra of four additional isotopologues, the ones with $H_2{}^{18}O$, HOD, DOH, and DOD, were assigned. The transitions of the $H_2{}^{18}O$, whose spectroscopic parameters are listed in the last columns of Table 2, display the same splittings as those observed for the parent species. For the three deuterated species, the water internal rotation splittings have not been observed presumably due to the heavier reduced mass of the required motion.[5] The rotational constants of the three deuterated isotopologues of TFA−water are listed in Table 3. The centrifugal distortion constants have been fixed at the values of the parent (all protonated) species.

All of the measured transition frequencies are available in the Supporting Information.

These rotational constants match only the calculated values of species I (Table 1), making the conformational assignment straightforward. The discrepancies are, indeed, less than 1%, which is quite satisfactory when taking into account that the calculated and the experimental values refer to the equilibrium and to the ground-state geometries, respectively. Also, the quartic centrifugal distortion parameters are in good agreement with the theoretical values. No lines belonging to the other conformer could be identified. This could be due to the conformational relaxation to the most stable conformer upon supersonic expansion. It has, indeed, been shown that this kind of relaxation takes place easily when the interconversion barrier is smaller than $2kT$,[41] where T is the temperature before supersonic expansion; $2kT$ is about 380 cm^{-1} at 0 °C, the pre-expansion temperature in our case.

Table 3. Spectroscopic Parameters of the Three Deuterated Isotopologues of TFA−water[a]

	TFA−HOD	TFA−DOH	TFA−DOD
A/MHz	1252.33(1)[b]	1274.47(1)	1236.158(1)
B/MHz	652.523(3)	653.994(3)	650.161(4)
C/MHz	493.0183(2)	498.1981(2)	490.4597(2)
σ^c/kHz	3.7	2.6	4.0
N^d	9	9	9

[a]The quartic centrifugal distortion parameters have been fixed at the values of the parent species. [b]Errors in parentheses are in units of the last digit. [c]RMS error of the fit. [d]Number of lines in the fit.

■ STRUCTURAL INFORMATION

An O_w−H···O_{eth} hydrogen bond and a weaker C−H···O_w interaction hold the two units together in the observed conformer of the complex, as shown in Figure 3.

Due to the internal rotation of water and, plausibly, to the Ubbelohde effect (the shortening of the hydrogen bond length upon H → D substitution),[42] the position of the water hydrogens is undetermined, and a tentative determination of their substitution coordinates[43] gave meaningless (imaginary) values. However, reliable values of the r_s substitution coordinates of the O_w atom have been obtained, as shown in Table 4, where the values from the partial r_0 structure are also given for comparison.

The partial r_0 structure was obtained by adjusting three structural parameters (R_{H12O17}, ∠C2H12···O17, and ∠O17···C2−H12C1) while keeping the remaining parameters fixed to their ab initio values in order to reproduce the experimental rotational constants of TFA−H_2O and TFA−$H_2{}^{18}O$. The fitted and derived hydrogen bond parameters are reported in Table 5 and are compared to the ab initio values. The full ab initio geometry (considered, for its vibrationless nature, as an

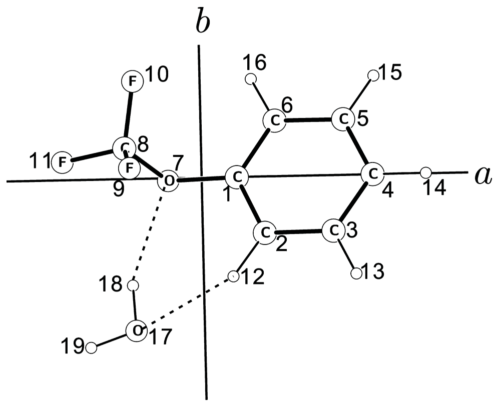

Figure 3. Sketch of the observed conformer of TFA–water with atom numbering.

Table 4. r_s Coordinates of the Water Oxygen Atom in TFA–Water

	a/Å	b/Å	c/Å
exptl.	±1.397(1)[b]	±3.0439(5)	±0.325(5)
calc.[a]	1.371	3.058	−0.500

[a]Calculated with the r_0 structure in Table 5. [b]Errors in parentheses are in units of the last digit.

Table 5. r_0 and r_e Hydrogen Bond Parameters of TFA–Water

	Fitted Parameters		
	R_{H12O17}/Å	∠C2H12···O17/°	∠O17···C2–H12C1/°
r_0	2.574(5)[a]	130.8(5)	−36.6(3)
r_e	2.447	132.0	−36.4
	Derived Parameters		
	R_{O7H18}/Å	∠O7···H18O17/°	
r_0	2.294(5)	140.5(5)	
r_e	2.170	143.1	

[a]Uncertainties (in parentheses) are expressed in units of the last digit.

equilibrium structure) is available in the Supporting Information.

■ CONCLUSIONS

Using Fourier transform microwave spectroscopy, we assigned the rotational spectra of five isotopologues of TFA–water. Water has the double role of proton donor and proton acceptor. The observed conformer is characterized, indeed, by an O_w–H···O_{eth} interaction, while a weaker C–H···O_w hydrogen bond also plausibly contributes to the stability of the complex. The fluorination of the CH_3 group not only changes the shape of the molecule but also modifies the kinds of interactions with water in the complex. In the complex anisole–water, water acts as proton donor and forms a strong hydrogen bridge (bifurcated) with the ether oxygen atom. Such an arrangement is no longer possible in TFA–water because the lone pairs of the water oxygen atom should overlap the π electron orbitals of the aromatic ring.

■ ASSOCIATED CONTENT

Supporting Information

Complete ref 37, MP2/6-311++G(d,p) geometry of the observed conformer, and tables of transition frequencies. This material is available free of charge via the Internet at http://pubs.acs.org.

■ AUTHOR INFORMATION

Corresponding Author

*E-mail: walther.caminati@unibo.it.

Notes

The authors declare no competing financial interest.

■ ACKNOWLEDGMENTS

We thank the Italian MIUR (PRIN Project 2010ERFKXL_001) and the University of Bologna (RFO) for financial support. Q.G. also thanks the China Scholarships Council (CSC) for financial support. M.V.L. gratefully acknowledges a FPI grant from the MICINN.

■ REFERENCES

(1) Vçhringer-Martinez, E.; Hansmann, B.; Hernandez-Soto, H.; Francisco, J. S.; Troe, J.; Abel, B. Water Catalysis of a Radical-Molecule Gas-Phase Reaction. *Science* **2007**, *315*, 497–501.

(2) Chabinyc, M. L.; Craig, S. L.; Regan, C. K.; Brauman, J. L. Gas-Phase Ionic Reations: Dynamics and Mechanism of Nucleophilic Displacements. *Science* **1998**, *279*, 1882–1886.

(3) Tait, M. J.; Franks, F. Water in Biological Systems. *Nature* **1971**, *230*, 91–94.

(4) Garrett, B. C. Ions at the Air/Water Interface. *Science* **2004**, *303*, 1146–1147.

(5) Evangelisti, L.; Caminati, W. Internal Dynamics in Complex of Water with Organic Molecules. Details of the Internal Motions in *tert*-Butylalcohol–Water. *Phys. Chem. Chem. Phys.* **2010**, *12*, 14433–14441.

(6) Caminati, W.; Dell'Erba, A.; Melandri, S.; Favero, P. G. Conformation and Stability of Ether–Water Adducts: Free Jet Absorption Millimeter Wave Spectrum of 1,4-Dioxane–Water. *J. Am. Chem. Soc.* **1998**, *120*, 5555–5558.

(7) Spoerel, U.; Stahl, W.; Caminati, W.; Favero, P. G. Jet-Cooled Rotational Spectra and Ab Initio Investigations of the Tetrahydropyran–Water System. *Chem.—Eur. J.* **1998**, *4*, 1974–1981.

(8) Caminati, W.; Moreschini, P.; Rossi, I.; Favero, P. G. The O···H–O Hydrogen Bond in the Gas Phase. Microwave Structure of Ethylene Oxide–Water. *J. Am. Chem. Soc.* **1998**, *120*, 11144–11148.

(9) Su, Z.; Wen, Q.; Xu, Y. Conformational Stability of the Propylene Oxide–Water Adduct: Direct Spectroscopic Detection of O···H–O Hydrogen Bonded Conformers. *J. Am. Chem. Soc.* **2006**, *128*, 6755–6760.

(10) Caminati, W.; Dell'Erba, A.; Maccaferri, G.; Favero, P. G. Conformation and Stability of Adducts of Cyclic Ammines with Water: Free Jet Absorption Millimeter-Wave Spectrum of Pyrrolidine–Water. *J. Am. Chem. Soc.* **1998**, *120*, 2616–2621.

(11) Caminati, W.; Favero, L. B.; Favero, P. G.; Maris, A.; Melandri, S. Intermolecular Hydrogen Bonding between Water and Pyrazine. *Angew. Chem., Int. Ed.* **1998**, *37*, 792–795.

(12) Caminati, W.; Moreschini, P.; Favero, P. G. The Hydrogen Bond between Water and Aromatic Bases of Biological Interest: Rotational Spectrum of Pyridazine–Water. *J. Phys. Chem. A* **1998**, *102*, 8097–8100.

(13) Melandri, S.; Sanz, M. E.; Caminati, W.; Favero, P. G.; Kisiel, Z. The Hydrogen Bond between Water and Aromatic Bases of Biological Interest: An Experimental and Theoretical Study of the 1:1 Complex of Pyrimidine with Water. *J. Am. Chem. Soc.* **1998**, *120*, 11504–11509.

(14) Conrad, A. R.; Teumelsan, N. H.; Wang, P. E.; Tubergen, M. J. A Spectroscopic and Computational Investigation of the Conforma-

tional Structural Changes Induced by Hydrogen Bonding Networks in the Glycidol−Water Complex. *J. Phys. Chem. A* **2010**, *114*, 336−342.

(15) Melandri, S.; Maris, A.; Favero, P. G.; Caminati, W. Free Jet Absorption Millimetre-Wave Spectrum and Model Calculations of Phenol−Water. *Chem. Phys.* **2002**, *283*, 185−192.

(16) Tubergen, M. J.; Andrews, A. M.; Kuczkowski, R. L. Microwave Spectrum and Structure of a Hydrogen-Bonded Pyrrole−Water Complex. *J. Phys. Chem.* **1993**, *97*, 7451−7457.

(17) Blanco, S.; López, J. C.; Alonso, J. L.; Ottaviani, P.; Caminati, W. Pure Rotational Spectrum and Model Calculations of Indole−Water. *J. Chem. Phys.* **2003**, *119*, 880−886.

(18) Blanco, S.; López, J. C.; Lesarri, A.; Alonso, J. L. Microsolvation of Formamide: A Rotational Study. *J. Am. Chem. Soc.* **2006**, *128*, 12111−12121.

(19) Alonso, J. L.; Cocinero, E. J.; Lesarri, A.; Sanz, M. E.; López, J. C. The Glycine−Water Complex. *Angew. Chem., Int. Ed.* **2006**, *45*, 3471−3474.

(20) Caminati, W.; Melandri, S.; Rossi, I.; Favero, P. G. The C−F···H−O Hydrogen Bond in the Gas Phase. Rotational Spectrum and Ab Initio Calculations of Difluoromethane−Water. *J. Am. Chem. Soc.* **1999**, *121*, 10098−10101.

(21) Caminati, W.; Melandri, S.; Maris, A.; Ottaviani, P. Relative Strengths of the O−H···Cl and O−H···F Hydrogen Bonds. *Angew. Chem., Int. Ed.* **2006**, *45*, 2438−2442.

(22) Feng, G.; Evangelisti, L.; Favero, L. B.; Grabow, J.-U.; Xia, Z.; Caminati, W. On the Weak O−H···Halogen Hydrogen Bond: A Rotational Study of $CH_3CHClF\cdots H_2O$. *Phys. Chem. Chem. Phys.* **2011**, *13*, 14092−14096.

(23) Caminati, W.; Maris, A.; Dell'Erba, A.; Favero, P. G. Dynamical Behavior and Dipole−Dipole Interactions of Tetrafluoromethane−Water. *Angew. Chem., Int. Ed.* **2006**, *118*, 6863−6866.

(24) Evangelisti, L.; Feng, G.; Écija, P.; Cocinero, E. J.; Castaño, F.; Caminati, W. The Halogen Bond and Internal Dynamics in the Molecular Complex of CF_3Cl and H_2O. *Angew. Chem., Int. Ed.* **2011**, *50*, 7807−7810.

(25) Gou, Q.; Feng, G.; Evangelisti, L.; Vallejo-López, M.; Spada, L.; Lesarri, A.; Cocinero, E. J.; Caminati, W. How Water Interacts with Halogenated Anesthetics: The Rotational Spectrum of Isoflurane−Water. *Chem.—Eur. J.* **2014**, DOI: 10.1002/chem.201303724 .

(26) Andrews, A. M.; Kuczkowski, R. L. Microwave Spectra of C_2H_4−H_2O and Isotopomers. *J. Chem. Phys.* **1993**, *98*, 791−795.

(27) Gutowsky, H. S.; Emilsson, T.; Arunan, E. Low *J* Rotational Spectra, Internal Rotation, and Structures of Several Benzene−Water Dimers. *J. Chem. Phys.* **1993**, *99*, 4883−4893.

(28) Gou, Q.; Feng, G.; Evangelisti, L.; Caminati, W. Lone-Pair···π Interaction: A Rotational Study of the Chlorotrifluoroethylene−Water Adduct. *Angew. Chem., Int. Ed* **2013**, *52*, 11888−11891.

(29) Onda, M.; Toda, A.; Mori, S.; Yamaguchi, I. Microwave Spectrum of Anisole. *J. Mol. Struct.* **1986**, *144*, 47−51.

(30) Federdel, D.; Herrmann, A.; Christen, D.; Sander, S.; Willner, H.; Oberhammer, H. Structure and Conformation of α,α,α-Trifluoroanisol, $C_5H_5OCF_3$. *J. Mol. Struct.* **2001**, *567−568*, 127−136.

(31) Kang, L.; Novick, S. E.; Gou, Q.; Spada, L.; Vallejo López, M.; Caminati, W. The Shape of Trifluoromethoxybenzene. *J. Mol. Spectrosc.* **2014**, in press, DOI: 10.1016/j.jms.2014.01.011.

(32) Giuliano, B. M.; Caminati, W. Isotopomeric Conformational Change in Anisole−Water. *Angew. Chem., Int. Ed.* **2005**, *44*, 603−606.

(33) Balle, T. J.; Flygare, W. H. Fabry−Perot Cavity Pulsed Fourier Transform Microwave Spectrometer with a Pulsed Nozzle Particle Source. *Rev. Sci. Instrum.* **1981**, *52*, 33−45.

(34) Grabow, J.-U.; Stahl, W.; Dreizler, H. A Multioctave Coaxially Oriented Beam-Resonator Arrangment Fourier-Transform Microwave Spectrometer. *Rev. Sci. Instrum.* **1996**, *67*, 4072−4084.

(35) Caminati, W.; Millemaggi, A.; Alonso, J. L.; Lesarri, A.; López, J. C.; Mata, S. Molecular Beam Fourier Transform Microwave Spectrum of the Dimethylether−Xenon Complex: Tunnelling Splitting and ^{131}Xe Quadrupole Coupling Constants. *Chem. Phys. Lett.* **2004**, *392*, 1−6.

(36) *MASTRO*, version 9.2; Schrödinger, LLC: New York, 2012.

(37) Frisch, M. J.; Trucks, G. W.; Schlegel, H. B.; Scuseria, G. E.; Robb, M. A.; Cheeseman, J. R.; Scalmani, G.; Barone, V.; Mennucci, B.; Petersson, G. A.; et al. *GAUSSIAN09*; Gaussian, Inc.: Wallingford, CT, 2009.

(38) Boys, S. F.; Bernardi, F. The Calculations of Small Molecular Interactions by the Differences of Separate Total Energies. Some Procedures with Reduced Errors. *Mol. Phys.* **1970**, *19*, 553−566.

(39) Pickett, M. H. The Fitting and Prediction of Vibration−Rotation Spectra with Spin Interactions. *J. Mol. Spectrosc.* **1991**, *148*, 371−377.

(40) Watson, J. K. G. In *Vibrational Spectra and Structure*; Durig, J. R., Ed.; Elsevier: New York/Amsterdam, The Netherlands, 1977; Vol. *6*, pp 1−89.

(41) See for example: Ruoff, R. S.; Klots, T. D.; Emilsson, T.; Gutowski, H. S. Relaxation of Conformers and Isomers in Seeded Supersonic Jets of Inert Gases. *J. Chem. Phys.* **1990**, *93*, 3142−3150.

(42) Ubbelohde, A. R.; Gallagher, K. J. Acid−Base Effects in Hydrogen Bonds in Crystals. *Acta Crystallogr.* **1955**, *8*, 71−83.

(43) Kraitchman, J. Determination of Molecular Structure from Microwave Spectroscopic Data. *Am. J. Phys.* **1953**, *21*, 17−25.

ChemPubSoc Europe

DOI: 10.1002/chem.201303724

CHEMISTRY A European Journal Full Paper

Rotational Spectroscopy

How Water Interacts with Halogenated Anesthetics: The Rotational Spectrum of Isoflurane–Water

Qian Gou,[a] Gang Feng,[a] Luca Evangelisti,[a] Montserrat Vallejo-López,[a, b] Lorenzo Spada,[a] Alberto Lesarri,[b] Emilio J. Cocinero,[c] and Walther Caminati*[a]

Abstract: The rotational spectra of several isotopologues of the 1:1 complex between the inhaled anesthetic isoflurane and water have been recorded and analyzed by using Fourier transform microwave spectroscopy. The rotational spectrum showed a single rotamer, corresponding to the configuration in which the most stable conformer of isolated isoflurane is linked to the water molecule through an almost linear C–H···O weak hydrogen bond. All transitions display a hyperfine structure due to the ^{35}Cl (or ^{37}Cl) nuclear quadrupole effects.

Introduction

The molecular mechanism describing the interactions of anesthetics with biological substrates has been the object of several investigations. Most evidences suggest that anesthesia may affect the organization of fat molecules, or lipids, in the outer membrane of a cell, potentially altering the ability to send signals along nerve cell membranes.[1] The full-scale experimental descriptions of anesthetic mechanisms are usually ascertained by using large-scale molecular modeling.[2]

The inhaled anesthetic isoflurane (1-chloro-2,2,2-trifluoroethyl difluoromethyl ether, $C_3H_2ClF_5O$, abbreviated to ISO hereafter), contains several different sites for stereospecific interaction, which might imply the interaction through weak hydrogen- or halogen bonding with neuronal ion channels and on the protein binding in the central nervous system.[1b] The intrinsic structural properties of bare ISO have been revealed in the isolation conditions of a supersonic expansion by using Fourier transform microwave (FTMW) spectroscopy,[3] and two conformers (*trans* and *gauche*) distinguished by the orientation of the difluoromethane group have been identified. These spectroscopic data allow the study on the intermolecular complex or hydration aggregates involving ISO.

[a] Q. Gou, Dr. G. Feng, Dr. L. Evangelisti, M. Vallejo-López, L. Spada, Prof. Dr. W. Caminati
Department of Chemistry
University of Bologna, Via Selmi 2, 40126, Bologna (Italy)
Fax: (+39) 0512099456
E-mail: walther.caminati@unibo.it

[b] M. Vallejo-López, Prof. Dr. A. Lesarri
Departamento de Química Física y Química Inorgánica
Universidad de Valladolid, 47011 Valladolid (Spain)

[c] Dr. E. J. Cocinero
Departamento de Química Física, Facultad de Ciencia y Tecnología
Universidad del País Vasco, (UPV-EHU)
Apartado 644, 48940 Bilbao (Spain)

Supporting information for this article is available on the WWW under http://dx.doi.org/10.1002/chem.201303724.

Understanding the solvation processes in the aqueous environments and its potential decisive influence on gas-phase reaction is of considerable importance.[4] In recent years, jet-cooled high resolution spectroscopy has been successfully applied to study a number of water–organic molecular adducts, providing detailed and precise information about the structures and dynamics of these non-covalent interaction systems.[5] Plenty of rotationally resolved investigations have shown the specificity and directionality of the weak interactions in molecular complexes involving water and organic molecules.

When forming the complex with water, ISO has several active sites that could bind with the solvent molecule through different interactions: 1) the ether oxygen could act as a proton acceptor, binding with water through O–H···O hydrogen bond; 2) thanks to the electron-withdrawing effect of the halogen atoms, the aliphatic hydrogen atoms could act as proton donors linking water with C–H···O weak hydrogen bonds; 3) halogen bonds could be formed between the halogen atoms and the negative site of water oxygen, resulting from the "σ-hole".[6] To investigate the kind of interaction that dominates the hydration aggregates of ISO, herein we conduct the investigation of 1:1 complex of ISO–H_2O with FTMW spectroscopy.

Results and Discussion

Theoretical calculations

We preliminarily explored the conformational space of the complex by Molecular Mechanics, using conformational search algorithms implemented in MacroModel 9.2 within the MMFFs force-field.[7] We found 88 different geometries within an energy window of 800 cm^{-1} which, at the MP2/6-311++G(d, p) level[8] converged to five plausible conformers. Further vibrational frequency calculations at the same level proved four conformers, shown in Table 1, to be real minima. These calcula-

Table 1. MP2/6-311++G(d,p) spectroscopic parameters of the plausible conformers of ISO–H_2O.

	T1	T2	G1	G2
ΔE [cm^{-1}]	40	235	791	0[a]
ΔE_{BSSE} [cm^{-1}]	99	0[b]	789	11
A [MHz]	1055	1014	1116	1058
B [MHz]	670	625	617	638
C [MHz]	626	584	566	553
$\lvert\mu_a\rvert, \lvert\mu_b\rvert, \lvert\mu_c\rvert$ [D]	3.4, 0.2, 0.8	0.4, 1.1, 0.8	0.7, 1.7, 0.7	2.0, 4.3, 1.9
D_J [kHz]	0.12	0.17	0.09	0.05
D_{JK} [kHz]	0.14	0.06	−0.16	0.20
D_K [kHz]	0.07	0.04	0.27	0.02
d_1 [kHz]	−0.04	−0.04	0.03	−0.02
d_2 [kHz]	−0.01	−0.04	−0.01	−0.01
χ_{aa} [MHz]	32.5	31.8	33.9	32.1
χ_{bb}–χ_{cc} [MHz]	−86.0	−20.8	−75.2	−15.2
χ_{ab} [MHz]	18.9	16.6	−0.1	11.2
χ_{ac} [MHz]	−7.3	−12.4	−0.3	−7.8
χ_{bc} [MHz]	29.2	52.0	−38.6	51.6

[a] $E/E_h = -1224.604444$. [b] $E/E_h = -1224.600173$.

tions provided, besides the relative energies, the rotational, ^{35}Cl nuclear quadrupole coupling and first-order centrifugal distortion constants. Also, the components of the electric dipole moments have been estimated. Two structural families, corresponding to the *trans* and *gauche* forms of the monomer (T and G, respectively, with $E_G - E_T = 159\ cm^{-1}$),[3] can be distinguished by the orientation of the $-CHF_2$ group with respect to the ether group of ISO. In each family, there are two different ways to link the two subunits together, labeled as "1" (C–H···O weak hydrogen bond, in which water acts as a proton acceptor) and "2" (O–H···O hydrogen bond, in which water acts as a proton donor). The calculations indicate that in the global minimum (G2) the configuration adopted by the ISO is apparently the less stable one (G) in the isolated monomer.[3] However, when basis set superposition errors (BSSE)[9] are taken into account, the *trans* form T2 turns out to be the global minimum. Nevertheless, the theoretical values are very close, predicting that three structures (T2, G2, and T1) are almost isoenergetic, these differences are within the error of the theoretical method (Table 1).

Rotational spectra

The rotational spectra of ISO–H_2O were predicted from the theoretical values of the rotational and quadrupole coupling constants of the four forms of the complex. After scanning wide frequency ranges, the spectrum of only one rotamer was detected and assigned in the supersonic expansion. Thirteen transitions (K_a from 0 to 6) of the μ_a-R branch with $J = 7 \leftarrow 6$ were assigned in the first stage. Three more μ_a-R bands with J_{upper} from 6 to 9 were then measured. Finally, we could measure six weaker μ_c-R transitions. No μ_b-type lines were observed possibly because of the quite small dipole moment component. Each transition is split into several component lines due to the quadrupole effect of the ^{35}Cl (or ^{37}Cl) nuclei, as shown, for example, in Figure 1 for the $7_{07} \leftarrow 6_{06}$ transition of the ^{35}Cl isotopologue.

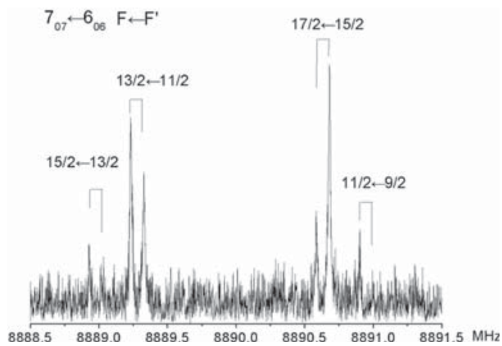

Figure 1. Recorded $7_{07} \leftarrow 6_{06}$ rotational transition of the observed conformer of ISO–H_2O showing the ^{35}Cl hyperfine structure. Each component line exhibits the Doppler doubling.

The frequencies were fitted to the Watson's "S" reduced semirigid-rotor Hamiltonian[10] within the I^r representation, given here in a simple form:

$$H = H_R + H_{CD} + H_Q \tag{1}$$

in which H_R represents the rigid-rotor Hamiltonian, the centrifugal distortion contributions are represented by H_{CD}, whereas H_Q is the operator associated with the interaction of the ^{35}Cl (or ^{37}Cl) nuclear electric quadrupole moment with the electric-field gradient at the Cl nucleus.[11] The spectroscopic constants were derived by direct diagonalization using Pickett's SPFIT program,[12]

Following the same procedure, the μ_a-type spectrum of the ^{37}Cl isotopomer has been measured and assigned in natural abundance. The determined parameters of both isotopologues are listed in Table 2.

Subsequently, the rotational spectra of three additional heavy water isotopologues (ISO-$H_2{}^{18}O$, ISO–DOH, ISO–D_2O) were successfully assigned. The rotational assignment of ISO–$H_2{}^{18}O$ was straightforward, and its spectroscopic constants are reported in the third column of Table 2. The rotational spectra of the deuterated species displayed some unexpected features, which raised some interpretation problems. On one hand, the rotational transitions of ISO–D_2O are split, apart from the quadrupole hyperfine structure, into doublets with component lines separated by about 1 MHz (see Figure 2), indicating a finite V_2 barrier hindering the internal rotation of the D_2O moiety in the complex. On the other hand, a single rotational spectrum of the ISO–DOH species could be assigned, suggesting the two water hydrogen atoms to be equivalent to each other; an ex-

Table 2. Spectroscopic parameters of the three isotopologues of ISO–H_2O.

	ISO(^{35}Cl)–H_2O	ISO(^{37}Cl)–H_2O	ISO–$H_2{}^{18}O$
A [MHz]	1034.7187(4)[a]	1018.05(2)	1007.4568(6)
B [MHz]	668.9313(3)	667.506(1)	654.782(2)
C [MHz]	624.0039(3)	618.1093(6)	618.1754(7)
D_J [kHz]	0.785(1)	0.8320(5)	0.95(1)
D_K [kHz]	0.608(6)	[0.608]	[0.608]
d_1 [kHz]	−0.310(1)	−0.335(4)	−0.46(1)
d_2 [kHz]	−0.0121(5)	[−0.0121][b]	−0.16(1)
χ_{aa} [MHz]	33.00(2)	25.60(7)	33.01(2)
χ_{bb}–χ_{cc} [MHz]	−77.92(8)	−66.24(8)	−57.32(8)
N[c]	139	36	43
σ [kHz][d]	3.3	3.7	4.1

[a] Uncertainties (in parentheses) are expressed in units of the last digit. [b] Fixed to the value obtained for normal species. [c] Number of transitions in the fit. [d] Standard deviation of the fit.

Table 3. Spectroscopic parameters of the isotopologues with deuterated water.[a]

	ISO(^{35}Cl)–D_2O		ISO(^{35}Cl)–HDO
	$m=0$	$m=1$	
A [MHz]	999.55(2)[b]	999.28(2)	1022.25(2)
B [MHz]	655.740(1)	655.870(2)	665.106(1)
C [MHz]	610.4737(6)	610.3869(7)	615.3569(5)
D_J [kHz]	0.698(5)	0.705(7)	0.637(6)
d_1 [kHz]	−0.268(4)	−0.266(6)	−0.242(4)
χ_{aa} [MHz]	32.1(2)		32.0(2)
χ_{bb}–χ_{cc} [MHz]	−48.4(8)		−65.36(8)
N[c]	62		37
σ [kHz][d]	6.4		5.8

[a] The D_K and d_2 centrifugal distortion parameters have been fixed to the values of the parent species. [b] Uncertainties (in parentheses) are expressed in units of the last digit. [c] Number of transitions in the fit. [d] Standard deviation of the fit.

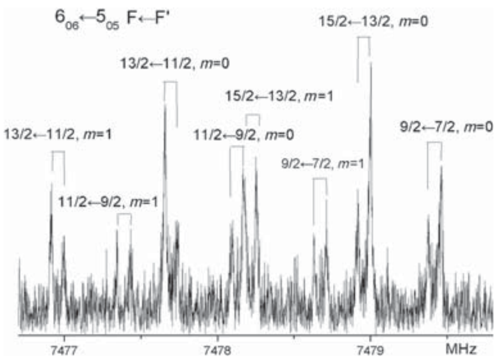

Figure 2. The internal rotation of water is apparent in the doubling of all hyperfine components of the $6_{06}\leftarrow 5_{05}$ rotational transition of ISO–D_2O. Each component is further split by an instrumental Doppler effect.

perimental evidence compatible with a near free or low V_2 barrier. Although it appears difficult to estimate relative populations from intensity measurements, it seems, from intensity measurements of some nearby transitions, that the monodeuterated species is almost as twice intense than the bideuterated and the normal species in appropriate H/D abundance ratio conditions. Probably the mass effects related to the considerable heavier top when we have D_2O rather than H_2O in the complex, makes the internal rotation effects observable in the first case, even within a low V_2 barrier. Similar effects have been observed previously in some complexes of water with organic molecules.[13]

The noticeable low values of the quadrupole coupling parameter χ_{bb}–χ_{cc} for the ISO–$H_2{}^{18}O$ and ISO–D_2O species with respect to that of the normal species are interpretable in terms of a considerable rotation of the principal inertial axes system upon isotopic substitution.

The transitions frequencies of the two torsional states of the bideuterated species have been fitted with a common set of quadrupole coupling constants. The spectroscopic parameters are shown in Table 3 for the two deuterated water isotopologues.

All measured transitions of the five isotopologues are given as Supporting Information.

Conformational assignment

Concerning the conformational assignment, the comparison of Tables 1 and 2 shows that the experimental rotational and quadrupole coupling constants match the theoretical values only for conformer T1. In addition, μ_b type spectra could not be observed, confirming the assignment to T1. This result is apparently in contrast with the theoretical conformational energies. However, the presence of T2 in the jet cannot be excluded totally due to its low μ_a dipole moment component, which is about 1/10 of the μ_a value of T1, the observed conformer. Since the spectrum is relatively weak, we cannot exclude the T2 conformer to be as much abundant as T1. Also for conformer G2 we could not observe any line, in spite of its high μ_a value. In this case, we can state that its abundance should not exceed 1/10 of that of T1.

Structural information

In the observed conformer, T1, water is linked to ISO through a C–H···O weak hydrogen bond (see Figure 3), and plausibly undergoes a near free internal rotation around its C_2 axis.

Within this hypothesis, the position of the water hydrogens is undetermined, and a tentative determination of the their substitution coordinates[14] gave meaningless (imaginary) values. However, reliable values of the r_s substitution coordinates of the Cl and O_{H_2O} atoms have been obtained, as shown in Table 4. The r_s values are in good accord with the values calculated with an effective partial r_0 structure, in which the hydrogen bond parameters have been fitted to the values $r_{O13H12}=2.153(3)$ Å and $\sphericalangle O13H12C2=180.0(4)^\circ$, respectively. Their ab initio values are (see the complete ab initio geometry in the Supporting Information): $r_{O13H12}=2.084$ Å and $\sphericalangle O13H12C2=175.9^\circ$, respectively.

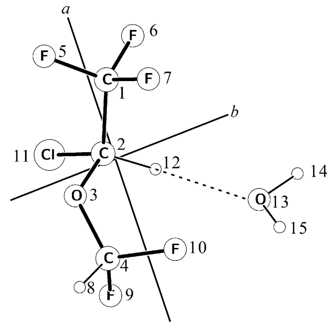

Figure 3. Sketch of the observed conformer of ISO–H_2O with atom numbering

Table 4. The r_s coordinates of substituted atoms of ISO–H_2O compared with calculated values

	a [Å]		b [Å]		c [Å]	
	Exptl	Calcd[a]	Exptl	Calcd	Exptl	Calcd
Cl	$\pm 0.573(3)$[b]	-0.601	$\pm 1.874(1)$	-1.874	$\pm 0.739(2)$	-0.728
O_{H_2O}	$\pm 1.611(1)$	1.535	$\pm 0.960(2)$	1.320	$\pm 2.419(1)$	-2.312

[a] Deduced from the partial r_0 structure (see the main text). [b] Uncertainties (in parentheses) are expressed in units of the last digit.

Conclusion

The rotational spectra of ISO–H_2O were studied with FTMW technique. The fitted rotational and quadrupole coupling constants matched the theoretical values straightforwardly to conformer T1, suggesting that ISO retains its preferred monomer structure in the adduct. However, the predicted O–H···O interaction through the ether oxygen, expected to be the global minimum has not been observed. The water subunit is thus linked to ISO, as a proton acceptor, through a linear C–H···O weak hydrogen bond. This behavior is quite different with respect to the adducts of H_2O with other ethers.[5a–e] It seems that the insertion of halogen atoms in an organic molecule favorites the formation of C–H···O interactions (with water acting as a proton acceptor), which is, indeed, the case of ISO–H_2O. Besides the normal species, four more isotopologues of the complex were also observed and assigned, consistent with this interpretation. The observed splitting in the bideuterated species and the indistinguishability of the two monodeuterated species, though apparently puzzling, could indicate an almost free internal rotation of water. Thus only the position of the water oxygen is determinable.

Experimental Section

Molecular clusters were generated in a supersonic expansion, under conditions optimized for the formation of the adduct. Details of the Fourier transform microwave spectrometer[15] (COBRA-type[16]), which covers the range 6.5–18 GHz, have been described previously.[17] A gas mixture of about 1% of isoflurane (commercial sample used without any further purification) in He at a stagnation pressure of $\approx$0.25 MPa was passed over a sample of H_2O (or $H_2{}^{18}O$, or D_2O) and expanded through a solenoid valve (General Valve, Series 9, nozzle diameter 0.5 mm) into the Fabry-Pérot cavity. The spectral line positions were determined after Fourier transformation of the time-domain signal with 8k data points, recorded with 100 ns sample intervals. Each rotational transition appears as doublets due to Doppler Effect. The line position is calculated as the arithmetic mean of the frequencies of the Doppler components. The estimated accuracy of the frequency measurements is better than 3 kHz. Lines separated by more than 7 kHz are resolvable.

Acknowledgements

We acknowledge Italian MIUR (PRIN project 2010ERFKXL_001) and the University of Bologna (RFO) for financial support. G.F. and Q.G. also thank the China Scholarships Council (CSC) for financial support. Financial support from the Spanish Ministry of Science and Innovation (CTQ2011-22923 and CTQ2012-39132), the Basque Government (Consolidated Groups, IT520-10) and UPV/EHU (UFI11/23) is gratefully acknowledged. M.V.L. gratefully acknowledges a FPI grant from the MICINN. E.J.C. acknowledges also a "Ramón y Cajal" contract from the MICINN. Computational resources and laser facilities of the UPV-EHU were used in this work (SGIker and I2Basque).

Keywords: conformation analysis · hydrogen bonds · rotational spectroscopy · rotamers · water

[1] a) N. P. Franks, W. R. Lieb, *Nature* **1994**, *367*, 607–614; b) A. S. Evers, C. M. Crowder, J. R. Balser, in *Foodman & Gilman's The Pharmacological Basis of Therapeutics*, 11th ed. (Eds.: L. L. Brunton, J. S. Lazo, K. L. Parker), McGraw-Hill, New York, **2006**, chap. 13.
[2] a) A. A. Bhattacharya, S. Curry, N. P. Franks, *J. Biol. Chem.* **2000**, *275*, 38731–38738; b) E. J. Bertaccini, J. R. Trudell, N. P. Franks, *Anesth. Analg.* **2007**, *104*, 318–324.
[3] A. Lesarri, A. Vega-Toribio, R. D. Suenram, D. J. Brugh, D. Nori-Shargh, J. E. Boggs, J.-U. Grabow, *Phys. Chem. Chem. Phys.* **2011**, *13*, 6610–6618.
[4] a) E. Vohringer-Martinez, B. Hansmann, H. Hernandez-Soto, J. S. Francisco, J. Troe, B. Abel, *Science* **2007**, *315*, 497–501; b) M. L. Chabinyc, S. L. Craig, C. K. Regan, J. L. Brauman, *Science* **1998**, *279*, 1882–1886; c) B. C. Garrett, *Science* **2004**, *303*, 1146–1147; d) M. J. Tait, F. Franks, *Nature* **1971**, *230*, 91–94.
[5] a) W. Caminati, A. Dell'Erba, S. Melandri, P. G. Favero, *J. Am. Chem. Soc.* **1998**, *120*, 5555–5558; b) W. Caminati, P. Moreschini, I. Rossi, P. G. Favero, *J. Am. Chem. Soc.* **1998**, *120*, 11144–11148; c) B. M. Giuliano, W. Caminati, *Angew. Chem.* **2005**, *117*, 609–612; *Angew. Chem. Int. Ed.* **2005**, *44*, 603–605; d) Z. Su, Q. Wen, Y. Xu, *J. Am. Chem. Soc.* **2006**, *128*, 6755–6760; e) Z. Su, Y. Xu, *Angew. Chem.* **2007**, *119*, 6275–6278; *Angew. Chem. Int. Ed.* **2007**, *46*, 6163–6166; f) L. Evangelisti, G. Feng, P. Écija, E. J. Cocinero, F. Castaño, W. Caminati, *Angew. Chem.* **2011**, *123*, 7953–7956; *Angew. Chem. Int. Ed.* **2011**, *50*, 7807–7810; g) W. Caminati, A. Maris, A. Dell'Erba, P. G. Favero, *Angew. Chem.* **2006**, *118*, 6863–6866; *Angew. Chem. Int. Ed.* **2006**, *45*, 6711–6714.
[6] a) A. C. Legon, *Phys. Chem. Chem. Phys.* **2010**, *12*, 7736–7747; b) T. Clark, M. Henneman, J. S. Murray, P. Politzer, *J. Mol. Model.* **2007**, *13*, 305–311.
[7] MASTRO, version 9.2, Schrödinger, LLC, New York, NY, **2012**.
[8] Gaussian 09, Revision B.01, M. J. Frisch, G. W. Trucks, H. B. Schlegel, G. E. Scuseria, M. A. Robb, J. R. Cheeseman, G. Scalmani, V. Barone, B. Mennucci, G. A. Petersson, H. Nakatsuji, M. Caricato, X. Li, H. P. Hratchian, A. F. Izmaylov, J. Bloino, G. Zheng, J. L. Sonnenberg, M. Hada, M. Ehara, K. Toyota, R. Fukuda, J. Hasegawa, M. Ishida, T. Nakajima, Y. Honda, O. Kitao, H. Nakai, T. Vreven, J. A. Montgomery, Jr., J. E. Peralta, F. Ogliaro, M. Bearpark, J. J. Heyd, E. Brothers, K. N. Kudin, V. N. Staroverov, R. Ko-

bayashi, J. Normand, K. Raghavachari, A. Rendell, J. C. Burant, S. S. Iyengar, J. Tomasi, M. Cossi, N. Rega, J. M. Millam, M. Klene, J. E. Knox, J. B. Cross, V. Bakken, C. Adamo, J. Jaramillo, R. Gomperts, R. E. Stratmann, O. Yazyev, A. J. Austin, R. Cammi, C. Pomelli, J. W. Ochterski, R. L. Martin, K. Morokuma, V. G. Zakrzewski, G. A. Voth, P. Salvador, J. J. Dannenberg, S. Dapprich, A. D. Daniels, Ö. Farkas, J. B. Foresman, J. V. Ortiz, J. Cioslowski, D. J. Fox, Gaussian, Inc., Wallingford CT, **2009**.
[9] S. F. Boys, F. Bernardi, *Mol. Phys.* **1970**, *19*, 553 – 566.
[10] J. K. G. Watson in *Vibrational Spectra and Structure, Vol. 6* (Ed.: J. R. Durig), Elsevier, New York/Amsterdam, **1977**, pp. 1 – 89.
[11] J. K. Bragg, *Phys. Rev.* **1948**, *74*, 533 – 538.
[12] H. M. Pickett, *J. Mol. Spectrosc.* **1991**, *148*, 371 – 377.
[13] L. Evangelisti, W. Caminati, *Phys. Chem. Chem. Phys.* **2010**, *12*, 14433.
[14] J. Kraitchman, *Am. J. Phys.* **1953**, *21*, 17 – 24.
[15] T. J. Balle, W. H. Flygare, *Rev. Sci. Instrum.* **1981**, *52*, 33 – 45.
[16] a) J.-U. Grabow, W. Stahl, *Z. Naturforsch. A* **1990**, *45*, 1043 – 1044; b) J.-U. Grabow, doctoral thesis, Christian-Albrechts-Universität zu Kiel, Kiel, **1992**; c) J.-U. Grabow, W. Stahl, H. Dreizler, *Rev. Sci. Instrum.* **1996**, *67*, 4072 – 4084; d) J.-U. Grabow, Habilitationsschrift, Universitat Hannover, Hannover, **2004**, http://www.pci.uni-hannover.de/~lgpca/spectroscopy/ftmw; e) Program available at http://www.pci.uni-hannover.de/~lgpca/spectroscopy/ftmw.
[17] W. Caminati, A. Millemaggi, J. L. Alonso, A. Lesarri, J. C. Lopez, S. Mata, *Chem. Phys. Lett.* **2004**, *392*, 1 – 6.

Received: September 23, 2013
Published online on January 8, 2014

Weak Hydrogen Bonds

DOI: 10.1002/anie.201309848

Probing the C–H⋯π Weak Hydrogen Bond in Anesthetic Binding: The Sevoflurane–Benzene Cluster**

Nathan A. Seifert, Daniel P. Zaleski, Cristóbal Pérez, Justin L. Neill, Brooks H. Pate, Montserrat Vallejo-López, Alberto Lesarri,* Emilio J. Cocinero, Fernando Castaño, and Isabelle Kleiner*

Abstract: *Cooperativity between weak hydrogen bonds can be revealed in molecular clusters isolated in the gas phase. Here we examine the structure, internal dynamics, and origin of the weak intermolecular forces between sevoflurane and a benzene molecule, using multi-isotopic broadband rotational spectra. This heterodimer is held together by a primary C–H⋯π hydrogen bond, assisted by multiple weak C–H⋯F interactions. The multiple nonbonding forces hinder the internal rotation of benzene around the isopropyl C–H bond in sevoflurane, producing detectable quantum tunneling effects in the rotational spectrum.*

Weak hydrogen bonds are characterized by very low interaction energies ($<20\,\mathrm{kJ\,mol^{-1}}$), making these forces especially sensitive to modulation and cooperativity. Model molecular clusters formed by haloalkanes and small organic molecules reveal how C–H⋯O,[1] C–H⋯S,[2] C–H⋯N,[3] or C–H⋯F–C[4] interactions tend to associate to maximize the number and strength of nonbonding forces, as illustrated by the nine simultaneous C–H⋯F contacts in the cage structure of the difluoromethane trimer.[5] Much less structural information is available on the weaker (dispersion-dominated) C–H⋯π interaction, despite its significance in organic, organometallic, and biological chemistry. Reviews by Nishio[6] and Desiraju and Steiner[7] based most of their conclusions on crystallographic and ab initio studies. Alternatively, rotational spectroscopy recently analyzed several clusters involving phenyl π acceptors,[8–11] in absence of perturbing crystal or matrix effects. In particular, F_3CH⋯benzene[8] represents a prototypical C–H⋯π(Ph) interaction, with the C–H bond pointing to the center of the aromatic ring. However, the short hydrogen bonding distance $r_{(\mathrm{H\cdots Benzene})} = 2.366(2)$ Å suggests a stronger interaction than that with other π acceptors, prompting our interest in systems with a less acidic hydrogen atom, larger size, and the possibility of competing interactions.

The sevoflurane–benzene cluster is interesting from a chemical and biological point of view. Sevoflurane ($(CF_3)_2HC\text{-}O\text{-}CF_2H$) is a common volatile anesthetic and the sevoflurane–benzene cluster might model local interactions with aromatic side chains at the protein receptors.[12] Chemically, sevoflurane combines different donor and acceptor groups, including oxygen lone pairs, several C–F "organic fluorine" bonds (recognized as weak acceptors), and two kinds of activated isopropyl and fluoromethyl C–H bonds. Recently, van der Veken et al. studied the vibrational spectrum of sevoflurane–benzene, reporting the observation of two different species.[13] However, the interpretation of the experimental data was largely based in quantum chemical calculations. In comparison, our rotational study has identified 46 separate high-resolution spectra from distinct isotopologues, accurately resolving the molecular structure and the internal dynamics of the benzene ring.

The results of the conformational screening of sevoflurane–benzene can be found in Figure 1 and Table 1 (five lowest-energy conformers). The most stable conformations contain a variety of weak hydrogen-bonding effects, mostly based on C–H⋯ π interactions originating in the isopropyl and fluoromethyl groups, and in combinations of C–H⋯F and C–H⋯π weak contacts. The predicted global minimum (conformer 1) shows an intriguing topology for benzene not seen in other conformers, where the eclipsing of one hydrogen

[*] N. A. Seifert, Dr. D. P. Zaleski, Dr. C. Pérez, Dr. J. L. Neill, Prof. B. H. Pate
Department of Chemistry, University of Virginia
McCormick Road, Charlottesville, VA 22904 (USA)
E-mail: brookspate@virginia.edu
Homepage: http://faculty.virginia.edu/bpate-lab/

M. Vallejo-López, Prof. A. Lesarri
Departamento de Química Física y Química Inorgánica
Facultad de Ciencias, Universidad de Valladolid
47011 Valladolid (Spain)
E-mail: lesarri@qf.uva.es
Homepage: http://www.uva.es/lesarri

Dr. E. J. Cocinero, Prof. F. Castaño
Departamento de Química Física
Facultad de Ciencia y Tecnología
Universidad del País Vasco (UPV-EHU)
Apartado 644, 48080 Bilbao (Spain)

Prof. I. Kleiner
Laboratoire Interuniversitaire de Systèmes Atmosphériques (LISA), CNRS/IPSL UMR 7583 et
Universités Paris Est et Paris Diderot
61 Av. General De Gaulle, 94010 Créteil (France)

[**] The authors from the University of Virginia acknowledge funding support from the NSF Major Research Instrumentation program (CHE-0960074). M.V.-L., A.L., E.J.C., and F.C. thank the MICINN and MINECO (CTQ-2011-22923, CTQ-2012-39132), the Basque government (IT520-10), and the UPV/EHU (UFI11/23) for funds. M.V.-L. and E.J.C. acknowledge a PhD grant and a "Ramón y Cajal" contract, respectively. Computational resources of the UPV-EHU were used in this work.

Supporting information for this article is available on the WWW under http://dx.doi.org/10.1002/anie.201309848.

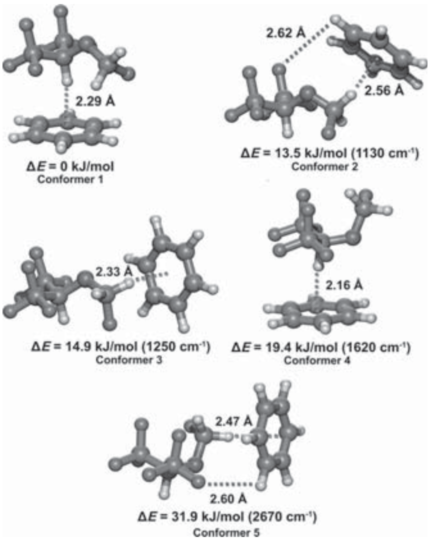

Figure 1. The predicted lowest-energy conformers of sevoflurane–benzene (MP2/6-311++g(d,p)).

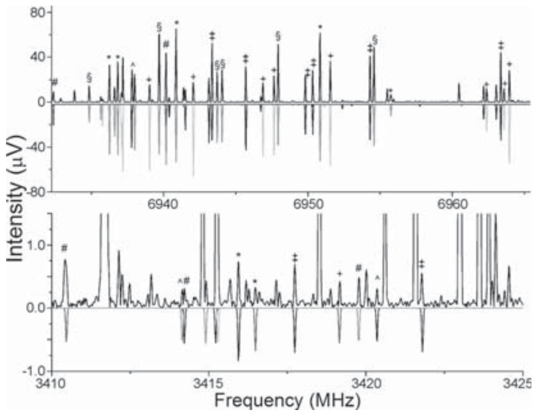

Figure 2. A section of the CP-FTMW spectrum of sevoflurane–[D$_1$]benzene (6.8 million acqusitions, positive traces). The six symbols correspond to a unique D isotopologue (negative traces for predictions). The bottom panel shows a selection of D/^{13}C double isotopologue transitions.

with the fluoromethyl group allows the other five hydrogens to be optimally staggered between the sevoflurane substituents. This arrangement makes it conceivable that some contribution arises from the two bifurcated and one single C−H···F interactions, which could enhance the attractive character of the primary C−H···π link. The simplicity of this optimally staggered C−H···π interaction is energetically favored by roughly 10.3–13.5 kJ mol^{-1}. Conformers 1 and 2 correspond to the observations of van der Veken et al., who found a population ratio of about 15:1 in favor of conformer 1 in Xe cryosolution, based on the intensities of the vibrational bands.[13]

The analysis of the rotational spectrum was possible thanks to recent advances in broadband (chirped-pulse) Fourier transform microwave (CP-FTMW) spectroscopy.[14,15] An overview of the 2–8 GHz MW spectrum is shown in Figure 2 and Figure S1 in the Supporting Information. The strongest transitions arise from the sevoflurane monomer (signal-to-noise ratio (SNR) ≈ 20000:1). The spectrum of the sevoflurane–benzene parent species was about 50 times weaker, more than sufficient to detect all independent spectra arising from each heavy-atom-monosubstituted isotopologue (^{13}C, ^{18}O) in natural abundance (0.2–1 %). Hyperfine splittings were immediately noticeable in the transitions of the complex, and eventually attributed to the internal rotation of the benzene monomer about the sevoflurane frame. The

Table 1: Predictions for rotational parameters and energetics of the lowest-energy conformers of sevoflurane–benzene in Figure 1.[a]

	Theory (MP2/M06-2X/B3LYP—6-311++G(d,p))				
	Conf. 1	Conf. 2	Conf. 3	Conf. 4	Conf. 5
A [MHz]	508/515/500	650/670/636	663/698/636	543/557/538	685/697/667
B [MHz]	376/379/319	264/263/209	256/253/211	358/355/305	273/279/228
C [MHz]	353/358/302	235/235/191	234/233/193	325/318/281	229/234/196
$\|\mu_a\|$ [D]	2.2/2.3/2.1	1.9/2.3/2.1	1.1/1.3/2.1	1.1/1.0/1.1	1.6/1.8/1.6
$\|\mu_b\|$ [D]	0.5/0.3/0.2	0.6/0.4/0.8	1.3/1.7/0.8	0.8/0.8/0.9	1.1/1.0/1.1
$\|\mu_c\|$ [D]	1.6/1.6/1.7	1.3/1.3/1.2	1.3/1.0/1.2	1.3/1.3/1.3	0.5/0.6/0.6
$\|\mu_{TOT}\|$ [D]	2.7/2.8/2.7	2.4/2.6/2.6	2.2/2.3/2.6	1.8/1.8/1.9	2.0/2.1/2.1
D_J [kHz]	0.02/0.02/0.07	0.02/0.01/0.1	0.02/0.01/0.07	0.02/0.02/0.04	0.008/0.007/0.05
D_{JK} [kHz]	0.004/0.01/0.2	0.2/0.2/−0.3	0.1/0.2/−0.03	0.08/0.1/0.3	0.1/0.1/0.04
D_K [kHz]	0.04/0.04/0.3	0.1/0.1/0.4	0.8/0.2/0.1	−0.07/−0.1/−0.2	0.2/0.1/−0.02
d_1 [Hz]	−2.8/−2.8/−14.4	1.4/−1.6/−5.6	1.0/0.7/−3.4	−2.6/−3.3/−7.0	−0.8/−0.5/−7.0
d_2 [Hz]	0.2/0.2/−0.7	0.6/−0.1/−0.2	0.3/0.2/−0.2	−0.3/−0.2/−0.3	0.0/0.1/−0.5
ΔG [kJ mol^{-1}]	0.0/0.0/0.0	8.6/4.5/−1.5	7.9/10.2/0.1	19.0/13.8/17.0	31.0/22.7/17.8
$\Delta(E+ZPE)$ [kJ mol^{-1}]	0.0/0.0/0.0	13.5/10.3/2.2	14.9/13.5/2.2	19.4/17.0/15.5	31.9/24.6/18.5
E_d [kJ mol^{-1}]	−17.8/−31.1/−20.5	−12.8/−20.9/−5.0	−11.9/−19.1/−5.3	−17.4/−26.1/−5.6	−12.4/−20.6/−4.4

[a] Rotational constants (A, B, C), electric dipole moment components (μ_α, α = a, b, c), Watson's S-reduced centrifugal distortion constants (D_J, D_{JK}, D_K, d_1, d_2), Gibbs free energies at 298 K and 1 atm (ΔG), electronic energies with zero-point corrections ($\Delta(E+ZPE)$) and dissociation energies (E_d).

Table 2: Experimental rotational constants for the parent species and the benzene ^{13}C and D isotopologues of sevoflurane–benzene (full listing in the Supporting Information).

Species	A [MHz][a]	B [MHz]	C [MHz]	Δ_J [kHz][b]	Δ_{JK} [kHz]	Δ_K [kHz]	N[c]	RMS [kHz]
parent (A)	508.42070(40)[d]	358.82931(13)	338.32685(13)	[0.03490]	[0.0550]	[−0.0630]	77	6.04
parent (B)	507.74250(60)	358.82020(12)	338.30995(12)	"	"	"	107	6.41
parent (avg)	508.08160(50)	358.82476(13)	338.31840(13)	"	"	"	–	–
5-D	505.704895(85)	356.433250(86)	335.438320(92)	0.03490(44)	0.0550(14)	−0.0630(16)	225	6.91
1-D	505.425300(95)	355.461685(38)	335.793300(41)	"	"	"	175	6.24
2-D	504.157430(60)	357.392938(38)	335.338172(35)	"	"	"	254	7.13
3-D	503.901760(58)	356.776863(34)	336.551764(34)	"	"	"	247	6.37
4-D	504.480480(54)	355.830667(33)	337.133881(31)	"	"	"	272	6.57
6-D	506.345460(81)	355.463814(29)	335.477671(28)	"	"	"	188	4.81
5-^{13}C	506.7452(77)	356.63733(29)	336.95711(22)	[0.03490]	[0.0550]	[−0.0630]	49	6.15
1-^{13}C	507.7542(70)	356.32317(20)	336.13907(22)	"	"	"	57	5.23
2-^{13}C	507.2520(41)	356.44752(14)	336.24013(15)	"	"	"	52	3.53
3-^{13}C	506.5724(49)	357.20783(16)	336.21528(17)	"	"	"	52	3.74
4-^{13}C	506.3589(71)	357.04374(21)	336.76461(21)	"	"	"	59	5.96
6-^{13}C	507.3754(94)	356.67671(27)	336.29174(30)	"	"	"	56	6.09

[a] Rotational parameters as defined in Table 1. [b] Centrifugal distortion fixed to the values for the 5-D isotopologue. [c] Number of measured transitions (N) and RMS deviation of the fit (frequency accuracy 10 kHz). [d] Standard error in parentheses in units of the last digit.

symmetry point group of the internal rotor is C_6, which contains four irreducible representations (A, B, E_1, and E_2). Therefore, each rotational transition is split into four separate symmetry components. We collect in Table 2 the experimental rotational constants derived for the parent species, for which the sixfold internal rotation barrier was determined as $V_6 = 32.8687(27)\ \text{cm}^{-1}$. The details of the barrier calculation will be reported separately. Isotopic substitutions in sevoflurane are similarly complicated by the internal rotation. However, substitutions on benzene break its C_6 symmetry, resulting in simpler asymmetric-top spectra. Our strategy was thus based on the use of a sample of monodeuterated benzene, allowing a manageable assignment of all the sevoflurane isotopologues in the cluster. The sensitivity of the experiment was so high that the doubly substituted D/^{13}C isotopologues in natural abundance could be detected with good intensity (e.g. SNR $\geq$ 3:1). Finally, and despite the extremely high spectral density, 33 of the 60 possible D/^{13}C isotopologues were assigned and every carbon had at least one associated isotopologue assignment. The spectral assignment was aided by automatic routines developed in Virginia.[16] The rotational parameters and experimental transitions for all 46 measured species are presented in Table 2 and Tables S1–S47 in the Supporting Information. No other conformations of sevoflurane–benzene were detected. Two sevoflurane homodimers will be reported separately.

The analysis of the multi-isotopic rotational spectra led to an accurate experimental structure for the cluster, including all heavy atoms and the six benzene hydrogens. Application of Kraitchman's equations[17] confirmed that the sevoflurane monomer[18] is not distorted upon complexation, as usually assumed for weak and moderately strong hydrogen bonds. Later, a least-squares fitting resulted in the ground-state-effective (r_0) structure.[19,20] The dimer has $3N-6 = 75$ independent degrees of freedom for a total of 138 experimental observations (three moments of inertia per species). Therefore, sevoflurane–benzene offers the possibility to determine a nearly full effective structure for a molecular complex, which is very rare. On assumption of ab initio constraints (M06-2X, Table S48) only for the positions of the three sevoflurane hydrogens and F-C-F bond angles, the molecular structure of Table S49 was obtained. A comparison with the theoretical geometries can be found in Figure 3, Figures S2 and S3, and Table S50. Interactive three-dimensional PDF representations can be found in Figures S4–S6.

Figure 3. Views of the sevoflurane–benzene structure. The ball-and-stick frameworks correspond to the M06-2X/6-311++g(d,p) geometry. The small spheres represent the experimental r_0 structure.

Consequently, we have addressed the structure, internal dynamics, and origin of the weak unions between sevoflurane and a benzene molecule through multi-isotopic rotational spectra. A single conformation was observed in the cold ($T_{rot} \approx 2$ K) supersonic jet, corresponding to the predicted global minimum primarily bound through the isopropyl C−H bond of sevoflurane. There is no indication of the second species with fluoromethyl bonding suggested from a weak band in the low-resolution IR spectra,[13] either because of thermal depopulation, or because of conformational relaxation in the jet. The C−H···π(Ph) weak hydrogen bond $r_{(\text{H}\cdots\text{Benzene})} = 2.401(16)$ Å is slightly longer than that in the complex with trifluoromethane ($r_{(\text{H}\cdots\text{Benzene})} = 2.366(2)$ Å), but still reflects the important activation role of the electronegative F and O atoms. The electrostatic contribution due to the interaction of the acidic hydrogen and the Lewis basic π benzene cloud likely enhances the C−H···π interaction with respect to aliphatic systems.[21] The geometry of the complex suggests that the main C–H···π interaction is modulated by secondary C–H···F weak contacts between three aromatic hydrogens and the fluorine atoms in sevoflurane. The calculated distances for the secondary interactions range from 3.095(14) Å in $OCH_2F\cdots H_1$ to 3.293(12)–3.531(15) Å in $CF_3\cdots H$ interactions. These values are 0.5–1 Å longer than the conventional fluorine hydrogen-bonding distances, but not unreasonable for bifurcated or secondary weak hydrogen bonds, as bonding distances up to 2.876–3.246 Å were identified in the difluoromethane trimer[5] and related clusters.[1-4] It is thus likely that the multiple weak fluorine hydrogen bonds are a contributor to the relative staggered orientation of the benzene ring and sevoflurane. An additional argument originates from the barrier hindering the internal rotation of the benzene moiety, which strikingly compares with the free torsion between the two subunits of $F_3CH\cdots$benzene.

The theoretical data outline the difficulty to treat dispersion forces. The B3LYP method fails to reproduce the cluster geometry, as first observed by a poor agreement with the rotational constants. The B3LYP C–H···π hydrogen bond is roughly 0.5 Å longer than the experimental value and it predicts the ring to be slightly tilted with respect to the C–H bond (98°). Conversely, the MP2 and M06-2X values (92.3° and 91.9°, respectively) agree fairly well with the r_0 determination (92.65(43)°). Significantly, in B3LYP the benzene ring is actually rotated approximately 25° from the eclipsing orientation of the global minimum. Thus, this optimal staggering is actually dependent on the proper treatment of the dispersion contribution to the C–H···π weak hydrogen bond. These results suggest that both electrostatics and dispersion play important roles in determining the complexation geometry of sevoflurane–benzene. Similar discrepancies of B3LYP were observed for $(\text{phenol})_2$.[10] In comparison, the MP2 and M06-2X methods with a modest Pople triple-ζ basis set acceptably account for the spectral results. MP2 and M06-2X mostly differ by a slight rotation in the benzene orientation, which could be attributed to the low-lying benzene torsional mode (14 cm^{-1}).

In conclusion, the new developments in broadband rotational spectroscopy lead to unparalleled levels of sensitivity for molecules and molecular clusters of increasing size (> 10–20 heavy atoms). A theoretical methodology with a balance between accuracy, computational cost, and portability is crucial for further experiments. As a result, rotational studies are essential in benchmarking the theoretical procedures for efficient description of weak nonbonding forces.

Received: November 12, 2013
Published online: February 12, 2014

Keywords: anesthetics · noncovalent interactions · rotational spectroscopy · weak hydrogen bonding

[1] a) Y. Tatamitani, B. Liu, J. Shimada, T. Ogata, P. Ottaviani, A. Maris, W. Caminati, J. L. Alonso, *J. Am. Chem. Soc.* **2002**, *124*, 2739; b) L. B. Favero, B. M. Giuliano, S. Melandri, A. Maris, P. Ottaviani, B. Velino, W. Caminati, *J. Phys. Chem. A* **2005**, *109*, 7402, and references therein.
[2] E. J. Cocinero, R. Sánchez, S. Blanco, A. Lesarri, J. C. López, J. L. Alonso, *Chem. Phys. Lett.* **2005**, *402*, 4.
[3] L. B. Favero, B. M. Giuliano, A. Maris, S. Melandri, P. Ottaviani, B. Velino, W. Caminati, *Chem. Eur. J.* **2010**, *16*, 1761.
[4] a) W. Caminati, S. Melandri, P. Moreschini, P. G. Favero, *Angew. Chem.* **1999**, *111*, 3105; *Angew. Chem. Int. Ed.* **1999**, *38*, 2924; b) W. Caminati, J. C. López, J. L. Alonso, J.-U. Grabow, *Angew. Chem.* **2005**, *117*, 3908; *Angew. Chem. Int. Ed.* **2005**, *44*, 3840.
[5] S. Blanco, S. Melandri, P. Ottaviani, W. Caminati, *J. Am. Chem. Soc.* **2007**, *129*, 2700.
[6] a) M. Nishio, M. Hirota, Y. Umezawa, *The CH/π Interaction, Evidence, Nature and Consequences*, Wiley-VCH, New York, **1998**; b) M. Nishio, *CrystEngComm* **2004**, *6*, 130; c) O. Takahashi, Y. Kohno, M. Nishio, *Chem. Rev.* **2010**, *110*, 6049; d) M. Nishio, *Phys. Chem. Chem. Phys.* **2011**, *13*, 13873.
[7] a) G. R. Desiraju, T. Steiner, *The weak Hydrogen Bond in Structural Chemistry and Biology*, IUC—Oxford Univ. Press, New York, **2001**; b) T. Steiner, *Angew. Chem.* **2002**, *114*, 50; *Angew. Chem. Int. Ed.* **2002**, *41*, 48.
[8] J. C. López, W. Caminati, J. L. Alonso, *Angew. Chem.* **2006**, *118*, 296; *Angew. Chem. Int. Ed.* **2006**, *45*, 290.
[9] a) M. Schnell, U. Erlekam, P. R. Bunker, G. von Helden, J.-U. Grabow, G. Meijer, A. van der Avoird, *Angew. Chem.* **2013**, *125*, 5288; *Angew. Chem. Int. Ed.* **2013**, *52*, 5180; b) M. Schnell, U. Erlekam, P. R. Bunker, G. von Helden, J.-U. Grabow, G. Meijer, A. van der Avoird, *Phys. Chem. Chem. Phys.* **2013**, *15*, 10207.
[10] a) A. L. Steber, J. L. Neill, D. P. Zaleski, B. H. Pate, A. Lesarri, R. G. Bird, V. Vaquero-Vara, D. W. Pratt, *Faraday Discuss.* **2011**, *150*, 227; b) N. A. Seifert, A. L. Steber, J. L. Neill, C. Pérez, D. P. Zaleski, B. H. Pate, A. Lesarri, *Phys. Chem. Chem. Phys.* **2013**, *15*, 11468.
[11] N. W. Ulrich, T. S. Songer, R. A. Peebles, S. A. Peebles, N. A. Seifert, C. Pérez, B. H. Pate, *Phys. Chem. Chem. Phys.* **2013**, *15*, 18148.
[12] a) H. Zhang, N. S. Astrof, J. H. Liu, J. H. Wang, M. Shimaoka, *FASEB J.* **2009**, *23*, 2735; b) H. Nury, C. Van Renterghem, Y. Weng, A. Tran, M. Baaden, V. Dufresne, J.-P. Changeux, J. M. Sonner, M. Delarue, P.-J. Corringer, *Nature* **2011**, *469*, 428.
[13] J. J. J. Dom, B. J. van der Veken, B. Michielsen, S. Jacobs, Z. Xue, S. Hesse, H.-M. Loritz, M. A. Suhm, W. A. Herrebout, *Phys. Chem. Chem. Phys.* **2011**, *13*, 14142.
[14] a) S. T. Shipman, B. H. Pate in *Handbook of High Resolution Spectroscopy* (Ed.: M. Quack, F. Merkt), Wiley, New York, **2011**, pp. 801–828; b) J. L. Neill, S. T. Shipman, L. Alvarez-Valtierra, A. Lesarri, Z. Kisiel, B. H. Pate, *J. Mol. Spectrosc.* **2011**, *269*, 21.
[15] a) C. Pérez, M. T. Muckle, D. Zaleski, N. A. Seifert, B. Temelso, G. C. Shields, Z. Kisiel, B. H. Pate, *Science* **2011**, *331-334*, 897; b) C. Pérez, S. Lobsiger, N. A. Seifert, D. P. Zaleski, B. Temelso, G. C. Shields, Z. Kisiel, B. H. Pate, *Chem. Phys. Lett.* **2013**, *571*, 1.
[16] Program Autofit, freely available from http://faculty.virginia.edu/bpate-lab/.
[17] a) J. Kraitchman, *Am. J. Phys.* **1953**, *21*, 17; b) C. C. Costain, *J. Chem. Phys.* **1958**, *29*, 864.
[18] A. Lesarri, A. Vega-Toribio, R. D. Suenram, D. J. Brugh, J.-U. Grabow, *Phys. Chem. Chem. Phys.* **2010**, *12*, 9624.
[19] H. D. Rudolph in *Advances in Molecular Structure Research, Vol. 1* (Eds.: M. Hargittai, I. Hargittai), JAI, Greenwich, **1995**, Chap. 3, pp. 63–114.
[20] Program STRFIT by Z. Kisiel, http://www.ifpan.edu.pl/~kisiel/prospe.htm.
[21] a) K. Shibasaki, A. Fujii, N. Mikami, S. Tsuzuki, *J. Phys. Chem. A* **2006**, *110*, 4397; b) K. Shibasaki, A. Fujii, N. Mikami, S. Tsuzuki, *J. Phys. Chem. A* **2007**, *111*, 753; c) R. C. Dey, P. Seal, S. Chakrabarti, *J. Phys. Chem. A* **2009**, *113*, 10113.

PCCP

PAPER

Weak C–H···N and C–H···F hydrogen bonds and internal rotation in pyridine–CH_3F†

Cite this: DOI: 10.1039/c3cp54430c

Received 19th October 2013,
Accepted 26th November 2013

DOI: 10.1039/c3cp54430c

www.rsc.org/pccp

Lorenzo Spada,[a] Qian Gou,[a] Montserrat Vallejo-López,[ab] Alberto Lesarri,[b] Emilio J. Cocinero[c] and Walther Caminati*[a]

The pulsed-jet Fourier transform rotational spectra of 4 isotopologues have been recorded for the most stable conformation of the molecular cluster pyridine–CH_3F. Two weak C–H···N and C–H···F hydrogen bonds link the two subunits of the complex. Structural information on the hydrogen bridges has been obtained. The internal rotation of the CH_3F subunit around its symmetry axis splits all rotational transitions into two (*A* and *E*) well resolved component lines, leading to a V_3 barrier height of 1.55(1) kJ mol^{-1}.

1 Introduction

Formation of weak hydrogen bonds (WHBs) is a common mechanism for molecular clustering in various aggregates, and their structural features in the solid state have been summarized in a book.[1] Blue shifts of the IR frequencies of the stretchings of the proton donor groups in cryogenic solutions have been observed for WHBs, in contrast to the red shifts typical of a standard hydrogen bond.[2] However, precise information on the energetics and on the structural and dynamical aspects of this kind of interaction is better determined in an environment free from the intermolecular interactions that take place in condensed media. Dissociation energies of complexes with the two subunits held together by WHBs have been estimated from centrifugal distortion effects within a pseudo-diatomic approximation following rotational (generally pulsed jet Fourier transform microwave, PJ-FTMW) studies. In this way, bond energies of a few kJ mol^{-1} have been estimated for the C–H···O,[3] C–H···N,[4] C–H···F–C,[5] C–H···Cl–C,[6] CH···S[7] and C–H···π[6,8] linkages. These energy values are similar to those of the van der Waals interactions, but the linkages maintain the same directional properties of "classical" hydrogen bonds. In addition, the Ubbelohde effect,[9] an alteration upon H → D substitution of the distances between the two constituent units, which has always been considered in conjunction with hydrogen bonding, has been recently pointed out also for the C–H···π WHB.[10] As to the investigations involving aromatic molecules, several complexes with CHF_3, the prototype C–H proton donor, have been studied. The investigation of the rotational spectrum of benzene–CHF_3 has shown that this complex is a symmetric top, with the two moieties held together through a C–H···π interaction,[8] and thus provided information on this kind of WHB. Replacing benzene with pyridine (Py), two high electronic density sites become available in the ring; then, besides the π-type form, a σ-type complex with a C–H···N and a C–H···F–C WHB was plausible, which turned out to be the global minimum.[4] What will happen when replacing in Py–CHF_3 the proton donor CHF_3 group with a less acidic group, such as CH_3F? Will weakening the WHB with a less acidic methylenic hydrogen finally result in a T-shape complex or will the in-plane conformation still be dominant? And how will the internal dynamics change, when a heavy internal rotor will be substituted with a very light top? The answers are given below.

2 Results and discussion

2.1 Theoretical calculations

We first explored the conformational space of Py–CH_3F by using molecular mechanics and conformational search algorithms implemented in MacroModel 9.2.[11] We found 28 configurations with energies below 50 kJ mol^{-1}. *Ab initio* MP2/6-311++G(d,p)[12] geometry optimizations were performed for all these configurations, and we found three stationary points below 5 kJ mol^{-1}. The three conformers were confirmed to be real minima with harmonic vibrational frequency calculations at the same level of theory.

We report in Table 1 the shapes, the spectroscopic parameters and the relative energies (ΔE and ΔE_0, the zero point

[a] *Department of Chemistry, University of Bologna, Via Selmi 2, I-40126, Bologna, Italy. E-mail: walther.caminati@unibo.it; Fax: +39-0512099456*
[b] *Departamento de Química Física y Química Inorgánica, Universidad de Valladolid, E-47011 Valladolid, Spain*
[c] *Departamento de Química Física, Facultad de Ciencia y Tecnología, Universidad del País Vasco, (UPV-EHU), Apartado 644, E-48940 Bilbao, Spain*

† Electronic supplementary information (ESI) available: Table of transitions of all the observed isotopomers and *ab initio* geometry of the observed complex. See DOI: 10.1039/c3cp54430c

Table 1 *Ab initio* shapes and spectroscopic parameters of the three most stable conformers of Py–CH_3F

	I	II	III
	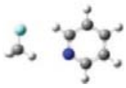		
A/MHz	4812.9	2879.0	2927.0
B/MHz	835.3	1271.6	1280.4
C/MHz	715.0	1233.3	1223.4
χ_{aa}/MHz	−2.91	1.94	2.86
$\chi_{bb} - \chi_{cc}$/MHz	−3.76	−5.04	−4.20
μ_a/D	−2.05	−0.29	0.91
μ_b/D	0.64	0.69	0.81
μ_c/D	0.0	0.39	−2.01
ΔE^a/cm^{-1}	6	13	0
$\Delta E_0{}^b$/cm^{-1}	0	211	217
E_D/kJ mol^{-1}	7.47	1.45	1.36

[a] Absolute energy = −387.062408 E_h. [b] Absolute energy zero point corrected = −386.93412 E_h.

energy) obtained for these three species. One of them is a σ-type complex, with the CH_3F moiety in the plane of the ring, and with two (C–H···N and C–H···F–C) WHBs connecting the two subunits. The other two forms are π-type complexes, with CH_3F perpendicular to the Py plane, and characterized by a C–H···π WHB. One can note that the zero point energy corrections invert the relative energies of the species, and that at the very end the σ-rotamer appears to be the most stable one.

We calculated the dissociation energies, including basis-set superposition error corrections (BSSE), by using the counterpoise procedure.[13]

2.2 Experimental section

A 1% gas mixture of methyl fluoride (purity 99%, available by Fluorochem) in helium was passed over a sample holder containing liquid pyridine, at a stagnation pressure of *ca.* 0.25 MPa. The best experimental conditions were found by cooling the molecular system at 273 K before expanding through the solenoid pulsed valve (General valve, series 9, nozzle diameter 0.5 mm) into the Fabry–Perot cavity at 5×10^{-4} mbar. The rotational spectrum, in the 6–18 GHz frequency region, was recorded using a COBRA-type[21] pulsed supersonic jet Fourier-transform microwave (FTMW) spectrometer,[22] described elsewhere.[23] Each rotational transition is split by the Doppler effect as a result of the coaxial arrangement of the supersonic jet and the resonator. The estimated accuracy of frequency measurements is better than 3 kHz and lines separated by more than 7 kHz are resolvable. Furthermore, the spectra of isotopologue adducts with CD_3F (99% enriched, purchased from Cambridge Isotope Laboratories, Inc.) and pyridine (^{15}N) (98% enriched available by Sigma Aldrich) were recorded.

2.3 Rotational spectra

According to the theoretical calculations (see Table 1) we focused our search on μ_a-type transitions of the expected most stable plane-symmetric conformer I. The assignment started with the lowest J predicted in our spectral region and, forthwith, the $5_{05} \leftarrow 4_{04}$ rotational transition was observed. It appears as a doublet of triplets according to the effect expected for the hindered internal rotation of the methyl group of methyl fluoride and to the appearance of the nuclear quadrupole hyperfine structure ($I(^{14}N) = 1$). After this, several other assignments were made up to $J = 9$ and some weaker μ_b-transitions were measured. No lines belonging to μ_c type transitions have been observed in agreement with the C_s symmetry of conformer I. All transition frequencies have been fitted with the XIAM program, based on the Combined Axis Method, CAM.[14] It supplies, apart from the rotational and centrifugal distortion constants, parameters with a clear physical meaning, such as the V_3 barrier to internal rotation, the angles ($\angle(i,g)$, $g = a, b, c$) between the internal rotation axis and the principal axes, and the moment of inertia of the internal top (I_α). In the fit, we used Watson's S reduced semirigid-rotor Hamiltonian (I^r representation).[15] The results are listed in Table 2.

One can immediately note that the rotational constants match the theoretical values only for conformer I, and so the conformational assignment is straightforward. Only the $\angle(i,a)$ angle is reported, because $\angle(i,b)$ is the complement to 90° of $\angle(i,a)$, and $\angle(i,c)$ is 90° from symmetry. I_α was poorly determined in the fit, so its values have been fixed to those of isolated CH_3F and CD_3F.[16] Additional information on the adduct structure and dynamics has been obtained from the microwave spectra of Py–CD_3F, Py(^{15}N)–CH_3F and Py(^{15}N)–CD_3F.

The internal rotation splittings were much smaller for the isotopologues containing the CD_3F moiety (due to the larger reduced mass of the motion), as shown in Fig. 1 for the $6_{06} \leftarrow 5_{05}$ transitions of the Py(^{15}N)–CH_3 and Py(^{15}N)–CD_3F species.

The lack of experimental signals from conformers II and III is plausibly due to conformational relaxation upon supersonic expansion, a process which easily takes place when the various conformers are connected through interconversion barriers of the order – or smaller than – 2 kT.[17]

Table 2 Experimental spectroscopic constants of the four measured isotopologues of pyridine–fluoromethane

	Py–CH_3F	Py(^{15}N)–CH_3F	Py–CD_3F	Py(^{15}N)–CD_3F
A/MHz	4833.037(2)[a]	4807.141(2)	4620.377(2)	4598.017(1)
B/MHz	835.9913(2)	835.9107(2)	789.9881(7)	789.8752(1)
C/MHz	716.6840(2)	716.0581(1)	681.1658(2)	680.5990(1)
D_J/kHz	0.3700(7)	[0.3700][b]	0.3095(7)	[0.3095]
D_{JK}/kHz	3.987(9)	[3.987]	3.41(3)	[3.41]
D_K/kHz	−2.8(5)	[−2.8]	—	—
d_1/kHz	−0.0568(8)	[−0.0568]	−0.045(1)	[−0.045]
d_2/kHz	−0.0130(4)	[−0.0130]	—	—
χ_{aa}/MHz	−2.942(8)	—	−3.11(2)	—
$\chi_{bb} - \chi_{cc}$/MHz	−3.738(7)	—	−3.67(1)	—
V_3/cm^{-1}	129.435(3)	129.631(5)	133.8(2)	134.4(1)
$I_\alpha{}^c$/uÅ^2	3.253	3.253	6.476	6.476
$\angle(i,a)$/°	88.030(1)	88.081(5)	87.22(2)	86.7(2)
N^d	168	28	114	28
σ^e/kHz	3.7	2.3	3.3	2.5

[a] Error in parentheses in units of the last digit. [b] Values in brackets fixed to the corresponding value of the parent species. [c] Fixed to the values of isolated CH_3F or CD_3F from ref. 16. [d] Number of lines in the fit. [e] Root-mean-square deviation of the fit.

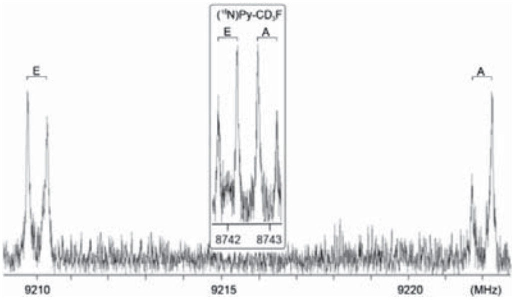

Fig. 1 Internal rotation splittings of the $6_{06} \leftarrow 5_{05}$ transitions of the $Py(^{15}N)–CH_3F$ and $Py(^{15}N)–CD_3$ isotopologues.

2.4 Structural information

The changes in the rotational constants in going from the parent species to the $Py(^{15}N)–CH_3F$ isotopologue allowed to calculate the substitution coordinates (r_s)[18] of the N atom. They are reported in Table 3, and are compared to the *ab initio* values (labeled as r_e).

The quite good agreement is a further confirmation of the conformational assignment. In addition, an effective partial r_0 structure was calculated by least-squares fit of the 12 rotational constants to adjust the $r_{N\cdots C}$ distance and the angle α (see Fig. 2), which determine the distance and the relative orientation of the two moieties in the complex.

All the remaining parameters were fixed to their *ab initio* values. The full *ab initio* geometry is given in the ESI.† The determined parameters are listed in Table 4, together with the corresponding *ab initio* values.

Table 3 The experimental substitution coordinates (r_s) of the nitrogen atom are in agreement with the *ab initio* values (r_e) of conformer I

	r_s	r_e
a/Å	±0.236(6)[a]	−0.227
b/Å[b]	±0.753(2)	0.767

[a] Error in parentheses in units of the last digit. [b] The c-coordinates have been fixed to 0 by symmetry.

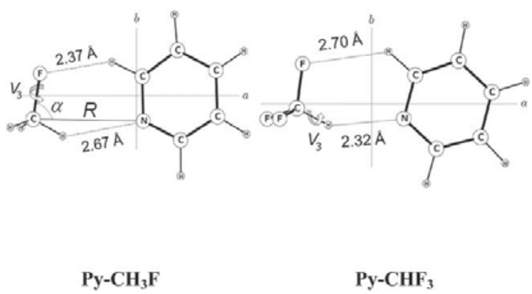

Fig. 2 Molecular structure, hydrogen bond parameters and internal rotation axes of $Py–CH_3F$ and $Py–CHF_3$.

Table 4 Effective structural parameters of the most stable conformer of $Py–CH_3F$

	r_0	r_e
R/Å	3.592(6)[a]	3.521
α/°	81.6(5)[a]	87.7

[a] Error in parentheses in units of the last digit.

2.5 Energetics

The hydrogen bond distances, $r_{H\cdots F}$ and $r_{H\cdots N}$, resulted to be 2.366 and 2.666 Å, respectively. These values are typical of WHBs. The corresponding values for $Py–CHF_3$ are reported to be 2.700 and 2.317 Å, respectively.[4] This comparison suggests a stronger H···N bond in $Py–CHF_3$, in agreement with the highest acidity of the single hydrogen of CHF_3. Conversely, the H···F linkage is stronger in $Py–CHF_3$. These parameters are shown in Fig. 2 for the two complexes. Looking at Fig. 2, one can note that the V_3 barriers in $Py–CH_3F$ (1.55 kJ mol^{-1}) and in $Py–CHF_3$ (0.52 kJ mol^{-1}) correspond to the breaking of the H···N or of the H···F WHBs, respectively. We can then state that for this kind of system, the H···N interaction is stronger than the H···F one. By assuming the complex to be formed by two rigid parts, and for cases when the stretching motion leading to its dissociation is almost parallel to the a-axis, it is possible to estimate its force constant according to:[19]

$$k_s = 16\pi^4(\mu R_{CM})^2[4B^4 + 4C^4 - (B - C)^2(B + C)^2]/(hD_J) \quad (1)$$

where μ, R_{CM}, and D_J are the reduced mass, the distance between the centers of mass and the first-order centrifugal distortion constant, respectively. R_{CM} has been estimated from the partial r_0 structure to be 4.64 Å. B and C are rotational constants of the complex. The obtained value is 6.4 N m^{-1}, corresponding to a harmonic stretching frequency of 67 cm^{-1}. From this value the dissociation energy can be estimated by assuming a Lennard-Jones potential function and using the approximated equation:[20]

$$E_D = 1/72k_sR_{CM}^2. \quad (2)$$

The value E_D = 11.4 kJ mol^{-1} has been obtained, in agreement with the *ab initio* value of 7.9 kJ mol^{-1}. This dissociation energy is slightly smaller than the value for $Py–CHF_3$ (14.9 kJ mol^{-1}),[4] in agreement with the strongest H···N interaction in this latter complex.

3 Conclusions

As described in the introduction, only one high resolution spectroscopy investigation, on $Py–CHF_3$,[4] was available in the literature to describe the features of the H···N WHB. In this second study on this topic, concerning $Py–CH_3F$, a molecular system apparently very similar to $Py–CHF_3$, we outline several differences between the two complexes, related both to the internal dynamics and to the chemical properties. From a spectroscopic point of view the internal rotation splittings in $Py–CH_3F$ are, in spite of a higher V_3 barrier, 3 orders of magnitude larger, because a heavy internal rotor (CF_3) is replaced by a light internal rotor (CH_3). The best parameter to describe the size of the splittings due to an internal rotor is the dimensionless reduced barrier *s*, which takes into account both the potential energy value and the reduced mass of the motion. Its values are 11.0 and 63.5 for Py–CH_3F and Py–CHF_3, respectively.

Looking at Fig. 2, one can note that the top internal rotations in Py–CH_3F and Py–CHF_3 break the H$\cdots$N and the H$\cdots$F linkages, respectively. As a consequence, the V_3 barriers correspond, in a first approximation, to the strengths of the two WHBs. Then, the higher V_3 barrier in Py–CH_3F suggests the H$\cdots$N WHB in Py–CH_3F to be quite stronger than the H$\cdots$F one in Py–CHF_3. We can also interpret the higher value of the H$\cdots$N distance in Py–CH_3F as an indication of a lower interaction energy.

Acknowledgements

We acknowledge Italian MIUR (PRIN 2010, project 2010ERFKXL_001) and the University of Bologna for financial support (RFO). Q. G. thanks the China Scholarships Council (CSC) for financial support. Financial support from the Spanish MICINN and MINECO (CTQ2011-22923 and CTQ2012-39132), the Basque Government (Consolidated Groups, IT520-10) and UPV/EHU (UFI11/23) is gratefully acknowledged. M.V.L. and EJC gratefully acknowledge the MICINN for a FPI grant and a ''Ramón y Cajal'' contract, respectively. Computational resources and laser facilities of the UPV-EHU were used in this work (SGIker and I2Basque). L. S. thanks Dr A. Maris for helping with theoretical calculations.

Notes and references

1 R. Desiraju and T. Steiner, *The Weak Hydrogen Bond*, Oxford University Press, Oxford, 1999.

2 B. J. van der Veken, W. A. Herrebout, R. Szostak, D. N. Shchepkin, Z. Havlas and P. Hobza, *J. Am. Chem. Soc.*, 2001, **123**, 12290; S. N. Delanoye, W. A. Herrebout and B. J. van der Veken, *J. Am. Chem. Soc.*, 2002, **124**, 7490; S. N. Delanoye, W. A. Herrebout and B. J. van der Veken, *J. Phys. Chem. A*, 2005, **109**, 9836; W. A. Herrebout, S. N. Delanoye and B. J. van der Veken, *J. Phys. Chem. A*, 2004, **108**, 6059; T. Van den Kerkhof, A. Bouwen, E. Goovaerts, W. A. Herrebout and B. J. van der Veken, *Phys. Chem. Chem. Phys.*, 2004, **6**, 358; B. J. van der Veken, S. N. Delanoye, B. Michielsen and W. A. Herrebout, *J. Mol. Struct.*, 2010, **976**, 97.

3 Y. Tatamitani, B. Liu, J. Shimada, T. Ogata, P. Ottaviani, A. Maris, W. Caminati and J. L. Alonso, *J. Am. Chem. Soc.*, 2002, **124**, 2739; S. Blanco, J. C. López, A. Lesarri, W. Caminati and J. L. Alonso, *ChemPhysChem*, 2004, **5**, 1779; J. L. Alonso, S. Antolinez, S. Blanco, A. Lesarri, J. C. López and W. Caminati, *J. Am. Chem. Soc.*, 2004, **126**, 3244; Y. Tatamitami and T. Ogata, *J. Mol. Spectrosc.*, 2003, **222**, 102; L. B. Favero, B. M. Giuliano, S. Melandri, A. Maris, P. Ottaviani, B. Velino and W. Caminati, *J. Phys. Chem. A*, 2005, **109**, 7402; P. Ottaviani, W. Caminati, L. B. Favero, S. Blanco, J. C. López and J. L. Alonso, *Chem.–Eur. J.*, 2006, **12**, 915.

4 L. B. Favero, B. M. Giuliano, A. Maris, S. Melandri, P. Ottaviani, B. Velino and W. Caminati, *Chem.–Eur. J.*, 2010, **16**, 1761.

5 W. Caminati, J. C. López, J. L. Alonso and J.-U. Grabow, *Angew. Chem.*, 2005, **117**, 3908; W. Caminati, J. C. López, J. L. Alonso and J.-U. Grabow, *Angew. Chem., Int. Ed.*, 2005, **44**, 3840; W. Caminati, S. Melandri, P. Moreschini and P. G. Favero, *Angew. Chem.*, 1999, **111**, 3105 (*Angew. Chem., Int. Ed.*, 1999, **38**, 2924); S. Blanco, J. C. López, A. Lesarri and J. L. Alonso, *J. Mol. Struct.*, 2002, **612**, 255; S. Blanco, S. Melandri, P. Ottaviani and W. Caminati, *J. Am. Chem. Soc.*, 2007, **129**, 2700.

6 L. F. Elmuti, R. A. Peebles, S. A. Peebles, A. L. Steber, J. L. Neill and B. H. Pate, *Phys. Chem. Chem. Phys.*, 2011, **13**, 14043; C. L. Christenholz, D.l A. Obenchain, S. A. Peebles and R. A. Peebles, *J. Mol. Spectrosc.*, 2012, **280**, 61.

7 E. J. Cocinero, R. Sanchez, S. Blanco, A. Lesarri, J. C. López and J. L. Alonso, *Chem. Phys. Lett.*, 2005, **402**, 4.

8 J. C. López, J. L. Alonso and W. Caminati, *Angew. Chem., Int. Ed.*, 2006, **45**, 290.

9 A. R. Ubbelohde and K. J. Gallagher, *Acta Crystallogr.*, 1955, **8**, 71.

10 Q. Gou, G. Feng, L. Evangelisti, D. Loru, J. L. Alonso, J. C. López and W. Caminati, *J. Phys. Chem. A*, 2013, DOI: 10.1021/jp407408f.

11 *MASTRO, version 9.3*, Schrödinger, LLC, New York, NY, 2012.

12 M. J. Frisch, G. W. Trucks, H. B. Schlegel, G. E. Scuseria, M. A. Robb, J. R. Cheeseman, J. A. Montgomery, Jr., T. Vreven, K. N. Kudin, J. C. Burant, J. M. Millam, S. S. Iyengar, J. Tomasi, V. Barone, B. Mennucci, M. Cossi, G. Scalmani, N. Rega, G. A. Petersson, H. Nakatsuji, M. Hada, M. Ehara, K. Toyota, R. Fukuda, J. Hasegawa, M. Ishida, T. Nakajima, Y. Honda, O. Kitao, H. Nakai, M. Klene, X. Li, J. E. Knox, H. P. Hratchian, J. B. Cross, C. Adamo, J. Jaramillo, R. Gomperts, R. E. Stratmann, O. Yazyev, A. J. Austin, R. Cammi, C. Pomelli, J. W. Ochterski, P. Y. Ayala, K. Morokuma, G. A. Voth, P. Salvador, J. J. Dannenberg, V. G. Zakrzewski, S. Dapprich, A. D. Daniels, M. C. Strain, O. Farkas, D. K. Malick, A. D. Rabuck, K. Raghavachari, J. B. Foresman, J. V. Ortiz, Q. Cui, A. G. Baboul, S. Clifford, J. Cioslowski, B. B. Stefanov, G. Liu, A. Liashenko, P. Piskorz, I. Komaromi, R. L. Martin, D. J. Fox, T. Keith, M. A. Al-Laham, C. Y. Peng, A. Nanayakkara, M. Challacombe, P. M. W. Gill, B. Johnson, W. Chen, M. W. Wong, C. Gonzalez and J. A. Pople, *GAUSSIAN03, Revision B.01*, Gaussian, Inc., Pittsburgh PA, 2003.

13 S. F. Boys and F. Bernardi, *Mol. Phys.*, 1970, **19**, 553.

14 H. Hartwig and H. Dreizler, *Z. Naturforsch., A: Phys. Sci.*, 1996, **51**, 923.

15 J. K. G. Watson, in *Vibrational Spectra and Structure*, ed. J. R. Durig, vol. 6, Elsevier, New York/Amsterdam, 1977, pp. 1–89.
16 J. Demaison, J. Breidung, W. Thiel and D. Papousek, *Struct. Chem.*, 1999, **10**, 129.
17 See for example: R. S. Ruoff, T. D. Klots, T. Emilson and H. S. Gutowski, *J. Chem. Phys.*, 1990, **93**, 3142.
18 J. Kraitchman, *Am. J. Phys.*, 1953, **21**, 17.
19 D. J. Millen, Determination of Stretching Force Constants of Weakly Bound Dimers from Centrifugal Distortion Constants, *Can. J. Chem.*, 1985, **63**, 1477.
20 S. E. Novick, S. J. Harris, K. C. Janda and W. Klemperer, *Can. J. Phys.*, 1975, **53**, 2007.
21 (*a*) J.-U. Grabow and W. Stahl, *Z. Naturforsch., A: Phys. Sci.*, 1990, **45**, 1043; (*b*) J.-U. Grabow, Doctoral thesis, Christian-Albrechts-Universitat zu Kiel, Germany, 1992; (*c*) J.-U. Grabow, W. Stahl and H. Dreizler, *Rev. Sci. Instrum.*, 1996, **67**, 4072.
22 T. J. Balle and W. H. Flygare, *Rev. Sci. Instrum.*, 1981, **52**, 33; W. Caminati, A. Millemaggi, J. L. Alonso, A. Lesarri, J. C. López and S. Mata, *Chem. Phys. Lett.*, 2004, **392**, 1.

Chemical Physics Letters 591 (2014) 216–219

Contents lists available at ScienceDirect

Chemical Physics Letters

journal homepage: www.elsevier.com/locate/cplett

Interactions between freons and aromatic molecules: The rotational spectrum of pyridine–difluoromethane

Montserrat Vallejo-López [a,b], Lorenzo Spada [a], Qian Gou [a], Alberto Lesarri [b], Emilio J. Cocinero [c], Walther Caminati [a,*]

[a] Dipartimento di Chimica 'G. Ciamician' dell'Università, Via Selmi 2, Bologna I-40126, Italy
[b] Departamento de Química Física y Química Inorgánica, Facultad de Ciencias, Universidad de Valladolid, Paseo de Belén, 7, Valladolid E-47011, Spain
[c] Departamento de Química Física, Facultad de Ciencia y Tecnología, Universidad del País Vasco, (UPV-EHU), Apartado 644, Bilbao E-48940, Spain

ARTICLE INFO

Article history:
Received 29 October 2013
In final form 15 November 2013
Available online 22 November 2013

ABSTRACT

The pulsed jet Fourier transform microwave spectrum of the molecular adduct pyridine–difluoromethane shows that the two subunits are linked to each other through a bifurcated $CH_2 \cdots N$ and a $CH \cdots F$ weak hydrogen bond. Energies and structural information of these links are given.

1. Introduction

Probably, after benzene, the prototype aromatic system, pyridine is the best-known heterocyclic aromatic molecule. It has many industrial and pharmaceutical applications and it is a ligand extensively used in coordination [1,2] and surface chemistry [3].

From a spectroscopic point of view, its simple structure has allowed the study of several adducts with several partner atoms or molecules. Depending on the nature of the chemical species linked to pyridine (Py from now on), π or σ type complexes have been observed, in relation to the Py interaction sites, that is the π system of the aromatic ring, or the n orbital of the nitrogen atom.

Py–Metal (metal = Li, Ca, and Sc) complexes have been produced in laser-vaporization molecular beams and studied by ZEKE spectroscopy and theoretical calculations [4]. It has been found that Li and Ca complexes prefer a σ bonding mode, whereas the Sc complex favors a π mode, with bond energies of 27.0, 49.1 and 110.6 kJ mol^{-1}, respectively.

Plenty of information on the typology and strengths of the non-bonding interactions of Py with its partners have been obtained also by rotational spectroscopy [5–20].

Py is the only aromatic molecule for which, thanks to its permanent dipole moment, the rotational spectra of all complexes with rare gases (except radon) have been reported. In all cases, a π-type complex has been observed [5–20], even for complexes with two rare gas atoms, which have a 'double' π arrangement, with one atom above and one below the ring [9,12,13]. The interaction energies are in the range 0.5–5 kJ mol^{-1}.

The molecular adducts of Py with other partners, apart from rare gases, studied by microwave (MW) spectroscopy displayed, to our knowledge, a σ-type arrangement. Four investigations are available, describing this kind of interaction, on the complexes of Py with simple molecules, such as CO [14], CO_2 [15], SO_2 [16] and SO_3 [17]. All of them are linked to the n orbital of Py, through formal C···N or S···N contacts. In the adduct with SO_3, Py acts as a Lewis base, donating its lone pair to the sulfur trioxide Lewis acid. The S–N bond becomes in this case a covalent bond, with a bond energy of about 120 kJ mol^{-1}.

Also complexes of Py with freons have a σ-type arrangement. This is the case of Py–CF_4, where the two subunits are held together by a $CF_3 \cdots N$ halogen bond, with the top undergoing a free rotation with respect to Py [18]. In Py–CHF_3, and Py–CH_3F two weak hydrogen bonds (WHB), C–H···N and C–H···F, are observed [19,20]. The barriers to internal rotation of the CHF_3 and of the CH_3F groups have been determined from the *A*–*E* splittings of the rotational transitions.

Unlike CF_4 (spherical top) and CHF_3 or CH_3F (symmetric tops), CH_2F_2 is an asymmetric top freon. We considered interesting to investigate the rotational spectrum of the Py–CH_2F_2 molecular adduct, for which multiple WHB interactions are possible between the constituent monomers. The obtained results are presented below.

2. Experimental

The rotational spectra of the complex were observed in a FTMW spectrometer [21] with a COBRA (Coaxial Oriented Beam and Resonator Axes) configuration [22] in the frequency range 6–18 GHz which has been described previously [23]. Briefly, the experimental detection is made up by three stages. The first step is the creation of the molecular pulse by opening the injection valve allowing the adiabatic expansion of our gas sample in the cavity. The macroscopic polarization of the molecular beam is the next stage. It

* Corresponding author. Fax: +39 051 2099456.
E-mail address: walther.caminati@unibo.it (W. Caminati).

0009-2614/$ - see front matter © 2013 Elsevier B.V. All rights reserved.
http://dx.doi.org/10.1016/j.cplett.2013.11.040

is generated by applying a microwave pulse into the Fabry–Perot resonator where the sample was previously introduced. Finally the following spontaneous molecular emission is digitalized in the time-domain and Fourier transformed in order to obtain the frequency of the rotational transitions of the system under study. Additionally, the coaxial arrangement in the cavity causes the splitting of the molecular signals into two different components due to the Doppler effect. Transitions separated by more than 7 kHz are resolvable with an estimated accuracy above 0.5 kHz.

A mixture of 2% CH_2F_2 in He was flown through commercial samples of Py or ^{15}N–Py (Aldrich) cooled at 0 °C, at pressures of ca. 0.3 MPa, and it is guided to a pulsed valve where the supersonic jet was created.

3. Computational methods

To explore the conformational landscape of our complex, molecular mechanics calculations were carried out using the Merck Molecular Force Field (MMFFs) [24] implemented in the program Macromodel 9.2 [25]. 62 different structures were identified within a window energy of 50 kJ mol^{-1}, and the provided geometries were later fully optimized with *ab initio* methods at MP2 level in order to get more reliable data for the plausible conformers. Frequency calculations were also performed, to check the nature of the stationary points and to estimate additional spectroscopic parameters, such as centrifugal distortion constants. After the re-optimization, only three conformers with relative energies below 5 kJ mol^{-1} were found (see Table 1), susceptible to be detected experimentally in the jet. All the calculations were performed with GAUSSIAN 09 [26] suite of programs and using the Pople triple-ζ 6-311++G(d,p) basis set.

To evaluate the dissociation energy of the complex, the geometries of the monomers were optimized and the respective energies, zero point corrected, were calculated. The obtained dissociation energy has finally been corrected for the Basis Set Superposition Error (BSSE) [27]. All obtained energies and spectroscopic parameters of the three most stable conformations are shown in Table 1.

4. Results

According to the theoretical predictions, the most stable conformer (see Table 1) is a near prolate top with a Ray's asymmetry parameter $\kappa \sim -0.97$ with two active selection rules: μ_a and μ_b. As long as the dipole moment is much stronger along the *a*-axis, μ_a-type *R* bands have been searched first. They are groups of lines evenly separated in frequency by a $B + C$ value. Two of these bands (J: 7←6 and 8←7) are shown in Figure 1. The experimental transition frequencies have been fitted using Pickett's SPFIT program [28] within semirigid Watson's Hamiltonian [29] in the symmetric reduction and I^r representation. An additional correction takes into account the quadrupole coupling effect [30] due to the non-spherical charge distribution in the ^{14}N nucleus. As a consequence of that hyperfine effect, each transition is split into several component lines, as it can be seen in Figure 2.

All obtained spectroscopic parameters are reported in Table 2. The experimental rotational constants are in good agreement with the theoretical values of conformer 1, showing that the conformer identified in the jet corresponds to the most stable species predicted by the theory. From the rotational constants, the inertial defect, Δ_c, has been calculated to be −4.59 uÅ^2. This value, although slightly higher than that expected for two methylenic hydrogens out of the plane, confirms the conformational assignment. The calculated values of Δ_c are, indeed, −3.75, −39.64 and −176.20 uÅ^2 for conformers 1, 2 and 3, respectively. Part of the unassigned transitions recorded in the spectrum could be identified with lines of Py–H_2O [31] or of the $(CH_2F_2)_n$ aggregates (with $n = 2$, 3 and 4) [32–34]. No other conformers were detected in the spectrum, despite the small energy gap between the other predicted structures stabilized by only two hydrogen bonds.

After the spectrum of the parent species, the one of the quadrupole-less complex with ^{15}N–Py was easily assigned. The obtained spectroscopic parameters are also shown in Table 2.

All measured transitions are available in the Supplementary Material.

When the intermolecular stretching motion leading to dissociation is almost parallel to the *a*-axis of the complex, it is plausible to derive the corresponding force constant within the pseudo diatomic approximation, through the equation [35]:

$$k_s = 16\pi^4(\mu R_{CM})^2[4B^4 + 4C^4 - (B - C)^2(B + C)^2]/(hD_J) \quad (1)$$

μ is the pseudo diatomic reduced mass, R_{CM} is the distance between the centers of the mass of the two subunits, and D_J is the centrifugal distortion constant. Moreover, assuming a Lennard–Jones type potential, the zero point dissociation energy of the complex can be derived applying the approximate expression [36]:

$$E_D = 1/72 k_s R_{CM}^2 \quad (2)$$

Hence, the dissociation energy of the complex was found to be 15.6 kJ mol^{-1}, relatively in good agreement with the *ab initio* value. In Table 3, we compare the dissociation energies of the complexes of Py with other freons. There we give the number and kind of interactions linking the freon molecules to Py. One can note that the lower dissociation energy is for Py–CF_4, where the interaction can be classified as halogen bond. The partially hydrogenated

Table 1
Spectroscopic parameters and relative energies of the three most stable conformations of Py–CH_2F_2.

	Conformer 1	Conformer 2	Conformer 3
	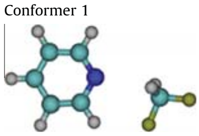	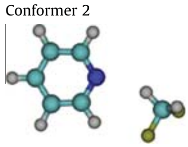	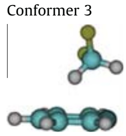
$A/B/C$/MHz	4407/587/520	3799/590/532	2383/891/838
$\chi_{aa}/\chi_{bb}/\chi_{cc}$/MHz	−4.34/1.00/3.34	−3.65/0.67/2.99	3.07/1.51/−4.58
$\mu_a/\mu_b/\mu_c$/D	−4.24/−0.72/0.0	−3.44/−0.43/−0.91	2.60/−0.38/−1.52
$D_J/D_{JK}/D_K$/kHz	0.11/1.38/4.60	0.62/−2.39/59.3	0.67/1.83/−0.25
d_1/d_2/Hz	−12.6/−1.91	48.0/−7.48	−9.77/16.5
ΔE_{ZPE}[a]/E_d[b]/kJ mol^{-1}	0.0[c]/11.8	1.6/10.5	4.7/3.8

[a] Zero point relative energies.
[b] Dissociation energy.
[c] Absolute energy is −486.151117 E_h.

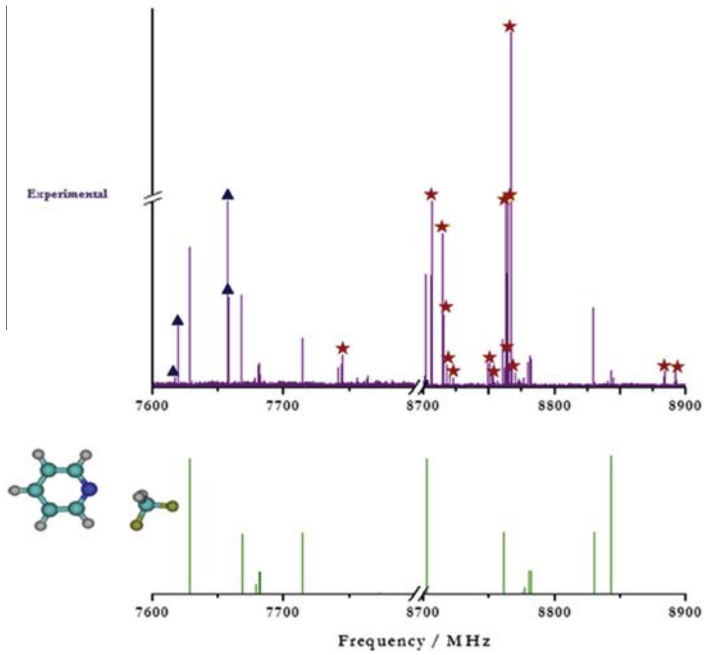

Figure 1. A section of the experimental spectrum of Py–CH_2F_2 is compared to the fitted frequencies. Line marked with a triangle belong to the oligomers of CH_2F_2, and those marked with a star belong to Py–H_2O.

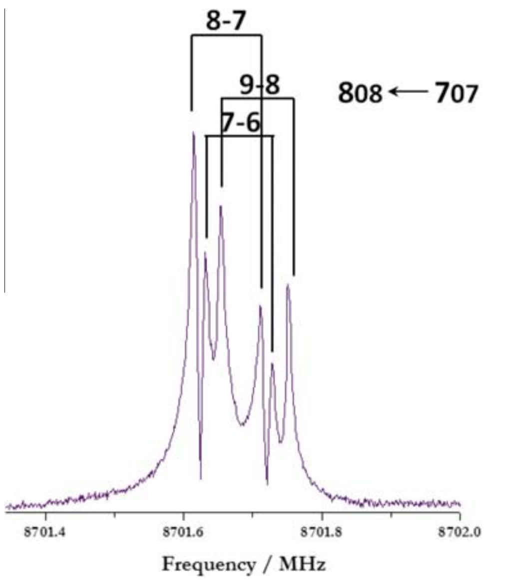

Figure 2. $8_{08} \leftarrow 7_{07}$ transition of the parent species, displaying the three $F \leftarrow F'$ ^{14}N quadrupole component lines.

freons, CHF_3, CH_3F and CH_2F_2 are linked to Py through C–H···N and C–H···F WHBs. However, in Py–CH_2F_2, where the CH_2···N is bifurcated, the dissociation energy is the largest one, according to three rather than to two WHBs.

Some structural information has been obtained from the six available rotational constants. First the Kraitchman [37] coordinates of the N atom were calculated in the principal axes system of the parent species. The obtained values are reported in Table 4, where they are compared to the *ab initio* data.

Table 2
Experimental spectroscopic parameters of the two isotopologues of the detected conformer of Py-CH_2F_2.

	$C_6H_5{}^{14}N \cdots CH_2F_2$	$C_6H_5{}^{15}N \cdots CH_2F_2$
A/MHz	4393.207 (2)[a]	4385.178 (3)
B/MHz	580.9088 (3)	580.6661 (5)
C/MHz	515.4690 (2)	515.1720 (3)
χ_{aa}/MHz	−4.14 (3)	–
χ_{bb}/MHz	0.85 (2)	–
χ_{cc}/MHz	3.29 (2)	–
D_J/kHz	0.1458 (9)	0.137 (2)
D_{JK}/kHz	2.166 (6)	2.17 (2)
d_1/Hz	−8.0 (9)	−8 (1)
d_2/Hz	−1.9 (2)	−1.8 (3)
N[b]	113	36
σ[c]/kHz	3.4	3.6

[a] Error in parentheses in units of the last digit.
[b] Number of lines in the fit.
[c] Root-mean-square deviation of the fit.

Table 3
Dissociation energies of complexes of pyridine with several freons.

Complex	Links	E_D/kJ mol^{-1}	Ref.
Py-CF_4	N···F_3C	10.0	[18]
Py-CH_3F	C–H···N C–H···F	11.4	[20]
Py-CHF_3	C–H···N C–H···F	14.9	[19]
Py-CH_2F_2	C–H_2···N C–H···F	15.6	This Letter

Table 4
r_s coordinates of the N atom in principal axes system of the parent molecule (c is zero by symmetry).

	a	b
r_s – exptl.	±0.602 (3)	±0.456 (3)
r_e – *ab initio*	−0.590	−0.437

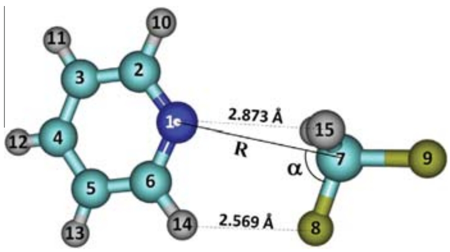

Figure 3. Drawing of Py-CH_2F_2 with the principal axes system and the main structural parameters.

A partial r_0 structure has been also determined by adjusting, with respect to the *ab initio* geometry, the N···C_{CH2F2} distance and the F_Z–C_{CH2F2}···N angle (the suffix *Z* is for *zusammen*, that is the *F* atom closer to the ring) in order to reproduce the experimental rotational constants of the two isotopologues. These parameters are labelled as *R* and α in Figure 3, and the *ab initio* geometry is given in Supplementary material. The maximum discrepancy between the calculated and experimental values was, after the fitting, 0.5 MHz. The values $R = 3.151(1)$ Å and $\alpha = 84.9(1)°$ have been obtained, with increases of 27 mÅ and of 0.6° with respect to the *ab initio* values. We could derive from these parameters the WHB lengths, which resulted to be $r_{N\cdots H} = 2.873$ Å and $r_{F\cdots H} = 2.569$ Å. These values are reported also in Figure 3. They are within the range of WHB's bond lengths. The latter value is intermediate with respect to the corresponding WHB bond lengths in Py–CHF_3 and Py–CH_3F, while $r_{N\cdots H}$ is larger than the corresponding values in the two homologues.

5. Conclusion

The observed conformer of Py–CH_2F_2 is stabilized by a small net of WHBs, that is a bifurcated CH_2···N and a CH···F links. Similar interactions have been found in Py–CHF_3, and Py–CH_3F, but the symmetric top conformation of CHF_3 and CH_3F allowed the determination, in the two latter cases, of their V_3 barriers to internal rotation, which represented extra data to size the strengths of the WHBs. It is possible, however, to set a strength order of the CH···N and a CH···F weak interactions within this small family of complexes of pyridine with freons. It should also be outlined that this kind of WHBs involving hetero aromatic molecules is supplied only by these three studies.

Acknowledgement

We thank Italian MIUR (PRIN project 2010ERFKXL_001) and the University of Bologna (RFO) for financial support. Q. G. thanks the China Scholarships Council (CSC) for financial support. Financial support from the Spanish Ministry of Science and Innovation (CTQ2011-22923 and CTQ2012-39132), the Basque Government (Consolidated Groups, IT520-10) and UPV/EHU (UFI11/23) is gratefully acknowledged. Computational resources and laser facilities of the UPV-EHU were used in this Letter (SGIker and I2Basque). M.V.L. and E.J.C. gratefully acknowledges the MICINN for a FPI grant and a 'Ramón y Cajal' contract, respectively.

Appendix A. Supplementary data

Supplementary data associated with this article can be found, in the online version, at http://dx.doi.org/10.1016/j.cplett.2013.11.040.

References

[1] R. Kempe, Eur. J. Inorg. Chem. (2003) 791.
[2] J. Ashmore, J.C. Green, L.H. Malcolm, M.L. Smith, C. Mehnert, E.J. Wucherer, J. Chem. Soc. Dalton Trans. 11 (1995) 1873.
[3] S. Haq, D.A. King, J. Phys. Chem. 100 (1996) 16957.
[4] S.A. Krasnokutski, D.-S. Yang, J. Chem. Phys. 130 (2009) 134313.
[5] C. Tanjaroon, W. Jäger, J. Chem. Phys. 127 (2007) 034302.
[6] A. Maris, W. Caminati, P.G. Favero, Chem. Comm. 23 (1998) 2625 (Cambridge).
[7] B. Velino, W. Caminati, J. Mol. Spectrosc. 251 (2008) 176.
[8] T.D. Klots, T. Emilsson, R.S. Ruoff, H.S. Gutowsky, J. Phys. Chem. 93 (1989) 1255.
[9] R.M. Spycher, D. Petitprez, F.L. Bettens, A. Bauder, J. Phys. Chem. 98 (1994) 11863.
[10] S. Melandri, G. Maccaferri, A. Maris, A. Millemaggi, W. Caminati, P.G. Favero, Chem. Phys. Lett. 261 (1996) 267.
[11] S. Tang, L. Evangelisti, B. Velino, W. Caminati, J. Chem. Phys. 129 (2008) 144301.
[12] L. Evangelisti, L.B. Favero, B.M. Giuliano, S. Tang, S. Melandri, W. Caminati, J. Phys. Chem. 113 (2009) 14227.
[13] S. Melandri, B.M. Giuliano, A. Maris, L. Evangelisti, B. Velino, W. Caminati, Chem. Phys. Chem. 10 (2009) 2503.
[14] R.P.A. Bettens, A. Bauder, J. Chem. Phys. 102 (1995) 1501.
[15] J.L. Doran, B. Hon, K.R. Leopold, J. Mol. Struct. 1019 (2012) 191.
[16] M.S. Labarge, J.-J. Oh, K.W. Hillig II, R.L. Kuczkowski, Chem. Phys. Lett. 159 (1989) 559.
[17] S.W. Hunt, K.R. Leopold, J. Phys. Chem. A 105 (2001) 5498.
[18] A. Maris, L.B. Favero, B. Velino, W. Caminati, J. Phys. Chem. A 117 (2013) 11289.
[19] L.B. Favero, B.M. Giuliano, A. Maris, S. Melandri, P. Ottaviani, B. Velino, W. Caminati, Chem. Eur. J. 16 (2010) 1761.
[20] L. Spada, Q. Gou, M. Vallejo-López, A. Lesarri, E. J. Cocinero, W. Caminati, *Phys. Chem. Chem. Phys.*, in press, http://dx.doi.org/10.1039/C3CP54430C.
[21] T.J. Balle, W.H. Flygare, Rev. Sci. Instrum. 52 (1981) 33.
[22] J.-U. Grabow, W. Stahl, H. Dreizler, Rev. Sci. Instrum. 67 (1996) 4072.
[23] W. Caminati, A. Millemaggi, J.L. Alonso, A. Lesarri, J.C. López, S. Mata, Chem. Phys. Lett. 392 (2004) 1.
[24] T.A. Halgren, J. Comput. Chem. 20 (1999) 730.
[25] Macromodel, Version 9.2, Schrödinger LLc., New York, NY, 2012.
[26] M. J. Frisch et al., Gaussian Inc., Wallingford CT, 2009.
[27] F. Boys, F. Bernardi, Mol. Phys. 19 (1970) 553.
[28] H.M. Pickett, J. Mol. Spectrosc. 148 (1991) 371.
[29] J.K.G. Watson, Aspects of Quartic and Sextic Centrifugal Effects on Rotational Energy Levels in 'Vibrational Spectra and Structure', Elsevier, Amsterdam, 1977.
[30] W. Gordy, L.R. Cook, 'Microwave Molecular Spectra', 3rd Edition, in: A. Weissberger (Ed.), Techniques of Chemistry, vol. XVIII, John Wiley & Sons Inc., New York, 1984.
[31] S. Blanco et al., Private communication.
[32] W. Caminati, S. Melandri, P. Moreschini, P.G. Favero, Angew. Chem. Int. Ed. 38 (1999) 2924.
[33] S. Blanco, S. Melandri, P. Ottaviani, W. Caminati, J. Am. Chem. Soc. 129 (2007) 2700.
[34] G. Feng, L. Evangelisti, I. Cacelli, L. Carbonaro, G. Prampolini, W. Caminati, Chem. Comm., 2013, Accepted for publication, http://dx.doi.org/10.1039/C3CC47206J.
[35] D. Millen, Can. J. Chem. 63 (1985) 1477.
[36] S.E. Novick, S.J. Harris, K.C. Janda, W. Klemperer, Can. J. Phys. 53 (1975) 2007.
[37] J. Kraitchman, Am. J. Phys. 21 (1953) 17.

CHEMISTRY
AN ASIAN JOURNAL

ACES

FULL PAPER

DOI: 10.1002/asia.201301722

Interactions between Freons: A Rotational Study of CH_2F_2–CH_2Cl_2

Qian Gou,[a] Lorenzo Spada,[a] Montserrat Vallejo-López,[a, c] Zbigniew Kisiel,[b] and Walther Caminati*[a]

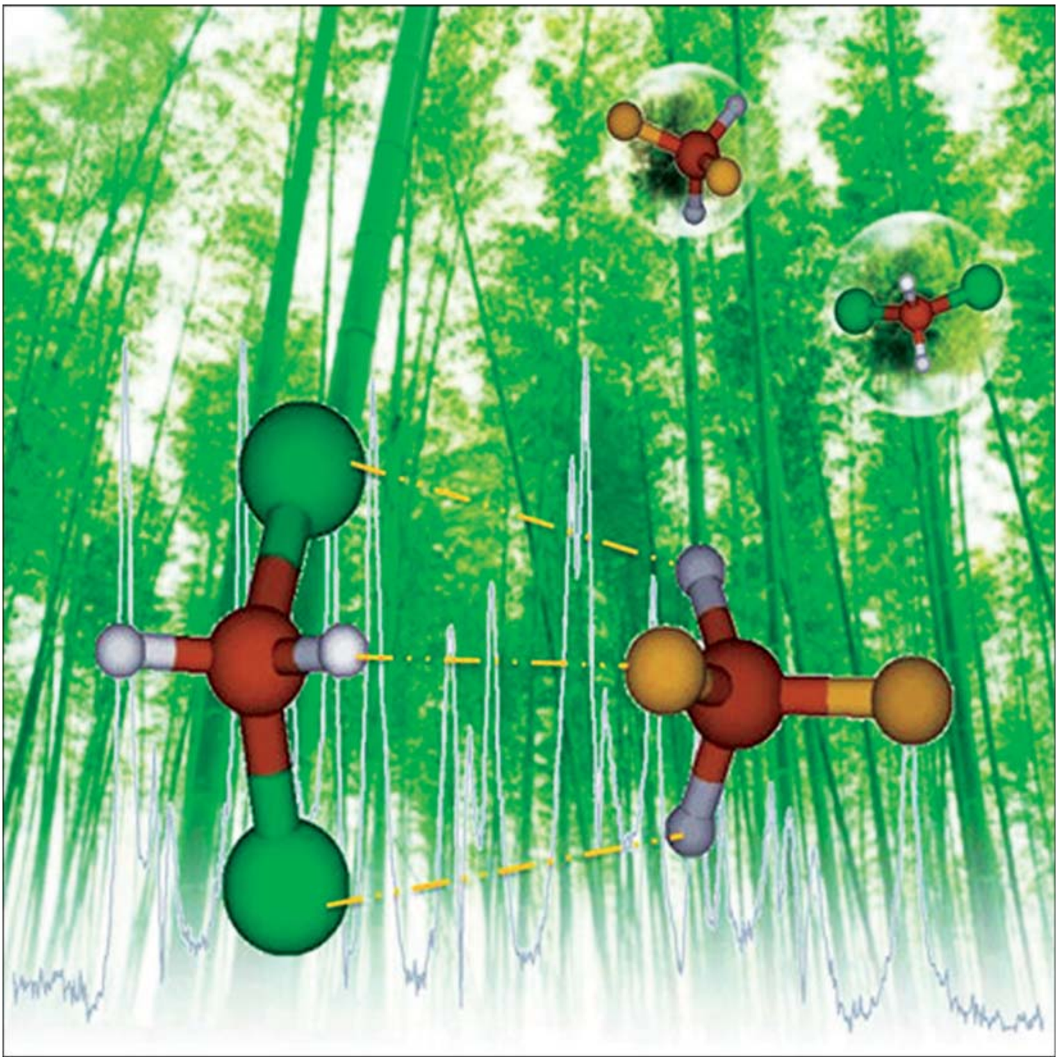

Abstract: The rotational spectra of two isotopologues of a 1:1 difluoromethane–dichloromethane complex have been investigated by pulsed-jet Fourier-transform microwave spectroscopy. The assigned (most stable) isomer has C_s symmetry and it displays a network of two C−H⋯Cl−C and one C−H⋯F−C weak hydrogen bonds, thus suggesting that the former interactions are stronger. The hyperfine structures owing to ^{35}Cl (or ^{37}Cl) quadrupolar effects have been fully resolved, thus leading to an accurate determination of the three diagonal (χ_{gg}; $g=a$, b, c) and the three mixed quadrupole coupling constants ($\chi_{gg'}$; g, $g'=a$, b, c; $g\neq g'$). Information on the structural parameters of the hydrogen bonds has been obtained. The dissociation energy of the complex has been estimated to be 7.6 kJ mol^{-1}.

Keywords: fluorine · freons · hydrogen bonds · non-bonding interactions · rotational spectroscopy

Introduction

In a recent IUPAC definition of the hydrogen bond, no explicit mention is given of the weak hydrogen bond (WHB);[1] as such, this weak interaction is still the subject of some controversy about its classification as a hydrogen bond. WHBs play an important role in chemistry and a vast amount of literature has been dedicated to this topic.[2]

WHBs such as C−H⋯O, C−H⋯N, and C−H⋯F−C are common in biological, atmospheric, and supramolecular chemistry.[3] Studies on such WHB have mainly been performed by using X-ray diffraction[4] and IR spectroscopy in rare-gas solutions.[5] However, this kind of experimental information on WHBs, from solid-state or solution-phase investigations, are contaminated by other intermolecular interactions that take place in condensed phases. Conversely, investigations on this kind of molecular system that are performed by using high resolution spectroscopic techniques, in particular pulsed-jet Fourier-transform microwave (FTMW) spectroscopy, provide precise data in an environment that is free from the interference of solvation and crystal-lattice effects.[6]

This technique has been used to obtain information on the C−H⋯O WHB from studies of the dimer of dimethyl ether[7] or of the adducts of some ethers, ketones, and aldehydes with some hydrogenated fluoro-freons, together with C−H⋯F linkages.[8] The C−H⋯N interaction has been described in rotational studies of the complexes of pyridine with mono-, di-, and tri-fluoromethane.[9]

[a] Q. Gou, L. Spada, M. Vallejo-López, Prof. W. Caminati
Dipartimento di Chimica "G. Ciamician"
Università di Bologna
Via Selmi 2, I-40126 Bologna (Italy)
Fax: (+39) 0512099456
E-mail: walther.caminati@unibo.it

[b] Prof. Z. Kisiel
Institute of Physics
Polish Academy of Sciences
Al.Lotnikow 32/46, 02-668 Warszawa (Poland)

[c] M. Vallejo-López
Permanent address:
Departamento de Química Física y Química Inorgánica
Facultad de Ciencias
Universidad de Valladolid
Paseo de Belén, 7, E-47011, Valladolid (Spain)

Supporting information for this article is available on the WWW under http://dx.doi.org/10.1002/asia.201301722.

Halogenated hydrocarbons have sites that can act as weak proton donors or weak proton acceptors, thereby leading to the easy formation of oligomers or hetero-adducts in which the subunits are held together by a 'net' of WHBs. Indeed, the aliphatic hydrogen atoms have been found to act as proton donors, thanks to the electron-withdrawing effect of the halogen atoms. Difluoromethane (CH_2F_2) can be regarded as the prototype for this kind of ambivalent molecules. Its oligomers, $(CH_2F_2)_n$, with $n=2$–4, have recently been characterized by FTMW spectroscopy. Rotational investigations of the dimer,[10] trimer,[11] and tetramer[12] of CH_2F_2 pointed out the existence of 3, 9, and 16 C−H⋯F−C WHBs, respectively. In the hetero-adduct CH_3F−CHF_3, the two subunits are linked together by three weak C−H⋯F−C WHBs, whilst the two subunits rotate through low V_3 barriers around their symmetry axes.[13]

Only one adduct between freon molecules that contain halogen atoms other than fluorine has been investigated by using rotational spectroscopy, that is, the adduct of CH_2ClF with FHC=CH_2, which presents a combination of C−H⋯F−C and C−H⋯Cl−C WHBs.[14] No complexes between freons with two heavy halogen atoms (Cl, Br, I) have been investigated, because, unlike the F atom, which has a nuclear spin quantum number of $I=1/2$, the other halogen atoms have $I=3/2$ or 5/2, thereby resulting in complicated quadrupole hyperfine structures in the rotational spectra of halogenated multi-molecular systems. From a spectroscopic point of view, in particular for systems that contain multiple quadrupolar nuclei, the interpretation of the rotational spectra can be a challenging task. For example, the rotational spectra of even simple molecules that contain two halogen atoms have only been reported in a few cases. Accurate information on the methylene di-halide series, CH_2Cl_2,[15] CH_2Br_2,[16] and CH_2I_2,[17] only became available in the last two decades. However, to the best of our knowledge, no information on their complexes is available. Herein, we report an investigation of the rotational spectrum of the 1:1 complex between CH_2Cl_2 and CH_2F_2 (freon 30 and freon 32), with the aim of determining the orientation of the subunits in the complex and ascertaining which WHB, that is, C−H⋯Cl−C or C−H⋯F−C, is more favorable.

Results and Discussion

Theoretical Calculations

Two isomers, which are both stabilized by three WHBs, are, by chemical intuition, expected to be the most stable forms of the title complex. The structures of the isomers are shown in Table 1. MP2/6-311++G(d,p) calculations, which were performed by using the Gaussian 03 program package,[18] confirmed this hypothesis. Table 1 also lists their relative energies (ΔE) and selected spectroscopic parameters for the investigation of the microwave spectrum. To obtain a better estimation of the energy differences, the intermolecular binding energies were counterpoise corrected (ΔE_{BSSE}) for the basis set superposition error (BSSE).[19] Isomer **I**, which contained two C–H···Cl–C and one C–H···F–C WHBs was slightly more stable than isomer **II**, which contained two C–H···F–C and one C–H···Cl–C WHBs. We also evaluated the dissociation energies, inclusive of the BSSE corrections, $E_{D(BSSE)}$. We did not calculate the zero-point-energy corrections.

Table 1. MP2/6-311++G(d,p) shapes and spectroscopic parameters of the two most stable forms of CH_2F_2–CH_2Cl_2.

	Isomer **I**	Isomer **II**
	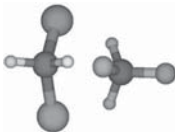	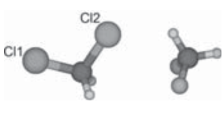
ΔE,ΔE_{BSSE}[a] [cm^{-1}]	0,0[b]	72,12
$E_{D(BSSE)}$[c] [$kJ\,mol^{-1}$]	7.0	6.9
A,B,C [MHz]	2706, 976, 792	3313, 870, 794
χ_{aa},$\chi_{bb}-\chi_{cc}$ (1) [MHz]	36.25, −45.14	−61.90, −8.14
χ_{ab},χ_{ac},χ_{bc} (1) [MHz]	−10.34, 7.84, 47.22[d]	−27.11, −17.04, −3.53
χ_{aa},$\chi_{bb}-\chi_{cc}$ (2) [MHz]		29.69, −96.32
χ_{ab},χ_{ac},χ_{bc} (2) [MHz]		−20.42, 3.43, 20.42
μ_a,μ_b,μ_c [D]	−1.5, −0.0, 0.0	2.9, 0.3, 0.4

[a] ΔE and ΔE_{BSSE} denote the energy difference with respect to the most stable isomer, without and with BSSE correction. [b] The absolute values are $-1197.020145\ E_h$ and $-1197.016320\ E_h$, respectively. [c] Dissociation energy. [d] For this isomer, the quadrupole coupling constants of Cl2 are the same as for Cl1, except for the signs of χ_{ab} and χ_{bc}.

Isomer **I** was calculated to be slightly distorted with respect to a C_s configuration, with the two F atoms in the plane of symmetry. However, it is well-known that, in similar cases, the vibrational ground-state wavefunction is symmetric with respect to the "near"-symmetry plane. Herein, we imposed C_s symmetry and, as a consequence, the quadrupole coupling constants of the two Cl atoms have the same value. This result is consistent, as shown below, with the experimental evidence.

Rotational Spectra

The spectrum was expected to be quite complicated for two reasons: 1) the presence of several abundant isotopologues ($^{35}Cl/^{35}Cl$, $^{35}Cl/^{37}Cl$, and $^{37}Cl/^{37}Cl$ in the ratio 9:6:1, according to the 75% and 25% natural abundance of ^{35}Cl and ^{37}Cl, respectively) and 2) the presence of two quadrupolar nuclei (^{35}Cl or ^{37}Cl) with a nuclear spin $I=3/2$ and with a relatively large nuclear electric quadrupole moment (Q).

Following the predictions from the computations, which showed that the μ_a dipole moment component was the largest one, we searched for the $J=5\leftarrow4$ μ_a-R band first and identified the intense $K=0$, 1 transitions of the parent species of isomer **I**. Each of the transitions was split into several quadrupole component lines, as shown in Figure 1 for the $5_{15}\leftarrow4_{14}$ transition.

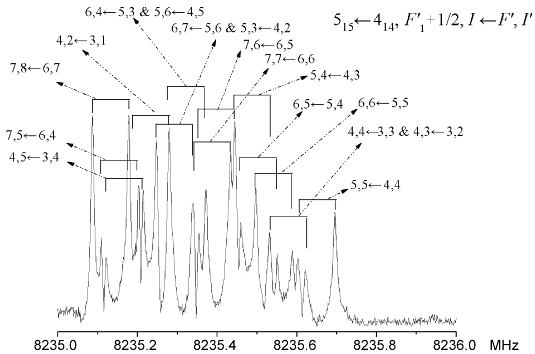

Figure 1. The recorded $5_{15}\leftarrow4_{14}$ rotational transition of the parent species of the observed isomer of CH_2F_2–CH_2Cl_2, which shows a hyperfine structure that originates from the two ^{35}Cl nuclei. Each component line exhibits its Doppler doubling.

Next, many additional μ_a-type transitions, with J_{upper} and K_a values of up to 8 and 3, respectively, were measured. Then, about 100 MHz below each transition of the observed $J=5$–4 band, a weaker set of transitions was observed, which belonged to the $^{35}Cl/^{37}Cl$ isotopologue. The intensities of these transitions were about 2/3 of those of the parent species, consistent with the natural relative abundance of the two isotopes and the existence of two equivalent $^{35}Cl/^{37}Cl$ isotopologues. This result confirmed the equivalence of the two Cl atoms and, consequently, the C_s symmetry of the complex.

The frequencies were fitted with Pickett's SPFIT program[20] by direct diagonalization of the Hamiltonian that consisted of Watson's "S" reduced semirigid-rotor Hamiltonian[21] in the I^r representation, augmented by the hyperfine Hamiltonian, according to Equation (1), in which H_R represents the rigid-rotor Hamiltonian, H_{CD} represents the centrifugal distortion contributions, and H_Q is the operator associated with the quadrupolar interaction of the ^{35}Cl (or ^{37}Cl) nuclei with the overall rotation.

$$H = H_R + H_{CD} + H_Q \quad (1)$$

The obtained spectroscopic constants are reported in Table 2. No μ_b-type transitions were observed, in accordance with the C_s symmetry of the isomer. The C_s symmetry makes the two ^{35}Cl atoms of the parent species equivalent to each other and, correspondingly, their quadrupole coupling constants have the same values. As mentioned above, the μ_a-type spectrum for the ^{35}Cl/^{37}Cl isotopologue has also been assigned and measured in natural abundance. Its spectroscopic parameters are listed in the second column of Table 2. In this case, the ^{35}Cl and ^{37}Cl nuclei are different from each other and, in addition, the geometrical symmetry of the complex is destroyed, so that two different sets of quadrupole coupling constants are required. Because a smaller number of lines were measured for this isotopologue, the d_1 and d_2 centrifugal distortion parameters were fixed at the values of the parent species, whilst the off-diagonal quadrupolar coupling constants, χ_{ab} and χ_{ac}, were fixed at the theoretical values. Disappointingly, we did not succeed in measuring at least four transitions of the ^{37}Cl/^{37}Cl isotopologue, because its abundance was only about 10% of that of the parent species.

Table 2. Spectroscopic parameters of the two isotopologues of CH_2F_2–CH_2Cl_2.

	^{35}Cl/^{35}Cl	^{35}Cl/^{37}Cl
A [MHz]	2663.073(3)[a]	2604.320(3)
B [MHz]	958.4016(2)	951.1963(1)
C [MHz]	785.1948(1)	775.4507(1)
D_J [kHz]	0.7171(7)	0.710(1)
D_{JK} [kHz]	10.813(6)	9.88(7)
d_1 [kHz]	−0.1604(7)	[−0.1604][b]
d_2 [kHz]	−0.0613(4)	[−0.0613][b]
$\chi_{aa}(^{35}\mathrm{Cl})$ [MHz]	37.399(5)	37.17(3)
$\chi_{bb}-\chi_{cc}$ (^{35}Cl) [MHz]	−43.68(2)	−42.34(3)
$\chi_{ab}(^{35}\mathrm{Cl})$ [MHz]	±9.00(7)	11.16[c]
$\chi_{ac}(^{35}\mathrm{Cl})$ [MHz]	7.0(1)	8.43[c]
$\chi_{bc}(^{35}\mathrm{Cl})$ [MHz]	∓49.71(6)	−50.03(2)
$\chi_{aa}(^{37}\mathrm{Cl})$ [MHz]		29.62(2)
$\chi_{bb}-\chi_{cc}(^{37}\mathrm{Cl})$ [MHz]		−35.44(2)
$\chi_{ab}(^{37}\mathrm{Cl})$ [MHz]		−7.52[c]
$\chi_{ac}(^{37}\mathrm{Cl})$ [MHz]		6.19[c]
$\chi_{bc}(^{37}\mathrm{Cl})$ [MHz]		39.23(1)
N[d]	349	160
σ[e] [kHz]	2.9	3.1

[a] Uncertainties (in parentheses) are standard deviations expressed in units of the last digit. [b] The numbers in parentheses are fixed at the values obtained for the parent species. [c] Fixed at the values obtained from the theoretical calculations. [d] Number of lines in the fit. [e] Standard deviation of the fit.

A comparison of the experimental spectroscopic parameters with the theoretical values for the two conformations in Table 1 leads to a straightforward assignment of the observed spectrum to isomer **I**, which is stabilized by two C−H···Cl−C and one C−H···F−C WHBs.

No lines belonging to isomer **II** were identified, despite the very small difference in complexation energy. This result could be due to conformational relaxation to the most stable isomer upon supersonic expansion. Indeed, it has been shown that this kind of relaxation takes place easily if the interconversion barrier is smaller than $2kT$.[22]

Structural Information

The C_s configuration of the observed isomer of CH_2F_2–CH_2Cl_2 is shown in Figure 2. From the rotational constants of the two isotopologues, it is possible to calculate the substitution coordinates, r_s,[23] of the Cl atom in the principal axes of the parent species. The obtained values are shown in Table 3 and are compared with the values of a partial r_0 structure.

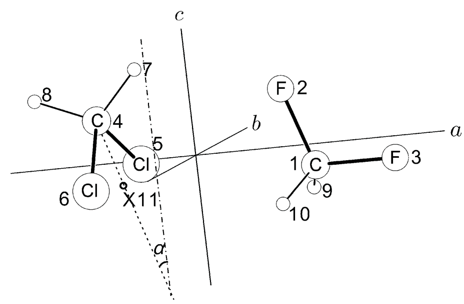

Figure 2. The observed isomer of CH_2F_2–CH_2Cl_2, with atom numbering and the positions of the principal axes. α denotes the angle between the bisector of the Cl-C-Cl valence angle and the bc plane.

Table 3. Experimental coordinates of the chlorine atoms in CH_2F_2–CH_2Cl_2.

	a [Å]	b [Å]	c [Å]
r_s	±1.399(1)	±1.466(1)	±0.223(7)
r_0[a]	−1.404	±1.473	−0.239

[a] Calculated from the r_0 structure in Table 4; the sign of the b coordinates depends on the specific Cl atom, owing to the symmetry.

The partial r_0 structure was obtained by adjusting three structural parameters (R_{C1C4}, ∢H7C4···C1, and ∢F2C1···C4), whilst keeping the remaining parameters fixed to their ab initio values (preserving the C_s symmetry), to reproduce the six experimental rotational constants. The obtained parameters are reported in Table 4 and compared to the ab initio values. From this partial r_0 structure, α (the angle between the Cl-C-Cl and bc planes) and the lengths of the three WHBs were derived (Table 4). The full ab initio geometry is available in the Supporting Information.

Table 4. Partial r_0 and r_e structures of CH_2F_2–CH_2Cl_2.

Fitted parameters	R_{C1C4} [Å]	∢H7C4···C1 [°]	∢F2C1···C4 [°]
r_0	3.755(1)[a]	62.5(1)	55.7(1)
r_e	3.751	63.5	50.4
Derived parameters	R_{F2H7} [Å]	R_{Cl5H9} [Å]	α [°][b]
r_0	2.489(2)	3.147(2)	11.8(1)
r_e	2.421	3.139	13.8

[a] Uncertainties (in parentheses) are expressed in units of the last digit. [b] The angle between the Cl-C-Cl plane and the *bc* inertial plane.

Quadrupole Coupling Constants

The nuclear quadrupole hyperfine structure considerably complicates the rotational spectrum, but its analysis can provide useful information on the structure and internal dynamics in the complex. This analysis would become possible if the principal nuclear quadrupole tensor could be determined, because, for a hyperfine nuclei terminal to a bond, this tensor is typically oriented to within 1° of the direction the relevant bond axis.[24] The only three non-zero components of the principal hyperfine tensor, $\chi_g = eQq_g$ ($g = x$, y, z), can be obtained from the quadrupole tensor that is experimentally determined in the principal inertial axes. The latter tensor consists of diagonal quadrupole coupling constants, χ_{aa}, χ_{bb}, and χ_{cc}, and off-diagonal χ_{ab}, χ_{bc} and χ_{ac} constants. Diagonalization of the corresponding 3×3 matrix results in three principal hyperfine tensor components, χ_{zz}, χ_{xx}, and χ_{yy}, which are conventionally labeled in such a way that χ_{zz} describes the molecular-field gradient around the axis close to the bond axis, which is, in this case, the C−Cl axis.

We performed the transformation by using the QDIAG program, available on the PROSPE website,[24–26] which also provided the rotation angles between the two axis systems. One of the more useful of these angles, θ_{zb}, allows an estimate of the ∢Cl-C-Cl valence angle from the relation ∢Cl-C-Cl = $(180-2\,\theta_{zb})$° The quadrupole asymmetry parameter $\eta = (\chi_{xx}-\chi_{yy})/\chi_{zz}$ is also evaluated. These parameters are compared in Table 5 with those for the CH_2Cl_2 monomer. The differences do not appear to be significant, thus suggesting that vibrational averaging in the cluster has little effect on the chlorine nuclear quadrupole hyperfine splitting.

Table 5. The principal quadrupole tensors, η, θ, and ∢Cl-C-Cl for CH_2Cl_2 and CH_2F_2–CH_2Cl_2.

	CH_2Cl_2[a]	CH_2F_2–CH_2Cl_2
χ_{zz} [MHz]	−75.4(2)	−74.16(6)
χ_{xx} [MHz]	33.4(2)	35.31(8)
χ_{yy} [MHz]	39.9414(2)	38.85(7)
η[b]	0.060(3)	0.048(1)
θ [°][c]	33.43(5)	33.6(1)
∢Cl-C-Cl [°][d]	113.1	112.7

[a] see Ref. [15]. [b] $\eta = (\chi_{xx}-\chi_{yy})/\chi_{zz}$. [c] This angle corresponds to θ_{za} for CH_2Cl_2 and θ_{zb} for CH_2F_2–CH_2Cl_2. [d] Estimate obtained from $180-2\theta$, compared with ∢Cl-C-Cl = 111.8° from the structural analysis of the monomer (see Ref. [15]).

Therefore, we can use the quadrupole orientation to calculate how much the Cl-C-Cl plane in the complex is tilted away from the *bc* plane. This result is quantified by using the tilt angle (α) as defined in Figure 2. The hyperfine estimate of this angle, as obtained from QDIAG, $\alpha = 10.6(1)$°, is close to the values from the ab initio geometry and from the partial r_0 structure, thereby providing additional independent confirmation of the determined structure.

Dissociation Energy

The intermolecular stretching motion that leads to the dissociation appears to be almost parallel to the *a* axis of the complex. By assuming that such a motion is separated from the other molecular vibrations, it is possible, within a pseudo-diatomic approximation, to estimate the stretching force constant according to Equation (2),[27] where μ is the pseudo-diatomic reduced mass and R_{CM} (3.771 Å) is the distance between the centers of mass of the two subunits; B, C, and D_J are the spectroscopic parameters reported in Table 2.

$$k_s = 16\pi^4 (\mu R_{CM})^2 [4B^4+4C^4-(B-C)^2(B+C)^2]/(hD_J) \qquad (2)$$

If then it is assumed that the intermolecular separation for this kind of complex can be described by a Lennard–Jones-type potential approximation, the dissociation energy can be evaluated from Equation (3),[28] thus leading to $E_D = 7.6\ \mathrm{kJ\,mol^{-1}}$, which is very close to the ab initio value ($E_{D(BSSE)} = 7.0\ \mathrm{kJ\,mol^{-1}}$).

$$E_D = 1/72\, k_s\, R_{CM}{}^2 \qquad (3)$$

In Table 6, we compare the dissociation energy of CH_2F_2–CH_2Cl_2 to those of some related adducts among freon molecules. From these data, it appears difficult to get a rule on the relative strengths of the C−H···Cl and C−H···F interactions.

Table 6. Binding energies of the investigated dimers of freons.

	WHBs	E_D [kJ mol^{-1}]	Reference
CH_3F···CHF_3	three C−H···F−C	5.3	[13]
CH_2F_2···CH_2F_2	three C−H···F−C	8.7	[10]
CH_2ClF···FHC=CH_2	one C−H···Cl−C one C−H_2···F−C	8.7	[14]
CH_2F_2···CH_2Cl_2	two C−H···Cl−C one C−H···F−C	7.6	this work

Conclusions

The microwave spectrum of CH_2F_2–CH_2Cl_2 represents an unprecedented investigation of this type of intermolecular complex by rotational spectroscopy. This cluster, which exists as a combination of two asymmetric molecules, contains two heavy quadrupolar nuclei (^{35}Cl or ^{37}Cl) with high nuclear spin quantum numbers and large electric nuclear quadrupole moments. The consequent complex hyperfine structure of each transition has been successfully analyzed and interpreted in terms of five or ten quadrupole coupling parameters, depending on the equivalence ($^{35}Cl/^{35}Cl$) or not ($^{35}Cl/^{37}Cl$) of the two Cl atoms. The complex has a plane of symmetry with two equivalent Cl atoms, as confirmed by the key available experimental data: 1) the existence of only one $^{35}Cl/^{37}Cl$ isotopologue with 2/3 intensity of that of the parent species; 2) the values of the Cl substitution coordinates; and 3) the number and values of the quadrupole coupling constants.

The detection of isomer **I**, in which the two subunits are linked to each other through two C−H···Cl−C and one C−H···F−C WHBs, rather than isomer **II**, in which the units are linked through two C−H···F−C and one C−H···Cl−C interactions, suggests that C−H···Cl−C is a stronger linkage than C−H···F−C.

Within a pseudo-diatomic approximation, in which the two subunits are considered to be rigid in the angular coordinates, the dissociation energy of this complex has been estimated to be of similar value to that of the dimer of CH_2F_2.

Experimental Section

The molecular clusters were generated in a supersonic expansion, under optimized conditions for the formation of the adduct. Details of the Fourier-transform microwave spectrometer[29] (COBRA-type[30]), which covers the range 6.5–18 GHz, have been described previously.[31]

A gaseous mixture of about 1% CH_2F_2 and CH_2Cl_2 (commercial samples used without further purification) in He at a stagnation pressure of about 0.5 MPa was expanded through a solenoid valve (General Valve, Series 9, nozzle diameter 0.5 mm) into the Fabry–Pérot cavity. The line positions were determined after Fourier transformation of the time-domain signal with 8k data points, recorded at sampling intervals of 100 ns. Each rotational transition appears as a doublet, owing to the Doppler Effect. The line position was calculated as the arithmetic mean of the frequencies of the Doppler components. The estimated accuracy of the frequency measurements was better than 3 kHz. Lines that were separated by more than 7 kHz were resolvable.

Acknowledgements

We acknowledge the Italian MIUR (PRIN project 2010ERFKXL_001) and the University of Bologna (RFO) for financial support. Q.G. also thanks the China Scholarships Council (CSC) for financial support. M.V.L. gratefully acknowledges a FPI grant from MICINN and Z.K. acknowledges a grant from the Polish National Science Centre (decision number DEC/2011/02A/ST2/00298).

[1] E. Arunan, G. R. Desiraju, R. A. Klein, .J. Sadlej, S. Scheiner, I. Alkorta, D. C. Clary, R. H. Crabtree, J. J. Dannenberg, P. Hobzal, H. G. Kjaergaard, A. C. Legon, B. Mennucci, D. J. Nesbitt, *Pure Appl. Chem.* **2011**, *83*, 1619–1636.
[2] For example, see: *The weak hydrogen bond in structural chemistry and biology*, *Vol. IX* (Eds.: G. R. Desiraju, T. Steiner), IUCr monographs on crystallography, Oxford University Press, Oxford, **2001**.
[3] For example, see: a) J.-M. Lehn, *Angew. Chem. Int. Ed. Engl.* **1988**, *27*, 89–112; *Angew. Chem.* **1988**, *100*, 91–116; b) J.-M. Lehn, *Angew. Chem. Int. Ed. Engl.* **1990**, *29*, 1304–1319; *Angew. Chem.* **1990**, *102*, 1347–1362; .
[4] For example, see: T. Steiner, *Angew. Chem. Int. Ed.* **2002**, *41*, 48–76; *Angew. Chem.* **2002**, *114*, 50–80.
[5] For example, see: S. N. Delanoye, W. A. Herrebout, B. J. Van der Veken, *J. Am. Chem. Soc.* **2002**, *124*, 11854–11855.
[6] For example, see: W. Caminati, J.-U. Grabow, *Microwave spectroscopy: Molecular systems* in *Frontiers of molecular spectroscopy* (Ed: J. Laane), Elsevier, Amsterdam, **2008**, Chapter 15, pp. 455–552.
[7] Y. Tatamitani, B. Liu, J. Shimada, T. Ogata, P. Ottaviani, A. Maris, W. Caminati, J. L. Alonso, *J. Am. Chem. Soc.* **2002**, *124*, 2739–2743.
[8] For example, see: a) J. L. Alonso, S. Antolínez, S. Blanco, A. Lesarri, J. C. López, W. Caminati, *J. Am. Chem. Soc.* **2004**, *126*, 3244–3249; b) Q. Gou, G. Feng, L. Evangelisti, M. Vallejo López, A. Lesarri, E. J. Cocinero, W. Caminati, *Phys. Chem. Chem. Phys.* **2013**, *15*, 6714–6718; c) S. Blanco, J. C. López, A. Lesarri, W. Caminati, J. L. Alonso, *ChemPhysChem* **2004**, *5*, 1779–1782; d) L. B. Favero, B. M. Giuliano, S. Melandri, A. Maris, P. Ottaviani, B. Velino, W. Caminati, *J. Phys. Chem. A* **2005**, *109*, 7402–7404; e) P. Ottaviani, W. Caminati, L. B. Favero, S. Blanco, J. C. López, J. L. Alonso, *Chem. Eur. J.* **2006**, *12*, 915–920.
[9] a) L. B. Favero, B. M. Giuliano, A. Maris, S. Melandri, P. Ottaviani, B. Velino, W. Caminati, *Chem. Eur. J.* **2010**, *16*, 1761–1764; b) M. Vallejo-López, L. Spada, Q. Gou, A. Lesarri, E. J. Cocinero, W. Caminati, *Chem. Phys. Lett.* **2014**, *591*, 216–219; c) L. Spada, Q. Gou, M. Vallejo-López, A. Lesarri, E. J. Cocinero, W. Caminati, *Phys. Chem. Chem. Phys.* **2014**, *16*, 2149–2153.
[10] W. Caminati, S. Melandri, P. Moreschini, P. G. Favero, *Angew. Chem. Int. Ed.* **1999**, *38*, 2924–2925; *Angew. Chem.* **1999**, *111*, 3105–3107; .
[11] S. Blanco, S. Melandri, P. Ottaviani, W. Caminati, *J. Am. Chem. Soc.* **2007**, *129*, 2700–2703.
[12] G. Feng, L. Evangelisti, I. Cacelli, L. Carbonaro, G. Prampolini, W. Caminati *Chem. Commun.* **2014**, *50*, 171–173.
[13] W. Caminati, J. C. López, J. L. Alonso, J.-U. Grabow, *Angew. Chem. Int. Ed.* **2005**, *44*, 3840–3844; *Angew. Chem.* **2005**, *117*, 3908–3912.
[14] C. L. Christenholz, D. A. Obenchain, S. A. Peebles, R. A. Peebles, *J. Mol. Spectrosc.* **2012**, *280*, 61–67.
[15] Z. Kisiel, J. Kosarzewski, L. Pszczólkowski, *Acta Phys. Polon. A* **1997**, *92*, 507–516.
[16] Y. Niide, H. Tanaka, I. Ohkoshi, *J. Mol. Spectrosc.* **1990**, *139*, 11–29.
[17] a) Z. Kisiel, L. Pszczólkowski, W. Caminati, P. G. Favero, *J. Chem. Phys.* **1996**, *105*, 1778–1785; b) Z. Kisiel, L. Pszczólkowski, L. B. Favero, W. Caminati, *J. Mol. Spectrosc.* **1998**, *189*, 283–290.
[18] Gaussian 03 (Revision B.01), M. J. Frisch, G. W. Trucks, H. B. Schlegel, G. E. Scuseria, M. A. Robb, J. R. Cheeseman, J. A. Montgomery, Jr., T. Vreven, K. N. Kudin, J. C. Burant, J. M. Millam, S. S. Iyengar, J. Tomasi, V. Barone, B. Mennucci, M. Cossi, G. Scalmani, N. Rega, G. A. Petersson, H. Nakatsuji, M. Hada, M. Ehara, K. Toyota, R. Fukuda, J. Hasegawa, M. Ishida, T. Nakajima, Y. Honda, O. Kitao, H. Nakai, M. Klene, X. Li, J. E. Knox, H. P. Hratchian, J. B. Cross, C. Adamo, J. Jaramillo, R. Gomperts, R. E. Stratmann, O. Yazyev, A. J. Austin, R. Cammi, C. Pomelli, J. W. Ochterski, P. Y. Ayala, K. Morokuma, G. A. Voth, P. Salvador, J. J. Dannenberg, V. G. Zakrzewski, S. Dapprich, A. D. Daniels, M. C. Strain, O. Farkas, D. K. Malick, A. D. Rabuck, K. Raghavachari, J. B. Foresman, J. V. Ortiz, Q. Cui, A. G. Baboul, S. Clifford, J. Cioslowski, B. B. Stefanov, G. Liu, A. Liashenko, P. Piskorz, I. Komaromi, R. L. Martin, D. J. Fox, T. Keith, M. A. Al-Laham, C. Y. Peng, A. Nanayakkara, M. Challacombe, P. M. W. Gill, B. Johnson, W. Chen, M. W. Wong, C. Gonzalez, J. A. Pople, Gaussian, Inc., Pittsburgh PA, **2003**..
[19] S. F. Boys, F. Bernardi, *Mol. Phys.* **1970**, *19*, 553–566.
[20] M. H. Pickett, *J. Mol. Spectrosc.* **1991**, *148*, 371–377.
[21] J. K. G. Watson in *Vibrational Spectra and structure*, *Vol. 6* (Ed.: J. R. Durig), Elsevier, New York/Amsterdam, **1977**, pp. 1–89.
[22] For example, see: R. S. Ruoff, T. D. Klots, T. Emilson, H. S. Gutowski, *J. Chem. Phys.* **1990**, *93*, 3142–3150.
[23] J. Kraitchman, *Am. J. Phys.* **1953**, *21*, 17–25.
[24] Z. Kisiel, E. Bialkowska-Jaworska, L. Pszczolkowski, *J. Chem. Phys.* **1998**, *109*, 10263–10272.

[25] Z. Kisiel in *Spectroscopy from Space* (Eds.: J. Demaison, K. Sarka, E. A. Cohen), Kluwer Academic Publishers, Dordrecht, **2001**, pp. 91–106.
[26] Z. Kisiel, *PROSPE–Programs for ROtational SPEctroscopy*, available at http://www.ifpan.edu.pl/~kisiel/prospe.htm.
[27] a) D. J. Millen, *Can. J. Chem.* **1985**, *63*, 1477–1479; b) W. G. Read, E. J. Campbell, G. Henderson, *J. Chem. Phys.* **1983**, *78*, 3501–3508.
[28] S. E. Novick, S. J. Harris, K. C. Janda, W. Klemperer, *Can. J. Phys.* **1975**, *53*, 2007–2015.
[29] T. J. Balle, W. H. Flygare, *Rev. Sci. Instrum.* **1981**, *52*, 33–45.
[30] a) J.-U. Grabow, W. Stahl, *Z. Naturforsch. A* **1990**, *45*, 1043–1044; b) J.-U., Grabow, doctoral thesis, Christian-Albrechts-Universität zu Kiel, Kiel, **1992**; c) J.-U. Grabow, W. Stahl, H. Dreizler, *Rev. Sci. Instrum.* **1996**, *67*, 4072–4084; d) J.-U. Grabow, Habilitationsschrift, Universität Hannover, Hannover, **2004**.
[31] W. Caminati, A. Millemaggi, J. L. Alonso, A. Lesarri, J. C. Lopez, S. Mata, *Chem. Phys. Lett.* **2004**, *392*, 1–6.

Received: December 28, 2013
Revised: January 21, 2014
Published online: February 26, 2014

